

**Revealing cancer vulnerabilities
through drug profiling and combination
therapy**

Doctoral thesis at the Medical University of Vienna
for obtaining the academic degree

Doctor of Philosophy

Submitted by

Branka Radić Sarikas

Supervisor:

Giulio Superti-Furga, PhD
CeMM Research Center for Molecular Medicine
Of the Austrian Academy of Sciences
Lazarettgasse 14/ AKH BT 25.3
1090 Vienna, Austria

Vienna, 12/2015

Declaration

This thesis contains published results, as well as unpublished data soon to be submitted for a publication. Thus, it is compiled in the cumulative format. In total, three manuscripts are included, the author of the thesis being a co-author on all of them, as well as two chapters of results not yet published.

The work performed by the author of this thesis was carried out at the laboratory of Prof. Dr. Giulio Superti-Furga, at the CeMM Research Center for Molecular Medicine of the Austrian Academy of Sciences in Vienna, Austria. The work was supported by the ASSET project (Analysing and Striking the Sensitivities of Embryonal Tumours), a collaborative project supported by the European commission's FP7 Health work Programme 2010 (FP7-Health-2010) under the theme "tackling diseases through systems biology approaches"

Manuscript #1 was published in *EuPA Open Proteomics*: "Enhancing Cognate Target Elution Efficiency in Gel-Free Chemical Proteomics" by Branka Radic-Sarikas, Uwe Rix, Alexey Stukalov, Manuela Gridling, André C. Müller, Jacques Colinge, Giulio Superti-Furga and Keiryn L. Bennett. *EuPA Open Proteom.* 2015 Dec 9: 43-53. Reprinted with permission. B.R.S. designed and performed experiments, analyzed and interpreted the data, made the figures and wrote the manuscript. U.R. designed experiments, interpreted the data and wrote the manuscript. A.S. performed bioinformatic data analysis. M.G. assisted in experiments. A.C.M. performed mass spectrometry. J.C. supervised the study. G.S.F. codesigned and supervised the study. K.L.B. codesigned and supervised the study and wrote the manuscript.

Manuscript #2 was published in *Nature*: "Stereospecific targeting of MTH1 by (S)-crizotinib as an anticancer strategy" by Kilian V. M. Huber, Eidarus Salah, Branka Radic, Manuela Gridling, Jonathan M. Elkins, Alexey Stukalov, Ann-Sofie Jemth, Camilla Göktürk, Kumar Sanjiv, Kia Strömberg, Therese Pham, Ulrika Warpman Berglund, Jacques Colinge, Keiryn L. Bennett, Joanna I. Loizou, Thomas Helleday, Stefan Knapp & Giulio Superti-Furga. *Nature.* 2014 Apr 10;508(7495):222-7. Reprinted with permission. K.V.M.H., E.S., B.R., M.G., J. M.E., J.I.L., A.-S.J., K.S. performed experiments. K.V.M.H. and G.S.-F. conceived the study. K.V.M.H., J.I.L., U.W.B., T.H., S.K. and G.S.-F. designed experiments. A.S., K.L.B. and J.C. performed mass spectrometry and bioinformatic data analysis. C.G., K.S., T.P. and U.W.B. performed animal experiments. K.V.M.H., S.K. and G.S.-F. wrote the manuscript. All authors contributed to the discussion of results and participated in manuscript preparation.

In the Results section we report yet unpublished results in the **chapter 3.3.**: "Phenotypic screens reveal neuroblastoma and Ewing sarcoma specific synergistic

combinations of clinically applicable targeted small molecules”. Branka Radic Sarikas designed and performed experiments, analyzed and interpreted the data, made the figures and wrote the manuscript. Kalliopi Tsafo (Novo Nordisk Foundation Center for Protein Research, Faculty of Health and Medical Sciences, University of Copenhagen, Copenhagen, Denmark) performed bioinformatic data analysis and interpreted the data. Georg Winter helped to set up MRM measurements and gave experimental advice. Kilian Huber helped to set up MRM measurements, gave experimental advice and interpreted the data. Kristina Bennet Emdal and Jesper Olsen (Novo Nordisk Foundation Center for Protein Research, Faculty of Health and Medical Sciences, University of Copenhagen, Copenhagen, Denmark) performed SILAC experiment and analyzed and interpreted the data. Cornelia Mutz (Children's Cancer Research Institute, Vienna, Austria) performed Annexin V experiments and analyzed the data. Stefan Kubicek gave experimental advice and designed experiments. Keiryn Bennett performed mass spectrometry. Heinrich Kovar (Children's Cancer Research Institute, Vienna, Austria) gave experimental advice. Giulio Superti-Furga codesigned and supervised the study.

Manuscript #3 was published in Nature Chemical Biology: “The solute carrier SLC35F2 enables YM155-mediated DNA damage toxicity” by Georg E Winter, Branka Radic, Cristina Mayor-Ruiz, Vincent A Blomen, Claudia Trefzer, Richard K Kandasamy, Kilian V M Huber, Manuela Gridling, Doris Chen, Thorsten Klampfl, Robert Kralovics, Stefan Kubicek, Oscar Fernandez-Capetillo, Thijn R Brummelkamp & Giulio Superti-Furga. Nat Chem Biol. 2014 Sep;10(9):768-73. Reprinted with permission. G.E.W. designed and performed experiments, analyzed and interpreted the data, made the figures and wrote the manuscript. B.R. designed and performed experiments, interpreted the data and prepared figures. C.M.-R. performed the mouse xenograft experiments, high-content microscopy and the comet assay. V.A.B. helped perform the haploid genetic screen and conducted statistical analysis. C.T. performed the RNA sequencing experiment and helped to perform MRM measurements. R.K.K. analyzed RNA sequencing data and performed statistical analysis. K.V.M.H. helped to set up MRM measurements and gave experimental advice. M.G. assisted with immunoblot analysis. D.C. created the Circos plot and a graphical display of insertion sites. T.K. operated the next-generation sequencer (Illumina HiSeq 2000) and helped with next-generation sequencing data handling. R.K. gave experimental advice and supervised next-generation sequencing. S.K. gave experimental advice and designed experiments. O.F.-C. designed the mouse xenograft study and analyzed and interpreted data. T.R.B. codesigned the study and gave experimental advice. G.S.-F. codesigned and supervised the study and wrote the manuscript.

Table of contents

| | |
|---|-----|
| Declaration..... | i |
| Table of contents | iv |
| Acknowledgements | vi |
| Abstract | vii |
| Zusammenfassung | ix |
| | |
| 1 Introduction..... | 1 |
| 1.1 Signal transduction and signaling networks in cancer | 1 |
| 1.2 Systems biology in cancer | 4 |
| 1.3 Cancer treatment..... | 6 |
| 1.3.1 Precision medicine and targeted therapy | 6 |
| 1.3.2 Resistance to targeted therapeutics..... | 8 |
| 1.4 Combination therapy..... | 9 |
| 1.5 Determination of synergy | 11 |
| 1.6 Identification of cellular targets of drugs..... | 12 |
| 1.6.1 Chemical proteomics | 14 |
| 1.7 Pediatric tumors..... | 16 |
| 1.7.1 Ewing sarcoma | 17 |
| 1.7.2 Neuroblastoma | 20 |
| 2 Aim | 23 |
| 3 Results..... | 24 |
| 3.1 Manuscript #1: Enhancing cognate target elution efficiency in gel-free chemical proteomics..... | 24 |
| 3.2 Manuscript #2: Stereospecific targeting of MTH1 by (S)-crizotinib as an anticancer strategy. | 36 |
| 3.3 Phenotypic screens reveal neuroblastoma and Ewing sarcoma specific synergistic combinations of clinically applicable targeted small molecules | 55 |
| 3.3.1 A parallel combinatorial drug screen reveals distinct disease specific drug-drug interactions | 56 |
| 3.3.2 Alterations in transport properties cause potent drug synergy in neuroblastoma | 57 |
| 3.3.3 Combination of PKC412 with IGF1R/INSR inhibitors is synergistic in Ewing sarcoma | 59 |

| | | |
|-------|---|-----|
| 3.3.4 | PKC412 target identification in the EWS-FLI1 altered signaling context..... | 60 |
| 3.3.5 | Synergistic effect of the drug combination comes from a particular alteration of phosphorylation events | 62 |
| 3.4 | Manuscript #3: The solute carrier SLC35F2 enables YM155-mediated DNA damage toxicity. | 71 |
| 4 | General discussion | 80 |
| 4.1 | Occurrence of resistance to targeted therapies..... | 80 |
| 4.2 | Mechanisms of action of therapeutics | 81 |
| 4.3 | Combinatorial drug treatment..... | 84 |
| 4.4 | Summary and outlook | 86 |
| 5 | Materials and Methods..... | 89 |
| 5.1 | Viability assays | 89 |
| 5.2 | Synergy determination | 89 |
| 5.3 | Apoptosis measurements..... | 89 |
| 5.4 | Colony formation assay | 90 |
| 5.5 | Real-time PCR analysis | 90 |
| 5.6 | Cell culture..... | 90 |
| 5.7 | Cell stimulation and immunoblotting..... | 91 |
| 5.8 | SILAC labeling | 91 |
| 6 | References | 92 |
| 7 | Abbreviations | 109 |

Curriculum Vitae

Publication list

Acknowledgements

I would like to thank my supervisor, Prof. Dr. Giulio Superti-Furga, for support and patience and for giving me the opportunity to do my PhD in his lab. I am very thankful for all the knowledge about science and about life that he shared with me. Giulio was the best party companion ever and a passionate Game of Thrones ally.

I would like to thank Dr. Keiryn Bennett for reinforcing my beliefs, patience and persistence. I am very thankful to the members of my PhD committee Dr. Robert Kralovics and Prof. Dr. Heinrich Kovar for their support and advice. Heinrich was essential for my introduction to the Ewing sarcoma community and he was a great influence.

CeMM is a great place and I feel privileged to be a part of it. I am grateful to all GSFies, an ever-changing but constantly positive group of people that I had the pleasure to work with over the years. The only thing I regret is that Dr. Uwe Rix couldn't stay my co-supervisor for longer. I learned a great deal from him even in this limited time and his support from across the seas meant a lot. I would especially like to thank Dr. Kilian Huber for numerous discussions, readiness to help and constant encouragement. Special thanks go to my permalicious friends and fellow colleagues, Johannes Bigenzahn and Astrid Fauster, the best possible companions on this journey. I am grateful to my desk neighbors, Georg Winter and Johannes Bigenzahn, for scientific input and help, funniest jokes and sharpest sarcasm.

Big thanks go:

to my dear friends who shared with me all the good and the bad and happily accepted my geekiness.

To my Beverly Hills crew – Jelena Milosevic Feenstra, Ferran Fece de la Cruz, Ashot Harutyunyan and Roberto Giambruno – for being purely awesome, fantastic and supportive.

To Jelena, my perfect little sister and my best friend, who is unconditionally always there for me. A true child of our parents! :-)

To my parents and my late granny Latinka, who firmly supported all my life decisions and sacrificed a lot for it; they always made me feel special and loved.

To the most daring man in the Universe, Srđan, who had the courage not only to marry me, but to do it during my PhD. His immense support and endless belief in me led me through the toughest moments. I felt loved each and every second and it was never, ever boring.

Abstract

Cancer is a complex heterogeneous disease for which there is no single one-size-fits-all treatment. Precision medicine is becoming a powerful tool for medical practice, as focus is put on inter-patient variability and understanding of the molecular signaling perturbations induced by malignant transformation. Conversely, deciphering the molecular mechanism of drugs in tumor cells can reveal insights into disease biology.

We set out to research therapeutics using systems-level approaches. First we developed a refined methodology to characterize the cellular target profiles of small molecules based on chemical proteomics. We have implemented a new strategy that evidently enhanced cognate target elution efficiency and proved to be effective and generically applicable, since the enhancement was evident in either in chemical immobilization of compounds on an inert matrix or biotinylated compounds on avidin-functionalized resins. This knowledge may lead to exploitation of the full potential of drug candidates, while revealing off-target effects that often lead to toxicity.

Using chemical proteomics, we discovered that MTH1 (NUDT1), a nucleotide pool sanitizing enzyme, has a global role in tumorigenesis. We showed that loss-of-function of MTH1 impairs the growth of KRAS mutant tumor cells and that MTH1 inhibitors cause DNA damage in cancer cells. Moreover, we found that the (S)-enantiomer of the kinase inhibitor crizotinib is a nanomolar inhibitor of MTH1 catalytic activity while (R)-crizotinib was inactive. All in all, our results suggest nucleotide pool homeostasis as an interesting intervention point for cancer therapy.

Combinations of inhibitors are proposed as a method to overcome the resistance caused by compensatory pathways and to lessen the toxic side effects through reduced dosing, which is especially appealing in pediatric tumors. Using a parallel phenotypic combinatorial screening approach, we identified disease specific interactions of targeted agents. .

We observed a highly potent synergy in neuroblastoma, between the kinase inhibitor lapatinib and anticancer compound YM155. We found that the inhibition of ABCB1 efflux transporter by lapatinib led to considerable increase in intracellular concentration of YM155; this allowed the prolonged and elevated cytotoxicity specific for resistant neuroblastoma cells expressing high levels of ABCB1. Next, we retrieved combinations specific for Ewing sarcoma; e.g. concomitant treatment with the clinically evaluated multikinase inhibitor PKC412 and IGF1R/INSR inhibitors proved to be strongly synergistic. We profiled PKC412 by chemical proteomics and found that the compound exerts its cytotoxic effect by inhibiting crucial Ewing sarcoma signaling routes. We showed that a particular drug combination-

induced alteration of phosphorylation events was responsible for the synergistic effect since a large portion of signaling events were unique for the combinatorial treatment.

Finally, we focused on the phenomenon of drug resistance and drug action. Although YM155 was developed as a survivin inhibitor, the precise molecular mechanism was unknown. We used a haploid genetic screen to reveal an absolute interdependency between YM155 action and SLC35F2, a member of the solute carrier protein family that is overexpressed in a number of malignancies. We further showed that YM155 conferred its cytotoxicity via DNA intercalation in cells expressing SLC35F2, leading to a DNA damage response and apoptotic cell death. This gene-drug interaction might offer a specific targeting strategy of DNA damage to tumor cells with elevated levels of SLC35F2 expression.

We used different techniques to profile drugs and drug combinations and characterize cancer vulnerabilities. The results demonstrate that a holistic, integrated systems pharmacology approach can contribute towards better understanding of cancer biology and identify new alternative therapeutic regimens.

Zusammenfassung

Krebs ist eine komplexe und heterogene Erkrankung, für die keine "one-size-fits-all" Behandlungsmodalität zur Verfügung steht. Die Methoden der Präzisionsmedizin entwickeln sich zu einem leistungsfähigen Werkzeug für die medizinische Praxis. Ihr Schwerpunkt liegt auf dem Verständnis der Variabilität zwischen Patienten und der durch die maligne Transformation induzierten molekularen Veränderungen zellulärer Signaltransduktion. Gleichzeitig ermöglicht das Verständnis der molekularen Wirkmechanismen von Arzneimitteln in Tumorzellen Einblicke in die zugrundeliegende Krankheitsbiologie.

Das Ziel dieser Arbeit war die Charakterisierung bestehender Medikamente mittels system-biologischer Verfahren. In einem ersten Schritt verbesserten wir eine spezifische Methode, um zelluläre Zielproteine von Arzneimitteln mittels "chemical proteomics" mit höherer Sensitivität zu identifizieren. Wir haben ein verbessertes Protokoll mit erhöhter Elutionseffizienz und detaillierterer Identifikation verschiedener Zielproteinsubklassen etabliert. Diese neue experimentelle Strategie ist sowohl für Arzneimittel mit chemischer Immobilisierung auf einer inerten Matrix als auch für biotinylierte Verbindungen an Avidin-funktionalisierten Adsorbentien anwendbar. Diese technische Verbesserung kann dazu beitragen sowohl das Wirkpotential bestehender Arzneimittelkandidaten zu erweitern als auch mögliche Nebeneffekte, die oft zu erhöhter Toxizität führen zu identifizieren.

Durch die Anwendung dieser neuen experimentellen "chemical proteomics" Strategie entdeckten wir, dass MTH1 (NUDT1), ein Nukleotidpool Erhaltungsenzym, eine globale Rolle in der Tumorgenese spielt. Wir konnten zeigen, dass der zelluläre Funktionsverlust von MTH1 das Wachstum von KRAS-mutierten Tumorzellen beeinträchtigt und darüber hinaus MTH1 Inhibitoren DNA-Schäden in Krebszellen verursachen. Anknüpfend konnten wir das (S)-Enantiomer des Kinaseinhibitors crizotinib als einen nanomolaren katalytischen MTH1 Inhibitor identifizieren wohingegen (R)-crizotinib keine Wirkung zeigte. Zusammenfassend enthüllen unsere Ergebnisse, dass die Nukleotidpool Homöostase einen neuen interessanten Angriffspunkt zur Krebstherapie darstellt.

Die Kombination von verschiedenen Therapeutika findet als Verfahren in der Klinik breite Anwendung um unter anderem Resistenzen, die durch veränderte und adaptierte Signaltransduktionswege induziert wurden, entgegenzutreten. Darüber hinaus kann eine Kombinationsbehandlung toxische Nebenwirkungen durch reduzierte Dosierung der Einzelsubstanz verringern. Dies ist eine besonders attraktive Eigenschaft bei der Behandlung von pädiatrischen Tumoren.

Mit Hilfe eines phänotypischen kombinatorischen Screening Ansatzes konnten wir tumorspezifische Kombinationen von zielgerichteten Krebstherapeutika identifizieren. Eine

hochwirksame Synergie konnten wir im Neuroblastom-Screening zwischen dem Kinaseinhibitor Lapatinib und dem Krebsmedikament YM155 identifizieren. Als Wirkmechanismus konnten wir die Inhibition des ABCB1 Transporters durch Lapatinib definieren, die zu einem erheblichen Anstieg der intrazellulären YM155 Konzentration führt. Dies ermöglicht eine längere und höhere Tumorzellzytotoxizität vor allem beim resistenten Neuroblastom mit erhöhter ABCB1 Expression. Ferner konnten wir spezifische Arzneimittelkombinationen für das Ewing-Sarkom (ES) identifizieren, wie zum Beispiel die gleichzeitige Behandlung mit dem Multi-Kinaseinhibitor PKC412 und IGF1R/INSR (Insulin-ähnlicher Wachstumsfaktor 1-Rezeptor und Insulin-Rezeptor) Inhibitoren. Wir charakterisierten in weiterer Folge das Zielproteinprofil von PKC412 unter Zuhilfenahme von "chemical proteomics". Dies verdeutlichte, dass die erhöhte zytotoxische Wirkung durch Hemmung von entscheidenden ES Signaltransduktionswegen zu Stande kommt. Wir konnten darüber hinaus zeigen, dass eine charakteristische Veränderung der Phosphorylierung verschiedener Signaltransduktionsproteine für die synergistische Wirkung verantwortlich ist. Ein großer Teil der Phosphorylierungsveränderungen war spezifisch für die kombinatorische Behandlung.

Abschließend lag der Fokus auf der Charakterisierung der Arzneimittelresistenz und Arzneimittelwirkung ausgewählter Therapeutika. YM155 wurde als Survivin-Inhibitor entwickelt, jedoch war der genaue molekulare Mechanismus der Krebszelltod Induktion unbekannt. Unter Verwendung eines haploiden genetischen Screening-Verfahrens konnten wir eine unabdingbare Abhängigkeit zwischen YM155 Wirkung und SLC35F2 Expression, einem Mitglied der "solute carrier" Proteinfamilie, die in einer Reihe von malignen Erkrankungen verstärkt exprimiert wird, identifizieren. Wir konnten außerdem zeigen, dass YM155 in SLC35F2 exprimierenden Zellen durch DNA-Interkalation zur Zytotoxizität und Apoptoseinduktion führt. Der Import von YM155 durch tumor- und patientenspezifische erhöhte Expression von SLC35F2 ermöglicht eine zielgerichtete und personalisierte Krebstherapie durch tumorspezifische Induktion von DNA-Schäden.

In dieser Arbeit haben wir verschiedene Technologien angewandt um Arzneimittel Wirkungen und Kombinationen mechanistisch zu untersuchen. Die Ergebnisse zeigen deutlich, dass ein integrierter System-Pharmakologie Ansatz zum verbesserten Verständnis der Krebsbiologie beitragen kann und die Identifikation neuer Therapiemodalitäten ermöglicht.

1 Introduction

1.1 Signal transduction and signaling networks in cancer

Unlike single-cell animals, multicellular organisms, such as humans, rely on the cooperation between the member cells that create them. They collaborate and communicate through a complex circuitry of signals, in order to keep the system operative. Moreover, all somatic lineages are pledged to eventually die and fine-tuning of these programs is essential for the well-being of an organism. Each cell has to be thoroughly guided and controlled to fulfill its purpose. Thus, correct interpretation of extracellular signals has a fundamental function in understanding the cellular behavior and the organism as a whole. Cancer can be described as a disease where this harmony is gravely disturbed. Here, individual clones of cells are taking the advantage of this fine-tuning for their own benefit. Malignant cells interfere with signaling networks and reprogram energy metabolism, thus enabling invasive growth and perpetual replication (Hanahan & Weinberg, 2011), as illustrated in Figure 1. Hence, tumorigenesis can be understood as an impairment of signaling transduction networks, where cellular processes and intercellular communication are perplexed (Kolch *et al*, 2015).

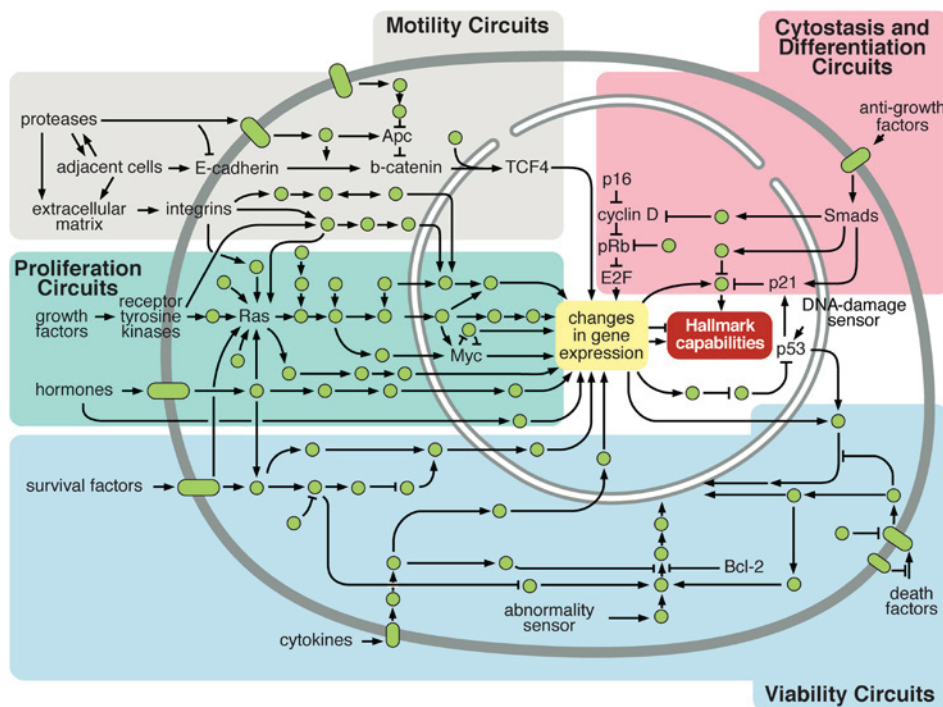


Figure 1. Intracellular signaling networks regulate the operations of the cancer cell. (taken from Hanahan & Weinberg, 2011)

Tumor suppressors normally inhibit proliferation; a loss-of-function mutation in these genes contributes to cancer. Proto-oncogenes, on the other hand, normally send positive signals for growth and proliferation. They are heavily deregulated in cancer, usually by mutations, and that allows unrestrained growth and replication of tumor cells, while their differentiation is inhibited. Mutant, overactive and/or over-expressed forms of proto-oncogenes are called oncogenes, and they are a result of gain-of-function mutations. Proteins encoded by proto-oncogenes are very often signal-transduction proteins, in addition to cell-cycle control proteins and transcription factors. Notably, Knudson hypothesis (Knudson, 1971) considers cancer a repercussion of several events, since a few lines of evidence support the conclusion that a single mutation is not sufficient to cause cancer. Communication between neighboring or distant cells is based on the ligand-receptor signaling axis. Receptors can be situated either on the cell surface (when receptors are transmembrane proteins) or inside the cell (in cases where the ligand enters the cell). Interestingly, the final response is not uniquely dependent on the receptor, but varies according to the cell type. Distinct target cells can react differently to the same stimulus, which adds another level of complexity to the signaling network. Another way of regulating these complex networks are feedback loops, which allow bistable (on/off switch) and oscillatory behavior. Here, a downstream molecule alters the activity of the upstream effector. Feedback loops can be positive, where the output prompts its own production. Positive feedback loops are very much used during development, since they allow all-or-none decisions. Feedback loops can also be negative, where the output hinders its own production. Negative feedback corrects fluctuations caused by varying input intensities and perturbations to the amplifier, resulting in a robust output and a correct response to stimuli (Kolch *et al*, 2015). Oncogenes and tumor-suppressor genes are often targeting the state transitions controlled by feedback.

The exemplar pathway where multiple feedback loops tightly regulate the signaling is the PI3K/AKT/mTOR pathway, which is critical in regulating multiple processes both in normal and cancer cells. mTOR (mechanistic target of rapamycin) belongs to the PI3K-related kinase family; it forms two large complexes - mTORC1 and mTORC2. mTORC1 controls a vast number of processes and senses diverse signals. In contrast to mTORC1, mTORC2 does not respond to nutrients, but both do sense growth factors. Both complexes have an important role in controlling a number of kinases, thus regulating homeostasis and growth. Hence, it is not surprising that activated mTOR signaling is implicated in cancer among other diseases which made mTOR an excellent target for cancer therapy. The FDA (Food and Drug Administration) approved in 2007 the rapamycin analogue temsirolimus for treatment of advanced-stage renal cell carcinoma, and there are a number of clinical trials underway using rapalogs. A pivotal role of mTOR in globally regulating cellular growth and

survival suggests that a very strong inhibition would cause ample side effects. However, therapeutic efficacy proved to be limited, most probably due to the numerous negative feedback loops (Laplane & Sabatini, 2012). AKT phosphorylation on threonine at position 308 (T308) was increased upon mTOR inhibition by rapalogs, which in turn caused cell survival (Peterson *et al*, 2009). Inhibition of the mTOR/PI3K pathway causes a rapid increase in signaling, through the compensatory activation of parallel pro-survival pathways. Furthermore, since the pathway is tightly regulated through negative feedback loops (Figure 2), over-activation of upstream pathways may occur if they are inhibited (Rozengurt *et al*, 2014).

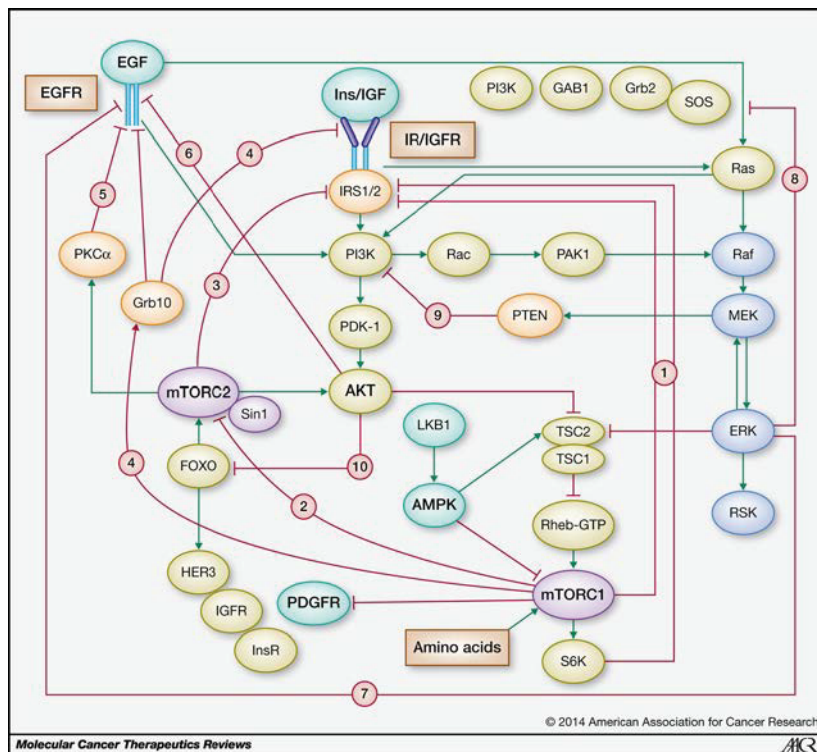


Figure 2. Feedback loops control signaling through the PI3K/mTOR and RAS/RAF/MEK/ERK pathways. Negative feedback loops are indicated by the red lines, while stimulatory connections are in green. (taken from Rozengurt *et al.*, 2014)

Combinations of inhibitors are suggested as a method to overcome the resistance caused by compensatory pathway activation that remodels topology and structure of signaling networks.

In the result part of this thesis a combination of two kinase inhibitors proved to be strongly synergistic in the signaling context of Ewing sarcoma and the effect was predominantly conveyed through thorough and combination-specific inhibition of the PI3K/mTOR signaling axis, inevitably by modulating complex feedback loops.

1.2 Systems biology in cancer

Cancer is often considered a microevolutionary process. It is a complex system of alterations and interactions that are constantly adjusting and reshaping. Although our understanding of intracellular processes has dramatically improved in the last few decades, as well as our knowledge on intercellular communication and tissue organization, many open questions remain. Ironically, a number of fundamental discoveries in cell biology have roots in cancer research. For instance, the investigation of abnormalities in cell growth and proliferation led to the discovery of proteins whose function was previously unknown. In this light, understanding cancer as an anomaly is even more challenging. Malignant phenotypes are determined by complex deregulations in multiple dimensions, from intracellular pathways to the organism as a whole.

Understanding the properties of a living organism as a result of complex interactions in biological systems is a subject of systems biology. Instead of reductionism, where individual effects are studied, systems biology aims for a holistic approach in understanding dynamics and complexity of living systems. Proper functioning of the cell is tightly regulated by homeostatic mechanisms that allow a measured response to environmental perturbations (Werner *et al*, 2014). These responses are severely altered in cancer (Figure 3). Genomic and epigenetic aberrations, together with environmental factors, lead to this global degeneracy; thus, integrative approaches are necessary to comprehend the underlying complexity of the malignant condition. A major requirement to achieve efficient cancer treatment is to identify crucial processes that are disrupted in cancer, which is even more challenging due to the intra- and intertumoral heterogeneity (Du & Elemento, 2015) and rewiring of networks as a result of molecular changes (Lee *et al*, 2012).

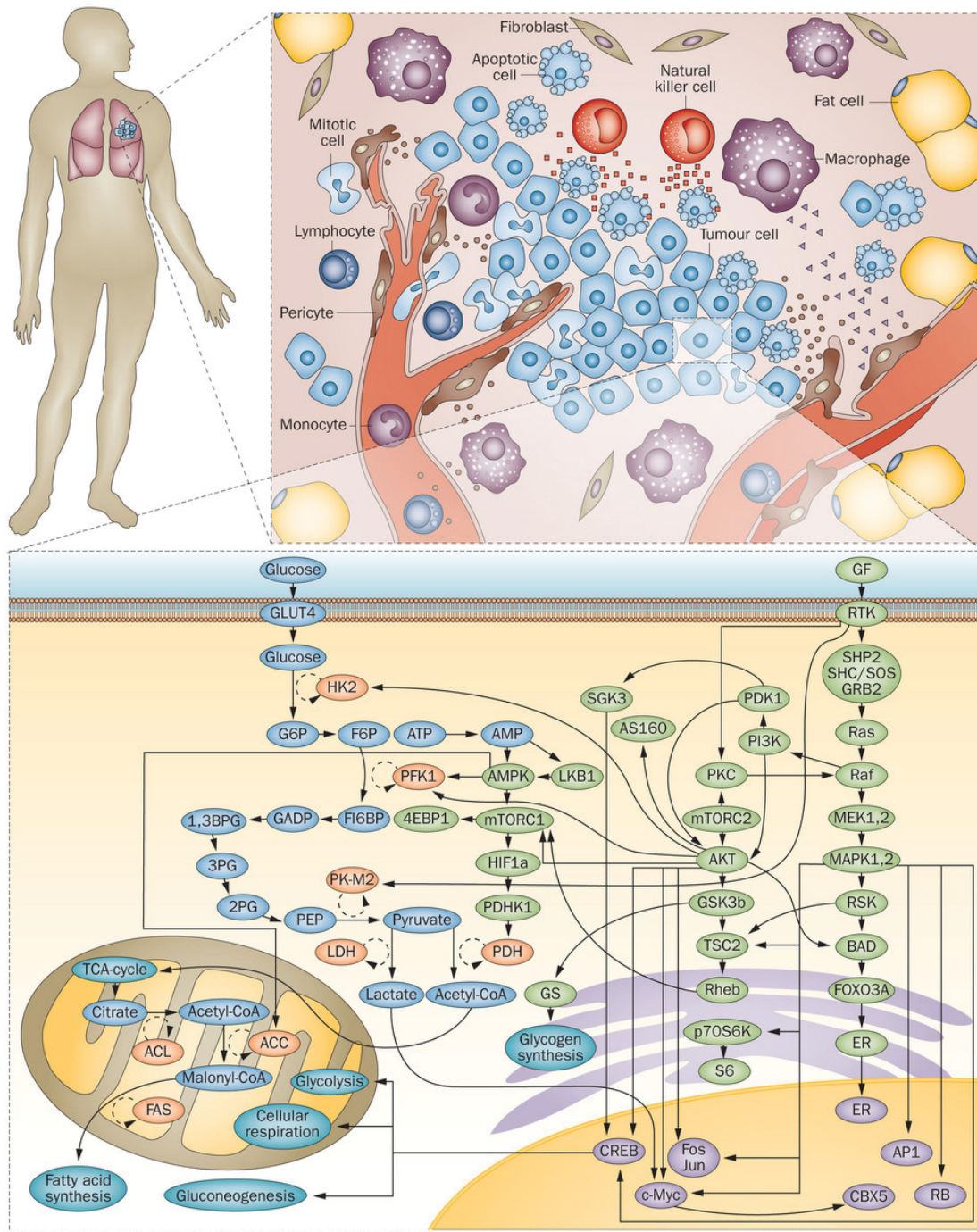


Figure 3. Complex interactions between different molecular networks within the cell. Processes within the body as a whole have to be tightly regulated. Malignant phenotype is characterized by the unbalance of complex interactions, caused by aberrations at the molecular level. Permission obtained from Visual Art © 2013 The University of Texas MD Anderson Cancer Center. (taken and adopted from Werner et al., 2014)

1.3 Cancer treatment

1.3.1 Precision medicine and targeted therapy

Current therapy of cancer is still mainly based on surgery, radiotherapy and standard chemotherapeutics that act on rapidly dividing cells. The whole concept depends on cancer cells susceptibility to these drugs since they divide more vigorously; however, it is quite far from any cancer specificity. Besides, it is arduous to eradicate every single cancer cell and most often the patients relapse. Even if they affect the same tissue, tumors can still differ tremendously in their mutations and other genetic drivers. They can be considered special molecular subtypes which might require different treatments due to their heterogeneity. Tumor heterogeneity is not a new concept; Rudolf Virchow already described it in his textbook *Cellular Pathology* in 1858. It is nowadays considered a major challenge in the therapy since it was shown that the appearance of resistant clones accounts for tumor relapse (Junttila & de Sauvage, 2013).

In difference to passenger mutations which are dispensable and do not contribute greatly to cancerogenesis drivers confer a proliferative advantage to cancer cells and lead to a malignant phenotype. Cancer cells become 'addicted' to the constitutive activation of these oncogenes. Simply put, the aim of targeted therapy is to selectively inhibit drivers of the particular cancer. This is the premise for personalized cancer treatment. This specificity allows for a greater therapeutic window and fewer side effects. It is important to note, however, that it is the whole complex signaling environment created by the driver mutations that should be targeted pharmacologically. Tumor heterogeneity is not simply a genetic variation; variations in signal transduction networks create context-dependent abnormalities (Kolch *et al*, 2015).

A famous example of a successful targeted approach is imatinib (Gleevec®), an inhibitor of the Bcr-Abl protein kinase (Druker *et al*, 1996). The chimeric Bcr-Abl protein causes abnormal proliferation and blocks apoptosis, leading to an abnormal amount of white blood cells, a hallmark of CML. Gleevec® binds to the Abl kinase domain in an inactive conformation and blocks the ATP binding site, thus preventing the catalytic activity of Bcr-Abl kinase. Administration of the drug leads to the removal of Philadelphia positive cells in almost all patients. Nonetheless, resistance still emerges in a number of patients, mostly in form of point mutations in the enzymatic pocket of Bcr-Abl. Even so, Gleevec® appears a 'magic bullet' and is often regarded as a proof of principle for targeted drug discovery.

There are other examples of personalized, targeted approaches in cancer therapy, although only a small subset of chemotherapy is based on targeting the genetic alterations

characterizing individual tumor. Trastuzumab is an anti-HER2 monoclonal antibody that can be administered to breast cancer patients with HER2 overexpression or amplification which accounts for approximately 20-25% of patients (Slamon *et al*, 1989). Furthermore, also some HER2-negative patients show responses (Slamon *et al*, 2011), arguing that the overall complex signaling context is what determines the efficacy. Small molecule kinase inhibitors such as gefitinib (Iressa®) and erlotinib (Tarceva®) bind to the ATP binding domain of EGFR kinase and thus inhibit EGFR downstream signaling. These targeted agents are given to non-small-cell-lung cancer (NSCLC) patients that harbor an EGFR mutation. It should be noted, however, that although according to the current guidelines all patients with any kind of EGFR mutations receive these drugs the overall effectiveness does depend on the particular mutation in the protein (Martini *et al*, 2011).

The RAS-RAF-MEK-ERK-MAP axis is one of the most important signaling pathways in cells; it mediates responses to growth signals and promotes survival. BRAF is a serine/threonine kinase, a member of the RAF family together with ARAF and CRAF. Activating BRAF mutations in the kinase domain, most often the V600E mutation, are present in 40-60% of patients with melanoma (Davies *et al*, 2002; Wan *et al*, 2004). Here, the phosphorylation of the kinase is mimicked by a negatively charged amino acid that replaces a conserved glutamic acid, thus leading to constitutive activation of the kinase. Vemurafenib (Zelboraf®) can block the mutated protein, but it is inactive against the wild type BRAF. Conversely, although the BRAF V600E allele occurs in some other cancer types, the response rates are poorer than in melanoma. Colorectal cancer patients, for example, have much lower response rates, although they harbor the very same mutation (Kopetz *et al*, 2015). This is one more indication that oncogenic mutations can lead to different phenotypes depending on the overall signaling environment, and ultimately it is the context that determines the final response to the therapy.

1.3.2 Resistance to targeted therapeutics

Although the detection of cancer-specific mutations is a valuable prediction tool, it is not the only prerequisite for a successful targeted therapy. As already mentioned, compensatory crosstalk, redundancy, and feedback loops are shaping the signaling network, and the driver mutation is simply a node in a complex system. Thus, it is not surprising that target-based discovery is facing limitations and challenges, due to the oversimplified view of the one target – one drug model. Furthermore, even when targeted therapies are efficient, the limiting factor of cancer therapy nowadays is the occurrence of resistance. Generally, two types of resistance can be distinguished: intrinsic or primary and acquired or secondary resistance. Intrinsic resistance exists before the treatment has started, since the tumor in that case consists of cells where resistance-mediating elements prevail. Acquired resistance, on the other hand, is a result of therapy occurring via various adaptive responses. Since tumors are heterogeneous, a sub-population of resistant clones can appear and convey resistance, since their trait is advantageous (Holohan *et al*, 2013). There are, however, several mechanisms of acquired resistance. It can occur through secondary mutations in the oncogene or changes in the expression levels of the drug target, or via activation of adaptive responses through development of bypass signaling pathways which are able to rewire and maintain the signaling that was initially inhibited by the drug. Sometimes this is exactly the key to successful combination therapy – the second drug is able to inhibit the bypass pathway and hence the combination can overcome the resistance (Crystal *et al*, 2014).

Deregulation of transporters that facilitate the influx and efflux of chemotherapeutic compounds is another well-recognized originator of drug resistance. Various carrier proteins are involved in drug transport, mostly from the SLC and ABC classes of membrane transporters. In fact, the first ever described ABC transporter was ABCB1 (MDR1 multidrug resistance protein 1) that was discovered due to its ability to pump out a number of drugs from the cell thus preventing them to carry out their effect. Cancer cells evolve to overexpress these transporters so they become resistant to all their substrates. This is a major hindrance in cancer treatment since this mechanism can affect a wide-range of cancer therapeutics rendering them ineffective. The most important transporters that confer multidrug resistance are ABCB1 (MDR1, P-gp), ABCG2 (BCRP, human breast cancer resistance protein) and ABCC1 (MRP1, multidrug resistance-associated protein) (Alisi *et al*, 2013) and their expression can be chemotherapy induced. In some primary untreated pediatric tumors, however, e.g. neuroblastoma, the multidrug resistance-associated genes are often overexpressed (Norris *et al*, 1996; Cialfi *et al*, 2010) and associated with poor

outcome (Fletcher *et al*, 2010). In the results part of this thesis we show that kinase inhibitor lapatinib was able to efficiently block the transporter essential for the export of another anticancer compound outside of the cell and thus revert resistance through synergistic effect. On the other hand, changes in drug import can influence the intracellular concentration as well and lead to a differential response depending on the expression of specific influx transporters on the cell surface. One such an example where this property can be used to target the cancer cells more effectively is a dependency of a small molecule on the import via a particular transporter such as in the case of the surviving suppressant YM155 and SLC35F2 (Winter *et al*, 2014); this is discussed in detail in chapter 3.4 of this thesis.

1.4 Combination therapy

There are several examples of successful targeted approaches, as discussed previously. However, even if initially efficacious, in most cases resistance eventually occurs. Secondary mutations, activation of compensatory pathways and upregulation of efflux transporters are predominant causes of acquired resistance. Sometimes these hurdles could be successfully overcome with the combination treatment.

The idea of combining drugs in chemotherapy emerged already in the 1950s. It was known that the successful tuberculosis treatment was dependent on a combination of drugs with different mechanism of action. Emil Frei and Emil Freireich, together with James Holland, all medical doctors at the National Cancer Institute, came to an idea to try a similar approach in ALL (acute lymphoblastic leukemia), a particularly aggressive type of childhood leukemia (Frei *et al*, 1958). They discovered that the simultaneous administration of a cocktail of anticancer drugs could lead to a complete remission in children with leukemia. Against cancer cells this combination acted synergistically, while toxic side effects were mitigated. Furthermore, the occurrence of drug resistance was deficient or at least postponed. Combination therapy soon became a standard, not only in leukemia, but in solid tumors as well. Conventional cancer treatment nowadays is still mostly based on combinations of cytotoxic agents that non-selectively kill rapidly dividing cells, although more personalized therapeutic strategies are paving their way into standard cancer care. One needs to systematically explore the concept of drug synergies to investigate the full potential of the approach.

The term synergy was derived from the Greek word *synergos* (συνεργός), which can be translated as “collaborator” or “working together”. One of the leaders in the field, W. R.

Greco, said: “Synergistic combinations are thought to be interesting. They are considered special. If you add a synergy to a group, you get a team.” However, a common perception of synergies is often blurring the interpretation of the synergistic effect in the context of drug combinations. Put shortly, a synergistic drug combination should be more potent than equally effective doses of its components (Greco *et al*, 1995; Lehár *et al*, 2007).

Combination treatment, especially in cancer and infectious diseases, is used not only to reduce the toxic side effects through reduced dosing, but to overcome and prevent resistance to single components and also to take advantage of simultaneous treatment that may become efficacious even though acting on individual targets might be insufficient (Zimmermann *et al*, 2007). The overly present problem of resistance is one of the limiting factors for a broader and more effective use of targeted agents. This issue can be addressed by conjunctive application of two or more drugs simultaneously. Mechanisms by which the beneficial effect is achieved may vary. In cases where cells become resistant by activating the parallel pathway, a synergistic effect is obtained by introducing the compound that inhibits that pathway and that may or may not be very effective on its own (Crystal *et al*, 2014). Synergy can also occur if one of the compounds is inhibiting a drug efflux pump, thus allowing the substrate molecule to maintain intracellular accumulation and exhibit its effect. Whatever the mechanism of a combinatorial effect, it is not an easy task to quantify and interpret it.

It is also important to note that *in vitro* synergy and therapeutic synergy are not equivalent. For therapeutic synergy, pharmacokinetic properties and toxicity profile of the combination play a pivotal role. Essentially, if a combination of drugs *in vitro* causes the effect that is unique and also more selective towards tumor cells, there is a high likelihood for therapeutic synergy. The final goal in therapeutic synergy is to have a more pronounced anti-cancer effect with applying lower concentrations of the drugs than in a single therapy; ideally, these drugs should also have only minor or no overlaps in their toxic profiles, thus less severe side effects. There was a considerable concern that therapeutic synergy carries a risk of synergistic side effects. This would inevitably happen if the side effect mechanisms would be well correlated with the main mechanism of the anti-cancer effect. It was shown, however, that synergies operate in a confined cellular background, which allows for greater specificity (Lehár *et al*, 2009).

1.5 Determination of synergy

In order to characterize the combinatorial drug (combo) effect as either antagonistic or synergistic, it is required to define a starting point: the assumption of a null reference which is the case when there is no interaction between the drugs. Various models define the null reference in different ways. The Bliss independence model (Bliss, 1939) is based on probabilistic independence; this means that a fractional response of the combination at given concentrations equals the sum of fractional responses of each of the drugs alone. Here, it is presumed that compounds act independently, on mutually non-exclusive sites, but each contributes to the result (Greco *et al*, 1996). The general form of the Bliss independence effects is equation [1]:

$$fa_{12} = fa_1 + fa_2 - fa_1fa_2, \quad [1]$$

where fa_1 , fa_2 and fa_{12} are fractions of possible response to the two drugs and their combination.

The Loewe additivity model (Loewe & Muischnek, 1926) defines a null hypothesis as a case where a drug would interact with itself, or its close analogue. Therefore, this model can also deal with cases where chemicals are perturbing a common pathway. Loewe additivity is usually quantified by a combination index score (CI) that is calculated using the Chou-Talalay method (Chou & Talalay, 1984). The equation for Loewe additivity [2] postulates:

$$1 = \frac{D1}{ID_{x,1}} + \frac{D2}{ID_{x,2}}, \quad [2]$$

where D stands for a concentration of the drug, $ID_{x,1}$ is a concentration of a drug 1 resulting in x % inhibition of the maximum effect of drug 1 and $ID_{x,2}$ is a concentration of drug 2 resulting in x % inhibition of the maximum effect of drug 2.

An overview of consensus terminology is given in Table 1 which is adopted from W.R.Greco (Greco *et al*, 1995). In short, if the combination effect equals the null hypothesis, it is defined as inertism, independence or additivity; if it is greater than predicted then it is a synergy, and if the effect is less than predicted it is called antagonism.

| | Both agents effective individually; Eq. [2] is the reference model | Both agents effective individually; Eq. [1] is the reference model | Only one agent effective individually | Neither agent effective individually |
|---|--|--|---------------------------------------|--------------------------------------|
| Combination effect greater than predicted | Loewe synergism | Bliss synergism | synergism | coalism |
| Combination effect equal to prediction from reference model | Loewe additivity | Bliss independence | inertism | inertism |
| Combination effect less than predicted | Loewe antagonism | Bliss antagonism | antagonism | |

Table 1. Consensus terminology for two-agent combined action concepts.

In order to probe as many combinations as possible in a screen, it is a common practice to test the effect only at single doses. However, the effect of varying concentrations (Greco *et al*, 1995) has to be considered. Small molecule drugs are often promiscuous, and their target profiles might vary based on the affinity towards particular targets. Consequently, synergistic profiles may be different at various concentration points. This can be addressed by testing dose series, or by using a factorial dose matrix. A dose matrix allows capturing synergy either if the high-dose effect is boosted (efficacy boosts), or if the effective concentration is shifted to lower doses (potency shifts) (Lehár *et al*, 2008). On the other hand, the screening costs grow rapidly with the increment of the drug combinations tested in factorial matrix design. Thus, a fine balance between the size of the chemical screening library and the assay fidelity has to be achieved.

1.6 Identification of cellular targets of drugs

For only a handful of drugs the exact mode of action is known. This holds true even for a large number of compounds used often and routinely in clinical practice. Even the new, “targeted” agents, that are created to bind to a specific target, are actually often interacting with a multitude of proteins, although their specificities may vary. There are two sides to the coin, though. On one hand, this promiscuity of small molecules can lead to various side effects, which are the consequence of interfering with additional unwanted targets. On the other, sometimes the favorable response is actually a result of the overall target profile of the drug, that may be more far-reaching than the specific one-target inhibition. Either way, it is

advantageous to know the exact target spectrum of a drug. For a number of widely used medicines, however, both the target and a side effects profile are not well understood. Perhaps the best example for this is aspirin or acetylsalicylic acid. In most countries it is used as an OTC (over the counter) drug and it is difficult even to estimate how many doses of aspirin are taken daily throughout the world. Still, it is largely unknown what causes its relatively common and sometimes severe side effects. Interestingly, if aspirin were to be newly marketed today, most probably it would not make it further than phase I trials. In this light, it becomes obvious that nowadays it is not easy to navigate through the complicated field of drug discovery and approval. Moreover, in the age of precision medicine, another level of complexity appears, since differences in among individuals are being recognized, including differential drug activity.

Target profiling of a chemical entity can be achieved through a number of approaches. Roughly, they can be divided in two big classes – functional genomic approaches and affinity-based approaches, with a number of additional in-silico knowledge-based and cellular profiling methods (Schirle & Jenkins, 2015). Next-generation sequencing technologies opened a possibility for the genome-wide screening and identifying genes that are relevant for the MoA of a compound. An insertional mutagenesis approach in the near-haploid KBM7 human cell line allowed assessing loss-of-function mutations that could rescue cells from compound induced toxicity and thus reveal targets that account for resistance to a particular agent (Carette *et al*, 2009). In chapter 3.4 of this thesis, this resistance-based approach is described in more detail through the discovery of a dependency of the small molecule YM155 on the solute carrier family member 35 F2 (SLC35F2) and this relationship being the main basis of DNA damage toxicity conferred by YM155.

The relatively recent introduction of CRISPR-Cas9 genome-editing technologies (Cong *et al*, 2013; Mali *et al*, 2013) provided new possibilities for MoA screens, either by transcriptional repression or activation (Konermann *et al*, 2014). CRISPR screens are comparable to RNAi or cDNA overexpression methods, but offer tighter precision control.

Affinity-based approaches are also applicable to identify the cellular interactors and target spectrum of a compound. The yeast-2-hybrid system, established in 1989 (Fields & Song, 1989), opened possibilities for discovering protein-protein interactions. Modifications of this system allowed not only the charting of DNA-protein and RNA-protein interactions but also small molecule-protein interaction screening and target profiling. Reverse yeast two-hybrid systems can be used to screen for agents able to disrupt protein-protein interactions, while ligand-based three-hybrid systems offer unbiased target deconvolution, although the downside is that it requires prior derivatization of a small molecule (Rezwan & Auerbach, 2012). Although these represent relatively quick and straightforward methods, poor

permeability of yeast for drugs as well as a limited coverage of the proteome by the cDNA libraries may pose a problem. Another way of identifying drug interactions is by monitoring the thermal stabilization of proteins upon binding of a compound. The cellular thermal shift assay (CETSA) in combination with quantitative mass spectrometry (Savitski *et al*, 2014; Huber *et al*, 2015) can be used to identify cellular proteins that are cellular targets of drugs or metabolites. The major disadvantage, however, is that the alterations in thermal stability are relatively irregular, since their extent can depend on the characteristics of a ligand and the protein itself, thus the use is probably limited to relatively focused studies.

1.6.1 Chemical proteomics

Compound affinity chromatography coupled to gel-free liquid chromatography mass spectrometry is another powerful approach for identifying the cellular target spectra of small molecules (Figure 4). Here, the compound of interest has to be immobilized on a solid phase, which sometimes requires chemical modification of a compound, usually by adding a suitable linker. The drug matrix is then incubated with cell or tissue lysates, followed by washing steps and elution of the bound interactors. Prior to the chemical proteomics experiment it is important to confirm that the cellular activity of the analogue is not changed. Competition pull-downs with the unmodified compound can be used to discriminate high-affinity binders from very abundant background proteins. Eluates can either be processed via SDS-PAGE or in a gel-free method they can directly be digested with trypsin and processed for subsequent MS analysis.

In chapter 3.1 of this thesis, target elution efficiency in various aspects of the chemical proteomics is discussed in detail. We showed that an improved elution strategy allows for higher specificity of cognate targets in a gel-free approach. In the results section 3.2, it is shown how chemical proteomics can help to elucidate dramatic differences in the mechanism of action as such as in the case of two enantiomers of an anti-cancer drug, e.g. the chiral kinase inhibitor crizotinib. The main limitation of chemical proteomics is that a number of potential targets cannot be captured by this method due to their localization since integral membrane proteins lose their conformation during the experimental process. Also, it is difficult to make a distinction between direct and indirect binders, although there are improvements in the field, as mentioned in the results section 3.1. On the other hand, the method is unbiased, proteome-wide and performed in a competitive, intact, cellular environment (Rix & Superti-Furga, 2009). Chemical proteomics contributes to the systems-level understanding of drug-induced perturbation of relevant pathways, complementing the

other 'omics' strategies. As described in the results part of this thesis, in-depth chemical proteomics and phosphoproteomics are able to reveal the effects of kinase inhibitors on signaling pathways and, together with knowledge-based approaches, depict the mechanism of a synergistic combinatorial effect.

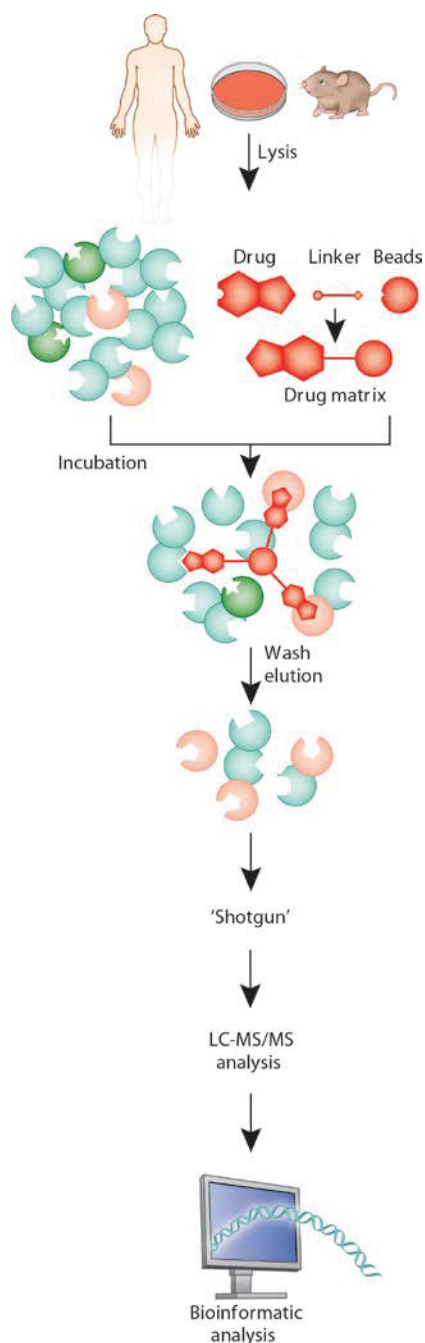


Figure 4. Schematic of compound-centric chemical proteomics experiment. (adopted from Rix et al., 2009)

1.7 Pediatric tumors

Adult cancers are characterized by accumulation of damage caused by both environmental and endogenous sources for decades before the disease onset and it is widely accepted that a high-rate of structural variations (SVs) is a good indicator of severance of disease. Tumors with a lot of SVs are expected to be more aggressive than the ones with more stable genomes. Next generation sequencing proved, however, that this is not an axiom in childhood tumors. No correlation between SVs and disease outcomes in childhood tumors has been reported so far (Chen *et al*, 2015). Additionally, pediatric cancers usually occur in non-self-renewing tissues and require fewer rounds of clonal expansion (Vogelstein *et al*, 2013). They are very diverse regarding their cells of origin, clinical features and onset time. Even their classification is done mostly according to the anatomic location. Since they arise at an early age, developmental processes mostly define their origin; cancer is then usually a consequence of altered regulation of normal tissue development. Furthermore, in childhood tumors only a few mutations were found in genes that code for druggable targets, thus rendering it more difficult to advance in targeted therapy. For a variety of solid tumors, the overall survival rate of pediatric patients was not significantly improved since 1975, and the situation is worse compared to children with other childhood cancers (Smith *et al*, 2014). In recurrent or metastatic neuroblastoma, Ewing sarcoma, osteosarcoma and rhabdomyosarcoma, the overall survival rate is below 30% (Cole & Maris, 2012; Leavey *et al*, 2008; Kempf-Bielack *et al*, 2005; Pappo *et al*, 1999) and many childhood cancer survivors experience long-term effects that affect negatively their quality of life.

Some of the biggest issues with current chemotherapy are the side effects, since the standard therapy regimen is based on agents affecting cells that rapidly divide; although cancer cells are more susceptible, the chemotherapeutic effect is far from being selective. Indeed, secondary adverse reactions are limiting factors for the treatment duration and dosages. The most common side effects include hair loss, nausea and vomiting, increased risk of infections, bruising, mouth sores, fatigue etc. In case of children and adolescent patients, the long-term effects are even more worrisome, as the consequences of the chemo and radiation therapy continue to influence their health and quality of life long after treatment. Severe aftereffects are often causing reproduction and sexual development problems, as infertility occurs quite often after the therapy and the development of sexual glands is altered. Former cancer patients usually face hormone imbalances and resultant growth problems, learning and memory issues as well as heart problems, etc. (www.cancer.net). Thus, also from this point of view it is evident that there is an increasing need for new, targeted, personalized regimens.

1.7.1 Ewing sarcoma

A vast number of childhood tumors have quiet genomes, and Ewing sarcoma has one of the quietest of all. STAG2 and TP53 are the only genes found to be commonly affected (Figure 5); these mutations often occur together and are linked to poor prognosis and relapse (Crompton *et al*, 2014; Tirode *et al*, 2014; Brohl *et al*, 2014).

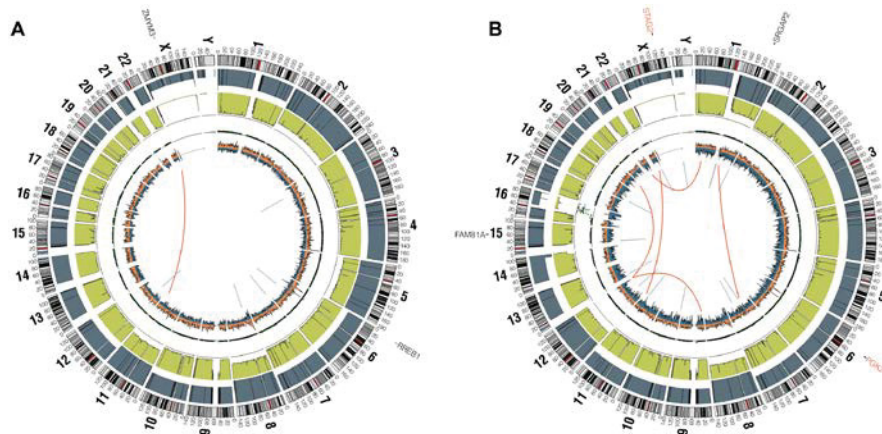


Figure 5. Circos-plots of exemplary Ewing sarcoma family tumors. The plot tracks represent somatic mutations, from outside circle: black - mutated genes including missense; red - indel and orange - nonsense; grey - genomic location; genome copy number alterations; green - lesser allele frequency. Tumor (A) has 2 somatic coding mutations; tumor (B) contains 4 somatic coding mutations (one of them a frameshift mutation in STAG2). (taken and adopted from Brohl *et al.*, 2014)

Various proto-oncogenes and tumor suppressor genes have important roles in development, and keeping the system at balance is a big prerogative for a healthy state. Not surprisingly, bone cancers usually occur in adolescents; this is related with factors involved in promoting growth of the skeletal system during puberty. Interestingly, a number of pediatric tumors are driven by fusion proteins, whose activity is sufficient for the cancerogenic transformation. One of these examples is Ewing sarcoma, an aggressive and rare, highly malignant cancer.

Ewing sarcoma is the second most common pediatric bone tumor but can develop in soft tissue as well (extra-skeletal Ewing sarcoma). The disease onset usually in adolescent years with peak occurrence between ages 10 and 20 (Burchill, 2008), but children and young adults can be affected as well. Long-term survival rates range from 65-75% for patients without observable metastases at diagnosis, to less than 30% in patients with recurrent or metastatic disseminated disease (Gaspar *et al*, 2015). During the last three decades only a minor advancement in outcome have been achieved (Gorlick *et al*, 2013).

Novel, specific and efficient therapeutic approaches are needed that exploit vulnerabilities of this particular cancer type.

Tumors previously classified as Ewing sarcoma family of tumors (ESFT), Askin's tumor and peripheral neuroectodermal tumor (PNET) are all now considered Ewing sarcomas (Hawkins, 2011). The EWSR1-ETS fusion is the defining molecular feature of these tumors, most commonly EWS and FLI1 (Delattre *et al*, 1992; May *et al*, 1993). The fusion oncoprotein is a result of a chromosomal translocation t(11:22) between the central exons of the EWSR1 (EWS) gene (Ewing sarcoma breakpoint region 1, at chromosome 22) to the central exons of an ETS (E-twenty-six) family gene, most commonly FLI1 (Friend leukemia integration 1, chromosome 11) (Figure 6). EWS-FLI1 causes global transcriptional changes since the potent transcriptional activator such as EWS domain gets fused to the highly conserved *ets* DNA binding domain of FLI1. Interestingly, higher number of EWS-FLI1 regulated genes is suppressed than induced (Kauer *et al*, 2009). Global alterations caused by EWS-FLI1 lead to a particular malignant condition that maintains de-differentiated cell state and promotes resistance to DNA-damaging agents (Riggi & Stamenkovic, 2007; Ban *et al*, 2008; Riggi *et al*, 2008; Awad *et al*, 2010; Lawlor & Thiele, 2012; Grohar & Helman, 2012). Additionally, the fusion protein can influence the post-translational processing (Herrero-Martin *et al*, 2011).

It was recently shown that EWS-FLI1 alters chromatin regulation and remodeling, acting as a crucial epigenetic modulator (Riggi *et al*, 2014; Tomazou *et al*, 2015). It produces changes in promoters, enhancers and super-enhancers, thus either repressing or activating its targets and provoking a genome-wide rewiring of gene regulatory regions. The oncogenic landscape of Ewing sarcoma is shaped by the fusion protein, on both transcriptional and regulatory level by various means of chromatin modulation (Riggi *et al*, 2014; Tomazou *et al*, 2015). Furthermore, pluripotent adult stem cells express high levels of polycomb proteins, which cause suppression of a large number of differentiation genes. Altered epigenetic regulation of polycomb target genes may create the receptive environment for the EWS-FLI1 activity and is associated with modifications of developmental transcription programs (Svoboda *et al*, 2014). On the other hand, sirtuins (class III histone deacetylases) are emerging as promising epigenetic drug targets in cancer (Huber & Superti-Furga, 2011). SIRT1 is highly expressed in Ewing sarcoma metastases (Ban *et al*, 2014), thus there is a strong motivation behind the use of SIRT1 inhibitors for treatment of metastatic disease in ES patients. All in all, better understanding of the exact mechanisms of epigenetic alterations would hopefully lead to novel therapeutic opportunities.

EWS-FLI1 is undoubtedly the biological driver of the disease. It mediates malignant transformation and drives the expression of risk proteins. Being a transcription factor, however, it is considered a very challenging drug target since it lacks a druggable pocket.

Thus, new therapeutic approaches should be tailored to specifically modulate the signaling landscape created by the oncofusion.

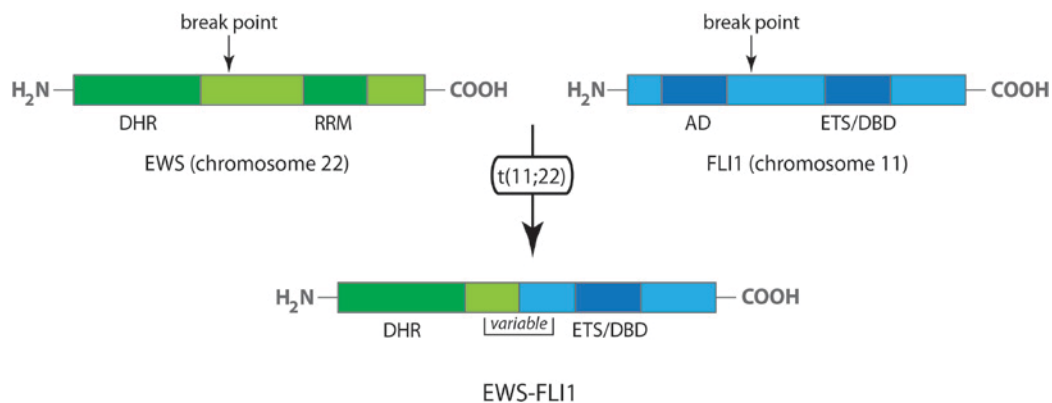


Figure 6. Schematic of EWS-FLI1 translocation. The N-terminal activation domain of EWS, with multiple degenerate hexapeptide repeats is fused with the C-terminal ETS DNA-binding domain (ETS-DBD) of FLI1. RRM - RNA recognition motif of EWS; AD - activation domain (AD) of FLI1. Bracketed region - multiple fusion types are the result of a variation in the sites of chromosomal break points. (made based on a scheme from Anderson *et al*, 2012)

A protein does not necessarily have to be mutated to appear as a promising therapeutic target. IGF1 is a growth factor deposited in the bone matrix, and its high levels influence Ewing sarcoma tumorigenesis. IGF1 is induced by the EWS-FLI1 fusion protein (Cironi *et al*, 2008) and the autocrine and paracrine loops triggered by it play a major role in neoplastic transformation by EWS-FLI1 (Toretzky *et al*, 1997; Scotlandi *et al*, 1996). Rising of IGF-1 levels in pubescence coincides with the peak incidence of the disease (Lissat *et al*, 2012). IGF1 stimulates IGF1R receptors and triggers growth and pro-survival pathways (PI3K and Ras), thus creating, a perfect niche for a neoplastic transfiguration of cells. The results of clinical trials with anti-IGF-1R antibodies and small molecules targeting IGF1R (as well as a heterodimer with insulin receptor, IGF1R/InsR) were often contradictory. Although a subset of patients would respond dramatically (Jiang *et al*, 2015), without a biomarker it was impossible to predict who the responders would be. Also, as expected, drug resistance eventually occurred, mostly through activation of bypass pathways (Subbiah *et al*, 2011; Naing *et al*, 2012) A proposition of a combination treatment that could contribute to a better and prolonged effect of an IGF1R inhibitor is discussed in the results section 3.3.

In a number of ES samples, upregulation of phosphorylated Akt, a hallmark of pathway activation (Sarbasov *et al*, 2005), was frequently observed (Scotlandi *et al*, 2005). Inhibition of mTOR can lead to the release of IGF1 (Kurmasheva *et al*, 2009) and several studies have shown that mTOR inhibitors are more effective when combined with IGF1R inhibitors than as single agents (Mita *et al*, 2008; Naing *et al*, 2012; Schwartz *et al*, 2015;

Demetri *et al*, 2013). In general, PI3K/AKT/mTOR pathway plays an important role in Ewing sarcoma progression, as in many other malignancies (Laplante & Sabatini, 2012; Janku, 2013). Another protein kinase, PRKCB (protein kinase PKC- β), can have prosurvival effect on Ewing sarcoma cells. Moreover, there is an overlap between genes modulated through PRKCB and EWS-FLI1, thus alterations caused by the fusion protein could be at least partially counteracted by inhibiting PRKCB (Surdez *et al*, 2012).

Although a number of molecular targets is identified in Ewing sarcoma (Jiang *et al*, 2015), such are tyrosine kinase inhibitors, IGF1R, mTOR and EWS-FLI1 related targets, the efficacy is still modest, due to the lack of biomarkers and drug resistance. Additionally, the origin of ES is not precisely known. Histologically, it is a very diverse tumor; as patients get older, the disease sites change from predominantly bone to the soft tissue. Although the so-called hen or egg problem in ES was phrased already a decade ago (Kovar, 2005) it is still a conundrum whether an incomplete differentiation program is enforced on a pluripotent precursor cell, or if the tumor stem cell is blocked in the differentiation by the fusion oncogene. EWS-ETS fusion is toxic to most of cell types, and attempts to generate animal models are ordinaarily unsuccessful. Certain embryonal mesenchymal and neuronal tissues, however, do tolerate EWS-ETS gene expression at defined developmental stages, and this contributes to the current opinion that Ewing sarcoma arises from mesenchymal or neural crest-derived stem or progenitor cell.

1.7.2 Neuroblastoma

Neuroblastoma arises from sympathoadrenal lineage of the neural crest during the development. It originates most commonly in adrenal medulla, but can occur in paraspinal sympathetic ganglia or chest ganglia. The mechanism by which sympathetic neuroblasts transform to malignant neuroblastoma cells is still uncertain. In the USA and Europe 8-10% of pediatric cancers are classified as neuroblastomas, thus making it the most common extracranial solid tumor in children (Maris *et al*, 2007; Smith *et al*, 2010; Gatta *et al*, 2014) and the most common cancer in infancy (Gurney *et al*, 1997). In children above approximately 12-18 months of age neuroblastomas are often metastatic and unresectable; survival rate with intensive multimodal therapy ranges from 40 to 50% (Maris *et al*, 2007; Kreissman *et al*, 2013). For most infants with neuroblastoma, however, the outcome is more favorable. Moreover, in a particular type of disease characterized by a specific pattern of metastases the spontaneous complete regression of cancer occurs, after only minimal chemotherapy or even without it (Diede, 2014; Matthay, 1998; Nickerson *et al*, 2000;

Pritchard & Hickman, 1994). There are several proposed mechanisms of tumor regression, but it is still uncertain how exactly this phenomenon occurs and what is the prevalence of spontaneous regression (Brodeur & Bagatell, 2014). On the other hand, disease can progress fiercely, despite the intensive therapy.

Neuroblastoma is a remarkably heterogeneous tumor that exhibit diverse clinical behavior. Based on cytogenetic profiles, neuroblastoma can be divided in three groups: subtype 1, 2A and 2B. In subtype 1 are hyperdiploid or triploid tumors with whole chromosome gains, with high expression levels of TrkA (tropomyosin receptor kinase A, NTRK1). Spontaneous regression can occur only in subtype 1. Near diploidy and segmental chromosomal abnormalities are characteristic for subtype 2, which is associated with older age and more severe phenotype with worse clinical outcome and poor prognosis. It can further be split in 2A and 2B, with 2B being the most aggressive tumors marked by NMYC amplification and 1p deletion. NMYC is a MYC related oncogene that was reported as the gene amplified in neuroblastoma cell lines and primary tumors (Kohl *et al*, 1983; Schwab *et al*, 1983). It is a transcription factor can activate expression of genes that promote proliferation and growth, metastasis, self-renewal, and angiogenesis, but suppress differentiation, cell cycle arrest and immune surveillance. About 25% of neuroblastomas have amplified NMYC (Huang & Weiss, 2013) resulting in NMYC protein overexpression.

INSS (International Neuroblastoma Staging System) defined a specific pattern of metastatic spread that was followed by spontaneous regression of the disease as neuroblastoma stage 4S. The International Neuroblastoma Risk Group (INRG) uses different classification, dividing patients in 16 categories, that are further broadly grouped into very low, low, intermediate and high risk classes (Cohn *et al*, 2009). In this system, 4S patients are in the MS (metastatic special) category. Patients with 4S/MS disease usually express TrkA (Nakagawara *et al*, 1993). Depending on the presence of its cognate ligand NGF (nerve growth factor) in the microenvironment cells expressing TrkA undergo differentiation into ganglion cells (if NGF is present) or programmed cell death (absence of NGF). Hence, the disease regression seen in infants might be a consequence of a delayed activation of apoptosis during the development provoked by the NGF deficiency (Brodeur, 2003). Relatively recent next-generation sequencing studies of neuroblastoma discovered only a few recurrent somatic mutations in high-risk disease, consistent with the observed low mutational burden in pediatric tumors. These are activating mutations in anaplastic lymphoma receptor tyrosine kinase ALK (Mosse *et al*, 2008; George *et al*, 2008; Chen *et al*, 2008; Janoueix-Lerosey *et al*, 2008) and the loss-of-function alterations in ATRX (α -thalassaemia/mental retardation syndrome X-linked), ARID1A and ARID1B (AT-rich interactive domain 1A and 1B), all associated with chromatin remodeling (Sausen *et al*, 2013; Diede, 2014). In case of MS tumors, no germline or non-silent somatic mutations have

been reported (Molenaar *et al*, 2012; Sausen *et al*, 2013). Altogether, these findings strengthened the hypothesis that epigenetic regulation could have a role in the etiology of neuroblastoma. Genome-wide methylation studies showed that frequently methylated regions are found in pathways related with apoptosis (Decock *et al*, 2011); additional studies are needed, however, to decipher the epigenetic regulation in various neuroblastoma tumors.

Regardless of the category, it is evident that new therapeutic strategies are needed in neuroblastoma. Dealing with the high risk disease poses a big challenge for pediatric oncologists, since there is still no curative treatment. Recently, immunotherapy emerged as an attractive option; neuroblastoma cells could selectively express lineage-specific cell surface markers that may not be present on non-embryonic tissues, granting specificity (Bosse & Maris, 2015). In a randomized phase 3 clinical trial the improved survival was demonstrated in neuroblastoma patients that received monoclonal antibody against the tumor-associated disialoganglioside GD2 (Yu *et al*, 2010). Currently, the search for differentially expressed cell surface molecules characteristic for neuroblastoma became one of the major focuses in the field. On the other hand, probably the most promising approach for the induction of tumor regression in susceptible neuroblastomas is the inhibition of TRKA pathway (Brodeur & Bagatell, 2014). It would be advantageous to rather induce apoptosis and regression of the tumor than to wait for it to spontaneously occur, since children with MS/4S stage often suffer from hepatomegaly and respiratory compromise.

2 Aim

Through the work presented in this thesis we wanted to improve the understanding of the relationship between anticancer drugs and cancer cells. Targeted, small molecule medicines exert their effects in a complex signaling environment altered by the malignant changes, where they perturb the system and cause detrimental effects ideally primarily to cancer cells. Cancer cells, on the other hand, have a vast potential to adapt and overcome destructive drug effects, thus the recurrent problem of resistance to targeted therapeutics. The aim was to contribute to the understanding of combinatorial drug treatment and drug-drug interactions, mechanisms of action and mechanisms of resistance to small molecules. By characterizing drug profiles we could investigate the biology of cancers through the differential response of cancer cells to chemical perturbations.

We were interested in improving target discovery tools. Although chemical proteomics (mass spectrometry based drug affinity approach) allowed profiling of a number of clinically relevant compounds, we observed that the detection of certain cognate drug targets was severely compromised and thus the method required optimization. We intended to discover a unique elution strategy that would improve target recovery and subsequent drug profiling.

We performed combinatorial phenotypic screens in three pediatric tumor entities in parallel in order to capture disease specific drug-drug interactions. We were interested in (i) discovering new synergistic drug combinations specific for neuroblastoma and Ewing sarcoma and (ii) deciphering the complex signaling alterations dependent on the EWS-FLI1 (EF) oncofusion, a biologic driver of Ewing sarcoma. We adopted a systems view on complexity of signaling alterations caused by EF, and employed different chemical biology approaches to profile relevant drugs and decipher global signaling events and synergistic drug effects specific for Ewing sarcoma.

Furthermore, we investigated a couple of intriguing compounds with an unknown mechanism of action: (i) compounds selectively cytotoxic in RAS-dependent cancers and (ii) YM155, a small molecule developed as a survivin inhibitor. We performed either chemical perturbation or insertional mutagenesis screens, in order to profile the drugs, identify cancer vulnerabilities and decipher resistance mechanisms.

3 Results

3.1 Manuscript #1: Enhancing cognate target elution efficiency in gel-free chemical proteomics.

Branka Radic-Sarikas, Uwe Rix, Alexey Stukalov, Manuela Gridling, André C. Müller, Jacques Colinge, Giulio Superti-Furga, Keiryn L. Bennett

We observed altered target profiles in the current chemical proteomic approach, probably due to particular elution conditions critically impacting the effectiveness of disruption of drug-protein interaction. To address that, a number of elution conditions were systematically assessed with the objective to discover a novel elution strategy that would improve the overall recovery of all classes of target proteins whilst maintaining compatibility with immunoblotting procedures which serve as an important quality control. This knowledge may lead to exploitation of the full potential of drug candidates, while revealing off-target effects that often lead to toxicity.



Enhancing cognate target elution efficiency in gel-free chemical proteomics



Branka Radic-Sarikas^{a,3}, Uwe Rix^{a,b,3}, Alexey Stukalov^{a,1}, Manuela Gridling^a, André C. Müller^a, Jacques Colinge^{a,2}, Giulio Superti-Furga^{a,c}, Keiryn L. Bennett^{a,*}

^a CeMM Research Center for Molecular Medicine of the Austrian Academy of Sciences, Vienna, Austria

^b Department of Drug Discovery, H. Lee Moffitt Cancer Center & Research Institute, Tampa, FL, USA

^c Center for Physiology and Pharmacology, Medical University of Vienna, Vienna, Austria

ARTICLE INFO

Article history:

Received 1 June 2015

Received in revised form 2 August 2015

Accepted 25 September 2015

Available online 30 September 2015

Keywords:

Chemical proteomics

Mass spectrometry gel-free

Double elution

Dasatinib

Sunitinib

ABSTRACT

Gel-free liquid chromatography mass spectrometry coupled to chemical proteomics is a powerful approach for characterizing cellular target profiles of small molecules. We have previously described a fast and efficient elution protocol; however, altered target profiles were observed. We hypothesised that elution conditions critically impact the effectiveness of disrupting drug-protein interactions. Thus, a number of elution conditions were systematically assessed with the aim of improving the recovery of all classes of proteins whilst maintaining compatibility with immunoblotting procedures. A double elution with formic acid combined with urea emerged as the most efficient and generically applicable elution method for chemical proteomics

© 2015 The Authors. Published by Elsevier GmbH. This is an open access article under the CC BY-NC-ND license (<http://creativecommons.org/licenses/by-nc-nd/4.0/>).

1. Significance

The majority of drugs are surprisingly promiscuous, thus a powerful approach to characterize the cellular target profiles of small molecules is imperative. An acid-based chemical proteomic elution protocol compatible with gel-free liquid chromatography mass spectrometry (LCMS) is effective; however, altered target profiles were observed. We have optimised and implemented a new strategy that decidedly enhanced cognate target elution efficiency. This was evident for both chemical immobilization of

compounds on an inert matrix and also for biotinylated compounds on avidin-functionalized resins.

2. Introduction

Understanding the molecular mechanisms of drugs is of utmost importance as this knowledge may guide target-based improvement of lead compounds; whilst revealing off-target effects that lead to toxicity [1–3]. If chemical entities could be matched to biological processes at the molecular level throughout the drug discovery and development process, the attrition rates for tool compounds and drugs could potentially decrease. Concomitantly, therapeutic efficacy should also improve. Thus, deciphering the target spectra of bioactive compounds can lead to exploitation of the full potential of drug candidates. Some examples where this is applicable are in aiding the identification of novel therapeutic applications or elucidating side effects [4–7]; and/or pharmacological tool compounds that are used to dissect complex biological processes [8]. There is a growing body of data that supports the notion that the majority of drugs are promiscuous and that the ‘one drug, one target’ paradigm seldom applies [9]. The more we understand drug properties, the more we realize that it is not so much the question of if a compound has off-targets, but how many there are and how these contribute to the biological effects. Several methods have been employed in the identification of small molecule-protein interactions, such as chemical proteomics or gene expression-based methods [3,5,10,11].

Abbreviations: MS, mass spectrometry; LC, liquid chromatography; LCMS, liquid chromatography mass spectrometry; iTRAQ, isobaric tags for relative and absolute quantitation; SDS, sodium dodecyl sulphate; CML, chronic myeloid leukemia; TEA, triethylamine; HPLC-MS, high-performance liquid chromatography mass spectrometry; TEAB, triethylammonium bicarbonate; FA, formic acid; ACN, acetonitrile; XX-NHS, biotin-biotinamidohexanoyl-6-aminohexanoic acid *N*-hydroxysuccinimide ester; DTT, dithiothreitol; TLCK, *N*-alpha-tosyl-L-lysiny-chloromethylketone; U/FA, 3 M urea and 50 mM FA; B, boiling; dNSAF, distributed normalized spectral abundance factor; dSAF, spectral abundance factor; uSpC, unique spectral count.

* Corresponding author. CeMM Research Center for Molecular Medicine of the Austrian Academy of Sciences, Lazarettgasse 14, AKH BT25.3, Vienna, 1090 Austria.

E-mail address: kbennett@cemm.oew.ac.at (K.L. Bennett).

¹ Present address: Max-Planck Institute of Biochemistry, Am Klopferspitz 18, D-82152 Martinsried/Munich, Germany.

² Present address: Institut de Recherche en Cancérologie de Montpellier, Campus Val d'Aurelle 34298 Montpellier, France.

³ These authors equally contributed to this work.

<http://dx.doi.org/10.1016/j.euprot.2015.09.002>

1876–3820/© 2015 The Authors. Published by Elsevier GmbH. This is an open access article under the CC BY-NC-ND license (<http://creativecommons.org/licenses/by-nc-nd/4.0/>).

Chemical proteomics is a post-genomic affinity chromatography-based approach that is enabled by modern mass spectrometry (MS) and bioinformatic capabilities [3,12–17]. There are various protocols in use, but the most widely-accepted procedure entails the elution of interacting proteins from a drug-affinity matrix with sodium dodecyl sulphate (SDS) followed by analysis of the eluate by one- or two-dimensional SDS-PAGE and *in situ* tryptic digestion of the proteins. In most cases, the resultant peptide mixture is analyzed by nano-liquid chromatography (LC) coupled to nano-electrospray (ESI) tandem MS [18]. Whereas this gel-based proteomic workflow (often referred to as GeLCMS) has been highly successful and has led to a number of landmark publications that describe several important novel drug-protein interactions [8,19–21], there are also a number of important limitations. These include high labor demand, high cost, and an increased risk of keratin contamination as a consequence of multiple sample handling steps. GeLCMS is also not directly compatible with quantitative proteomic approaches that utilize post-digestion chemical labeling with isobaric tags (e.g., iTRAQ, TMT) [22]. Therefore, gel-free proteomic methods are receiving more widespread interest.

We have recently shown that adaptation of a gel-free approach resulted in a significant reduction in sample preparation and MS instrument time, and ultimately led to an increase in absolute numbers of identified proteins [23]. Target recovery was also improved such that a 5-fold decrease in the protein input was enabled without loss of data quality [23]. Furthermore, we have demonstrated the compatibility of our approach with subsequent relative quantitative proteomics using iTRAQ labeling [24,25]. Despite these advancements, the method has only been used in a few studies from our groups [26–30], as there were some questions raised concerning cognate target recovery (especially for receptor tyrosine kinases, RTKs) and decreased immunoblot efficiency. For example, the detection of the BCR-ABL fusion oncoprotein, which is the biochemical hallmark of chronic myeloid leukemia (CML) and a major drug target of several kinase inhibitors (e.g., imatinib and dasatinib), was compromised. This observation was apparent with dot blots and western gel-based immunoblot assays. Therefore, we hypothesized that elution conditions critically impact the effectiveness of disrupting drug-protein interactions. Subsequently, the final drug-protein profile can be altered. Surprisingly, this aspect is rarely addressed and often overlooked in biochemical approaches linked to mass spectrometry-based proteomics. Thus, the ultimate aim of this current study was to systematically and thoroughly assess a number of different elution conditions to determine the best, yet generic, protocol that efficiently eluted a broad range of cognate targets encompassing several protein classes. Dasatinib was initially selected as the test compound. This drug is a multi-kinase inhibitor approved for the treatment of patients with imatinib-resistant CML and BCR-ABL-positive acute lymphoblastic leukemia (ALL). Dasatinib is not only a potent inhibitor of the large 210 kDa fusion protein BCR-ABL [31], but also of the cytosolic TEC family kinase BTK [6] and the membrane-bound receptor tyrosine kinase DDR1 [21]. In addition, we have previously generated a dasatinib analog suitable for chemical proteomics that we have validated and successfully employed in different studies [21,32,33].

A number of elution conditions were assessed with the objective to improve: (i) compatibility with immunoblot analysis, which is an important quality control; and (ii) the overall recovery of *bona fide* targets. The protocol optimized on the coupleable analog of dasatinib was further extended to a biotinylated derivative of the drug; and also to a second compound with a different target profile. Compared to dasatinib, sunitinib [34] inhibits a complementary fraction of kinases [28]. The drug is an oral, multi-targeted kinase inhibitor, which has been approved for treatment of imatinib-resistant gastrointestinal stromal tumor and

renal cell carcinoma. Additionally, sunitinib is in clinical trials for CML and myelodysplastic syndromes. Sunitinib is a potent inhibitor of receptor tyrosine kinase c-KIT [35], and the serine/threonine protein kinase PRKAA1 (AMPK1 α) and CAMK2 [36]. Overall, we could show that our optimized elution method brought a universal improvement in elution efficiency with two different drug-coupling strategies and two different kinase inhibitors.

3. Materials and methods

3.1. Chemicals

All chemicals used were of analytical grade, unless stated otherwise and obtained from commercial suppliers.

3.2. Biological material

K562 and HEL cells were obtained from DSMZ (Deutsche Sammlung von Mikroorganismen und Zellkulturen). Antibodies used were rabbit polyclonal anti-DDR1, anti-BTK (E9) and anti-KIT (C-19) (Santa Cruz Biotechnology, Santa Cruz, CA); and anti-ABL (21–63) (generated in house).

3.3. Compounds and immobilization

Dasatinib and sunitinib were purchased from Selleck Biochem (Houston, Texas Area). *c*-dasatinib was synthesized by WuXi PharmaTech (Shanghai, China) [21], and *c*-sunitinib was obtained from Indus Biosciences Private Limited (Hyderabad, India) through Gateway Pharma (Freeland, UK). Compounds were immobilized on NHS-activated Sepharose 4 Fast low (Amersham Biosciences, Amersham, UK). Beads were washed with dimethyl sulfoxide (DMSO) and incubated overnight with 1 mM compound and 100 mM triethylamine (TEA) at room temperature (RT) with constant agitation. After incubation, the supernatant was analyzed by high-performance liquid chromatography mass spectrometry (HPLCMS) in order to determine whether the compound was completely immobilized. Unreacted functional groups were subsequently blocked with 0.8 M ethanolamine for at least 8 h at RT, washed with DMSO and either stored at 4 °C in isopropyl alcohol or used immediately for affinity chromatography. For the biotinylated drug experiments, *c*-dasatinib was incubated with biotin amidohexanoyl-6-aminohexanoic acid *N*-hydroxysuccinimide ester (biotin-XX-NHS, Sigma-Aldrich, St. Louis, MO) in the presence of TEA overnight at RT with constant agitation. The supernatant was then analyzed by HPLC-MS for residual reagents and the reaction yield. Dasatinib coupled to biotin was incubated with UltraLink immobilized streptavidin plus beads (Pierce, Rockford, IL) on a roto-shaker for 30 min at 4 °C and used for affinity chromatography.

3.4. Affinity purification

The same affinity purification protocol was used for *c*-dasatinib, *c*-sunitinib and *c*-dasatinib-XX-biotin. K562 and HEL cell lysates were prepared using a lysis buffer comprised of 50 mM Tris-HCl (pH 7.5), 100 mM NaCl, 0.2% NP-40, 5% glycerol, 1.5 mM MgCl₂, 25 mM NaF, 1 mM Na₃VO₄, 1 mM phenylmethylsulfonyl fluoride (PMSF), 1 mM dithiothreitol (DTT), 10 μ g/mL *N*-alpha-tosyl-L-lysyl-chloromethylketone (TLCK), 1 μ g/mL leupeptin, 1 μ g/mL aprotinin, and 10 μ g/mL soybean trypsin inhibitor. In order to minimize sample variability, cell lysates were prepared in large batches, aliquoted and stored at –80 °C until required. Before application to the pre-equilibrated affinity matrices, cell suspensions were clarified by centrifugation. Lysates (5 and 10 mg total protein for K562 and HEL, respectively) were incubated with drug-

coupled affinity matrices for 2 h at 4 °C. After a brief centrifugation, the lysates were transferred to 2 mL Bio-Spin disposable chromatography columns (BioRad, Hercules, CA). Columns were washed with lysis buffer and then with 50 mM HEPES–NaOH buffer (pH 7.5) supplemented with 0.5 mM EDTA (pH 8.0) and 100 mM NaCl. Retained proteins were eluted in several ways: (i) immediate elution without incubation; (ii) heat denaturation by boiling (B) at 100 °C, either for 5 min or 1 h; and (iii) incubation for 1 h at 57 °C or 60 °C. As elution agents, the following freshly-prepared stocks were used: (i) 250 μ L 100 mM FA; (ii) 300 μ L 6 M urea; (iii) 300 μ L 1 M NaCl; (iv) 300 μ L 25% CH₃CN (acetonitrile, ACN); (v) 300 μ L 50% CH₃CN; (vi) 250 μ L 3 M urea, 50 mM FA (U/FA); (vii) 250 μ L 0.5M NaCl, 50 mM FA (NaCl/FA); (viii) 250 μ L 50% CH₃CN, 50 mM FA (ACN/FA); (ix) HEPES buffer; and (x) 30 μ L sodium dodecyl sulfate (SDS) sample buffer (Laemmli buffer) combined with boiling for 4 min. In some cases, a double elution procedure was applied (denoted as .2). After elution with a given agent (e.g., FA or U/FA), the eluate was collected in a glass vial and re-loaded onto the drug-affinity matrix and the flow-through collected a second time. On any occasion where FA was used either as a single agent or in combination with other components, proteins were eluted into a glass vial containing either 62.5 μ L (FA elution alone) or 31.25 μ L (combinations with FA) 1 M triethylammonium bicarbonate (TEAB) to neutralize the acidic eluate. Whenever FA was not used, retained proteins were eluted directly into a glass vial using a higher volume of eluting agent to maintain the same final volume for all eluates throughout the experiments. For ACN or ACN/FA and ACN/FA.2, eluted proteins were lyophilised by vacuum centrifugation and reconstituted in 100 mM TEAB. After elution of the proteins, the same sample preparation protocols were used throughout. An aliquot of each eluate (100 μ L) was removed for immunoblot analysis and denatured by boiling for 4 min with Laemmli buffer. In an initial screen with c-dasatinib where four selected elution methods were compared to a standard FA protocol, one biological replicate of each was analysed as technical duplicates. For the U/FA.2 elution pulldowns with c-dasatinib and c-sunitinib, five and two biological replicates were analysed, respectively. Experiments conducted with c-dasatinib-XX-biotin consisted of four biological replicates.

3.5. Immunoblot analysis

For the western blot experiments, eluates containing Laemmli buffer were separated by 1D SDS-PAGE on a 7% polyacrylamide gel. Blotting was performed for 1 h onto a nitrocellulose transfer membrane (Protran BA 85, 0.45 μ m). After blocking with either 5% non-fat dry milk or 3% BSA in TBS/Tween, the membrane was incubated with the primary antibody overnight at 4 °C and then for 1 h at RT with the secondary antibody. The signal was detected using radiographic films after incubation with chemi-luminescence detection reagent (ECL normal or ECL plus, GE Healthcare Bio-Sciences, Uppsala, Sweden). For the dot blot experiments, eluates containing Laemmli buffer were spotted onto a nitrocellulose membrane using a Bio-Dot apparatus (Biorad, Hercules, CA) as previously described [37]. The membrane was dried, rehydrated and analyzed by immune staining. Two 1:5 serial dilutions of the eluates were used throughout to extend the dynamic range of the immunoblot signal. This was essential to observe subtle differences in intensity.

3.6. Solution tryptic digestion of eluted proteins and sample preparation for liquid chromatography mass spectrometry

Based on the immunoblot experiments, non-acidic eluates were not analysed by LCMS. The TEAB-neutralized acidic eluates, however, were reduced with 500 mM DTT at 56 °C for 1 h (final

concentration DTT approximately 10 mM) and alkylated with 1 M iodoacetamide for 30 min at room temperature in the dark (final concentration iodoacetamide approximately 55 mM). Depending on the preceding elution procedure and prior to digestion with trypsin, samples were diluted with 500 mM TEAB to a concentration of 250 mM NaCl or 1.5 M urea. All final volumes of the various samples were kept constant throughout. Digestion was performed with sequencing grade modified porcine trypsin (Promega, Madison, WI) overnight at 37 °C. Eluates were desalted using stage tips [38] (3 \times 5% of the digest volume per drug pulldown), concentrated in a vacuum centrifuge (Eppendorf, Hamburg, Germany) to approximately 2 μ L and then reconstituted with 24 μ L 5% FA. All samples were analysed by LCMS as technical replicates.

3.7. Liquid chromatography mass spectrometry

Mass spectrometry was performed on an linear trap quadrupole (LTQ) Orbitrap Velos mass spectrometer (ThermoFisher Scientific, Waltham, MA) using Xcalibur version 2.1.0 SP1.1160. The instrument was coupled to an Agilent 1200HPLC nanoflow systems (dual pump with one precolumn and one analytical column) (Agilent Biotechnologies, Palo Alto, CA) via a nano-electrospray ion source using a liquid junction (Proxeon, Odense, Denmark). Solvents for LCMS separation of the digested samples were as follows: solvent A consisted of 0.4% FA in water and solvent B consisted of 0.4% FA in 70% methanol and 20% isopropanol. Eight microlitres of the tryptic peptide mixture were automatically loaded from a thermostatted microautosampler onto a trap column (Zorbax 300SB-C18 5 μ m, 5 \times 0.3 mm, Agilent Biotechnologies, Palo Alto, CA) with a binary pump at a flow rate of 45 μ L/min. TFA (0.1%) was used for loading and washing the precolumn. After washing, the peptides were eluted by back-flushing onto a 16 cm fused silica analytical column with an inner diameter of 50 μ m packed with C18 reversed phase material (ReproSil-Pur 120C18-AQ, 3 μ m, Dr. Maisch GmbH, Ammerbuch-Entringen, Germany). The peptides were eluted from the analytical column with a 27 min gradient ranging from 3 to 30% solvent B, followed by a 25 min gradient from 30 to 70% solvent B and, finally, a 7 min gradient from 70 to 100% solvent B at a constant flow rate of 100 nL/min [39]. The analyses were performed in a data-dependent acquisition mode and dynamic exclusion for selected ions was 60 s. A top 15 collision-induced dissociation (CID) method was used, and a single lock mass at m/z 445.120024 [Si(CH₃)₂O]₆ [40] was employed. Maximal ion accumulation time allowed in the CID mode was 50 ms for MSⁿ in the LTQ and 500 ms in the C-trap. Automatic gain control was used to prevent overfilling of the ion traps and was set to 5000 in the MSⁿ mode for the LTQ and 10⁶ ions for a full FTMS scan. Intact peptides were detected 60,000 resolution at m/z 400 [39].

3.8. Data analysis

The acquired raw MS data files were processed with msconvert (ProteoWizard Library v2.1.2708) and converted into Mascot generic format (.mgf) files. The resultant peak lists were searched against the human Swiss-Prot database version v2011.06_20110609 or v2011.12_20111220 (35683 and 35879 sequences, respectively, including isoforms as obtained from varsplic.pl) with the search engines Mascot (v2.3.02, MatrixScience, London, U.K.) and Phenix (v2.5.14, GeneBio, Geneva, Switzerland). Submission to the search engines was via a Perl script that performs an initial search with relatively broad mass tolerances (Mascot only) on both the precursor and fragment ions (\pm 10 ppm and \pm 0.6 Da, respectively). High-confidence peptide identifications were used to calculate independent linear transformations for both precursor and fragment ion masses that

would minimize the mean square deviation of measured mass from theoretical. These recalibrating transformations were applied to all precursor and fragment ions prior to a second search with narrower mass tolerances (± 4 ppm and ± 0.3 Da). One missed tryptic cleavage site was allowed. Carbamidomethyl cysteine and oxidized methionine were set as fixed and variable modifications, respectively. To validate the proteins, Mascot and Phenyx output files were processed by internal parsers. Proteins with ≥ 2 unique peptides above a score T1, or with a single peptide above a score T2, were selected as unambiguous identifications. For validated proteins fulfilling either the T1 or T2 criteria, any additional peptides with a score $>T3$ were also accepted. For Mascot and Phenyx, T1, T2, and T3 peptide scores were 16, 40, and 10; and 5.5, 9.5, and 3.5, respectively (P -value $< 10^{-3}$). For each data set the validated peptides retrieved by the two algorithms were merged, any spectral conflicts discarded and proteins grouped according to shared peptides. A false discovery rate (FDR) of $< 1\%$ and $< 0.1\%$ (including the peptides exported with lower scores) was determined for proteins and peptides by applying the same procedure against a reversed database. To compare the efficiency of the elution protocols, the distributed normalized spectral abundance factors (dNSAF) [41] were used as a measure of protein abundance.

$$\text{dSAF}_i = \frac{1}{L_i} \left(\text{uSC} + \sum_{k=1}^{N_{\text{ssep}}(i)} \frac{\text{uSC}_i}{\sum_{l=1}^{N_{\text{sprot}}(k)} \text{uSC}_l} \text{sSC}_{i,k} \right) \quad (1)$$

$$\text{dNSAF} = \frac{\text{dNSAF}_i}{\sum_{i=1}^N \text{dNSAF}_i} \quad (2)$$

Briefly, the distributed spectral abundance factor (dSAF) of protein i is the weighted sum of the spectral counts divided by protein length. The weight of unique spectral counts (uSC) is 1, whereas the weight of spectra for k -th shared peptide ($\text{sSC}_{i,k}, k = 1, 2, \dots, N_{\text{ssep}}(i)$) is the ratio of unique spectral counts of protein i and the sum of all unique spectral counts for $N_{\text{sprot}}(k)$ proteins that share k -th peptide. Finally, dSAF is normalized to the total sum of dSAFs in the specific LCMS analysis to obtain dNSAF (2). For each drug, the effect of each elution protocol on the abundance of the two protein groups was assessed: known targets and interactors ('T'), and known contaminants ('C': spectrin, actin, myosin, vimentin, haemoglobin subunits, histone and ribosomal proteins, heterogeneous ribonuclear proteins, POTE ankyrin domain family members). Specifically, the following generalized linear regression

model was applied to dNSAF data:

$$A_{ij} = a_0 + a_i + p_{G(i), P(j)} + q_{i, P(j)} + b_{B(j)} + e_j + d_{i, B(j)}, \quad (3)$$

$$\log(\text{dNSAF}_{ij}) \propto \text{Normal}(A_{ij}), \quad (4)$$

$$I_{ij} \propto \text{Bernoulli}(\text{logit}^{-1}(\alpha A_{ij} + \beta)), \quad (5)$$

where $i = 1, 2, \dots, N$ and $j = 1, 2, \dots, M$ specify the protein and LCMS analysis, respectively, and A_{ij} is the abundance of i -th protein in the j -th experiment. A_{ij} takes into account the following factors: a_0 —the average protein abundance; $a_0 + a_i$ —the average abundance of i -th protein; $p_{G(i), P(j)}$ —the average effect of the elution protocol ($P(j)$) on a given group of proteins ($G(i)$, either targets or contaminants); $q_{i, P(j)}$ —the protocol effect on the individual protein; e_j —the normalization term for the j -th LCMS analysis; $b_{B(j)}$ and $d_{i, B(j)}$ account for the global and protein-specific effects of the $B(j)$ -th batch of LCMS analyses. The equation (4) links the observed dNSAF_{ij} to A_{ij} . Bernoulli-logit model (5) is used to properly account for missing data: protein identification ($I_{ij} = 1$) or absence ($I_{ij} = 0$) in a given experiment is linked to inferred abundance A_{ij} , where parameters α and β are learned from the data.

The model (3)–(5) enables an assessment of how a given protocol affects the abundance of specific protein groups (either targets or contaminants) and individual proteins. At the same time, these protocol-specific effects are decoupled from batch-specific and individual LCMS data variations. The Bayesian methodology was adopted and the model (3)–(5) was fit to the experimental data using STAN [42] to obtain the posterior distributions for all the model parameters. The posterior distributions for protein group-specific protocol effects ($p_{J,C}$) were used to estimate the overall protocol efficiencies:

$$\text{Eff}(J) = (p_{J,T} - p_{J,C}) - (p_{0,T} - p_{0,C}). \quad (6)$$

That is, $\text{Eff}(J)$ reports how much the target proteins (T) are enriched over the contaminants (C) when using protocol J in comparison to the 0-th reference protocol (U/FA). It follows from (6) that $\text{Eff}(J)$ is positive for more efficient protocols, and one-sided P -value

$$P(\text{Eff}(J) \leq 0) \quad (7)$$

provides the statistical significance of this hypothesis.

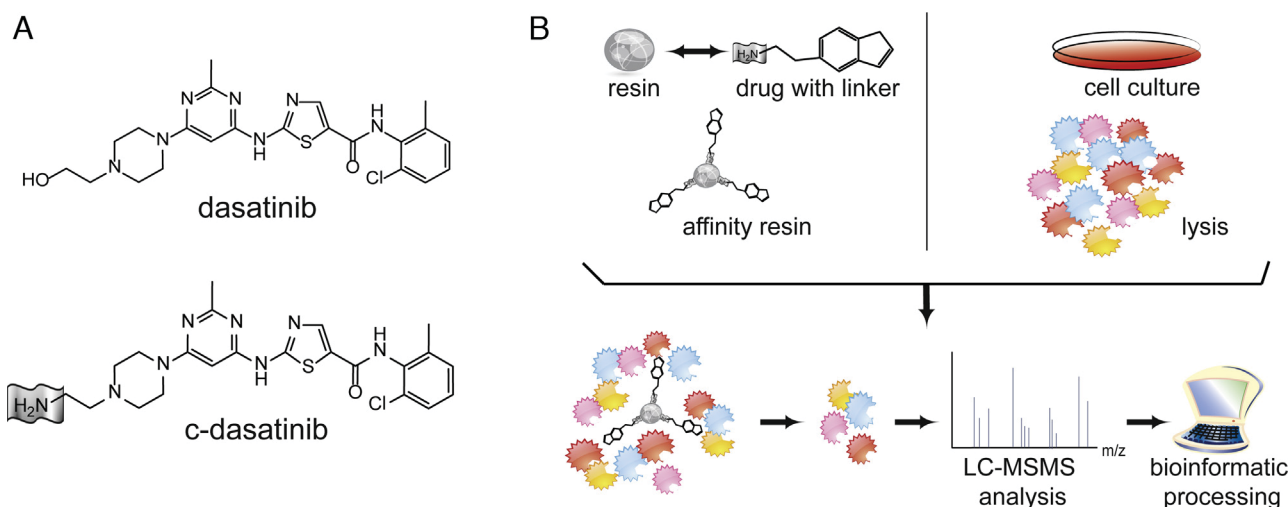


Fig. 1. Overview of the experimental approach. (A) Chemical structure of dasatinib and c-dasatinib. The latter is the chemically-modified version of dasatinib that can be coupled to sepharose beads via a linker. (B) The overall workflow of a chemical proteomic experiment.

4. Results and discussion

4.1. Combining formic acid with denaturing reagents improves detection of BCR-ABL, DDR1 and BTK by immunoblotting.

The dasatinib analog (Fig. 1A) was coupled to NHS-sepharose beads and the resultant drug affinity matrix was incubated with cell extracts from the chronic myelogenous leukemia (CML) cell line K562 (5 mg protein per pulldown) (Fig. 1B). A number of different elution reagents and/or conditions were used: (i) 100 mM formic acid (FA); (ii) 6 M urea (U) [43]; (iii) 1 M NaCl; (iv) 25% acetonitrile (ACN) [44,45]; (v) 50% ACN [44]; (vi) 3 M urea, 50 mM FA (U/FA); (vii) 0.5 M NaCl, 50 mM FA (NaCl/FA); (viii) 50% ACN, 50 mM FA (ACN/FA); (ix) HEPES buffer; and (x) 4 × SDS sample buffer (Laemmli buffer). The latter is the traditional method for gel-based approaches and acts as a control for evaluating the protein targets of a drug by immunoblot analyses. Elution with 100 mM FA (no incubation of the proteins on the affinity matrices) is our previously-established, standard elution procedure for gel-free drug pull-down experiments [23]. All elution protocols assessed were compared to this 'standard protocol'. Reagents

were evaluated at RT or 100 °C (B) for 4 min or 1 h. A 1 h incubation at 57 °C and 60 °C was also assessed for the urea and ACN elutions, respectively. It has been previously suggested that the efficiency of protein elution may be improved when incubating at higher temperatures [44]. In the early stages of the study, one goal was to establish a reproducible immunoblotting method that would enable a rapid comparison between selected elution methods. The dot blot approach allows the direct application of a sample onto a membrane without prior separation by electrophoresis. Furthermore, proteins are transferred by microfiltration. This eliminates any variability caused by the transfer of a protein from a gel. Based on previous experiments with dasatinib, three antibodies (c-ABL, DDR1 and BTK) were selected. These proteins are *bona fide* dasatinib targets [6,21,31] and belong to different kinase classes: non-receptor kinases from ABL and TEC family (c-ABL and BTK, respectively) and receptor tyrosine kinase (DDR1). The differences between the elution methods were assessed by direct comparison to the standard elution procedure (Fig. 2). When used as single agents (Fig. 2A), both 6 M urea (lane 3) and 1 M NaCl (lane 7) gave a weaker signal for both c-ABL and DDR1 than the standard FA elution (lane 2). When the samples were boiled (B) for 4 min,

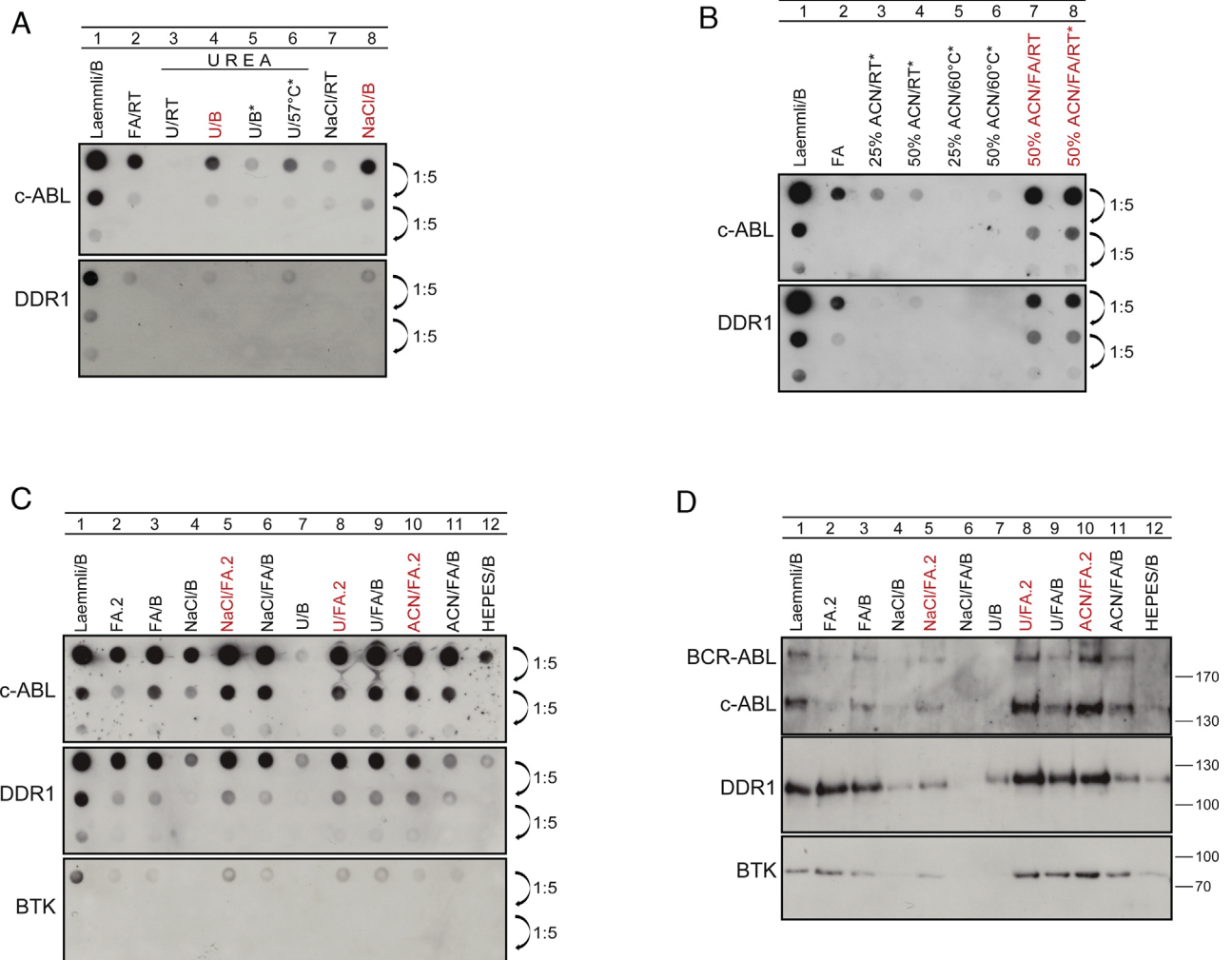


Fig. 2. Combination of formic acid with denaturing reagents improves elution efficiency for BCR-ABL, DDR1 and BTK. (A) Anti-ABL and anti-DDR1 dot blots of pull-downs eluted with urea and NaCl. Five-fold serial dilutions from each eluate were also loaded. B, boiled; *, 1 h incubation of the elution agent on the column. (B) Anti-ABL and anti-DDR1 dot blots of pull-downs eluted with different concentrations of acetonitrile and combined with formic acid. Five-fold serial dilutions from each eluate were also loaded. *, 1 h incubation of the elution agent on the column. (C) Anti-ABL, anti-DDR1 and anti-BTK dot blots of pull-downs eluted with various elution agents and procedures. Double application of the eluate to the column is denoted as .2. Five-fold serial dilutions from each eluate were also loaded. B, boiling. (D) Anti-ABL, anti-DDR1 and anti-BTK western blots of pull-downs eluted with same agents and conditions as in (C), B, boiling. (For interpretation of the references to color in the text, the reader is referred to the web version of this article.)

however, the results were in the same range as the standard protocol or even slightly improved (lanes 4 and 8, highlighted in red). A longer incubation time of 1 h (indicated by asterisks) with urea at 57 °C (lane 6) or 100 °C (lane 5) did not lead to any visible improvement in elution efficiency. The ACN elution was also weak (Fig. 2B). Even after a 1 h incubation at RT (lanes 3 and 4) or 60 °C (lanes 5 and 6), ACN as a single elution agent only resulted in a faint to no signal. Nevertheless, when ACN was combined with FA (lanes 7 and 8, highlighted in red), signal intensity was markedly improved. Regardless of whether the proteins were immediately eluted from the drug affinity matrix or after a 1 h incubation period, the 50% ACN/50 mM FA combination at RT enhanced the elution and immunoblot efficiency to an extent comparable to the Laemmli control (lane 1). This experimental condition was also notably improved over the standard FA elution (lane 2).

As the combination of ACN with FA at RT led to a significant improvement in signal intensity, our next step was to evaluate the effect on protein elution from the drug affinity matrix when all of the selected reagents were combined with FA. Furthermore, we reasoned that more proteins could be retrieved if the eluate was applied to the column twice. Regardless of the reagent chosen, the eluate was collected, applied to the column a second time, and the

eluate again collected in a glass vial (denoted as .2 in all ensuing text). At this point too, an improvement in elution efficiency by boiling the samples was not excluded. Thus, to assess whether boiling of the samples alone is sufficient to potentiate elution efficiency, HEPES buffer was included in the panel of elution agents. Dot and western blot analyses of the various eluates for c-ABL, DDR1 and BTK (Fig. 2C and D) showed that the elution efficiency was markedly enhanced for all three targets when denaturing agents were combined with formic acid. A double elution with 50 mM FA combined with either 0.5 M NaCl (NaCl/FA.2) (Fig. 2C, lane 5, highlighted in red); 3 M urea (U/FA.2) (lane 8, highlighted in red); and 50% ACN (ACN/FA.2) (lane 10, highlighted in red) all showed an increase in elution efficiency over the standard procedure where formic acid was used as a single agent and at a higher concentration of 100 mM (lane 2). Also, it was observed that in most cases boiling of the samples did not lead to enhancement of the signal intensity (lanes 6, 9, 11, 12). In some instances, quite the contrary a weaker signal was apparent compared to the counterparts that were not boiled (see lane 11 compared to lane 10). Furthermore, boiling of the HEPES eluate (lane 12) did not result in increased protein recovery. Thus, we concluded that the combination of a selection of agents with FA is

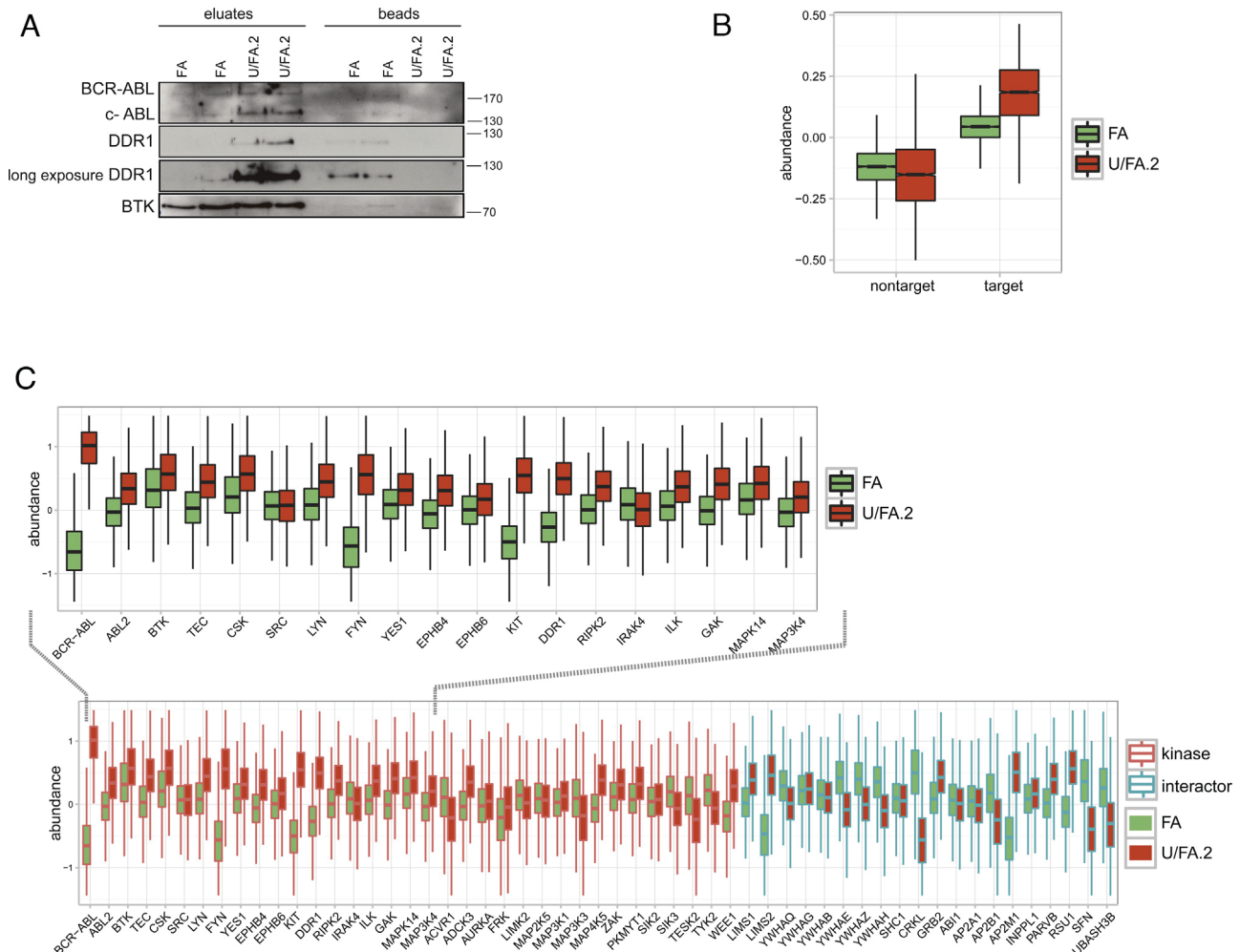


Fig. 3. Formic acid/urea double elution improved the identification of dasatinib targets by gel-free liquid chromatography mass spectrometry. (A) Anti-ABL, anti-DDR1 and anti-BTK western blots of pull-downs eluted with either FA or U/FA.2, plus the beads sequentially eluted with Laemmli buffer. (B) Comparison of the overall abundance between FA and U/FA.2. (C) The majority of the cognate kinase targets of dasatinib are more abundant with U/FA.2 than FA alone. This is particularly noticeable for the main target of dasatinib, BCR-ABL. An integrated plot showing differences in protein abundance between the FA alone and the U/FA.2 elution methods. Kinases and kinase-interacting proteins are indicated in the red and blue box plots, respectively. Recovery of all major kinase targets was improved with U/FA.2, whilst the majority of the kinase-interacting proteins are less abundant. Five biological replicates were analysed (two technical replicates each). (For interpretation of the references to color in this figure legend, the reader is referred to the web version of this article.)

sufficient for signal improvement, and this holds true for all three selected targets of dasatinib: ABL, receptor tyrosine kinase DDR1 and the TEC kinase family member, BTK.

BCR-ABL is the main target of dasatinib. Similarly, c-ABL is also one of the primary targets. As shown in Fig. 2D, both proteins were recognized by the anti-ABL antibody as evidenced by bands detected for ABL and BCR-ABL at approximately 140 kDa and 210 kDa, respectively. As mentioned previously, one of the main issues with the current 100 mM FA standard elution method is the inability to retrieve ABL proteins with high efficiency from the dasatinib-coupled affinity matrix. This was already apparent from the dot blot, and is particularly noticeable in the first 5-fold dilution series (Fig. 2C, upper panel, lane 2). Excluding HEPES (lane 12) and U/B (lane 7), the recovery with FA was lower than all the other elution methods assessed. Even more striking is this difference on the western blot (Fig. 2D). Here the signal in the FA eluate is almost completely absent for both BCR-ABL and ABL (upper panel, lane 2). Conversely, the recovery of these proteins with U/FA.2 (lane 8, highlighted in red) and ACN/FA.2 (lane 10, highlighted in red) was even higher than that observed with Laemmli buffer (lane 1). The difference was not as pronounced with the two other dasatinib targets, DDR1 and BTK. Nevertheless, an improvement was still observed when the same set of elution procedures was used; namely U/FA.2 (middle and lower panels, lane 8, highlighted in red), U/FA/B (lane 9), ACN/FA.2 (lane 10, highlighted in red) and ACN/FA/B (lane 11). In addition, NaCl/FA.2 (lane 5, highlighted in red) also showed a slight improvement in elution efficiency. This was particularly noticeable for BCR-ABL and ABL. An overall comparison of these data showed that on the immunoblot level, an improvement in the recovery of selected dasatinib targets was achieved in all instances when formic acid was combined with a denaturing reagent.

4.2. Combining formic acid with denaturing reagents improved detection of dasatinib targets by mass spectrometry.

We next asked the question: whether improvement in target recovery as observed from the immunoblot analyses would also translate into a higher quality data set by LCMS. Therefore, the most promising elution methods as determined by immunoblot, i.e., FA.2, U/FA.2, NaCl/FA.2, and ACN/FA.2 were screened by LCMS (Supplementary Table S1). The spectral count values were used as an indicator of target importance; as this represents a combination of target affinity and abundance [46]. When the average spectral counts (from two technical replicates) of selected elution methods were compared for relevant dasatinib targets, we observed that FA.2 did not show an increase in elution efficiency. This led to the conclusion that the double elution alone is not sufficient to improve the standard method. Rather, it is the joint effect of the double elution together with the appropriate combination of elution reagents. When the other elution methods were compared to the standard FA protocol, the most striking difference was observed for BCR-ABL. An almost four-fold increase in average spectral counts was apparent for the U/FA.2 and ACN/FA.2 elutions (from 15 spectral counts with FA alone; to 55 and 61.5, respectively, for the alternate elution methods). Apart from the substantial increase in the elution efficiency of ABL kinases, the data obtained from the LCMS screen of the proteins eluted with U/FA.2 and ACN/FA.2 appeared to be comparable to the standard method. Nonetheless, both elution methods displayed a noticeable improvement in the immunoblot experiments (Fig. 2C and D). The U/FA.2 and ACN/FA.2 immunoblot and LCMS data were quite similar; however, due to the simplicity of the sample preparation only the U/FA.2 method was investigated further (see below). To confirm that the observed increase in cognate target recovery was due to improved elution and not as a consequence of other factors

such as downstream sample loss, Laemmli buffer was added to the beads after the proteins had been eluted. The beads were boiled for 5 min and loaded onto a gel together with the eluates. For all three of the targets (ABL, DDR1 and BTK) assessed by immunoblot, a clear improvement in elution with U/FA.2 compared to the standard FA was evident. In support of this observation, residual protein on the beads was not apparent for U/FA.2 (Fig. 3A). Conversely, some protein was retained on the beads when FA alone was used.

To assess both the robustness and consistency of the new method, five new cycles of FA and U/FA.2 elution experiments were conducted and analysed by LCMS (Fig. 3B and C, Supplementary Table S2). Compared to FA alone (Fig. 3B, light green), elution with U/FA.2 (red) resulted in higher target recovery. The list of dasatinib targets consisted of all validated protein kinase targets and indirect binders of the drug, i.e., the interactors of target kinases [6,21,29,47–50]. When specifically assessing the kinase targets of dasatinib, the target enrichment was even more evident (Fig. 3C). The majority of the kinases were more abundant in U/FA.2 compared to the standard FA eluates. Contingent on previously-published data using gel-based approaches [21,33,48], the dasatinib targets identified with the U/FA.2 elution accurately reflected the expected distribution of primary and secondary interactors. In addition to the dramatic difference observed with BCR-ABL, ABL2, kinases from the SRC family (LYN, FYN, YES1 and c-SRC), and the negative regulator c-SRC kinase (CSK) showed improvement. The TEC family kinases (BTK and TEC) are prominent interactors of dasatinib [6] and were also eluted more efficiently. Likewise, the receptor tyrosine kinases DDR1, KIT, EPHB4 and EPHB6 and the serine–threonine kinases (GAK, MAPK14, MAP3K4) were also identified with higher spectral count abundances. RIPK2 was also eluted with higher efficiency. This kinase is a member of the receptor-interacting protein (RIP) family of serine/threonine protein kinases, and is a known target of dasatinib that has not been reported with other ABL kinase inhibitors (e.g., imatinib, nilotinib or ponatinib) [51].

One of the drawbacks of chemical proteomics is that it is often difficult to distinguish direct from indirect targets. With the U/FA.2 elution method, however, the contribution from several non-kinase proteins was reduced (Fig. 3C), e.g., 14-3-3 proteins, CRKL, UBASH3B, etc. This apparent reduction (as determined by spectral counts) may reflect a decrease in MS sampling for these proteins due to the concurrent increase in sampling of the now more efficiently eluted true interactors. On the other hand, the integrin-linked kinase ILK together with the non-kinase interaction partners LIMS1, LIMS2, PARVB and RSU1 were consistently observed with notably improved recovery (Fig. 3C). These molecules form a very robust IPP complex (ILK, PINCH and parvin complex) [52] and thus, do not follow the same trend as other non-kinase proteins. Rather, these too were eluted more efficiently with U/FA.2. Based on our spectral counting approach, the data generated from the U/FA.2 elution method suggested that this particular combination of reagents may aid in refining the distinction between direct and indirect interacting proteins.

4.3. U/FA.2 is an elution method of choice for biotinylated compounds

Although the widely-applied chemical immobilization of a bioactive small molecule on an inert matrix has proven highly-successful in many chemical proteomic studies; there are a few drawbacks. Synthesising a coupleable analog of a compound is not always straightforward. An alternative is to utilise the well-established biotin/avidin affinity purification system. Here, modification of a small molecule with a biotin tag enables the non-covalent capture of drug-protein complexes by (strept) avidin.

Previous observations from our group (data not shown) revealed that the standard formic acid-based elution method did not result in sufficient recovery of proteins when using biotinylated compounds as the bait; thereby precluding a successful analysis of such drug target interactions by gel-free LCMS. We therefore evaluated, if the elution method optimized in the preceding section would be more successful with respect to the identification of proteins that are enriched with a biotinylated small molecule. To answer this question, dasatinib was biotinylated (Fig. 4A), attached to streptavidin beads, incubated with K562 cell lysates (5 mg total protein per experiment) and eluted using the various methods described earlier (urea, NaCl, ACN), with or without boiling, in combination with formic acid and with a double elution. Initial dot blot analyses with an ABL-specific

antibody confirmed the feasibility of this molecule as a chemical proteomic probe as the elution with Laemmli buffer (positive control) readily recovered ABL proteins (Fig. 4B, lane 1). Strikingly, but consistent with previous observations [23], no signal was evident following elution with 100 mM formic acid (Fig. 4B, upper panel, lane 2). The complete absence of the main target of dasatinib was also confirmed by western blot (Fig. 4B, lower panel, lane 2). In contrast, the double elution with urea combined with formic acid produced an excellent immunoblot signal (Fig. 4B, upper panel, lane 8, highlighted in red; lower panel, lane 4, highlighted in red) which was comparable to that obtained with Laemmli buffer (lane 1). LCMS analysis of these eluates (Supplementary Table S3) strengthened the notion that U/FA.2 is the method of choice to elute target proteins of biotin-coupled drugs (Fig. 4C). Target

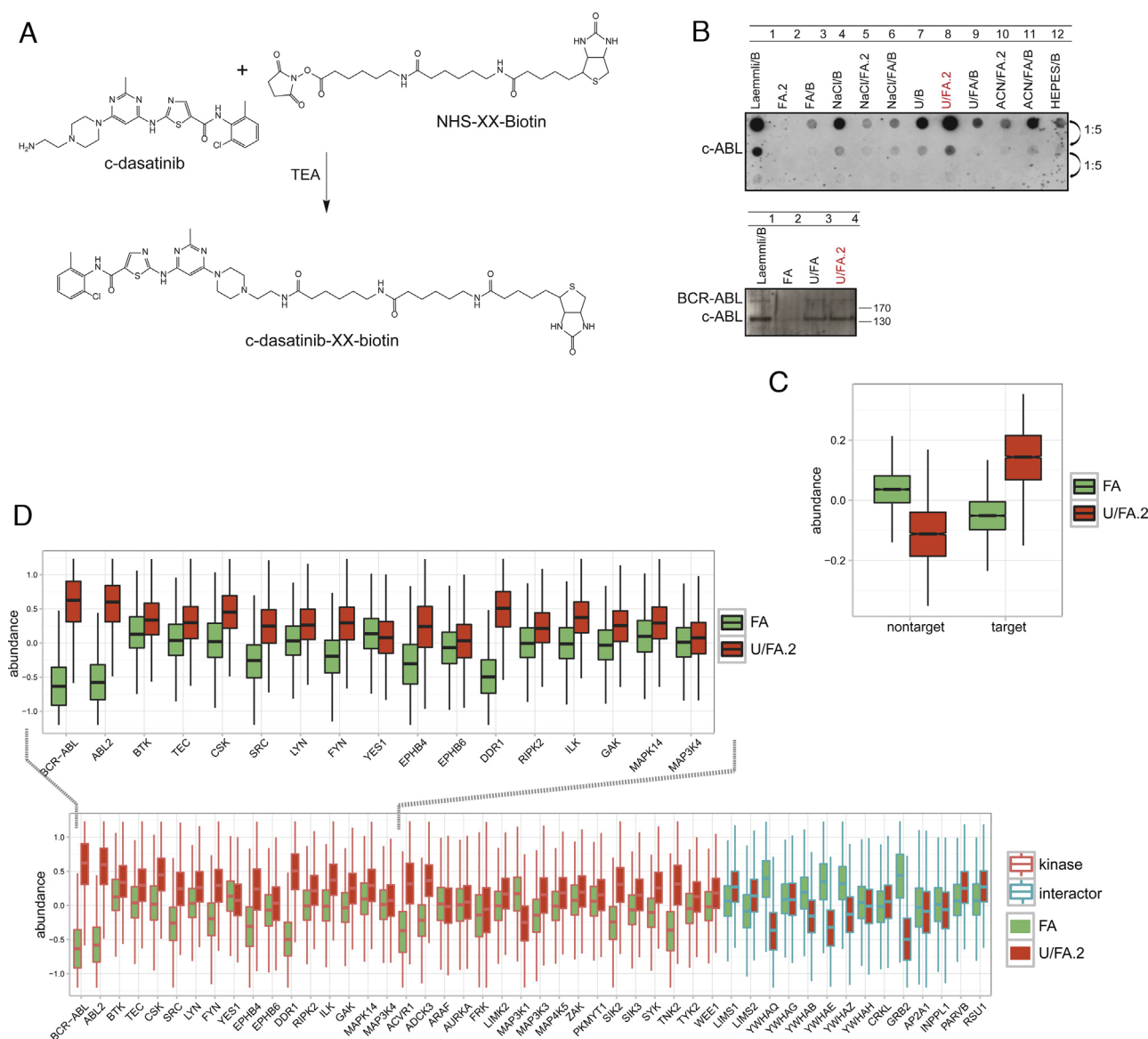


Fig. 4. Double elution with formic acid combined with urea improved the elution of proteins bound to biotinylated dasatinib. (A) Reaction to produce the biotinylated version of c-dasatinib for coupling to streptavidin beads. (B) Upper panel: anti-ABL dot blot of the pull-downs that were eluted with the various elution agents and procedures that were used in the c-dasatinib pull-downs. Five-fold serial dilutions from each eluate were also loaded. Double application of the eluate to the column is denoted as .2. B, boiled. Lower panel: anti-ABL western blot of pull-downs performed with the positive control (Laemmli), standard (FA) and U/FA (both single and double elution). Immunoblot signal for ABL is completely absent when the standard elution with 100 mM FA was used, whilst the signal is strong in the U/FA and U/FA.2 pull-downs. (C) Comparison of overall abundances between FA and U/FA.2. Four biological replicates were analysed (two technical replicates each). (D) The majority of cognate kinase targets of dasatinib are more abundant in U/FA.2 than FA. BCR-ABL was completely absent in the FA pull-downs, but had the highest recovery compared to other kinase targets when U/FA.2 was used as the elution method. An integrated plot showing differences in abundances between the FA and U/FA.2 elution methods is shown. Kinases and kinase-interacting proteins are indicated in the red and blue box plots, respectively. Recovery of all major kinase targets was improved with U/FA.2, whilst the majority of the kinase-interacting proteins (excluding the IPP complex) are less abundant. (For interpretation of the references to color in this figure legend, the reader is referred to the web version of this article.)

protein abundance was highly enriched for U/FA.2 (red) compared to FA alone (green). At the same time, non-target protein abundance was reduced. In addition, the ratio between target and non-target proteins was unfavorable for FA alone; whereas for the U/FA.2 elution, proteins that specifically interact with dasatinib were recovered with considerably higher abundance. This was even more apparent when specific dasatinib kinase targets were compared (Fig. 4D). In the FA pulldowns (green), BCR-ABL was completely absent, but was identified with high abundance by U/FA.2 elution (red). All other major targets of dasatinib were observed when the U/FA.2 elution method was applied, and in all cases recovery was enhanced compared to the standard method. Well-known targets that were identified with a notably higher abundance were ABL2 and receptor tyrosine kinases (DDR1, EPHB4). Several SRC and SRC-related kinases (CSK, LYN, FYN, and c-SRC), SYK, TNK2 (ACK1) and the serine-threonine kinases, ILK, GAK, MAPK14, MAP3K3 etc. were also observed with higher abundance (Fig. 4D). Perhaps even more remarkable than the observations made with the covalent drug immobilization experiments, was that all the secondary interactors (excluding the robust IPP complex) were identified with lower abundance (Fig. 4D). Furthermore, for both drug coupling approaches the increase in target recovery with U/FA.2 (Fig. 6A, red circles) was particularly noticeable for tyrosine kinases (including receptor tyrosine kinases). This observation was emphasised as the target recovery of RTKs with FA elution method was particularly underwhelming.

Differences in target profiles between chemically-coupled and biotinylated drug data were minor (Fig. 6A, two tones of orange). Moreover, excluding the kinases TESK (not enriched in the U/FA.2 eluate with c-dasatinib, and not identified in the c-dasatinib-biotinylated pulldowns) and ARAF (not enriched in the U/FA.2 eluate with c-dasatinib-XX-biotin, and not identified in the c-dasatinib pulldowns) (Fig. 6A, green); for all dasatinib targets U/FA.2 was more efficient than FA. Finally, the data led us to conclude that the observed improvement in the eluted protein profiles is not constrained to a particular class of kinases, but rather, to the overall increase in target capture (Fig. 6A).

4.4. Elution with the combination of formic acid and urea also improved identification of cognate targets of sunitinib

We next evaluated if the improvements observed with the U/FA.2 method were unique to dasatinib and target proteins; or if this would also translate to other drug-protein interactions. Therefore, sunitinib [34] was selected. Similar to dasatinib, this compound also has multiple targets, but the profile only displays minimal overlap with dasatinib [7,28,53]. Affinity chromatography with c-sunitinib was performed on human erythroid leukemia cells (Fig. 5A). HEL cells are known to express the RTK c-KIT, which is a cognate target of sunitinib. The data revealed that both FA and U/FA.2 elution successfully eluted c-KIT as shown by immunoblotting (Fig. 5B). Consistent with our previous observations using

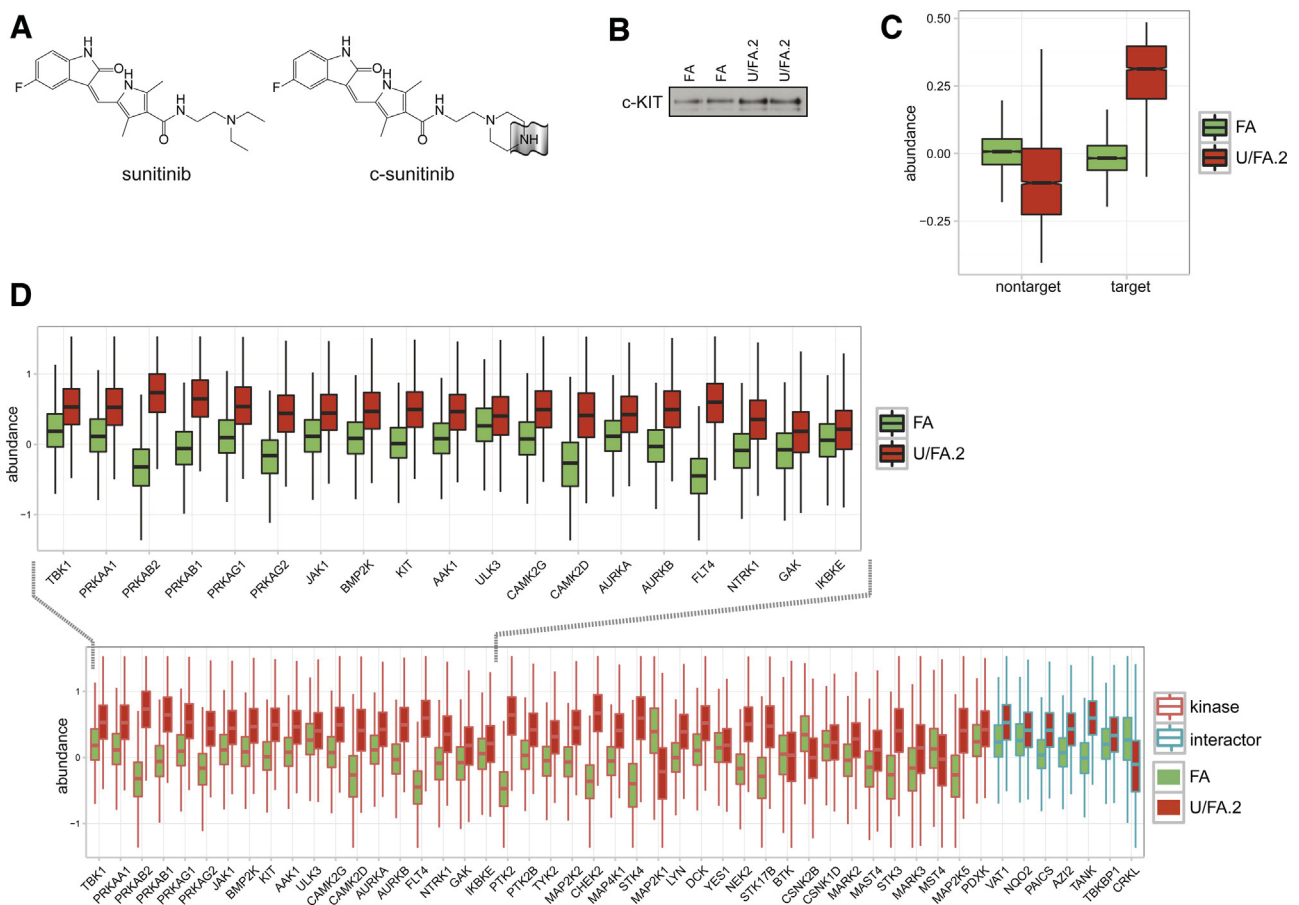


Fig. 5. Formic acid/urea double elution improved the identification of sunitinib targets. (A) Chemical structure of sunitinib and c-sunitinib. The latter is the chemically-modified version of sunitinib that can be coupled to sepharose beads via a linker. (B) Anti-KIT western blot of FA and U/FA.2 pulldowns. Immunoblot signal for U/FA.2 is stronger compared to the standard elution with 100 mM FA. (C) Comparison of overall abundances between FA and U/FA.2. A strong increase in abundance is observed for target proteins with U/FA.2. Two biological replicates were analysed (two technical replicates each). (D) The majority of cognate kinase targets of sunitinib are more abundant in U/FA.2 than FA. An integrated plot showing differences in abundances between the FA and U/FA.2 elution methods is shown. Kinases and kinase-interacting proteins are indicated in the red and blue box plots, respectively. (For interpretation of the references to color in this figure legend, the reader is referred to the web version of this article.)

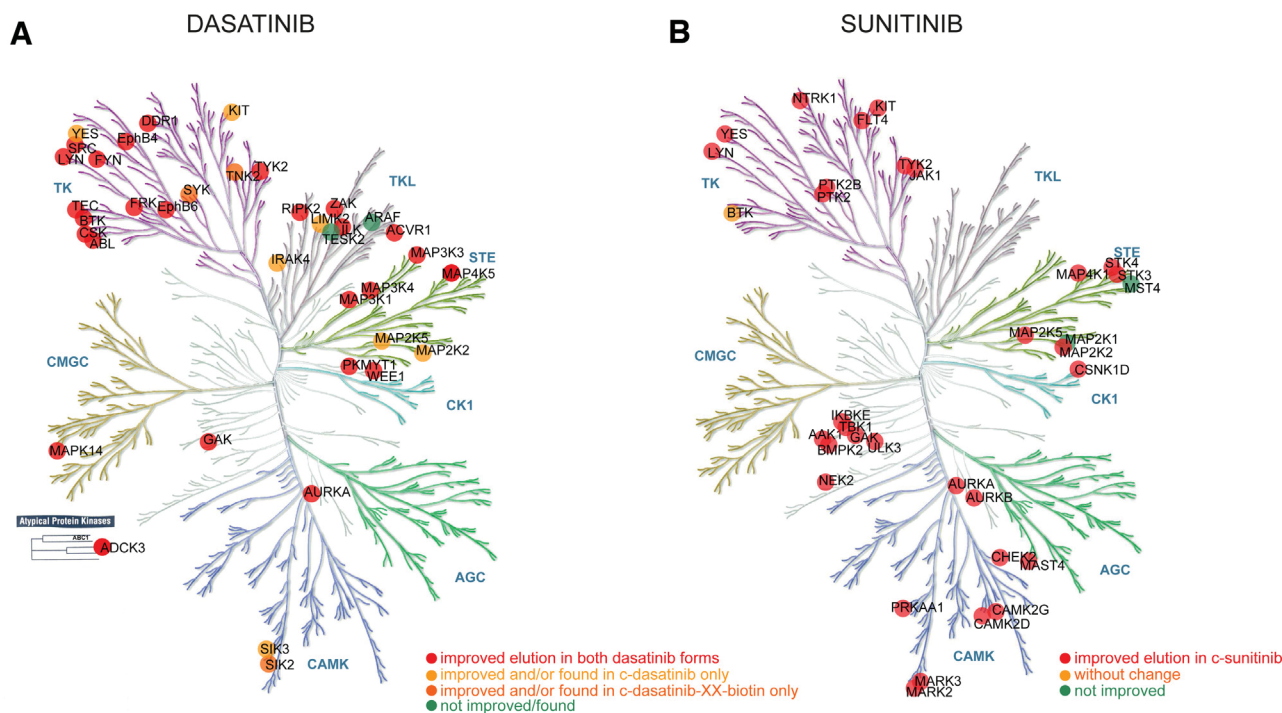


Fig. 6. Displayed on the kinome tree in red are the kinases that were observed with a higher abundance in the U/FA.2 elution method. The improvement in eluted protein profiles is not constrained to a particular class of kinases, but rather, the overall increase in target capture. (A) Kinome tree representation for both dasatinib coupling approaches. Kinases that were recovered with either c-dasatinib or c-dasatinib-XX-biotin are depicted in two different tones of orange, respectively. Kinases that had a higher recovery with the standard method are displayed in green. (B) In red are the kinases that were observed with a higher abundance in the U/FA.2 elution method in sunitinib pull-downs. The improvement in eluted protein profiles is not constrained to a particular branch and it is mostly reciprocal to dasatinib target distribution. Kinases that had same recovery are depicted in orange; the ones that had a higher recovery with the standard method are displayed in green. Illustration reproduced courtesy of Cell Signaling Technology, Inc. (www.cellsignal.com). (For interpretation of the references to color in this figure legend, the reader is referred to the web version of this article.)

dasatinib, U/FA.2 elution resulted in an improved recovery of c-KIT. Furthermore, subsequent LCMS analysis showed that both methods led to the identification of a large number of kinase targets. The overall elution efficiency across all targets, however, was dramatically enhanced with the urea/formic acid double elution (Fig. 5C). This improvement was particularly apparent when the data from other targets of sunitinib was compared, e.g., c-KIT, PRKAA1 (5'-AMP-activated protein kinase 1 alpha, AMPK1 α), or TBK1. As for dasatinib, this improvement was not restricted to a particular branch of the kinome tree (Fig. 6. A and B). Indirect binding proteins of kinases, such as regulatory subunits and multicomponent kinase complex partners of 5'-AMP-activated protein kinase (PRKAB1, PRKAB2, PRKAAG1, PRKAAG2 etc), or TBK1 (TANK, TBKBP1, AZI2) (Fig. 5D) also showed marked improvement. Furthermore, a number of non-dasatinib kinase targets were eluted more efficiently. These include tyrosine kinases JAK1, FLT4, NTRK1, PTK2 (FAK), PTK2B (FAK2) etc.; and serine/threonine NAK kinases (AAK1, BMP2K, GAK), IKK-related kinases (IKKBE, TBK1), and NEK kinases (NEK2). Calcium/calmodulin dependent protein kinases such as CAMK2D and CAMK2D were strongly enriched in the U/FA.2 eluates, in addition to CHEK2, MARK2 and MARK3. This data showed that the improvement in protein recovery observed with the U/FA double elution is widely applicable and not just restricted to a single drug or individual target protein thereof.

5. Conclusion

In this study, we report the successful optimization of chemical proteomics coupled to gel-free mass spectrometry. By introducing an adapted double elution method that is beneficial for both standard drug immobilization protocols and biotinylated drugs, we

could retrieve all cognate targets with higher efficiency compared to our previously preferred method. In general, the combination of a denaturing agent with formic acid led to an increase in the elution efficiency of drug targets; despite the fact that the concentration of formic acid was 2-fold lower. The double elution with a combination of 3 M urea and 50 mM formic acid resulted in paramount target recovery without comparable enrichment of non-specific proteins. This was not constrained neither to a particular branch of the kinome dendrogram, nor to a single drug. Furthermore, the success of this elution protocol with biotinylated compounds offers a promising prospect of also capturing covalent drug-protein interactions. We believe this adapted elution method will improve the characterization of cellular target profiles of small molecules. It is mild, rapid, affordable and efficient, and allows a wide spectrum of proteins to be captured in a single chemical proteomic experiment.

Conflict of interest

The authors declare no competing financial interests.

Author contributions

The manuscript was written with contributions from all authors. All authors have given approval to the final version of manuscript.

Acknowledgment

Research in our groups at CeMM is supported by the Austrian Academy of Sciences and the ASSET project funded by the

European Union within the FP7 framework. B.R.S. is financed by the ASSET project (HEALTH-F4-2010-259348).

Appendix A. Supplementary data

Supplementary data associated with this article can be found, in the online version, at <http://dx.doi.org/10.1016/j.euprot.2015.09.002>.

References

- [1] B.K. Wagner, P.A. Clemons, Connecting synthetic chemistry decisions to cell and genome biology using small-molecule phenotypic profiling, *Curr. Opin. Chem. Biol.* 13 (2009) 539–548.
- [2] J. Lee, M. Bogyo, Target deconvolution techniques in modern phenotypic profiling, *Curr. Opin. Chem. Biol.* 17 (2013) 118–126.
- [3] U. Rix, G. Superti-Furga, Target profiling of small molecules by chemical proteomics, *Nat. Chem. Biol.* 5 (2009) 616–624.
- [4] D.A. Tuveson, N.A. Willis, T. Jacks, J.D. Griffin, S. Singer, C.D. Fletcher, et al., STI571 inactivation of the gastrointestinal stromal tumor c-KIT oncoprotein: biological and clinical implications, *Oncogene* 20 (2001) 5054–5058.
- [5] E.J. Licitra, J.O. Liu, A three-hybrid system for detecting small ligand-protein receptor interactions, *Proc. Natl. Acad. Sci. U. S. A.* 93 (1996) 12817–12821.
- [6] O. Hantschel, U. Rix, U. Schmidt, T. Burckstummer, M. Kneidinger, G. Schutze, et al., The Btk tyrosine kinase is a major target of the Bcr-Abl inhibitor dasatinib, *Proc. Natl. Acad. Sci. U. S. A.* 104 (2007) 13283–13288.
- [7] M.I. Davis, J.P. Hunt, S. Herrgard, P. Ciceri, L.M. Wodicka, G. Pallares, et al., Comprehensive analysis of kinase inhibitor selectivity, *Nat. Biotechnol.* 29 (2011) 1046–1051.
- [8] K. Godl, J. Wissing, A. Kurtenbach, P. Habenberger, S. Blencke, H. Gutbrod, et al., An efficient proteomics method to identify the cellular targets of protein kinase inhibitors, *Proc. Natl. Acad. Sci. U. S. A.* 100 (2003) 15434–15439.
- [9] J. Drews, Case histories, magic bullets and the state of drug discovery, *Nat. Rev. Drug Discov.* 5 (2006) 635–640.
- [10] C. Chidley, H. Haruki, M.G. Pedersen, E. Muller, K. Johnsson, A yeast-based screen reveals that sulfasalazine inhibits tetrahydrobiopterin biosynthesis, *Nat. Chem. Biol.* 7 (2011) 375–383.
- [11] J. Lamb, E.D. Crawford, D. Peck, J.W. Modell, I.C. Blat, M.J. Wrobel, et al., The connectivity map: using gene-expression signatures to connect small molecules, genes, and disease, *Science* 313 (2006) 1929–1935.
- [12] G.C. Adam, E.J. Sorensen, B.F. Cravatt, Trifunctional chemical probes for the consolidated detection and identification of enzyme activities from complex proteomes, *Mol. Cell. Proteomics* 1 (2002) 828–835.
- [13] H. Daub, K. Godl, D. Brehmer, B. Klebl, G. Muller, Evaluation of kinase inhibitor selectivity by chemical proteomics, *Assay Drug Dev. Technol.* 2 (2004) 215–224.
- [14] D.A. Jeffery, M. Bogyo, Chemical proteomics and its application to drug discovery, *Curr. Opin. Biotechnol.* 14 (2003) 87–95.
- [15] H. Katayama, Y. Oda, Chemical proteomics for drug discovery based on compound-immobilized affinity chromatography, *J. Chromatogr. B* 855 (2007) 21–27.
- [16] U. Kruse, M. Bantscheff, G. Drews, C. Hopf, Chemical and pathway proteomics: powerful tools for oncology drug discovery and personalized health care, *Mol. Cell. Proteomics* 7 (2008) 1887–1901.
- [17] S.-E. Ong, M. Schenone, A.A. Margolin, X. Li, K. Do, M.K. Dou, et al., Identifying the proteins to which small-molecule probes and drugs bind in cells, *Proc. Natl. Acad. Sci. U. S. A.* 106 (2009) 4617–4622.
- [18] J. Rappsilber, M. Mann, Analysis of the topology of protein complexes using cross-linking and mass spectrometry, *CSH Protoc.* 2007 (2007) pdb prot4594.
- [19] Y. Oda, T. Owa, T. Sato, B. Boucher, S. Daniels, H. Yamanaka, et al., Quantitative chemical proteomics for identifying candidate drug targets, *Anal. Chem.* 75 (2003) 2159–2165.
- [20] D. Brehmer, Z. Greff, K. Godl, S. Blencke, A. Kurtenbach, M. Weber, et al., Cellular targets of gefitinib, *Cancer Res.* 65 (2005) 379–382.
- [21] U. Rix, O. Hantschel, G. Durnberger, L.L. Remsing Rix, M. Planyavsky, N.V. Fernbach, et al., Chemical proteomic profiles of the BCR-ABL inhibitors imatinib, nilotinib, and dasatinib reveal novel kinase and nonkinase targets, *Blood* 110 (2007) 4055–4063.
- [22] P.L. Ross, Y.N. Huang, J.N. Marchese, B. Williamson, K. Parker, S. Hattan, et al., Multiplexed protein quantitation in *Saccharomyces cerevisiae* using amine-reactive isobaric tagging reagents, *Mol. Cell. Proteomics* 3 (2004) 1154–1169.
- [23] N.V. Fernbach, M. Planyavsky, A. Muller, F.P. Breitwieser, J. Colinge, U. Rix, et al., Acid elution and one-dimensional shotgun analysis on an Orbitrap mass spectrometer: an application to drug affinity chromatography, *J. Proteome Res.* 8 (2009) 4753–4765.
- [24] E.B. Haura, A. Muller, F.P. Breitwieser, J. Li, F. Grebien, J. Colinge, et al., Using iTRAQ combined with tandem affinity purification to enhance low-abundance proteins associated with somatically mutated EGFR core complexes in lung cancer, *J. Proteome Res.* 10 (2011) 182–190.
- [25] G.E. Winter, U. Rix, S.M. Carlson, K.V. Gleixner, F. Grebien, M. Gridling, et al., Systems-pharmacology dissection of a drug synergy in imatinib-resistant CML, *Nat. Chem. Biol.* 8 (2012) 905–912.
- [26] G.E. Winter, U. Rix, A. Lissat, A. Stukalov, M.K. Mullner, K.L. Bennett, et al., An integrated chemical biology approach identifies specific vulnerability of Ewing's sarcoma to combined inhibition of aurora kinases A and B, *Mol. Cancer Ther.* 10 (2011) 1846–1856.
- [27] K.V. Huber, E. Salah, B. Radic, M. Gridling, J.M. Elkins, A. Stukalov, et al., Stereospecific targeting of MTH1 by (S)-crizotinib as an anticancer strategy, *Nature* 508 (2014) 222–227.
- [28] M. Gridling, S. Ficarro, F.P. Breitwieser, L. Song, K. Parapatics, J. Colinge, et al., Identification of kinase inhibitor targets in the lung cancer microenvironment by chemical and phosphoproteomics, *Mol. Cancer Ther.* (2014) .
- [29] U. Rix, J. Colinge, K. Blatt, M. Gridling, Rix L.L. Remsing, K. Parapatics, et al., A target-disease network model of second-generation BCR-ABL inhibitor action in Ph+ ALL, *PLoS One* 8 (2013) e77155.
- [30] V. Borgdorff, U. Rix, G.E. Winter, M. Gridling, A.C. Muller, F.P. Breitwieser, et al., A chemical biology approach identifies AMPK as a modulator of melanoma oncogene MITF, *Oncogene* 33 (2014) 2531–2539.
- [31] L.J. Lombardo, F.Y. Lee, P. Chen, D. Norris, J.C. Barrish, K. Behnia, et al., Discovery of N-(2-chloro-6-methyl-phenyl)-2-(6-(4-(2-hydroxyethyl)-piperazin-1-yl)-2-methylpyrimidin-4-ylamino) thiazole-5-carboxamide (BMS-354825), a dual Src/Abl kinase inhibitor with potent antitumor activity in preclinical assays, *J. Med. Chem.* 47 (2004) 6658–6661.
- [32] M. Kneidinger, U. Schmidt, U. Rix, K.V. Gleixner, A. Vales, C. Baumgartner, et al., The effects of dasatinib on IgE receptor-dependent activation and histamine release in human basophils, *Blood* 111 (2008) 3097–3107.
- [33] J. Li, U. Rix, B. Fang, Y. Bai, A. Edwards, J. Colinge, et al., A chemical and phosphoproteomic characterization of dasatinib action in lung cancer, *Nat. Chem. Biol.* 6 (2010) 291–299.
- [34] L. Sun, C. Liang, S. Shirazian, Y. Zhou, T. Miller, J. Cui, et al., Discovery of 5-[5-fluoro-2-oxo-1,2-dihydroindol-(3Z)-ylidenemethyl]-2,4-dimethyl-1H-pyrrole-3-carboxylic acid (2-diethylaminoethyl) amide, a novel tyrosine kinase inhibitor targeting vascular endothelial and platelet-derived growth factor receptor tyrosine kinase, *J. Med. Chem.* 46 (2003) 1116–1119.
- [35] J. Hartmann, L. Kanz, Sunitinib and periodic hair depigmentation due to temporary c-kit inhibition, *Arch. Dermatol.* 144 (2008) 1525–1526.
- [36] R. Kumar, M.C. Crouthamel, D.H. Rominger, R.R. Gontarek, P.J. Tummino, R.A. Levin, et al., Myelosuppression and kinase selectivity of multikinase angiogenesis inhibitors, *Br. J. Cancer* 101 (2009) 1717–1723.
- [37] T. Burckstummer, K.L. Bennett, A. Preradovic, G. Schutze, O. Hantschel, G. Superti-Furga, et al., An efficient tandem affinity purification procedure for interaction proteomics in mammalian cells, *Nat. Methods* 3 (2006) 1013–1019.
- [38] J. Rappsilber, Y. Ishihama, M. Mann, Stop and go extraction tips for matrix-assisted laser desorption/ionization, nano-electrospray, and LC/MS sample pretreatment in proteomics, *Anal. Chem.* 75 (2003) 663–670.
- [39] K.L. Bennett, M. Funk, M. Tschernutter, F.P. Breitwieser, M. Planyavsky, C. Ubaida Mohien, et al., Proteomic analysis of human cataract aqueous humour: comparison of one-dimensional gel LCMS with two-dimensional LCMS of unlabelled and iTRAQ(R)-labelled specimens, *J. Proteomics* 74 (2011) 151–166.
- [40] J.V. Olsen, L.M. de Godoy, G. Li, B. Macek, P. Mortensen, R. Pesch, et al., Parts per million mass accuracy on an Orbitrap mass spectrometer via lock mass injection into a C-trap, *Mol. Cell. Proteomics* 4 (2005) 2010–2021.
- [41] Y. Zhang, Z. Wen, M.P. Washburn, L. Florens, Refinements to label free proteome quantitation: how to deal with peptides shared by multiple proteins, *Anal. Chem.* 82 (2010) 2272–2281.
- [42] Stan Development Team. Stan: A C++ Library for Probability and Sampling, Version 2.4 2014.
- [43] L.O. Narhi, D.J. Caughey, T. Horan, Y. Kita, D. Chang, T. Arakawa, Effect of three elution buffers on the recovery and structure of monoclonal antibodies, *Anal. Biochem.* 253 (1997) 236–245.
- [44] B.S. Parekh, H.B. Mehta, M.D. West, R.C. Montelaro, Preparative elution of proteins from nitrocellulose membranes after separation by sodium dodecyl sulfate-polyacrylamide gel electrophoresis, *Anal. Biochem.* 148 (1985) 87–92.
- [45] M.J. Towle, K.A. Salvato, J. Budrow, B.F. Wels, G. Kuznetsov, K.K. Aalfs, et al., In vitro and in vivo anticancer activities of synthetic macrocyclic ketone analogues of halichondrin B, *Cancer Res.* 61 (2001) 1013–1021.
- [46] J. Colinge, U. Rix, K.L. Bennett, G. Superti-Furga, Systems biology analysis of protein-drug interactions, *Proteomics Clin. Appl.* 6 (2012) 102–116.
- [47] O. Hantschel, U. Rix, G. Superti-Furga, Target spectrum of the BCR-ABL inhibitors imatinib, nilotinib and dasatinib, *Leuk. Lymphoma* 49 (2008) 615–619.
- [48] M. Bantscheff, D. Eberhard, Y. Abraham, S. Bastuck, M. Boesche, S. Hobson, et al., Quantitative chemical proteomics reveals mechanisms of action of clinical ABL kinase inhibitors, *Nat. Biotechnol.* 25 (2007) 1035–1044.
- [49] L.C. Kim, U. Rix, E.B. Haura, Dasatinib in solid tumors, *Expert Opin. Investig. Drugs* 19 (2010) 415–425.
- [50] L.L. Remsing Rix, U. Rix, J. Colinge, O. Hantschel, K.L. Bennett, T. Stranzl, et al., Global target profile of the kinase inhibitor bosutinib in primary chronic myeloid leukemia cells, *Leukemia* 23 (2009) 477–485.
- [51] E.K. Greuber, P. Smith-Pearson, J. Wang, A.M. Pendergast, Role of ABL family kinases in cancer: from leukaemia to solid tumours, *Nat. Rev. Cancer* 13 (2013) 559–571.
- [52] K.R. Legate, E. Montanez, O. Kudlacek, R. Fassler, ILK, PINCH and parvin: the tIPP of integrin signalling, *Nat. Rev. Mol. Cell Biol.* 7 (2006) 20–31.
- [53] T. Anastassiadis, S.W. Deacon, K. Devarajan, H. Ma, J.R. Peterson, Comprehensive assay of kinase catalytic activity reveals features of kinase inhibitor selectivity, *Nat. Biotechnol.* 29 (2011) 1039–1045.

3.2 Manuscript #2: Stereospecific targeting of MTH1 by (S)-crizotinib as an anticancer strategy.

Huber KV, Salah E, Radic B, Gridling M, Elkins JM, Stukalov A, Jemth AS, Göktürk C, Sanjiv K, Strömberg K, Pham T, Berglund UW, Colinge J, Bennett KL, Loizou JI, Helleday T, Knapp S, Superti-Furga G

We observed that SCH51344, a phenotypic “RAS inhibitor”, directly targets MTH1, a nucleotide pool sanitizing enzyme whose inhibition suppresses tumor growth. We validated MTH1 as the causal target for the antiproliferative effects of the drug and performed an MTH1 inhibitor screen to find more favorable candidates; the clinically approved kinase inhibitor crizotinib showed high affinity towards MTH1. Chemical proteomic approach allowed deciphering the complete target spectrum of both crizotinib enantiomers. Targeting homeostasis of the cellular nucleotide pool emerged as a promising option for cancer therapy.

Stereospecific targeting of MTH1 by (S)-crizotinib as an anticancer strategy

Kilian V. M. Huber¹, Eidarus Salah², Branka Radic¹, Manuela Gridling¹, Jonathan M. Elkins², Alexey Stukalov¹, Ann-Sofie Jemth³, Camilla Göktürk³, Kumar Sanjiv³, Kia Strömberg³, Therese Pham³, Ulrika Warpman Berglund³, Jacques Colinge¹, Keiryn L. Bennett¹, Joanna I. Loizou¹, Thomas Helleday³, Stefan Knapp² & Giulio Superti-Furga¹

Activated RAS GTPase signalling is a critical driver of oncogenic transformation and malignant disease. Cellular models of RAS-dependent cancers have been used to identify experimental small molecules, such as SCH51344, but their molecular mechanism of action remains generally unknown. Here, using a chemical proteomic approach, we identify the target of SCH51344 as the human mutT homologue MTH1 (also known as NUDT1), a nucleotide pool sanitizing enzyme. Loss-of-function of MTH1 impaired growth of KRAS tumour cells, whereas MTH1 overexpression mitigated sensitivity towards SCH51344. Searching for more drug-like inhibitors, we identified the kinase inhibitor crizotinib as a nanomolar suppressor of MTH1 activity. Surprisingly, the clinically used (R)-enantiomer of the drug was inactive, whereas the (S)-enantiomer selectively inhibited MTH1 catalytic activity. Enzymatic assays, chemical proteomic profiling, kinome-wide activity surveys and MTH1 co-crystal structures of both enantiomers provide a rationale for this remarkable stereospecificity. Disruption of nucleotide pool homeostasis via MTH1 inhibition by (S)-crizotinib induced an increase in DNA single-strand breaks, activated DNA repair in human colon carcinoma cells, and effectively suppressed tumour growth in animal models. Our results propose (S)-crizotinib as an attractive chemical entity for further pre-clinical evaluation, and small-molecule inhibitors of MTH1 in general as a promising novel class of anticancer agents.

Mutations in RAS isoforms are prevalent in human cancers, accompanied by poor prognosis and low survival, highlighting the need to develop new therapies^{1–3}. Direct modulation of RAS activity has posed a significant challenge in drug discovery. Therefore, alternative approaches have been used, for example by interfering with RAS posttranslational modifications to prevent maturation and translocation of the active protein to the plasma membrane^{4–6}. In addition, phenotypic screens have been used to search for small molecules that selectively target RAS-transformed cancer cells⁷. In 1995, this led to the discovery of a compound termed SCH51344 that suppressed the anchorage-independent growth of RAS-transformed fibroblasts⁸. As SCH51344 did not affect MAPK signalling, which is thought to be the primary mediator of RAS oncogenic activity, a novel but enigmatic mode of action was proposed⁹.

Identification of MTH1 as the main target of SCH51344

We set out to identify the cellular targets of SCH51344 using a chemical proteomic strategy (Fig. 1a). We generated a SCH51344 affinity probe (Fig. 1b) which we incubated with lysates of KRAS-positive SW480 cells, which are sensitive to SCH51344, and analysed the binding proteins by mass spectrometry. High-affinity binders were discriminated against highly abundant low-affinity proteins by competition with the free unmodified compound. Bioinformatic analysis revealed the human 7,8-dihydro-8-oxoguanine triphosphatase MTH1 (also known as NUDT1) and adenosine kinase (ADK) as the primary cellular targets of SCH51344 (Fig. 1c). MTH1 has been implicated in aiding RAS-transformed cells to overcome oncogene-induced senescence by preventing reactive oxygen species (ROS)-induced DNA damage¹⁰. On the contrary, little was known about the role of ADK in malignant disease, but in line with published RNA interference data¹¹ we did not observe any growth impairment of SCH51344-sensitive⁸ PANC1 human pancreatic carcinoma cells upon treatment with the ADK inhibitor

ABT-702 (data not shown). We therefore focused on MTH1 as the most likely relevant target of SCH51344. Having confirmed the binding of SCH51344 to MTH1 in both SW480 and DLD1 cells by immunoblot (Extended Data Fig. 1a), we used isothermal titration calorimetry (ITC) to determine a K_d value of 49 nM for SCH51344 (Fig. 1d and Extended Data Fig. 1b). MTH1 is a homologue of the bacterial mutT, a nucleotide pool sanitizing enzyme which cleaves oxidized nucleotides such as 8-oxo-deoxyguanosinetriphosphate (8-oxo-dGTP), thereby converting the triphosphates into the corresponding monophosphates¹². The hydrolysis reaction ensures that the oxidized nucleotides can no longer be recognized by DNA polymerase, preventing the mispairing of bases during replication and thus transversion mutations^{13,14}. To investigate the effect of SCH51344 on MTH1 catalytic activity we monitored the production of pyrophosphate (PPi) as a result of nucleotide triphosphate hydrolysis¹⁵. We determined half-maximum inhibitory concentration (IC₅₀) values of 215 nM, 410 nM and 675 nM for SCH51344 against the MTH1 substrates dGTP, 8-oxo-dGTP and 2-OH-dATP, respectively, confirming a direct effect of SCH51344 on MTH1 catalytic activity (Fig. 1e). To validate MTH1 as the causal target for the antiproliferative effects of SCH51344, we transfected human SW480 and DLD1 cells with *NUDT1* (MTH1) short interfering RNA that impaired colony formation (Fig. 1f). Stable knockdown using lentiviral short hairpin RNAs¹⁶ phenocopied results obtained using the inhibitor (Extended Data Fig. 1c). Conversely, overexpression of MTH1¹⁰ reduced sensitivity of SW480 cells against SCH51344 (Fig. 1g and Extended Data Fig. 1d), mechanistically corroborating the evidence that MTH1 is the main cellular target of SCH51344.

The (S)-crizotinib enantiomer inhibits MTH1 activity

Because SCH51344 has not been evaluated in a clinical setting, we decided to screen for other, more potent MTH1 inhibitors with favourable

¹CeMM Research Center for Molecular Medicine of the Austrian Academy of Sciences, 1090 Vienna, Austria. ²Nuffield Department of Clinical Medicine, Structural Genomics Consortium, University of Oxford, Old Road Campus Research Building, Roosevelt Drive, Oxford OX3 7DQ, UK. ³Science for Life Laboratory, Division of Translational Medicine and Chemical Biology, Department of Medical Biochemistry and Biophysics, Karolinska Institutet, 17121 Stockholm, Sweden.

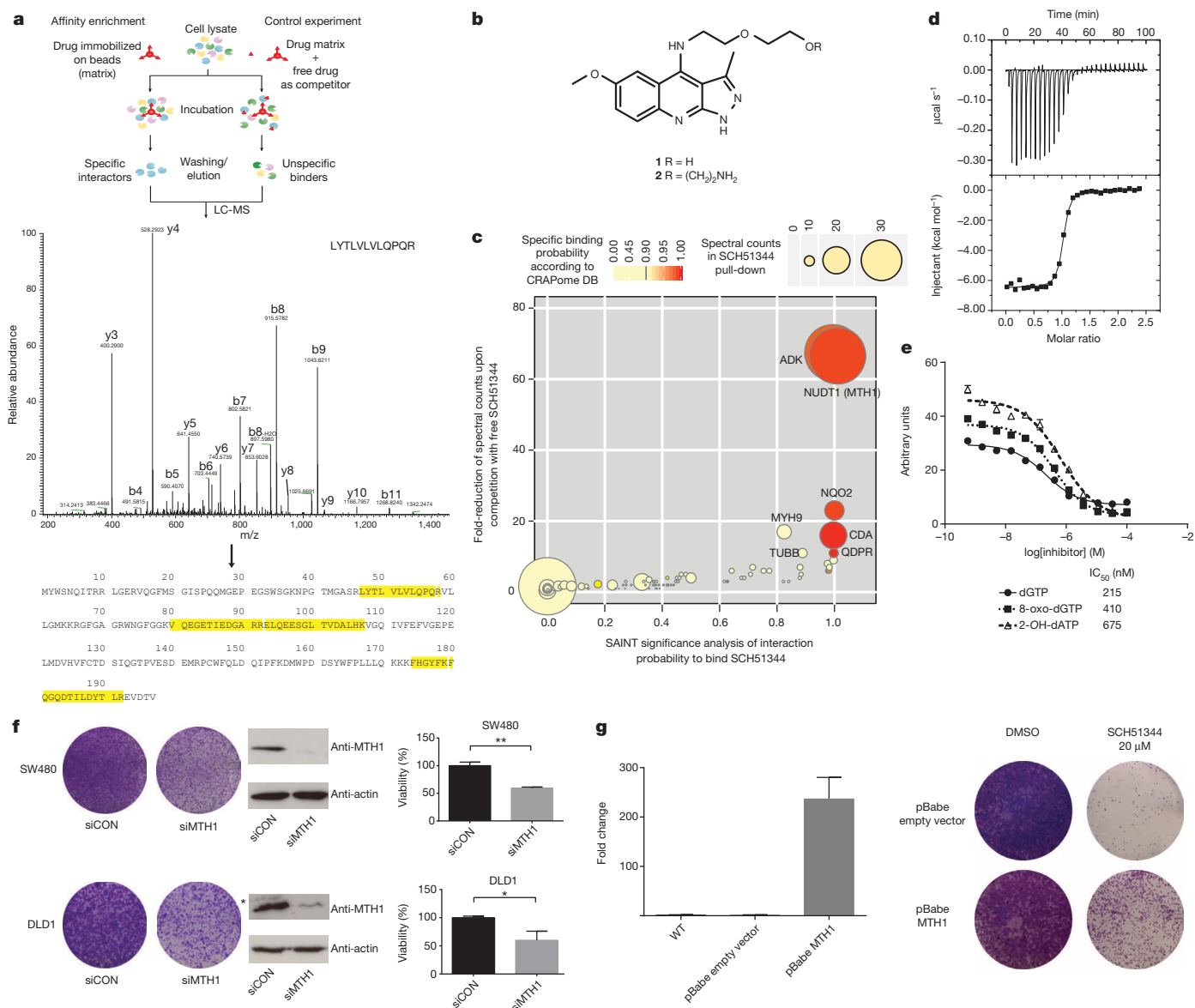


Figure 1 | MTH1 is the target of SCH51344. **a**, Representation of the chemical proteomic workflow. **b**, Structures of SCH51344 (1) and the probe used for affinity purification (2). **c**, Results from mass-spectrometry-based proteomic affinity purification experiment using SAINT and competition analysis. Data shown are based on two independent experiments for each condition ($n = 2$ per condition), and each replicate was analysed in two technical replicates. **d**, ITC data for MTH1 with SCH51344. The measured K_d was 49 nM ($n = 1$). **e**, SCH51344 inhibits hydrolysis of the MTH1 substrates dGTP, 8-oxo-dGTP and 2-OH-dATP, respectively. Data are shown for two

technical replicates ± s.e.m. and are representative of at least duplicate experiments ($n \geq 2$). **f**, Silencing of MTH1 by siRNA impairs colony formation of KRAS-positive SW480 (top) and DLD1 (bottom) cells. Data shown as mean ± s.e.m. and images are representative of triplicate experiments ($n = 3$) ($P < 0.05$, t -test). Asterisk denotes unspecific band. **g**, MTH1 overexpression as monitored by real-time PCR (left) restores SW480 cell viability upon SCH51344 treatment (right). Data shown as mean ± s.e.m. and images are representative of three independent experiments ($n = 3$). WT, wild type.

pharmacokinetic and pharmacodynamic properties. On the basis of substrates and active site architecture we proposed that kinase inhibitors may target MTH1. Screening a kinase inhibitor collection in a thermal shift stability assay¹⁷ we found that the dual c-MET/ALK inhibitor crizotinib^{18,19} exhibited high affinity towards MTH1 (data not shown). Crizotinib recently received approval for the treatment of EML4-ALK-positive non-small cell lung cancer (NSCLC) and is in several other clinical trials^{20–23}. However, using the catalytic MTH1 assay, we found that crizotinib batches obtained from different vendors resulted in varying IC_{50} values. This could not be explained by impurities or degradation products as analytical data were in accordance with literature¹⁸. Because crizotinib bears a chiral centre, we speculated that variable amounts of crizotinib stereoisomers may occur in different batches of inhibitor. We prepared and tested both the pure, clinically used (*R*)- as well as the so

far unexplored (*S*)-enantiomer of crizotinib in the MTH1 catalytic assay, which suggested that the screening hit batch contained a racemic mixture. We found that pure (*S*)-crizotinib was a low nanomolar MTH1 inhibitor whereas the (*R*)-enantiomer gave IC_{50} values in the micromolar range (Fig. 2a). These data were confirmed by direct-binding assays (ITC), indicating a 16-fold higher affinity of the (*S*)-enantiomer towards MTH1 (Fig. 2b and Extended Data Fig. 2a). Using K_m concentrations of substrates^{12,15}, we determined average IC_{50} values of 330 nM and 408 nM for (*S*)-crizotinib and the MTH1 substrates 8-oxo-dGTP and 2-OH-dATP, respectively ($n = 2$). Consistent with these data, (*S*)-crizotinib efficiently inhibited colony formation of SW480 cells and KRAS-mutated PANC1 cells, similar to SCH51344 (Fig. 2c, d). *In vitro* K_d measurements indicated that (*S*)-crizotinib was considerably less potent than the (*R*)-enantiomer against the established targets ALK, MET and ROS1 (Extended

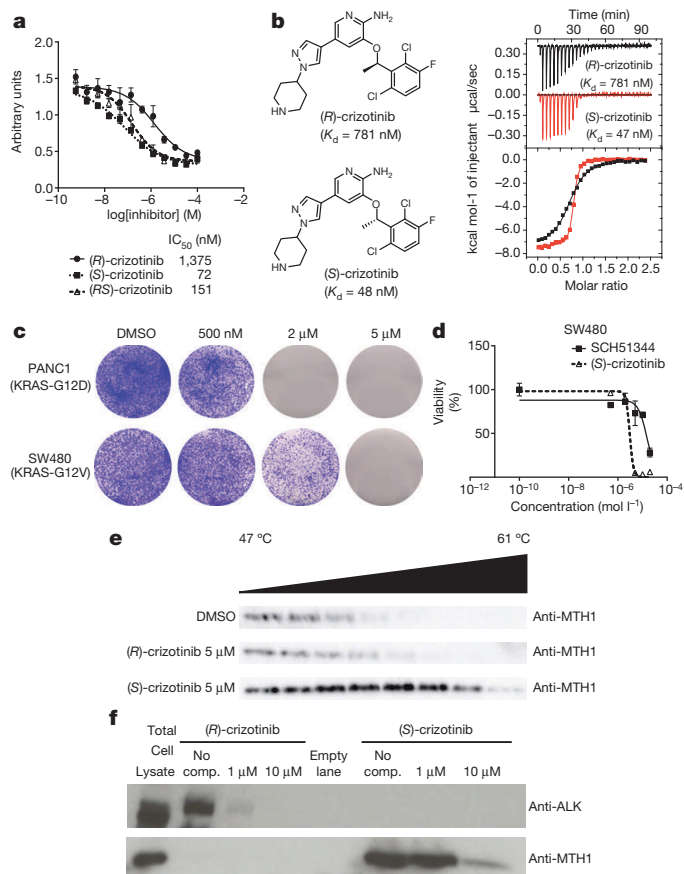


Figure 2 | (*S*)-Crizotinib is a nanomolar MTH1 inhibitor. **a**, MTH1 catalytic assay. Data are shown for both crizotinib enantiomers and the racemic mixture at 100 μ M dGTP. Results indicate two technical replicates \pm s.e.m. representative of at least duplicate experiments ($n \geq 2$). **b**, ITC for MTH1 with (*R*)- and (*S*)-crizotinib ($n = 1$). **c**, (*S*)-Crizotinib inhibits colony formation of PANC1 and SW480 cells. Images are representative of three independent experiments ($n = 3$). **d**, Comparison of antiproliferative efficacy of (*S*)-crizotinib versus SCH51344 against SW480 cells. Data shown as mean \pm s.e.m. for three independent experiments ($n = 3$). **e**, Cellular thermal shift assay showing MTH1 target engagement by (*S*)-crizotinib in intact KRASV12-expressing BJ cells. Images are representative of two independent experiments ($n = 2$). **f**, The (*S*)-crizotinib affinity probe selectively binds MTH1, but not ALK, in SW480 lysates, whereas the (*R*)-enantiomer exerts inverse properties.

Data Fig. 2b). Treatment of SW480 cells with a specific c-MET inhibitor, a potential off-target for (*S*)-crizotinib¹⁸, did not lead to the detection of any significant effects on proliferation (Extended Data Fig. 2c). However, investigating whether MTH1 overexpression could rescue SW480 cells from cell death induced by (*S*)-crizotinib in a similar manner as for SCH51344, we failed to observe any significant shift in IC_{50} values (Extended Data Fig. 2d), raising the question whether other targets contributed to the cell killing effect. We started investigating whether MTH1 was indeed targeted by (*S*)-crizotinib in intact cells. If a cellular protein is bound by a chemical agent, it is stabilized by the physical engagement compared to the non-engaged counterpart²⁴. In a cellular thermal shift assay using BJ-KRASV12 cells, (*S*)-crizotinib, in contrast to (*R*)-crizotinib, efficiently stabilized MTH1 validating the differential targeting within cells (Fig. 2e).

Specificity of (*S*)-crizotinib and analysis of binding mode

To further investigate the ability of the two crizotinib enantiomers to engage cellular proteins, we derived chemical probes suitable for drug pull-downs (Supplementary Information). We tested two derivatized

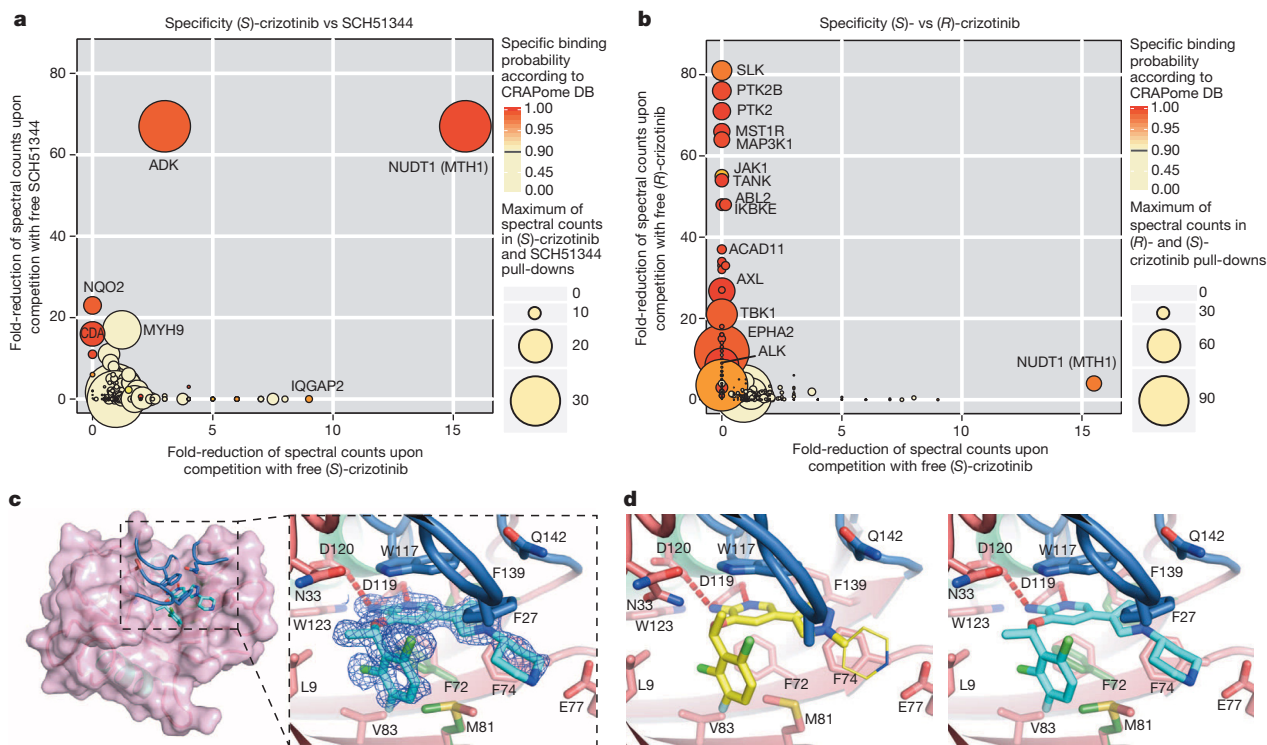


Figure 3 | Specificity and MTH1 co-crystal structure of (*S*)-crizotinib. **a**, **b**, Comparison of (*S*)-crizotinib specificity versus SCH51344 (**a**) and (*R*)-crizotinib (**b**). MTH1 is the only shared target with SCH51344 and is specific to (*S*)-crizotinib when compared to (*R*)-crizotinib. Data represent two independent experiments for each condition ($n = 2$ per condition), and each replicate was analysed in two technical replicates. **c**, Co-crystal structure of (*S*)-crizotinib and MTH1. MTH1 is in pink with light green α -helices and

the loops covering the binding site in blue. Hydrogen-bonding interactions are shown by dashed red lines. **d**, MTH1 interactions with (*R*)- and (*S*)-crizotinib. Left panel shows (*R*)-crizotinib in yellow; the thinner lines indicate part of the (*R*)-crizotinib that was not resolved in the electron density. Right panel shows (*S*)-crizotinib in cyan; alternate protein conformations in the absence of (*S*)-crizotinib are shown in dark green.

compounds for their ability to target ALK and MTH1 in SW480 cell extracts. The two enantiomers were remarkably specific for their cognate targets (Fig. 2f). If MTH1 was indeed the key target of (*S*)-crizotinib in other RAS-transformed cells, it should rank at the top of the specific interactors in an unbiased chemical proteomic experiment as done before with SCH51344. MTH1 was by far the most specific and prominent interactor of (*S*)-crizotinib (Extended Data Fig. 2e). Plotting the chemical proteomic results of SCH51344 and (*S*)-crizotinib against each other singled out MTH1 as the only common high-significance interactor (Fig. 3a). We also performed the reciprocal analysis with (*R*)-crizotinib which identified a plethora of protein kinases, all efficiently competed by free drug, but not MTH1 (Extended Data Fig. 2f). Notably, comparison of both profiles did not reveal any proteins that were significantly bound by both enantiomers (Fig. 3b). To exclude that either crizotinib enantiomer may target kinases of low abundance we interrogated a panel of 456 different recombinant kinases (KINOMEScan, Extended Data Fig. 3)²⁵. In line with the chemoproteomic results the two enantiomers showed a remarkable stereoselectivity with very distinct profiles. The few kinases to which (*S*)-crizotinib showed some affinity were not calculated to be significantly inhibited. (*R*)-Crizotinib not only bound to ten times more kinases, but was also predicted to efficiently inhibit at least ten of them, including the well characterized cognate targets ALK and MET, but also LCK, IRAK1, JAK3, LOK (also known as STK10) and SLK. To understand the differences in MTH1 binding, we co-crystallized both (*R*)- and (*S*)-crizotinib with recombinant protein. The structure revealed an unfavourable eclipsed conformation of the methyl group at the chiral centre and a chlorine substituent on the benzyl ring is likely to reduce the energetic favourability of (*R*)-crizotinib binding

(Fig. 3c, d and Extended Data Figs 4 and 5). ITC data confirmed that the difference in binding between (*R*)- and (*S*)-crizotinib was entirely entropic and therefore not due to different binding interactions with the protein (Fig. 2b).

MTH1 inhibitors induce DNA damage in cancer cells

Because MTH1 is thought to prevent incorporation of oxidized nucleotides into DNA, we reasoned that our new MTH1 inhibitors should increase the content of genomic 8-oxo-guanine, and thus induce DNA damage. Immunofluorescence staining for both 53BP1 (also known as TP53BP1) and autophosphorylated ATM, specific markers for DNA damage, was increased in SW480 cells treated with MTH1 inhibitors (Fig. 4a and Extended Data Fig. 6a). 53BP1 foci, which we also observed in cells transfected with MTH1-siRNA, were enriched in nuclei of cells with higher levels of 8-oxo-guanine owing to increased genomic incorporation (Extended Data Fig. 6b, c). We also tried to quantify the oxidized nucleotides by high-performance liquid chromatography coupled with mass spectrometry; however, due to high experimental background, we failed to obtain reliable results. Because accumulation of 8-oxo-guanine should activate base-excision repair (BER)¹⁶ and induce DNA single-strand breaks, we tested our inhibitors in an alkaline comet assay. Both (*S*)-crizotinib as well as SCH51344, but not (*R*)-crizotinib, yielded a significant tail moment, similar to cells transfected with MTH1-siRNA (Fig. 4b). Addition of the purified 8-oxo-guanine- or 2-hydroxy-adenine-specific DNA glycosylases, OGG1 and MUTYH, increased tail moments for (*S*)-crizotinib markedly, providing evidence for strong accumulation of these lesions upon inhibitor treatment (Extended Data Fig. 6d). MTH1 overexpression significantly reduced the number of DNA single-strand

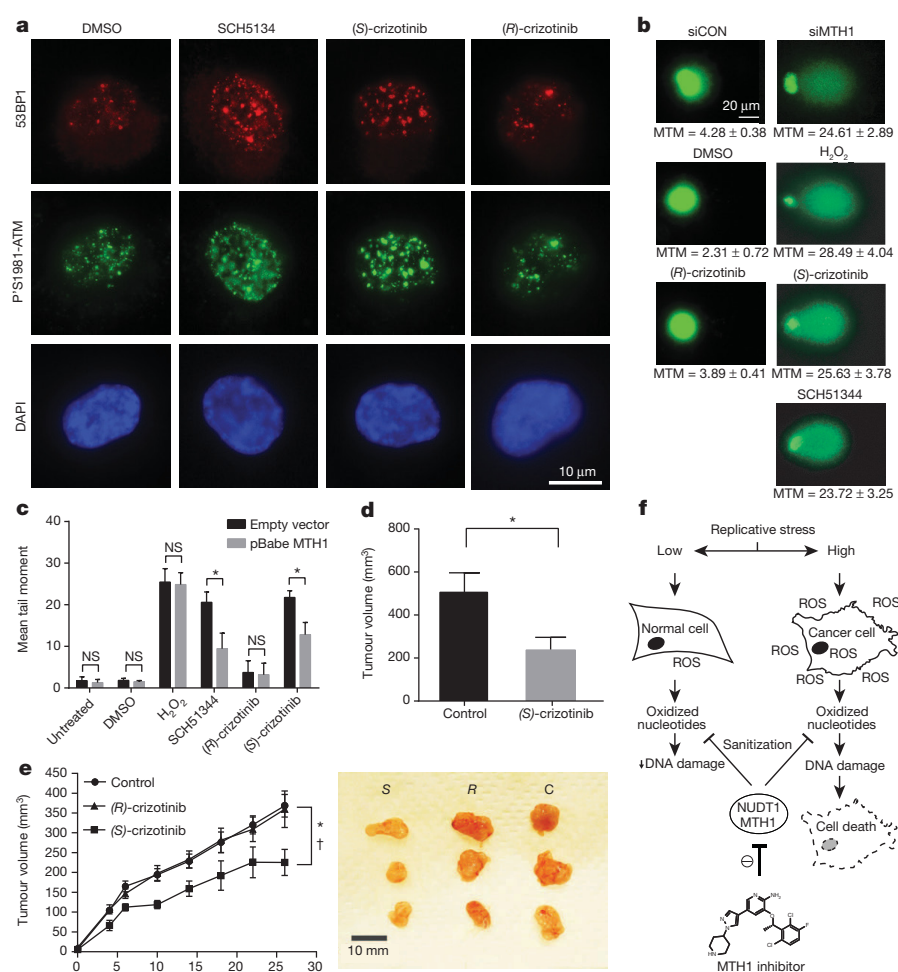


Figure 4 | (*S*)-Crizotinib is a selective MTH1 inhibitor with *in vivo* anticancer activity. **a**, The MTH1 inhibitors SCH51344 (5 μ M) and (*S*)-crizotinib (2 μ M), but not (*R*)-crizotinib (2 μ M), induce DNA damage as indicated by an increase in 53BP1 foci and ATM autophosphorylation. Images are representative of three independent experiments ($n = 3$). **b**, Comet assay. Similar to MTH1 gene silencing both SCH51344 (5 μ M) and (*S*)-crizotinib (2 μ M), but not (*R*)-crizotinib (2 μ M), induce DNA single-strand breaks. H₂O₂ was used as a positive control (150 μ M, 10 min). Images are representative of three independent experiments ($n = 3$); data are shown as mean \pm s.d. MTM, mean tail moment. **c**, MTH1 overexpression reduces the number of DNA single-strand breaks induced by SCH51344 and (*S*)-crizotinib. Compound concentrations are as in **b**. Data are shown as mean \pm s.d. based on three independent experiments ($n = 3$). NS, not significant. **d**, Results from SW480 mouse xenograft study. Effect on tumour growth following 35-day treatment with the MTH1 inhibitor (*S*)-crizotinib (25 mg per kg, subcutaneously daily; data are shown as mean \pm s.e.m., $n = 8$ per group). **e**, (*S*)-Crizotinib, but not (*R*)-crizotinib, impairs tumour growth in an SW480 colon carcinoma xenograft model (50 mg per kg, orally, daily). Data show mean \pm s.e.m., $n = 7-8$ animals per group. Statistical analysis performed by two-way repeat measurement ANOVA, Sidak's multiple comparison; * $P < 0.05$ (*S*)-crizotinib vs control; † $P < 0.05$ (*S*)-crizotinib vs (*R*)-crizotinib. Images depict representative tumours for each treatment group (C, control). **f**, Proposed mechanism for MTH1-inhibitor-induced cancer cell death.

breaks induced by (*S*)-crizotinib as well as SCH51344, but not by H₂O₂ (Fig. 4c and Extended Data Fig. 6e), providing evidence for MTH1 being the functionally relevant target. To explore the role of p53 in the cellular response to MTH1 suppression¹⁶ we created an SW480 Tet-on system²⁶ allowing for the inducible expression of p53 shRNAs and treated the cells with our inhibitors (Extended Data Fig. 7), which indicated a p53-independent mode of action. Treatment of SW480 cells expressing anti-MTH1 shRNA with the ATM- and ATR-inhibitors KU55933 and VE821, respectively, also did not display any differential effects (Extended Data Fig. 8). Similarly, *Atm*^{-/-} mouse embryonic fibroblasts were equally sensitive to MTH1 inhibitors as their *Atm*-proficient counterparts. Investigating cell lines bearing additional mutations in DNA repair genes, we found that HCT116 cells deficient for p21 were particularly sensitive to (*S*)-crizotinib. We tested our inhibitors in BJ skin fibroblasts that were either wild type, immortalized by hTERT, or transformed by SV40T and/or mutant KRAS. Both SCH51344 and (*S*)-crizotinib showed highest toxicity towards the SV40T and KRASV12 cells (Extended Data Fig. 9). Importantly, when we treated wild type BJ cells with (*R*)- or (*S*)-crizotinib, we found that the (*S*)-enantiomer did not show any increased toxicity on non-transformed cells. Among a panel of human cancer cell lines, we consistently observed a strong antiproliferative effect for (*S*)-crizotinib, in line with its lower catalytic assay IC₅₀ value. To explore the *in vivo* potential of (*S*)-crizotinib to impair tumour growth we performed mouse xenograft studies using SW480 cells. These experiments indicated that (*S*)-crizotinib, but not the (*R*)-enantiomer, was able to impair overall tumour progression as well as specifically reduce tumour volume by more than 50% (Fig. 4d, e and Extended Data Fig. 10a–c). This suggested that the two enantiomers have clearly diverse antitumour profiles and was consistent with their distinct molecular mechanism of action.

Targeting nucleotide pool homeostasis as cancer therapy

Increased levels of ROS in fast-proliferating cancer cells impair nucleotide pool homeostasis and contribute to mutations and DNA damage¹⁰. Removal of oxidized nucleotides by MTH1 may relieve cancer cells from proliferative stress and thereby represent a vulnerability factor and an attractive target for anticancer compounds (Fig. 4f)²⁷. MTH1 levels are increased in RAS-expressing cancers (Extended Data Fig. 10d) ranging from lung cancer^{28,29} to renal carcinoma³⁰, supportive of the notion that there is a connection between oncogenic transformation and oxidative stress. A potential more global role of MTH1 in tumorigenesis is supported by the observed antiproliferative effects for the inhibitors on cancer cells transformed by mechanisms other than RAS mutations (Extended Data Fig. 9c)⁸. Although prolonged clinical application will need to be evaluated critically in light of an increased long-term tumour burden in *Mth1*^{-/-} (also known as *Nudt1*^{-/-}) mice, the mild phenotype of these knockout animals³¹, and the specificity of MTH1 inhibitors speak for an appropriate therapeutic window. We propose that MTH1, together with other enzymes controlling sanitization of oxidized nucleotides, may represent a new attractive targeting strategy for difficult-to-treat tumours that display high levels of replicative and oxidative stress. The identification of the chemical mirror image of a recently clinically approved anticancer agent, crizotinib, as a nanomolar inhibitor of a yet pharmacologically unexploited cellular process, argues for further high-priority pre-clinical and clinical studies. A thorough investigation of the pharmacodynamics and pharmacokinetic properties of (*S*)-crizotinib will be necessary to understand why overexpression of MTH1 failed to rescue its cell-killing effects under the conditions tested. Until then, the possibility remains that targets other than MTH1 contribute to the effects of (*S*)-crizotinib. Whereas (*S*)-crizotinib is technically a new chemical entity and would require a new, separate drug approval process, the fact that it differs from a safe and bioavailable drug only in one chiral centre makes it somewhat more likely to have favourable, drug-like properties³² and thus may be auspicious for an efficient evaluation of the potential therapeutic merits.

METHODS SUMMARY

Drug-affinity matrices were prepared by immobilizing 25 nmol of compound on 50 µl *N*-hydroxysuccinimide (NHS)-activated Sepharose 4 Fast Flow beads (GE Healthcare Bio-Sciences AB, Uppsala, Sweden). Detailed procedures for affinity chromatography, elution and mass spectrometry analyses are provided in the supporting information.

Online Content Any additional Methods, Extended Data display items and Source Data are available in the online version of the paper; references unique to these sections appear only in the online paper.

Received 22 March 2013; accepted 4 March 2014.

Published online 2 April 2014.

1. Pylyayeva-Gupta, Y., Grabocka, E. & Bar-Sagi, D. RAS oncogenes: weaving a tumorigenic web. *Nature Rev. Cancer* **11**, 761–774 (2011).
2. Parada, L. F., Tabin, C. J., Shih, C. & Weinberg, R. A. Human EJ bladder carcinoma oncogene is homologue of Harvey sarcoma virus *ras* gene. *Nature* **297**, 474–478 (1982).
3. Der, C. J., Kroniris, T. G. & Cooper, G. M. Transforming genes of human bladder and lung carcinoma cell lines are homologous to the *ras* genes of Harvey and Kirsten sarcoma viruses. *Proc. Natl Acad. Sci. USA* **79**, 3637–3640 (1982).
4. Dekker, F. J. et al. Small-molecule inhibition of APT1 affects Ras localization and signaling. *Nature Chem. Biol.* **6**, 449–456 (2010).
5. Xu, J. et al. Inhibiting the palmitoylation/depalmitoylation cycle selectively reduces the growth of hematopoietic cells expressing oncogenic *Nras*. *Blood* **119**, 1032–1035 (2012).
6. Zimmermann, G. et al. Small molecule inhibition of the KRAS–PDEδ interaction impairs oncogenic KRAS signalling. *Nature* **497**, 638–642 (2013).
7. Yagoda, N. et al. RAS–RAF–MEK-dependent oxidative cell death involving voltage-dependent anion channels. *Nature* **447**, 865–869 (2007).
8. Kumar, C. C. et al. SCH 51344 inhibits *ras* transformation by a novel mechanism. *Cancer Res.* **55**, 5106–5117 (1995).
9. Walsh, A. B., Dhanasekaran, M., Bar-Sagi, D. & Kumar, C. C. SCH 51344-induced reversal of RAS-transformation is accompanied by the specific inhibition of the RAS and RAC-dependent cell morphology pathway. *Oncogene* **15**, 2553–2560 (1997).
10. Rai, P. et al. Enhanced elimination of oxidized guanine nucleotides inhibits oncogenic RAS-induced DNA damage and premature senescence. *Oncogene* **30**, 1489–1496 (2011).
11. Barbie, D. A. et al. Systematic RNA interference reveals that oncogenic KRAS-driven cancers require TBK1. *Nature* **462**, 108–112 (2009).
12. Fujikawa, K. et al. The oxidized forms of dATP are substrates for the human MutT homologue, the hMTH1 protein. *J. Biol. Chem.* **274**, 18201–18205 (1999).
13. Oka, S. et al. Two distinct pathways of cell death triggered by oxidative damage to nuclear and mitochondrial DNAs. *EMBO J.* **27**, 421–432 (2008).
14. Yoshimura, D. et al. An oxidized purine nucleoside triphosphatase, MTH1, suppresses cell death caused by oxidative stress. *J. Biol. Chem.* **278**, 37965–37973 (2003).
15. Svensson, L. M. et al. Crystal structure of human MTH1 and the 8-oxo-dGMP product complex. *FEBS Lett.* **585**, 2617–2621 (2011).
16. Rai, P. et al. Continuous elimination of oxidized nucleotides is necessary to prevent rapid onset of cellular senescence. *Proc. Natl Acad. Sci. USA* **106**, 169–174 (2009).
17. Fedorov, O. et al. Specific CLK inhibitors from a novel chemotype for regulation of alternative splicing. *Chem. Biol.* **18**, 67–76 (2011).
18. Cui, J. J. et al. Structure based drug design of crizotinib (PF-02341066), a potent and selective dual inhibitor of mesenchymal-epithelial transition factor (c-MET) kinase and anaplastic lymphoma kinase (ALK). *J. Med. Chem.* **54**, 6342–6363 (2011).
19. Zou, H. Y. et al. An orally available small-molecule inhibitor of c-Met, PF-2341066, exhibits cytoreductive antitumor efficacy through antiproliferative and antiangiogenic mechanisms. *Cancer Res.* **67**, 4408–4417 (2007).
20. Camidge, D. R. et al. Activity and safety of crizotinib in patients with ALK-positive non-small-cell lung cancer: updated results from a phase 1 study. *Lancet Oncol.* **13**, 1011–1019 (2012).
21. Kwak, E. L. et al. Anaplastic lymphoma kinase inhibition in non-small-cell lung cancer. *N. Engl. J. Med.* **363**, 1693–1703 (2010).
22. Gerber, D. E. & Minna, J. D. ALK inhibition for non-small cell lung cancer: from discovery to therapy in record time. *Cancer Cell* **18**, 548–551 (2010).
23. Butrynski, J. E. et al. Crizotinib in ALK-rearranged inflammatory myofibroblastic tumor. *N. Engl. J. Med.* **363**, 1727–1733 (2010).
24. Martinez Molina, D. et al. Monitoring drug target engagement in cells and tissues using the cellular thermal shift assay. *Science* **341**, 84–87 (2013).
25. Fabian, M. A. et al. A small molecule-kinase interaction map for clinical kinase inhibitors. *Nature Biotechnol.* **23**, 329–336 (2005).
26. Zuber, J. et al. An integrated approach to dissecting oncogene addiction implicates a Myb-coordinated self-renewal program as essential for leukemia maintenance. *Genes Dev.* **25**, 1628–1640 (2011).
27. Sakumi, K. et al. *Ogg1* knockout-associated lung tumorigenesis and its suppression by *Mth1* gene disruption. *Cancer Res.* **63**, 902–905 (2003).
28. Speina, E. et al. Contribution of hMTH1 to the maintenance of 8-oxoguanine levels in lung DNA of non-small-cell lung cancer patients. *J. Natl Cancer Inst.* **97**, 384–395 (2005).

29. Kennedy, C. H., Cueto, R., Belinsky, S. A., Lechner, J. F. & Pryor, W. A. Overexpression of *hMTH1* mRNA: a molecular marker of oxidative stress in lung cancer cells. *FEBS Lett.* **429**, 17–20 (1998).
30. Okamoto, K. *et al.* Overexpression of human *mutT* homologue gene messenger RNA in renal-cell carcinoma: evidence of persistent oxidative stress in cancer. *Int. J. Cancer* **65**, 437–441 (1996).
31. Tsuzuki, T. *et al.* Spontaneous tumorigenesis in mice defective in the *MTH1* gene encoding 8-oxo-dGTPase. *Proc. Natl Acad. Sci. USA* **98**, 11456–11461 (2001).
32. Hutt, A. J. Chirality and pharmacokinetics: an area of neglected dimensionality? *Drug Metabol. Drug Interact.* **22**, 79–112 (2007).

Supplementary Information is available in the online version of the paper.

Acknowledgements The team at CeMM was supported by the Austrian Academy of Sciences, the GEN-AU initiative of the Austrian Federal Ministry for Science and Research, and “ASSET”, a project funded by the European Union within FP7. S.K., E.S. and J.M.E. are grateful for financial support from the SGC, a registered charity (number 1097737) that receives funds from the Canadian Institutes for Health Research, the Canada Foundation for Innovation, Genome Canada, GlaxoSmithKline, Pfizer, Eli Lilly, Takeda, AbbVie, the Novartis Research Foundation, Boehringer Ingelheim, the Ontario Ministry of Research and Innovation and the Wellcome Trust (Grant No. 092809/Z/10/Z). E.S. was supported by the European Union FP7 Grant No. 278568 “PRIMES”. T.H. was supported by the Torsten and Ragnar Söderberg Foundation, the Knut and Alice Wallenberg Foundation, the Swedish Research Council, the European Research Council and the Swedish Cancer Society. J.I.L. was supported by the European Union FP7 Career Integration Grant (PCIG11-GA-2012-321602) and an FWF Grant (P24766-B20). We are grateful to D. Treiber, J. Hunt, P. Gallant and G. Pallares from

DiscoverX for the KdELECT and scanMAX studies. We thank W. Lindner and N. Maier for chiral HPLC analyses, R. Lichtenecker for NMR measurements, A. C. Müller for the annotation of the MS/MS spectrum, M. Brehme for help with the figures, and H. Pickersgill and G. Vladimer for critically reading the manuscript. We are very grateful to the following colleagues for the respective reagents: S. Lowe for the miR30 vectors and pMPLP-p53; R. Weinberg for pLKO.1 shMTH1 and pBABE-puro plasmids; W. Berger for SW480, DLD1 and SW620 cells; R. Oehler for PANC1 cells; W. Hahn and A. Gad for BJ-hTERT, BJ-hTERT-SV40T, BJ-hTERT-SV40T-KRASV12 cells, B. Vogelstein for p53^{-/-} and p21^{-/-} HCT116 cells; C. Gasche for LoVo and HCT15 cells; A. Nussenzweig for *Atm* wild type and *Atm*^{-/-} mouse embryonic fibroblasts.

Author Contributions K.V.M.H., E.S., B.R., M.G., J. M.E., J.I.L., A.-S.J., K.S. performed experiments. K.V.M.H. and G.S.-F. conceived the study. K.V.M.H., J.I.L., U.W.B., T.H., S.K. and G.S.-F. designed experiments. A.S., K.L.B. and J.C. performed mass spectrometry and bioinformatic data analysis. C.G., K.S., T.P. and U.W.B. performed animal experiments. K.V.M.H., S.K. and G.S.-F. wrote the manuscript. All authors contributed to the discussion of results and participated in manuscript preparation.

Author Information Atomic coordinates for MTH1 in complex with (*R*)- and (*S*)-crizotinib have been deposited at the Protein Data Bank under accession codes 4c9w ((*R*)-crizotinib) and 4c9x ((*S*)-crizotinib), respectively. The protein interactions from this publication have been submitted to the IntAct database (<http://www.ebi.ac.uk/intact/>) and assigned the identifier EBI-9232460. Reprints and permissions information is available at www.nature.com/reprints. The authors declare competing financial interests: details are available in the online version of the paper. Readers are welcome to comment on the online version of the paper. Correspondence and requests for materials should be addressed to G.S.-F. (gsuperti@cemmm.oeaw.ac.at).

METHODS

Cell culture. BJ, H1437, H2122, H23, H358, H460, HCT116 and U2OS cells were obtained from ATCC and DMSZ. SW480, DLD1 and SW620 cells were kindly provided by W. Berger, PANC1 were a gift from R. Oehler. The BJ-hTERT, BJ-SV40T and BJ-RASV12 were provided by W. Hahn. HCT116 p53^{-/-} and HCT116 p21^{-/-} were used by permission of B. Vogelstein. LoVo and HCT15 were a gift from C. Gasche. *Atm* wild type and *Atm*^{-/-} mouse embryonic fibroblasts were provided by A. Nussenzweig. All cells were cultured in the recommended media containing 10% fetal bovine serum and 10 U ml⁻¹ penicillin/streptomycin (Gibco) and checked for mycoplasma by PCR or ELISA before experimental use.

Immunoblotting. The following antibodies were used according to manufacturer's instructions: rabbit anti-MTH1 (NB100-109, Novus Biologicals)¹⁶, rabbit anti-actin (AAN01, Cytoskeleton), mouse anti-tubulin (DM1A, Abcam), goat anti-p53 (C-19, Santa Cruz Biotechnology), goat Alexa Fluor 680 anti-mouse IgG (Life Technologies).

Expression of recombinant MTH1. Codon-optimised human *NUDT1* complementary DNA subcloned into a pETM-11 vector (G. Stier, EMBL) featuring a His-tag and TEV site was obtained from GenScript (GenScript, NJ, USA) and expressed in the *Escherichia coli* strain BL21 DE3 (Life Technologies). After collecting, bacteria were lysed using buffer (50 mM Tris-HCl pH 7.5, 500 mM NaCl, 5% glycerol, 5 mM β-mercaptoethanol, 1 mM PMSF) containing lysozyme (Sigma-Aldrich) and DNase I (Roche). His-tagged protein was purified with NiNTA agarose (Qiagen), washed with buffer, and eluted with an imidazole gradient. Following removal of the His-tag by incubation with TEV protease, fractions were dialysed and purified using size-exclusion chromatography (Sephadex, GE Healthcare). Protein concentration of the purified fractions was determined by ultraviolet absorbance ($A_{280\text{nm}}$). The identity of the protein was confirmed by MALDI-TOF and protein activity determined by kinetic analysis which gave values in accordance with literature data¹⁵.

MTH1 catalytic assay. Half-maximal inhibitory concentrations (IC₅₀) were determined using a luminescence-based assay as described previously¹⁵ with some minor modifications. Briefly, serial dilutions of compounds were dissolved in assay buffer (100 mM Tris-acetate pH 7.5, 40 mM NaCl and 10 mM Mg(OAc)₂ containing 0.005% Tween-20 and 2 mM dithiothreitol (DTT)). Upon addition of MTH1 recombinant protein (final concentration 2 nM), plates were incubated on a plate shaker for 15 min at room temperature. After addition of the substrate dGTP (Fermentas, final concentration 100 μM), 8-oxo-dGTP (TriLink Biotechnologies, final concentration 13.2 μM), or 2-OH-dATP (Jena Bioscience, final concentration 8.3 μM) the generation of pyrophosphate (PPi) as a result of nucleotide triphosphate hydrolysis by MTH1 was monitored over a time course of 15 min using the PPLight Inorganic Pyrophosphate Assay kit (Lonza Rockland). IC₅₀ values were determined by fitting a dose-response curve to the data points using nonlinear regression analysis using the GraphPad Prism software.

siRNA experiments. Both a commercial MTH1-siRNA set (SMARTpool ON-TARGETplus, Dharmacon) as well as a custom-synthesized siRNA (Sigma-Aldrich) were obtained. The custom siRNA sequence was CGACGACAGCUACUGGUUU, AllStars Negative Control siRNA (Qiagen) was used as control. For transfections, cells were seeded in 24-well plates at approximately 30% confluency 24 h before siRNA treatment. The next day, medium was aspirated and transfections performed with INTERFERin (Polyplus) according to manufacturer's instructions using a final siRNA concentration of 10 nM. Cells were incubated for 2–3 days, washed, detached with trypsin and replated in six-well plates. After 7–10 days, medium was aspirated, cells were washed with PBS, fixed with ice-cold methanol, stained with crystal violet solution (0.5% in 25% methanol) and left to dry overnight. For quantification of results, ultraviolet absorbance of crystal violet was determined at 595 nm following solubilisation by 70% ethanol. Data were analysed using the GraphPad Prism software (*t*-test, *P* < 0.05).

Target engagement assay. The ability of compounds to interact with, and thereby stabilize the target in intact cells, was analysed essentially as described by Molina *et al.*²⁴. Briefly, BJ SV40T RASV12-cells cultured in T150 flasks to 80% confluency, were treated with cell media containing 1% DMSO and 5 μM either (R) or (S)-crizotinib for 3 h. After treatment, cells were detached with trypsin, collected by centrifugation and subsequently resuspended in TBS. The cell suspension was aliquoted into eight PCR tubes and heated for 3 min to 47, 49, 51, 53, 54, 57, 59 or 61 °C. Subsequently, cells were lysed using liquid nitrogen and three repeated cycles of freeze-thawing. Precipitated proteins were separated from the soluble fraction by centrifugation at 17,000g for 20 min. Soluble proteins, collected in the supernatant, were kept at -80 °C until western blot analysis. Half of each aliquot was loaded onto 4–25% SDS-PAGE gels, blotted on nitrocellulose membranes and analysed using the MTH1-antibody from Novus Biologicals at a concentration of 1:500.

Cloning of miR30-based shRNAs. To obtain inducible anti-p53-TRMPV-Neo miR30 shRNAs, pMLP plasmids containing p53-targeting sequences³³ were digested with EcoRI and XhoI, followed by ligation into the TRMPV-Neo vector²⁶.

Retro- and lentivirus production. For stable knockdown and MTH1 overexpression studies, 293T cells were transfected with helper plasmids and either pBABE-puro (Addgene plasmid 1764) or pBabe puro MTH1 (Addgene plasmid 21295), pLKO-eGFP-shRNA-control, pLKO.1 shMTH1-1 (Addgene plasmid 21297), or pLKO.1 shMTH1-2 (Addgene plasmid 21298). SW480 cells were then treated with 48 h supernatants containing polybrene (8 μg ml⁻¹) for 3 h. The next day cells were selected with puromycin (5 μg ml⁻¹). Tet-on competent SW480 were established by transduction of cells with pMSCV-rtTA3-IRES-EcoR-PGK-PuroR²⁶. After selection with puromycin (5 μg ml⁻¹), cells were transduced with TRMPV-Neo-shRNAs using Plat-E cells and ecotropic packaging. After subsequent selection with G418 (1 mg ml⁻¹) the expression of shRNAs was induced using doxycycline (2 μg ml⁻¹) and monitored by FACS.

Real-time PCR analysis. Total RNA was isolated using the RNeasy Mini Kit (Qiagen). 500 ng RNA was reverse transcribed using oligo(dT) primers using RevertAid Reverse Transcriptase (Fermentas). Quantitative PCR was carried out on a RotorGene RG-600 (Qiagen) PCR machine using the SensiMix SYBR kit (Bioline). Results were quantified using the 2^{-ΔΔC_t} method, using GAPDH expression levels for normalization.

Primer sequences. NUDT1-F 5'-CTCAGCGAGTTCTCTCTGG -3'; NUDT1-R 5'-GGAGTGGAAACCAGTAGCTGTC-3'.

Colony formation assay. One day before treatment, 5 × 10³ or 10⁴ cells were seeded per well in six-well plates and incubated for 24 h. The next day DMSO (equal to highest amount of compound dilution, maximum 0.2%) or compounds in increasing concentrations were added and cells incubated at 37 °C, 5% CO₂, for 7–10 days. After washing with PBS (Gibco), cells were fixed with ice-cold methanol, stained with crystal violet solution (0.5% in 25% methanol) and left to dry overnight. For quantification of results, ultraviolet absorbance of crystal violet was determined at 595 nm following solubilisation by 70% ethanol. Data were analysed using nonlinear regression analysis using the GraphPad Prism software.

Proliferation rate measurements. Population doublings were determined as described¹⁶. Briefly, 10⁵ cells were plated in triplicate in six-well plates followed by addition of drug or DMSO 6 h later and counting the number of cells every three days, after which 10⁵ cells were replated for the next count. The numbers were converted into population doublings using the following formula: (log(no. of cells counted) - log(no. of cells plated))/log(2).

Comet assay. Cells were treated with compounds for 3 or 6 days, upon which DNA single-strand breaks were assayed using the comet assay under alkali conditions. For the H₂O₂ control, cells were treated with H₂O₂ (Sigma-Aldrich) in PBS at 150 μM for 10 min. Cells were washed twice with PBS, collected using a rubber scraper, pelleted by centrifugation, resuspended in PBS and mixed with 1% low-gelling-temperature agarose (Sigma type VII) that was maintained at 37 °C. The mixture of cells and agarose was layered onto frosted glass slides pre-coated with 0.5% agarose and slides were placed on ice to gel. Slides were maintained in the dark for all subsequent steps. Slides were immersed in pre-chilled lysis buffer (2.5 M NaCl, 0.1 M EDTA, 10 mM Tris-HCl pH 7.70, 1% Triton X-100, 1% DMSO) for 1 h, washed in pre-chilled distilled water 3 times for 20 min and incubated for 45 min in pre-chilled alkaline electrophoresis buffer (50 mM NaOH, 1 mM EDTA, 1% DMSO, pH 12.8). After electrophoresis for 25 min at 25 V, slides were placed at 4 °C overnight, in the dark. The following day, slides were neutralized with 0.4 M Tris-HCl pH 7.0 for 1 h and stained with SYBR Gold (Invitrogen, diluted 1:10,000 in distilled water) for 30 min. Comet tail moments (defined as the average distance migrated by the DNA multiplied by the fraction of DNA in the comet tail) were scored using the CellProfiler cell image analysis software. For the OGG1/MUTYH enzyme modified comet assay, 150,000 U2OS cells were seeded in triplicate on six-well plates. After overnight incubation, cells were treated either with buffer or (S)-crizotinib (5 μM) for 24 h. Cells (10⁶ per ml) suspended in 1.2% low melting agarose were layered over the first layer of a 1% agarose gel on a frosted slide. Slides were then stored at 4 °C overnight in lysis buffer containing 100 mM sodium EDTA, 2.5 M NaCl, 10 mM Tris-HCl (pH 10), 1% Triton X-100 and 10% DMSO. After incubation, slides were washed 2 × 15 min each with enzyme buffer (40 mM HEPES, 0.1 M KCl, 0.5 mM EDTA and 0.2 mg ml⁻¹ BSA, pH 8 adjusted with KOH). OGG1 or MUTYH in enzyme buffer were added on top and slides were incubated at 37 °C for 45 min. After incubation, alkaline denaturation with alkali buffer (300 mM NaOH, 1 mM sodium EDTA) was done in an electrophoresis chamber for 20 min. Electrophoresis was then conducted at 25 V and 300 mA in the same buffer for 30 min. Slides were later neutralised with neutralising buffer (250 mM Tris-HCl (pH 7.5)) for at least 30 min, and then stained with 20 μM YOYO-1 dye. Images were acquired with a confocal microscope and analysed using comet score software.

Indirect immunofluorescence. Cells were treated with compounds for 3 days, following which they were adhered to glass coverslips, washed with PBS and then fixed with 3% paraformaldehyde in PBS for 20 min. Fixed cells were rinsed with PBS and permeabilized with 0.5% Triton-X-100 for 5 min. PBS washed slides

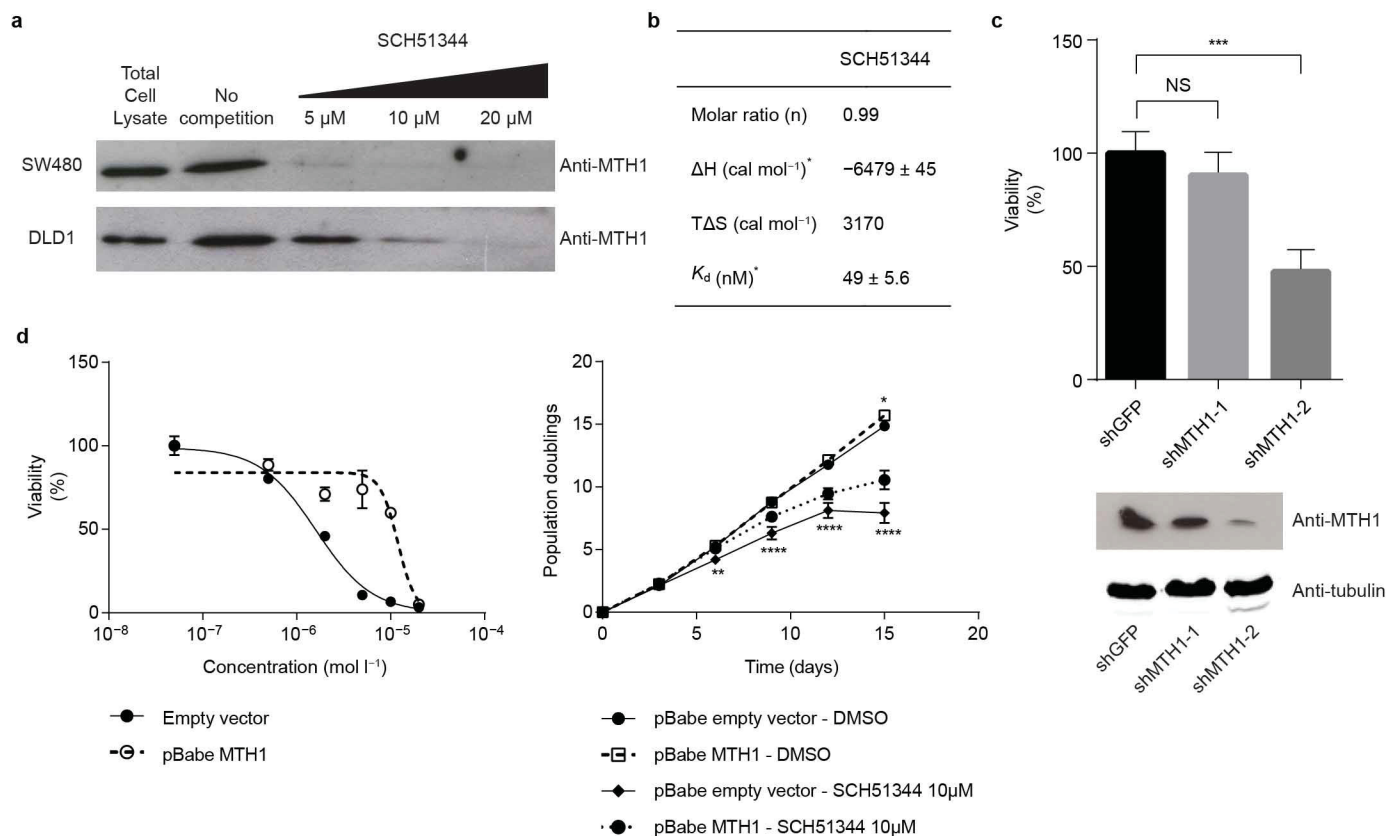
were incubated for 1 h with 10% FCS and 0.1% Triton-X-100 in PBS following which cells were stained with an anti-53BP1 monoclonal antibody (H-300, Santa Cruz, diluted 1:600), in combination with an 8-oxoguanine antibody (2Q2311, AbCam, diluted 1:400), where indicated, in 10% FCS and 0.1% Triton-X-100 in PBS. After rinsing with PBS coverslips were incubated with an Alexa Fluor 568 goat anti-rabbit IgG secondary antibody in combination with an Alexa Fluor 488 anti-mouse IgM secondary antibody, where indicated, for 1 h (Invitrogen, diluted 1:400) in 10% FCS and 0.1% Triton-X-100 in PBS. After a PBS wash, DNA was counterstained with DAPI (Sigma-Aldrich) for 10 min and the coverslips were mounted in Fluorescent Mounting Medium (Dako). Images were analysed with a Zeiss fluorescent microscope at $\times 63$ magnification with supporting software.

Xenograft study. All animals were acclimatised for one week, and had free access to water and food during the experiment. Animals were under a 12 h light cycle, and temperature, humidity and housing according to laboratory animal guidelines and regulations. The group size was based on previous experience on variability of tumour growth within control groups. Animals were grouped based on body weight, exclusion/inclusion criteria were pre-established in the ethical permit, and outliers in body weight were excluded. When assessing tumour volume, the experimenter was blinded. Tumour volume and body weight were analysed using two-way ANOVA (GraphPad Prism 4.0, GraphPad Software Inc.) and pairwise Bonferroni comparisons between groups, using a general linear model with repeat measures with experimental groups (treatment, control) as between factors and day as within-subject factor. Sidak's post hoc test was used for further analysis of significant interactions.

SCID mice (female, 5–6 weeks, Scanbur, Germany, $n = 8$ per group) were injected subcutaneously with 10^6 SW480 cells together with a matrix gel (1:1) in the sacral area. Treatment was initiated 1 day after cell inoculation. Vehicle or MTH1 inhibitor was administered subcutaneously once daily at 25 mg per kg for 35 days. MTH1 inhibitor was diluted in 1% DMSO, 10% ethanol, 10% Cremophor, 10% Tween 80, 69% PBS. Tumour size was measured twice weekly and body weight once weekly. At termination, a gross post-mortem inspection was performed; blood was collected for haematological parameters and aspartate aminotransferase (ASAT), alanine aminotransferase (ALAT) and creatinine measurements. For oral dosing, SCID mice (female, 5–6 weeks, Scanbur, Germany, (S)-crizotinib group, $n = 8$; (R)-crizotinib group, $n = 7$; control group, $n = 8$) were injected subcutaneously with 10^6 SW480 cells together with Matrigel (1:1) in the sacral area and two days later treatment was initiated. Vehicle, (S)-crizotinib or (R)-crizotinib were administered by oral gavage once daily for 26 days. The compounds were diluted in sterile water. Tumour size was measured twice weekly (calculated as length \times width \times width \times 0.52). The mice were weighed at least once weekly. At termination, a gross post-mortem inspection was performed. All experiments involving animals followed protocols approved by Stockholms Norra Djurförsöksetiska Nämnd (laboratory animal ethical committee Stockholm) and were in compliance with 2010/63/EU directive.

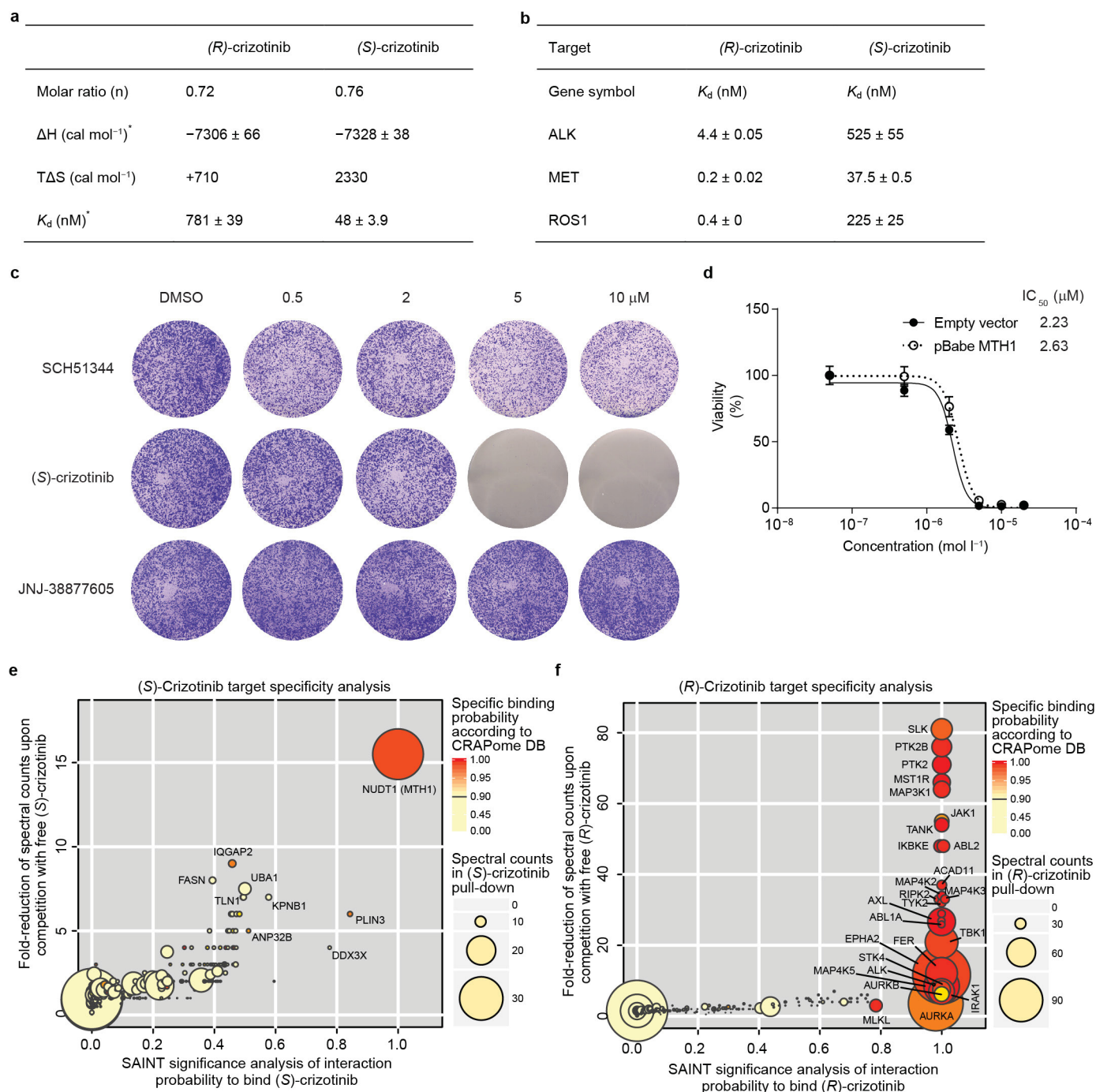
Statistical analysis. Unless stated otherwise, a normal distribution of data was assumed and appropriate test were applied.

33. Aksoy, O. *et al.* The atypical E2F family member E2F7 couples the p53 and RB pathways during cellular senescence. *Genes Dev.* **26**, 1546–1557 (2012).



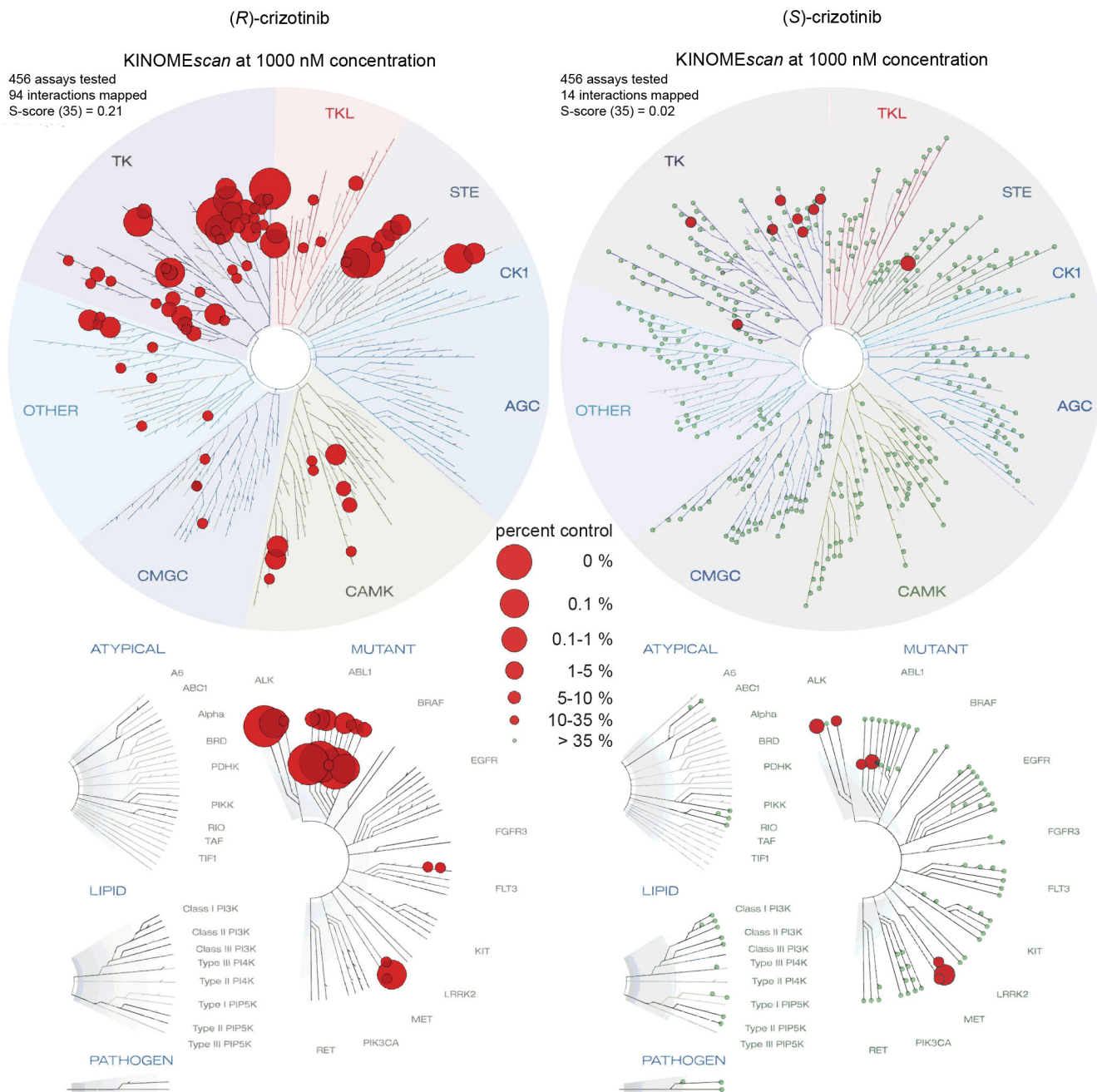
Extended Data Figure 1 | Confirmation of MTH1 as the main cellular target of SCH51344. **a**, Immunoblot showing a dose-dependent competition between MTH1 and free SCH51344 for the affinity probe ($n = 1$ per condition). **b**, Isothermal titration calorimetry results for SCH51344. Data were measured at 15 °C in 50 mM Tris-HCl pH 7.8, 150 mM NaCl. Errors given in the table represent the error of the nonlinear least squares fit to the experimental data ($n = 1$). **c**, Stable knockdown of MTH1 by shRNA reduces SW480 cell viability in a colony formation assay. Data are shown as mean \pm s.e.m. and are based on three independent experiments ($n = 3$). Asterisks indicate significance by one-way ANOVA; NS, not significant. **d**, MTH1 overexpression decreases

SW480 sensitivity towards SCH51344 as reflected by a shift in IC_{50} value (left). Data are shown as mean \pm s.e.m. and are based on three independent experiments ($n = 3$). Similarly, MTH1 overexpression partially restores SW480 proliferation as compared to empty vector at a sub-lethal dose of SCH51344 (right). Notably, the overall proliferation rate is comparable for empty vector- and pBabe-MTH1-transduced cells. Bottom asterisks indicate significance between SCH51344-treated empty vector and pBabe-MTH1 cells as calculated by two-way ANOVA; DMSO-treated empty vector versus DMSO-treated pBabe-MTH1 is not significant except for the last data point. Data are shown as mean \pm s.e.m. and are based on three independent experiments ($n = 3$).



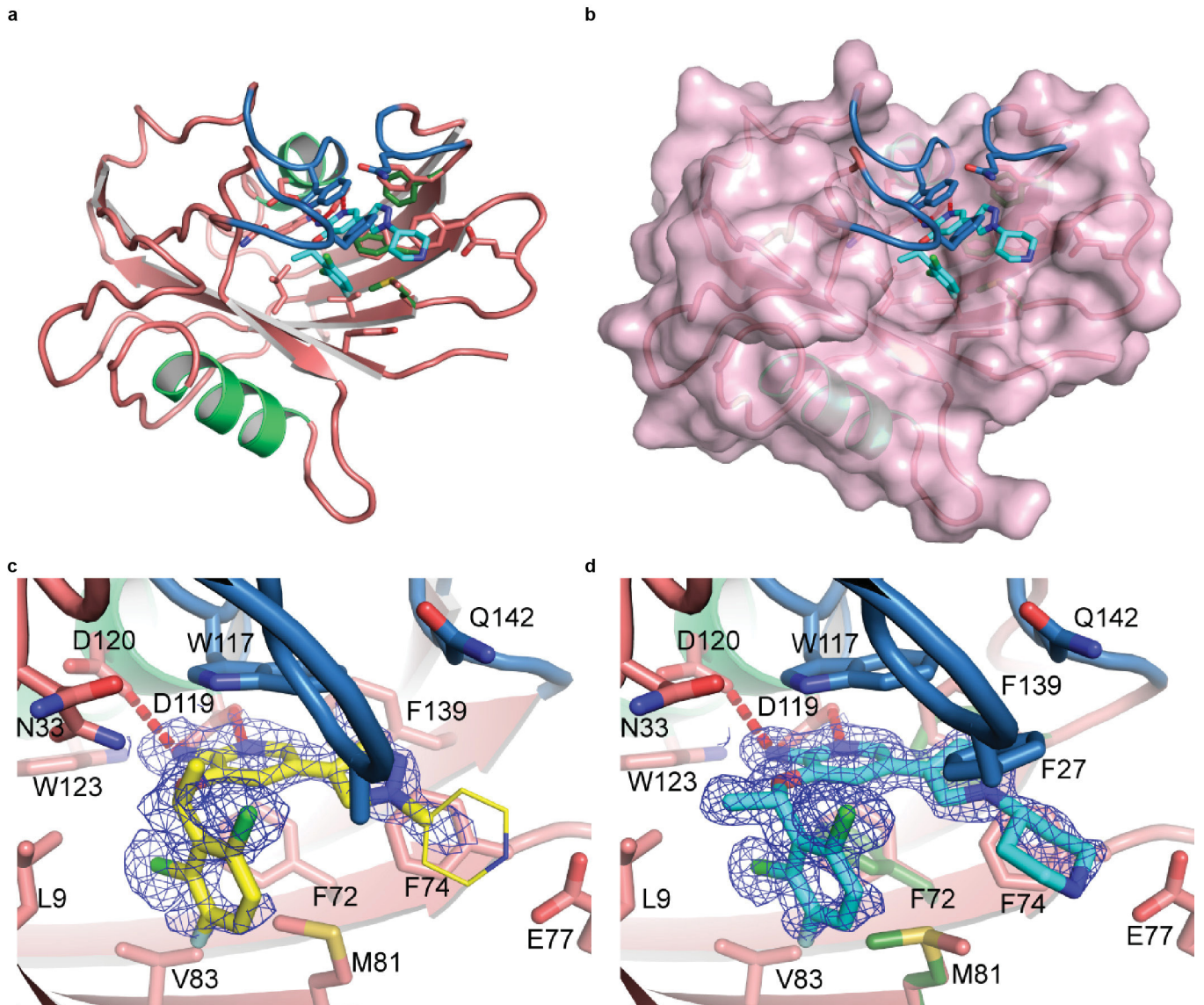
Extended Data Figure 2 | (*S*)-Crizotinib target specificity. **a**, Isothermal titration calorimetry results for both crizotinib enantiomers. Data were measured at 15 °C in 50 mM Tris-HCl pH 7.8, 150 mM NaCl. *Error given in the table represent the error of the nonlinear least squares fit to the experimental data ($n = 1$). **b**, K_d binding constants of both crizotinib enantiomers for the (*R*)-crizotinib cognate targets ALK, MET and ROS1. Data are shown as mean ± s.e.m. ($n = 2$). **c**, Pharmacologic *c*-MET kinase inhibition by a highly potent inhibitor (JNJ-38877605, *c*-MET $IC_{50} = 4$ nM) does not suppress growth of KRAS-mutated SW480 cells in contrast to the MTH1 inhibitors SCH51344 and (*S*)-crizotinib. Images are representative of three independent experiments ($n = 3$). **d**, MTH1 overexpression does not alter SW480 sensitivity towards (*S*)-crizotinib. Data are shown as mean ± s.e.m. and

are based on three independent experiments ($n = 3$). **e**, (*S*)-Crizotinib target specificity analysis. Comparison of the probability of true interaction (SAINT) versus the magnitude of spectral count reduction upon competition with the free compound. MTH1 is clearly the only significant target identified by chemoproteomics as further supported by a high spectral count (disc diameter) and very low frequency of appearance in AP-MS negative control experiments found in the CRAPome database (colour code). **f**, In contrast, analysis of (*R*)-crizotinib targets reveals a large number of kinases as specific interactors of the clinical enantiomer. Data shown in panels **e** and **f** are based on two independent experiments for each condition ($n = 2$ per condition), and each replicate was analysed in two technical replicates.



Extended Data Figure 3 | KINOMEScan results for both crizotinib enantiomers. Screening of both (R)- and (S)-crizotinib against a panel of 456 recombinant human protein kinases indicates a marked difference in the ability of the two enantiomers to bind kinases. (R)-crizotinib has high affinity towards a large number of kinases, including its cognate targets MET, ALK and

ROS1. Selectivity Score or S-score is a quantitative measure of compound selectivity. It is calculated by dividing the number of kinases that compounds bind to by the total number of distinct kinases tested, excluding mutant variants. $S(35) = (\text{number of non-mutant kinases with } \%Ctrl < 35) / (\text{number of non-mutant kinases tested})$.



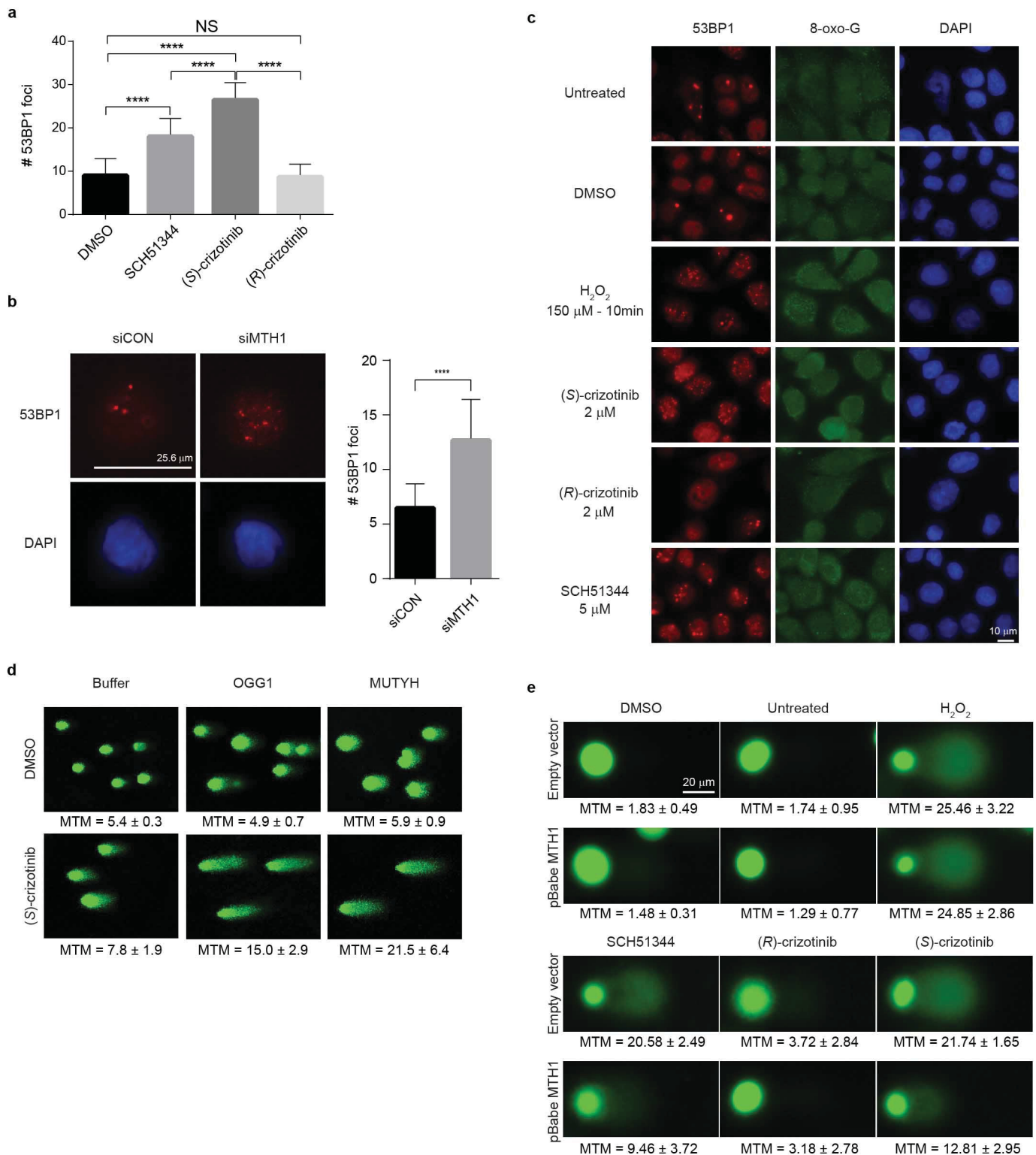
Extended Data Figure 4 | Co-crystal structures of (S)- and (R)-crizotinib bound to MTH1. **a**, MTH1 crystal structure overview with (S)-crizotinib. (S)-Crizotinib is shown in cyan, MTH1 is in pink with light green alpha-helices and the loops covering the binding site in blue. **b**, As **a** with a molecular surface shown covering MTH1 apart from the binding site loops. **c**, MTH1 crystal

structures with (R)- and (S)-crizotinib showing $2F_o - F_c$ electron density maps contoured at 1σ . (R)-Crizotinib is shown in yellow, MTH1 is in pink with light green alpha-helices and the loops covering the binding site in blue. **d**, As **c** except with (S)-crizotinib shown in cyan.

| a | | | b | | |
|--------------------------|---|---|---|---|---|
| | MTH1 : (R)-crizotinib | MTH1 : (S)-crizotinib | | MTH1 : (R)-crizotinib | MTH1 : (S)-crizotinib |
| Reservoir solution | 30% PEG4000, 0.2 M (NH ₄) ₂ SO ₄ | 24% PEG4000, 0.2 M (NH ₄) ₂ SO ₄ | Data collection | | |
| Volume of protein : | 50 : 100 | 50 : 100 | Space group | <i>P</i> 22 ₁ 2 ₁ | <i>P</i> 22 ₁ 2 ₁ |
| Volume of reservoir (nL) | | | Cell dimensions | | |
| Temperature (°C) | 4 | 20 | <i>a</i> , <i>b</i> , <i>c</i> (Å) | 36.2, 60.0, 66.9 | 36.2, 60.0, 67.0 |
| | | | α , β , γ (°) | 90, 90, 90 | 90, 90, 90 |
| | | | Resolution (Å) | 44.64-1.65 (1.68-1.65)* | 36.20-1.20 (1.22-1.20)* |
| | | | <i>R</i> _{merge} | 0.077 (0.369) | 0.054 (0.566) |
| | | | <i>I</i> / σ (<i>I</i>) | 8.2 (2.6) | 10.4 (2.2) |
| | | | Completeness (%) | 99.8 (97.4) | 99.6 (99.8) |
| | | | Redundancy | 4.2 (3.2) | 3.9 (4.0) |
| | | | Refinement | | |
| | | | Resolution (Å) | 44.64-1.65 | 36.23-1.20 |
| | | | No. reflections | 17128 | 43840 |
| | | | <i>R</i> _{work} / <i>R</i> _{free} | 0.148 / 0.218 | 0.146 / 0.182 |
| | | | No. atoms | | |
| | | | Protein | 1268 | 1355 |
| | | | Ligand/ion | 51 | 60 |
| | | | Water | 155 | 229 |
| | | | B-factors | | |
| | | | Protein | 15.1 | 14.2 |
| | | | Ligand/ion | 30.0 | 20.4 |
| | | | Water | 32.1 | 33.1 |
| | | | R.m.s deviations | | |
| | | | Bond lengths (Å) | 0.009 | 0.008 |
| | | | Bond angles (°) | 1.35 | 1.32 |

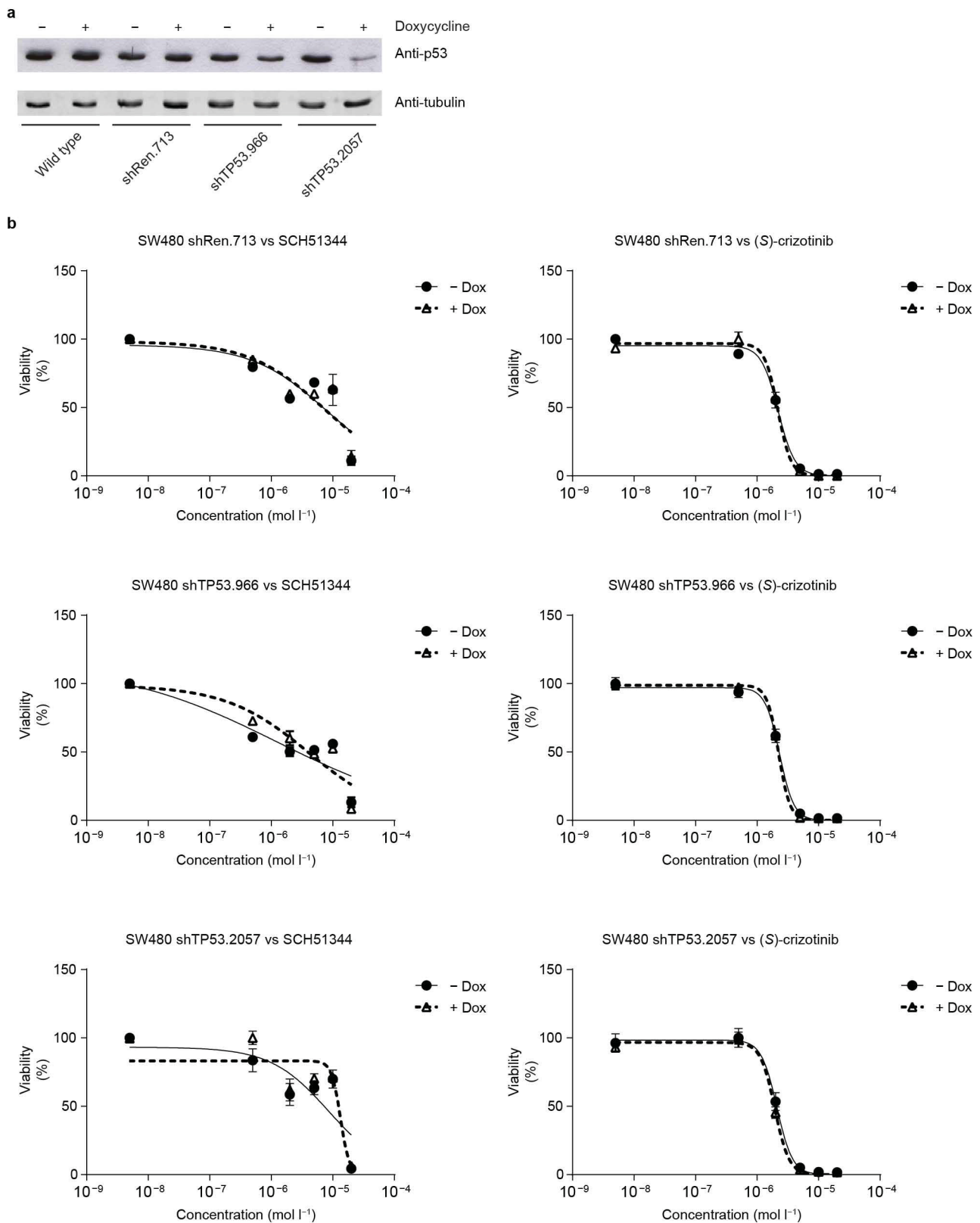
Each dataset was collected from a single crystal.
*Highest resolution shell is shown in parenthesis.

Extended Data Figure 5 | Data collection and refinement statistics. **a**, Crystallization of MTH1 complexes. **b**, Data collection and refinement statistics.



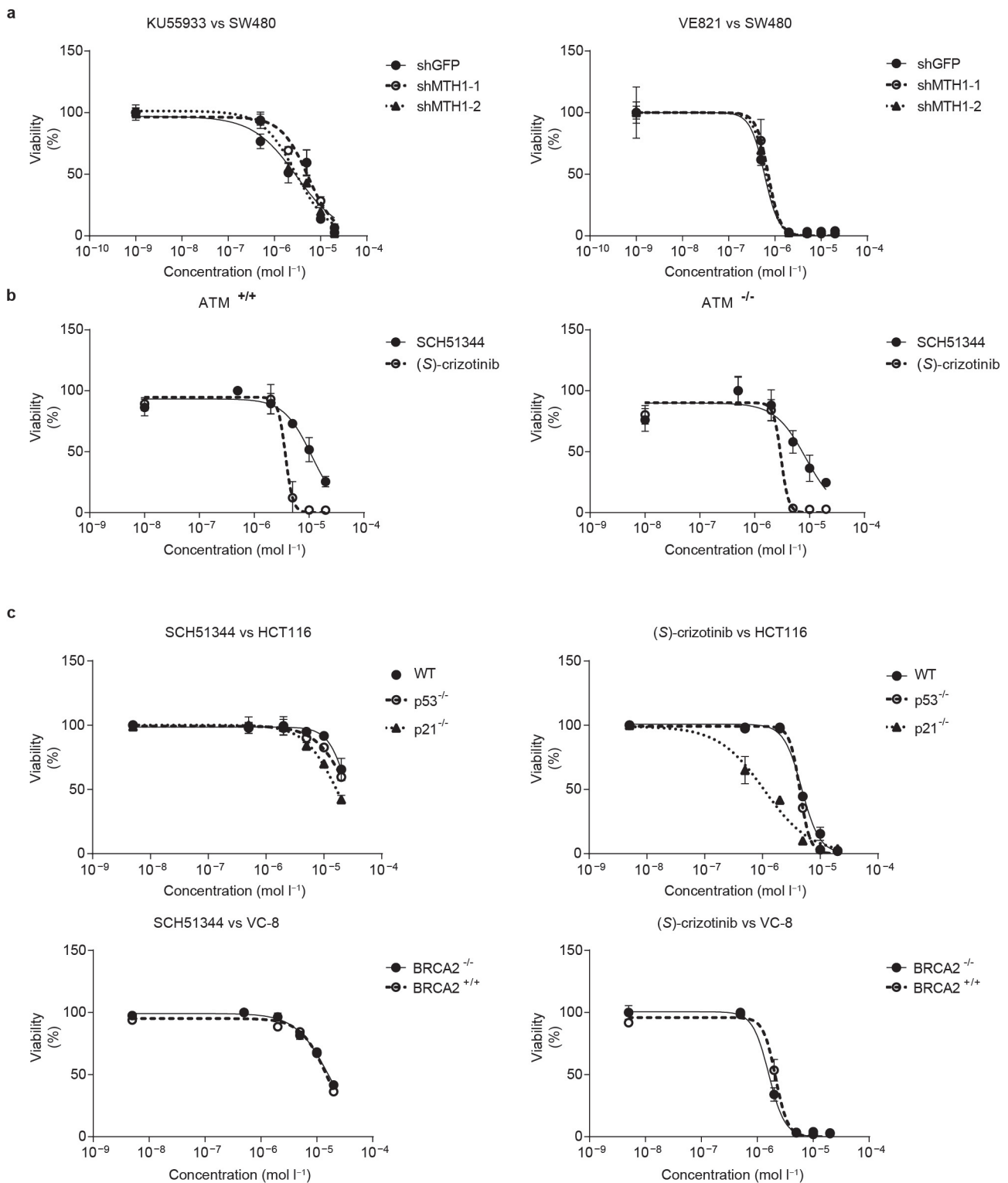
Extended Data Figure 6 | MTH1 suppression by siRNA or small-molecule inhibitors induces DNA damage. **a**, Quantification of 53BP1 foci formation in SW480 cells upon MTH1 inhibitor treatment. Concentrations are 5 μ M for SCH51344 and 2 μ M for each crizotinib enantiomer. Data are shown as mean \pm s.d. ($n = 3$). Asterisks indicate significance by two-way ANOVA; NS, not significant. **b**, In line with results obtained for the MTH1 inhibitors SCH51344 and (S)-crizotinib, transient knockdown of MTH1 also induces formation of 53BP1 foci in SW480 cells. Images are representative and data are shown as mean \pm s.d. based on three independent experiments ($n = 3$) ($P < 0.05$, t -test). **c**, Formation of 53BP1 foci correlates with increased 8-oxo-guanine staining in SW480 cells treated with the MTH1 inhibitors SCH51344

and (S)-, but not (R)-crizotinib. Images are representative of three independent experiments ($n = 3$). **d**, Modified OGG1-MUTYH comet assay. Treatment of U2OS cells with the MTH1 inhibitor (S)-crizotinib (5 μ M) induces formation of DNA single-strand breaks due to activation of endogenous base excision repair. Addition of the 8-oxo-guanine- and 2-hydroxy-adenine-specific DNA glycosylases OGG1 and MUTYH leads to an increase in the mean tail moment (MTM) due to increased DNA cleavage at lesion sites. Data are shown as mean \pm s.e.m. of three independent experiments ($n = 3$). **e**, The occurrence of DNA single-strand breaks induced by the MTH1 inhibitors SCH51344 and (S)-crizotinib is significantly decreased in SW480 cells overexpressing human MTH1 compared to empty vector transfected cells. Concentrations used are as in **c**. Numbers depict MTM \pm s.d.;



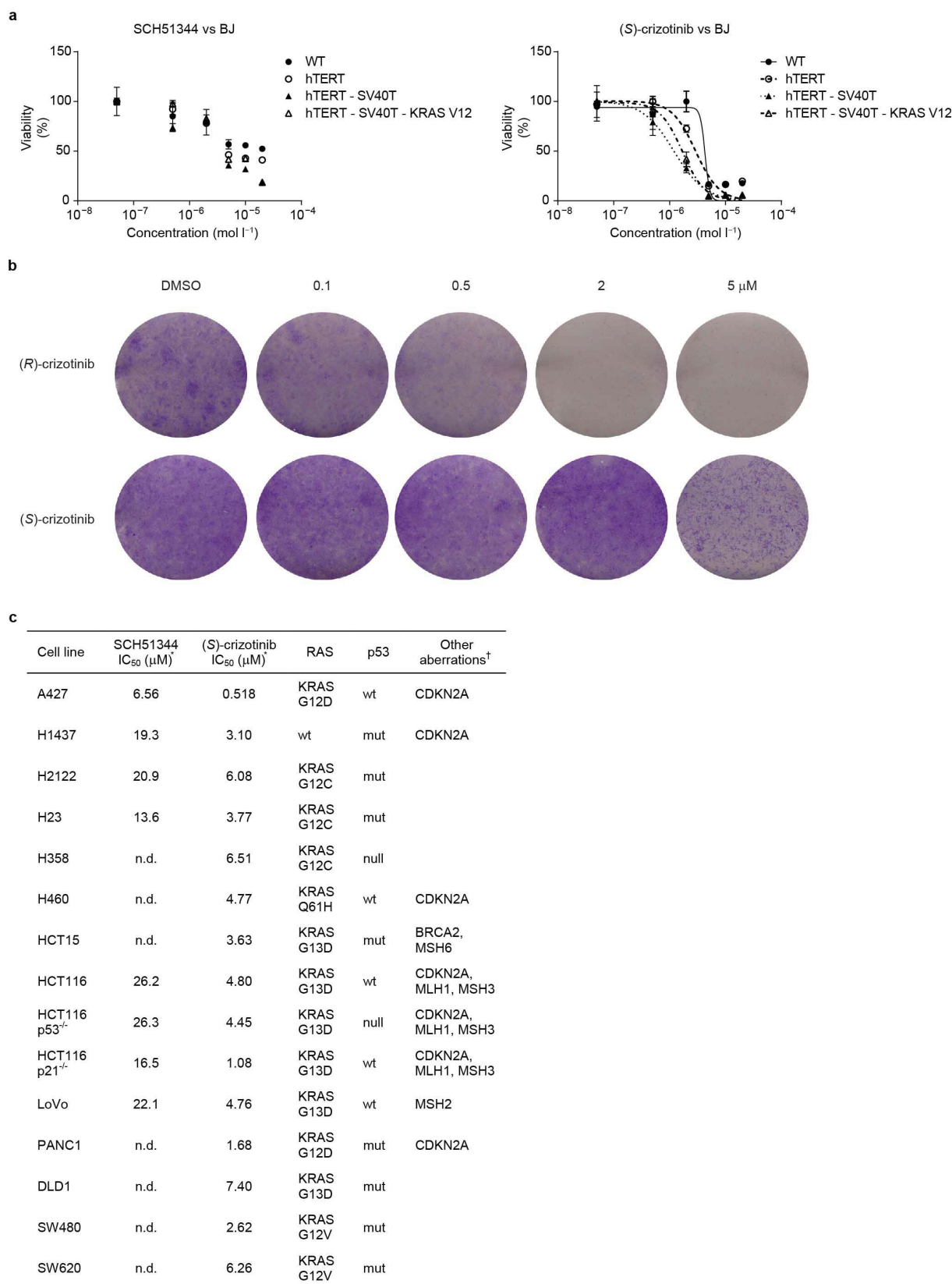
Extended Data Figure 7 | MTH1 inhibitor efficacy is not affected by loss of p53. **a**, Western blot evaluation of p53-shRNA knockdown efficiency. **b**, Viability curves from colony formation assays of SW480 cells expressing inducible non-targeting (shRen.713), or targeting anti-p53 shRNAs. Cells were cultured for 2 days either with or without doxycycline, plated in triplicate in

six-well plates, and drugs added 24 h later. Colonies were stained with crystal violet and quantified using ultraviolet absorbance after dye solubilisation with ethanol. Data are shown as mean \pm s.e.m. and are based on three independent experiments ($n = 3$).



Extended Data Figure 8 | Interplay of MTH1 activity and DNA damage proteins. **a**, Stable knockdown of MTH1 does not alter SW480 sensitivity towards ATM (KU55933) or ATR (VE821) kinase inhibition. Data are shown as mean \pm s.e.m. and are based on three independent experiments ($n = 3$). **b**, Conversely, ATM status does not affect MTH1 inhibitor efficacy in immortalized mouse embryonic fibroblasts. Data are shown as mean \pm s.e.m. and are based on three independent experiments ($n = 3$). **c**, As observed for

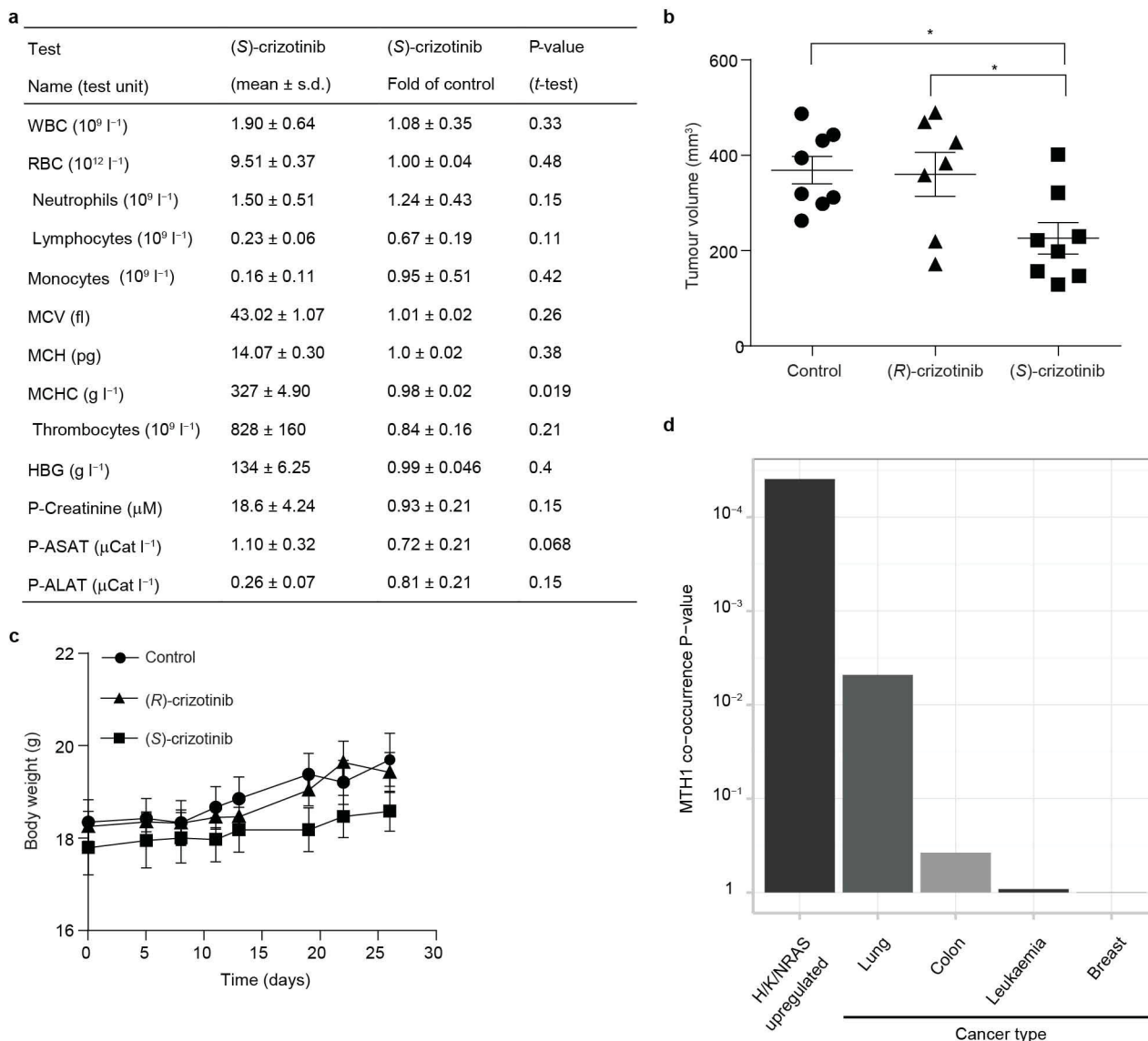
SW480, loss of p53 does not impair the sensitivity of KRAS-mutant HCT116 towards MTH1 inhibitors; however, p21^{-/-} cells are more sensitive, in particular to the more potent MTH1 inhibitor (S)-crizotinib (top). Data are shown as mean \pm s.e.m. and are based on three independent experiments ($n = 3$). WT, wild type. Similarly, BRCA2 function does not alter MTH1 inhibitor sensitivity of VC-8 cells (bottom). Data are shown as mean \pm s.e.m. and are based on three independent experiments ($n = 3$).



*Values represent average from triplicate experiments ($n = 3$).
 †Mutation data are adapted from COSMIC (n.d., not determined).

Extended Data Figure 9 | MTH1 inhibitors exert selective toxicity towards transformed cells. **a**, BJ cells transformed by KRASV12 or SV40T are more sensitive to the MTH1 inhibitors SCH51344 and (S)-crizotinib than wild type fibroblasts or cells immortalized by telomerase expression. Data are shown as mean \pm s.e.m. for three independent experiments ($n = 3$). **b**, (S)-Crizotinib does not exhibit any increased unspecific cytotoxicity compared to

(R)-crizotinib. In contrast, the (R)-enantiomer significantly impairs the growth of untransformed BJ skin fibroblasts at low micromolar concentrations in a colony formation assay. Compounds were added 24 h after seeding the cells and plates were incubated for 10 days, washed, fixed, and stained with crystal violet. Images are representative of two independent experiments ($n = 2$). **c**, IC₅₀ values for MTH1 inhibitors tested against a cancer cell line panel.



Extended Data Figure 10 | Xenograft supplementary data and Oncomine MTH1 meta-analysis. **a**, Mouse haematology and liver/heart/kidney parameters comparing treatment versus controls. SCID mice ($n = 8$ per group) were subcutaneously administered vehicle or (S)-crizotinib (25 mg per kg) for 35 days. Blood samples were obtained by orbital bleeding (under anaesthesia); blood parameters were analysed using whole blood and ASAT, ALAT and creatinine were analysed in EDTA-collected plasma by the Karolinska Universitetslaboratoriet, Clinical Chemistry. The mean values of white blood cells (WBC), red blood cells (RBC), neutrophils, lymphocytes, monocytes, mean corpuscular volume (MCV), mean cell haemoglobin (MCH), mean cell haemoglobin concentration (MCHC) from the different groups are presented

in the table. The results did not show any significant differences between control and treated groups apart from a minor change in MCHC. **b**, Effect of (R)-crizotinib (50 mg per kg, orally, daily), (S)-crizotinib (50 mg per kg, orally, daily) or vehicle on tumour volume at day 26 in SW480 xenograft mice. Individual data are shown, $n = 7-8$ animals per group. Statistical analysis performed by two-way repeat measurement ANOVA, followed by Sidak's multiple comparison. **c**, Effect of treatment on body weight. Data show mean \pm s.e.m. **d**, Meta-analysis of Oncomine data. MTH1 expression strongly correlates with upregulated RAS, which is also reflected by the fact that cancers with high prevalence of RAS mutations such as lung and colon carcinoma express higher levels of MTH1 than other unrelated cancer types.

3.3 Phenotypic screens reveal neuroblastoma and Ewing sarcoma specific synergistic combinations of clinically applicable targeted small molecules

A synergistic drug combination is supposed to be more potent than equally effective doses of its components (Greco *et al*, 1995), thus providing additional benefit to patient over a simple increase in single dosages. Furthermore, the occurrence of drug resistance is prevented or at least postponed. In this study, using a parallel combinatorial screening approach, we aimed to identify combinations of targeted agents that act highly synergistically and exclusively in the specific disease context. A drug library focused on clinically relevant agents allowed us to discover combinations that could be translated to patients relatively easily. Moreover, investigating specific drug-drug interactions in a particular disease landscape can lead to improved understanding of differences in cancer biology. We focused on pediatric tumors; they are basically developmental diseases, with only a few mutations found in genes that code for druggable targets. Although improved, the overall survival rate is still rather low in the aggressive forms of pediatric tumors and many childhood cancer survivors experience long-term effects of chemotherapy.

Neuroblastoma is the most common cancer in infancy (Gurney *et al*, 1997) and the most common extracranial solid tumor in children (Maris *et al*, 2007; Smith *et al*, 2010; Gatta *et al*, 2014). It is a remarkably heterogeneous tumor; to address this, we used isogenic cell line systems in which we could control for the expression of the main prognostic factors in neuroblastoma: NMYC and TRKA. Perhaps a major factor that contributes to the therapeutic failure in neuroblastoma is the occurrence of resistance (Alisi *et al*, 2013) caused by the overexpression of drug efflux transporters. We found that kinase inhibitor lapatinib strongly synergizes with potent cytotoxic compound YM155 by inhibiting ABCB1 transporter, thus reverting intrinsic and/or acquired resistance to YM155 in neuroblastoma cells.

Ewing sarcoma is a highly malignant tumor that occurs mostly in bones, but can affect soft tissue as well. The focus on inhibiting signaling pathways associated with the fusion oncoprotein is comprehensible when one considers that its biological driver EWS-FLI1 is a challenging drug target, being a transcriptional factor. However, early excitement that came from the availability of small molecules that can target molecules associated with Ewing sarcoma progression, such as mTOR, IGF1R PDGFR, VEGFRs, AURKA, PARP1 and GD2 (Jiang *et al*, 2015), came to an end after rather disappointing clinical data, where acquired resistance was one of the main issues. Combination therapy is an attractive alternative, in Ewing sarcoma as well as in other childhood cancers. The importance of the IGF axis in

Ewing sarcoma and other cancers was recognized almost two decades ago. The activated IGF1R pathway is necessary for malignant transformation by EWS-FLI1 (Toretzky *et al*, 1997; Scotlandi *et al*, 1996). Although in a certain number of patients the response to IGF1R inhibitors was dramatic, the overall rate was discouraging. We found that IGF1R inhibitors strongly synergize with PKC412, a compound that was already previously shown to be potent in Ewing sarcoma in vitro and in vivo (Boro *et al*, 2012). The combination of these two agents caused cell death by a mechanism that was clearly more than a pure sum of the individual effects. Furthermore, deeper analysis of all specific drug-drug interactions detected in the screen enabled a better understanding of the Ewing sarcoma signaling landscape.

3.3.1 A parallel combinatorial drug screen reveals distinct disease specific drug-drug interactions

We selected an initial library of targeted agents that were either clinically approved or in clinical trials, with an emphasis on safety for use in pediatric patients. The library was comprised of carefully selected compounds that illustrated current chemotherapeutic landscape of pediatric tumors (Figure 7A). In order to define a most efficient and representative sub-library for the combinatorial screen, first we determined potencies of an initial panel of small molecules in three pediatric tumor entities - Ewing sarcoma (ASP14 cell line), neuroblastoma (SH-SY5Y cell line) and medulloblastoma (UW28 cell line). Only drugs that were robustly and potently cytotoxic as single agents in each of the three tumor types were included in the combo sub-library. Since the aim was to capture disease-specific synergies, we created equal primary conditions to be able to pointedly compare combinatorial effects observed in parallel screens. Namely, all screens were done using equivalent specific sub-libraries based on half-inhibitory single drug concentrations that varied between the disease entities. A factorial dilution matrix approach was used, enabling us to capture drug associations in detail (Lehár *et al*, 2008). Thirty-six point concentration matrices were centered around IC_{50} values for each given drug and the combinatorial effect was calculated based on the Loewe additivity approach. Loewe additivity can be quantified by the combinatorial index (CI), i.e. the theorem of Chou-Talalay (Chou & Talalay, 1984). This method was used for the screen analysis since it is the most relevant reference in medical applications (Lehár *et al*, 2008). Due to a rapid augmentation of the number of data points with every additional compound in a concentration matrix based screening design, we applied strong criteria and deliberately selected a relatively small number of drugs that

potently inhibited cancer cell growth. On average, we found more combinations to be strongly synergistic than usually seen in combinatorial screens, most probably due to the directed library design approach (Figure 7B-D). The results varied between different screens, with the lowest rate of synergistic events in medulloblastoma and the highest in the Ewing sarcoma screen. Pediatric tumors have quiet genomes without acquired mutations typical for adult cancers. This led to speculations of a similar signaling context, since childhood tumors are determined by developmental processes, during which a number of tumor suppressors and proto-oncogenes have distinct roles. We observed, however, a relatively high specificity of the combinatorial events in the parallel screens.

3.3.2 Alterations in transport properties cause potent drug synergy in neuroblastoma

We focused on a highly potent synergy between kinase inhibitor lapatinib and anticancer compound YM155 (Figure 8A). In 2007 dual EGFR/HER2 kinase inhibitor lapatinib was approved by FDA for the combination therapy for breast cancer patients already using capecitabine, and in 2010 for women with HER2 positive metastatic breast cancer. It was also in phase II clinical trials for a number of malignant conditions in young patients. YM155 (sepantronium bromide) was in phase II clinical trials for single and combination therapy in a variety of cancer types. It causes downregulation of survivin, whilst its major mechanism of action is the induction of DNA damage (Winter *et al*, 2014; Chang *et al*, 2015). The interaction between these two agents was confined to a relatively small window of opportunity, only within a small subset of concentration (Figure 8B) but there reaching up to 70% more inhibition than predicted by the Bliss independence model. Moreover, it occurs in the lower, clinically relevant dose range; this concentration of lapatinib is achievable in pediatric patients and considerably lower than the serum limit (Karajannis *et al*, 2012; Fouladi *et al*, 2013). YM155 has worse pharmacokinetic profile compared to lapatinib; still, desired plasma combo concentration for YM155 is achievable and well tolerated in patients (Kudchadkar *et al*, 2015). Next, we confirmed the synergy in a long-term assay (Figure 8D) where the compounds were applied at 10- or 15-fold lower concentrations than their respective IC_{50} in SH-SY5Y cell line. Not surprisingly, single drugs at these concentrations were unable to cause cell death; the combination, however, was toxic to almost entire cell population. We observed marked global expression changes upon combinatorial treatment in SH-SY5Y, but little or no significantly regulated genes when SH-SY5Y cells were treated with single drugs (Figure 8C). The number of significantly regulated

genes resulting from treatment with either of the drugs alone was relatively low. When the two compounds were combined, however, broad alterations in the transcriptome were observed, with 1158 genes significantly upregulated and 1221 genes significantly downregulated.

NMYC proto-oncogene is amplified in neuroblastoma and correlated with advanced stages of the disease and with aggressiveness and poor prognosis (Brodeur et al, 1984; Seeger et al, 1985). To check whether lapatinib and YM155 synergize if signaling landscape is altered by NMYC we used engineered SH-SY5Y that allowed inducible expression of this gene (Figure 8F), since SH-SY5Y cell line has only one copy of NMYC. We could confirm that the effect was not NMYC dependent, since high degree of synergy was preserved not only when expression of NMYC was induced in SH-SY5Y, but also in NMYC-amplified IMR5-75 cell line that expresses high levels of NMYC (Figure 8F). In difference to NMYC, neuroblastomas that express NTRK1 (or TRKA, a member of TRK family of neurotrophin receptors) are likely to spontaneously regress or differentiate, depending on the presence of its ligand (NGF) (Brodeur et al, 2009). The most promising approach to induce spontaneous regression is the NTRK1 pathway inhibition (Brodeur & Bagatell, 2014). SH-SY5Y with ectopic expression of NTRK1 upon induction with NGF showed slightly reduced synergistic potential compared to the wild type cells (Figure 8E). The pattern of the effect was conserved, since the strongest synergy was detected at lowest concentrations. We concluded that lapatinib and YM155 synergize regardless of the NMYC and NTRK1 status.

Intrigued by the high potency of synergy between lapatinib and YM155, we hypothesized that an “on/off” type of mechanism might be responsible for the effect. Neuroblastoma is often associated with overexpression of a number of ABC transporters, leading to intrinsic resistance to various therapeutics (Norris *et al*, 1996; Cialfi *et al*, 2010). Indeed, when we compared the IC₅₀ of YM155 in SH-SY5Y with Ewing sarcoma and medulloblastoma cells from our panel, we noted a dramatic difference in sensitivity, with values ranging from ~ 1 nM in ASP14 to ~ 250 nM in SH-SY5Y (Figure 8H). We tested if lapatinib interferes with intracellular concentration of YM155, using multiple reaction-monitoring assay. Lapatinib dramatically increased amount of YM155 in the cell (Figure 8G), probably by inhibition of the export of YM155. Lapatinib was shown to inhibit both ABCB1 and ABCG2 transporters (Dai *et al*, 2008). YM155 is a substrate of ABCB1 (Iwai *et al*, 2011) and neuroblastoma cell lines resistant to YM155 are shown to have high levels of ABCB1 (Lamers *et al*, 2012). Neuroblastomas are known to express high levels of ABCC1 transporter as well (Alisi *et al*, 2013; Yu *et al*, 2015). We found that lapatinib increased intracellular concentration of YM155 to a larger extent than cyclosporine A, a known inhibitor of ABCB1; conversely, pre-treatment with MK-571 and KO143, inhibitors of ABCC1 and ABCG2 transporter, respectively, did not influence the amount of YM155 inside the cell

(Figure 8G). Synergy between YM155 and lapatinib emerged as neuroblastoma specific in our parallel screens. When combination was tested in ASP14 Ewing sarcoma cell line we observed mild to strong antagonism (Figure 8I). Ewing sarcoma tumors in general have lower expression of ABCB1, as reported in CCLE (Cancer Cell Line Encyclopedia) (Barretina *et al*, 2012) and neither lapatinib nor cyclosporine A could influence the intracellular concentration of YM155 in ASP14 (Figure 8I). Thus, the dramatic synergistic effect observed when lapatinib and YM155 were combined was characteristic for ABCB1 expressing neuroblastoma and a consequence of prolonged and potentiated cytotoxic effect of YM155 enabled by ABCB1 inhibition by the second drug, lapatinib.

3.3.3 Combination of PKC412 with IGF1R/INSR inhibitors is synergistic in Ewing sarcoma

A number of drug-drug interactions proved to be specific for Ewing sarcoma, allegedly a consequence of particular signaling alterations caused by EWS-FLI1 (Figure 9A). These disease specific synergies between the drugs could serve as a promising starting point for a precision approach to clinically target Ewing sarcoma unique vulnerabilities. In this light, we focused on characterizing the combination between a PKC/KIT inhibitor and an IGF1R/INSR inhibitor.

We were curious about disease specific potent drug combinations that emerged from the screens. PKC412, a staurosporine derivative annotated as PKC/KIT inhibitor, strongly synergized with all small molecule IGF1R inhibitors present in the combinatorial sub-library (Figure 9B). PKC412 is an oral, multi-targeted kinase inhibitor in Phase III clinical trial for treatment of patients with FLT3-mutated acute myeloid leukemia (AML) and in Phase II for mast cell leukemia (MCL) and aggressive systemic mastocytosis (ASM). PKC412 has been shown to induce apoptosis of Ewing sarcoma cells *in vitro* and *in vivo* (Boro *et al*, 2012). Both BMS-754807 and OSI-906 are oral, reversible ATP-competitive antagonists of IGF1 receptor that, unlike anti-IGF1R monoclonal antibodies, block also the insulin receptor and the hybrid dimers (IGF1R/INSR) which is advantageous in cancer treatment (Avnet *et al*, 2009; Zhang *et al*, 2007). In a number of preclinical tumor models induction of INSR signaling by insulin or IGF2 (Morrione *et al*, 1997) has been implicated. Strong synergism observed uniquely in ASP14 between PKC412 and both IGF-1R/INSR inhibitors was recapitulated in validation experiments, with the same factorial design of matrix pair-wise testing of serial dilutions as in the screen.

In addition to Loewe additivity CI model, we tested the effect by the second most used mathematical model for the synergy determination - the Bliss independence model (Bliss, 1939). We observed strong synergy at a broad array of concentrations, which demonstrates a relatively wide window of opportunity (Figure 9C). Moreover, the synergy was confirmed in a long-term assay, where the combination efficiently inhibited the colony formation of ASP14 cells to a much larger extent than either of the drugs alone (Figure 9D). We then checked whether this potentiation is a consequence of alteration of influx or efflux caused by either of the drugs. Small molecules require transporters for the import and the export from cells, and inhibition of these pumps can severely interfere with the intracellular concentration of a drug necessary to exert its effect. Changes in the drug transport, however, did not seem to account for the mechanism of synergy, since neither of the drugs was interfering with the intracellular concentration of the other drug partner, as shown by mass spectrometry based multiple reaction-monitoring assay (Figure 9E). Next, Annexin V immunostaining and subsequent FACS analysis affirmed the increased frequency of dead and apoptotic cells in the combo treated sample (Figure 9F), to a greater extent than the drugs alone. Finally, we tested the combination in a panel of Ewing sarcoma cell lines that differed regarding sensitivity to single agents and had different types of EWS-FLI1 fusion. All of them displayed a synergistic effect, expressed as a change in equipotent IC₅₀ concentrations, including the ASP14 parental A673 cell line (Figure 9G). Taken together, these data showed that the combination of PKC412 and an IGF1R/INSR inhibitor exhibited strong synergy in the context of Ewing sarcoma.

3.3.4 PKC412 target identification in the EWS-FLI1 altered signaling context

Currently available IGF1R/INSR inhibitors vary in their target specificity; they are often inhibiting receptor tyrosine kinases beyond the IGF1R and INSR family. OSI-906 and BMS-754807, however, were shown to be rather specific (Chen & Sharon, 2013). While for OSI-906 there are no reported potent off-targets (Chen & Sharon, 2013), BMS-754807 can inhibit few other kinases to various extents, most potently MET, RON, TRKA, TRKB, AURKA and AURKB although with markedly lower selectivity than IGF1R and INSR (Carboni *et al*, 2009). We observed similar synergistic potential between PKC412 and both IGF1R/INSR inhibitors, indicating that the IGF1 axis inhibition is vital for the synergy to occur. Still, it was indecipherable which portion of the broad target spectrum of PKC412 is responsible for its effect in Ewing sarcoma. PKC412 is a multi-targeted, promiscuous kinase inhibitor,

recognized mostly for treatment of FLT3 mutated leukemia. FLT3 is poorly expressed in Ewing sarcoma and the target spectrum of PKC412 in this context was uncharted. PKC412 was shown to be a modulator of EWS-FLI1 target gene expression (Boro *et al*, 2012). We treated ASP14 cells with either relatively high-dose PKC412 (5 μ M) or combinatorial treatment at previously determined combo concentrations and did not observe any significant changes in expression levels of NKX.2, NROB1 and PHLDA1, all transcriptionally regulated by EF (Smith *et al*, 2006; Kinsey *et al*, 2006; Boro *et al*, 2012), although the expression levels changed dramatically upon EWS-FLI1 knockdown (Figure 10A).

In order to deconvolute the target profile of PKC412 in Ewing sarcoma, we used a mass spectrometry based drug affinity chromatography method, i.e. chemical proteomics (Figure 10B). A coupleable analog of PKC412 (Borgdorff *et al*, 2014) was immobilized on sepharose beads and affinity purification of interacting proteins from lysates of ASP14 cells was performed as described in chapter 3.1. To be able to distinguish relevant targets in the Ewing sarcoma background, we performed reciprocal analyses with ASP14 cells where expression of EWS-FLI1 had been genetically suppressed by means of an inducible shRNA for 72h (Figure 12D). Although remnants of the fusion protein were still detectable at that point, the overall presence and the impact of EWS-FLI1 were significantly impaired, thus allowing us to distinguish a Ewing sarcoma relevant PKC412 target profile. This was compelling, especially in the context of specificity of the synergistic effect between PKC412 and the IGF1R/InsR inhibitor. Prior to the LC-MSMS analysis, drug pull-down samples from both ASP14 wt and EWS-FLI1 (EF) knock-down (kd) conditions were checked via Western blot for presence of Aurora kinase A (AURKA), a known target of PKC412 and one of the kinases upregulated by the EF oncoprotein (Winter *et al*, 2011). As expected, AURKA was much more abundant in the WT compared to the EF kd and it was specifically bound by the drug, as confirmed by the effective competition experiment. Conversely, although still moderately present in the lysates, AURKA was not detected in the EF kd experiment, hence we were able to confirm a differential target profile as hypothesized (Figure 10C) In-depth analysis of the ASP14 chemical proteomic experiment revealed further interactors of PKC412 (Figure 10D). In line with its reported promiscuity, the compound target spectrum was spread across the kinome tree (Figure 10E). Both tyrosine and serine-threonine kinases were inhibited by the drug. Interestingly, though, when we compared small molecule-protein interactions reported in STITCH ('search tool for interactions of chemicals') (Kuhn *et al*, 2008) with high confidence with the target profile we retrieved, we did not find a considerable overlap (Figure 10F), in line with the expected distinct mechanism of a drug in a particular signaling context. Nonetheless, 16 cognate targets in overlap with STITCH and additional previously non-reported interactors of PKC412 illustrated the signaling landscape in Ewing sarcoma as suggested by the observed drug profile. When all reliable targets were mapped

onto established cellular pathways, a few signaling routes emerged as crucial for conveying the effect of the drug.

Changes in calcium-dependent signalling mechanisms are frequently altered and remodeled in cancer cells, including Ca^{2+} sensors and effectors, for instance calmodulin (CAM) and its downstream targets, such as CAM kinase (CAMK) (Means, 2000), calcineurin (Klee *et al*, 1998) and protein kinase C (PKC) (Roderick & Cook, 2008). CAMK are serine-threonine kinases that are usually related to learning and memory processes. It was shown, however, that CAMKI or CAMKII inhibition can alter tumor cell proliferation in breast cancer and osteosarcoma (Rodriguez-Mora *et al*, 2005; Yuan *et al*, 2007). Moreover, an emerging body of evidence showed that these enzymes can also modulate cancer invasion capacity (Wang *et al*, 2015). Almost the whole class of CAMKII kinases was captured in a complex with PKC412, as well as other cognate calcium signaling kinases, such as PRKCA, PRKCB and PDGFRB, arguing for a thorough blockade of the pathway. Furthermore, it was reported that in Ewing sarcoma insulin pathways promote proliferation and malignancy (Garofalo *et al*, 2011). Interestingly, it was shown that PDGFR is involved in mediating resistance to BMS-754807 in human rhabdomyosarcoma model (Huang *et al*, 2010). We detected a number of confident interactors that are notably insulin signaling related according to the KEGG database (PDK1, PRKAA2, PRKAB1, PRKAB2) and reported in competition binding assays (Davis *et al*, 2011). Overlap between the mTOR and insulin pathways pointed to another binder of PKC412, ULK3 (Unc-51 Like Kinase 3), a known regulator of autophagy. This serine-threonine kinase seems to be dependent on EWS-FLI1, since it was not found in EF reduced environment (Figure 10F), thus potentiating its impact in the Ewing sarcoma context. We are currently investigating this relationship further. Altogether, we concluded that PKC412 exerted its cytotoxic effect by inhibiting crucial ES cancer cell signaling routes – calcium, insulin and mTOR pathways.

3.3.5 Synergistic effect of the drug combination comes from a particular alteration of phosphorylation events

Following up on the chemical proteomic analysis, we set out to investigate the consequences of single and combinatorial drug treatment on signaling networks. We compared four different conditions (DMSO treated, PKC412, BMS-754807 and combo (combination of the two drugs)) using a quantitative proteomics approach (Olsen & Mann, 2013), where we combined stable isotope labeling by amino acids in cell culture (SILAC) (Ong *et al*, 2002) and high-resolution liquid chromatography–tandem mass spectrometry

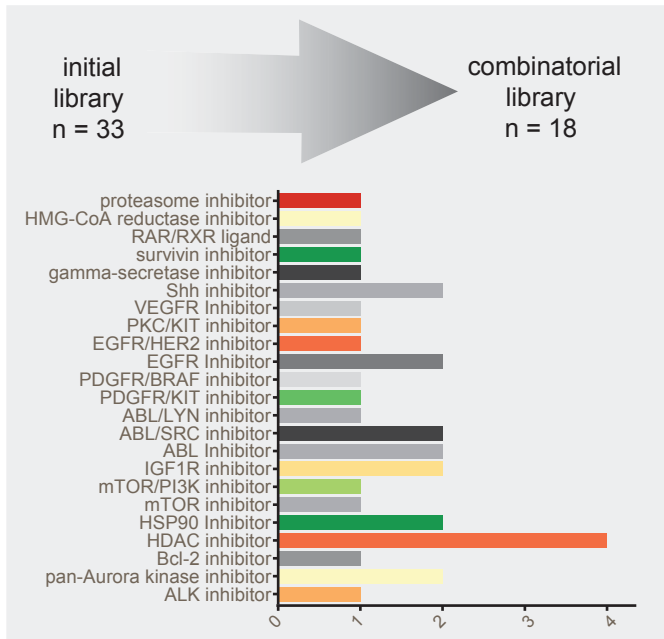
(LC-MS/MS). In order to analyze the phosphoproteome, we treated serum starved ASP14 cells with compounds and then stimulated them with serum for 20 minutes (Figure 12A). We identified and quantified 13,228 phosphorylation sites on 3,586 proteins that were confident numbers in accordance with published studies (Figure 11A) (Olsen *et al*, 2006; Emdal *et al*, 2015).

As expected, the majority of phosphorylation sites deregulated by single drug treatments were overlapping with the combo. Curiously, out of 667 downregulated sites by the combinatorial treatment, more than half (386) were uniquely altered by combo (Figure 12B). The same particularity was observed with the compound-induced upregulation of phosphorylation sites, arguing for the exclusive mechanism of the synergistic effect. KEGG pathway enrichment analysis of combo downregulated sites showed a strong preference for MAPK and mTOR signaling, as well as the insulin pathway (Figure 12F). The overall effect of the combinatorial treatment that we observed was truly synergistic in nature - it encompassed single effects of both of the drugs and supplemented an exclusive combinatorial response. We implemented a cluster-dependent sequence motif analysis of the phosphorylation sites and observed a strong preference for PKC/AKT and MAPK motifs (Figure 12C). Interestingly, an ATM/ATR motif was upregulated by combinatorial treatment, most probably due to the activation of stress related DNA damage inducing pathways.

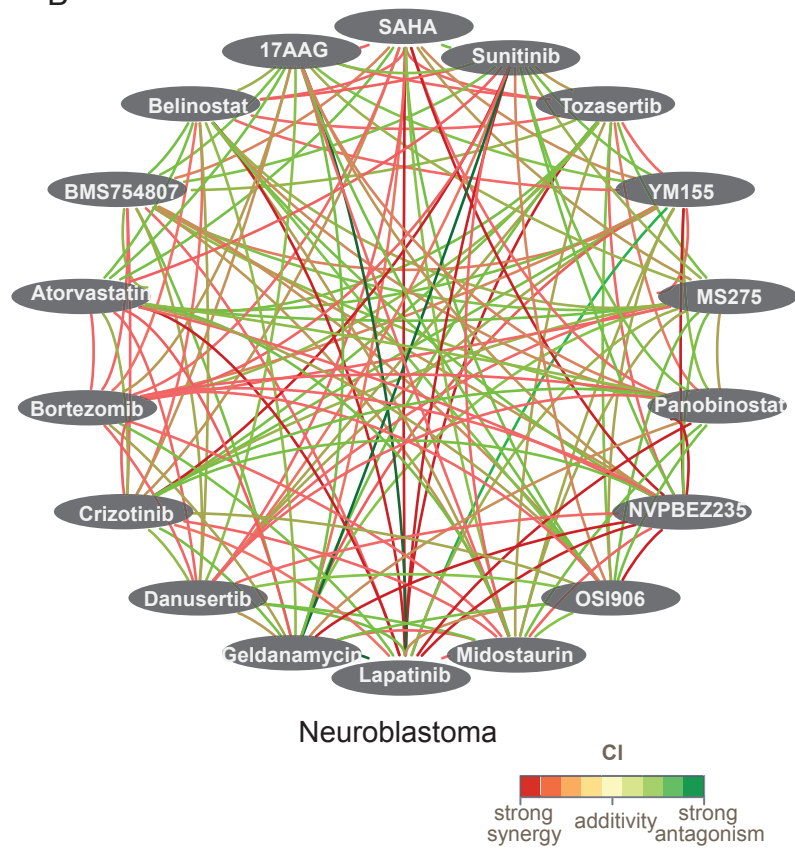
The ASP14 cell line allows for the conditional knockdown of EWS-FLI1 in a doxycycline dependent manner (Tirado *et al*, 2006). We tested the temporal resolution of the knockdown and selected the 72h point (Figure 12D) at which the cells were still not entering oncogene induced senescence and while the knockdown efficiency was satisfying. We compared the downstream signaling events in EWS-FLI1 “on” and “off” setting in same controlled conditions (upon starvation, drug treatment and short stimulation with serum). Combo treatment massively downregulated TORC2 dependent AKT S473 phosphorylation, even to a larger extent than the mTOR (dual mTORC1 and mTORC2) inhibitor torin 1 (Figure 12E); interestingly, upon EF knockdown the effect was markedly weaker. Also, an effect on AKT S473 phosphorylation by BMS-754807 was abolished when EF was reduced. Neither torin 1 nor rapamycin (mTORC1 inhibitor) had an effect on AKT T308 phosphorylation, a catalytic site for AKT activation. Combo treatment, however, notably decreased the phosphorylation also at this site, seemingly suppressing the feedback loop. Interestingly, phosphorylation of a downstream TORC1 effector p70S6 kinase (S6K) was also potently inhibited by combinatorial treatment, while no effect at all was observed in cells with reduced EF. Hence, PKC412 and BMS-754807 combined treatment was particularly effective only when the signaling pathways were alternated by EWS-FLI1 and in that context only, importantly, the combinatorial effect led to more potent pathway inhibition than if either of the drugs was applied alone.

The combo treatment indicated an overrepresentation of PKA and CaMKII motifs for downregulated sites (Figure 11E), in concordance with PKC412 chemical proteomics data. Curiously, for a number of relevant phosphoproteins we observed considerably stronger downregulation when drugs were applied together compared to PKC412 alone at the same concentration. For instance, this was true for a number of Ca²⁺/calmodulin dependent kinases (CAMK2D, DAPK2, CAMK1, PRKCB); some of those have been shown to be PKC412 targets but the overall effect was decidedly potentiated by the second drug.

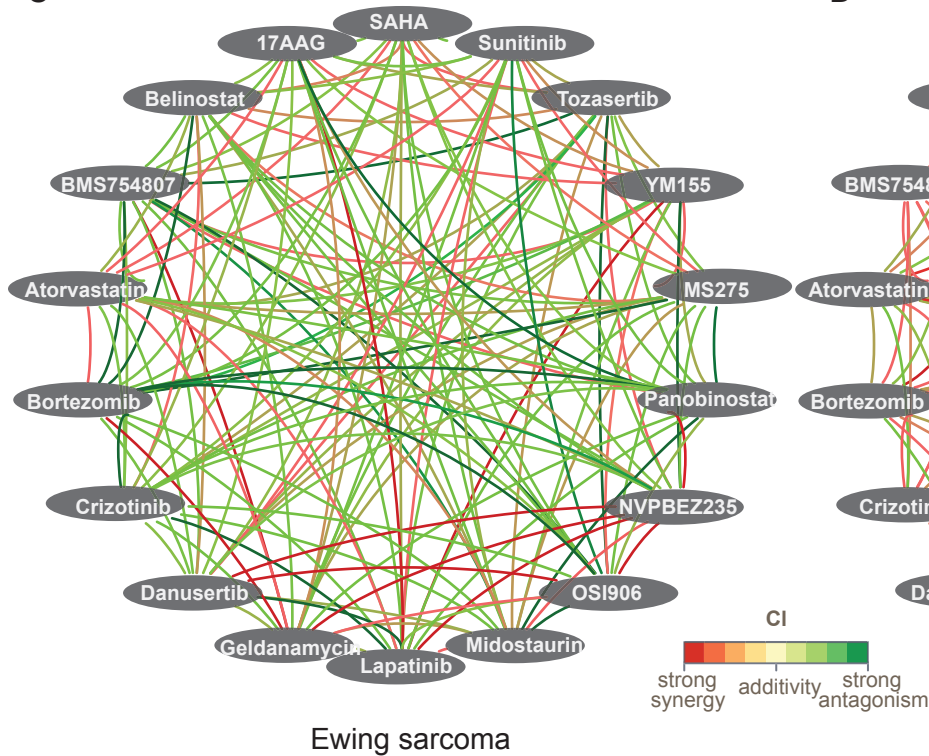
A



B



C



D

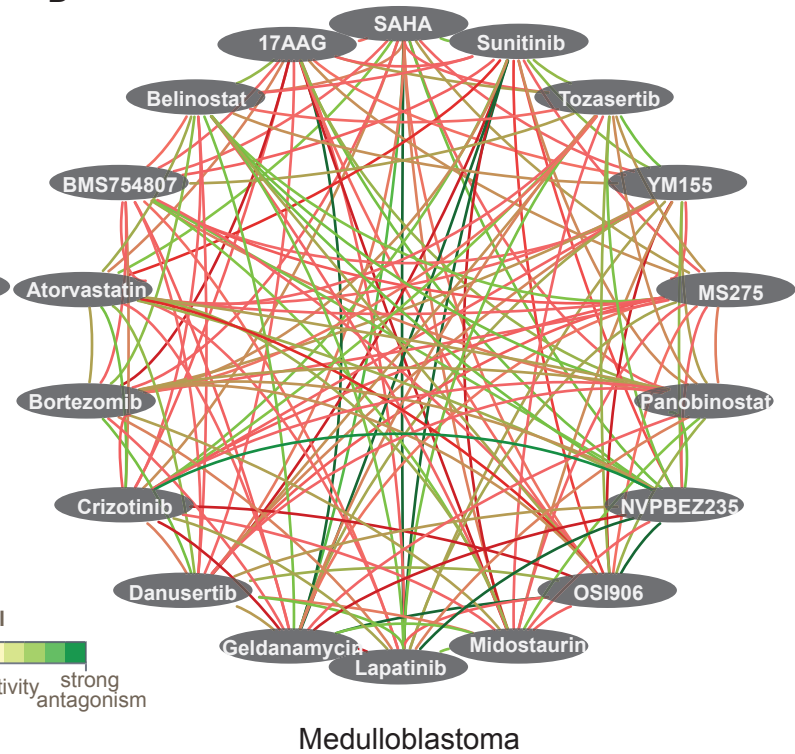


Figure 7. Drug synergy screens in three pediatric tumor entities (A) Initial drug library (grey and colored bars) and sub-library for the combinatorial screen (colored bars). (B-D) Drug-drug interactions found in combinatorial drug screens in (B) neuroblastoma, (C) Ewing sarcoma and (D) medulloblastoma.

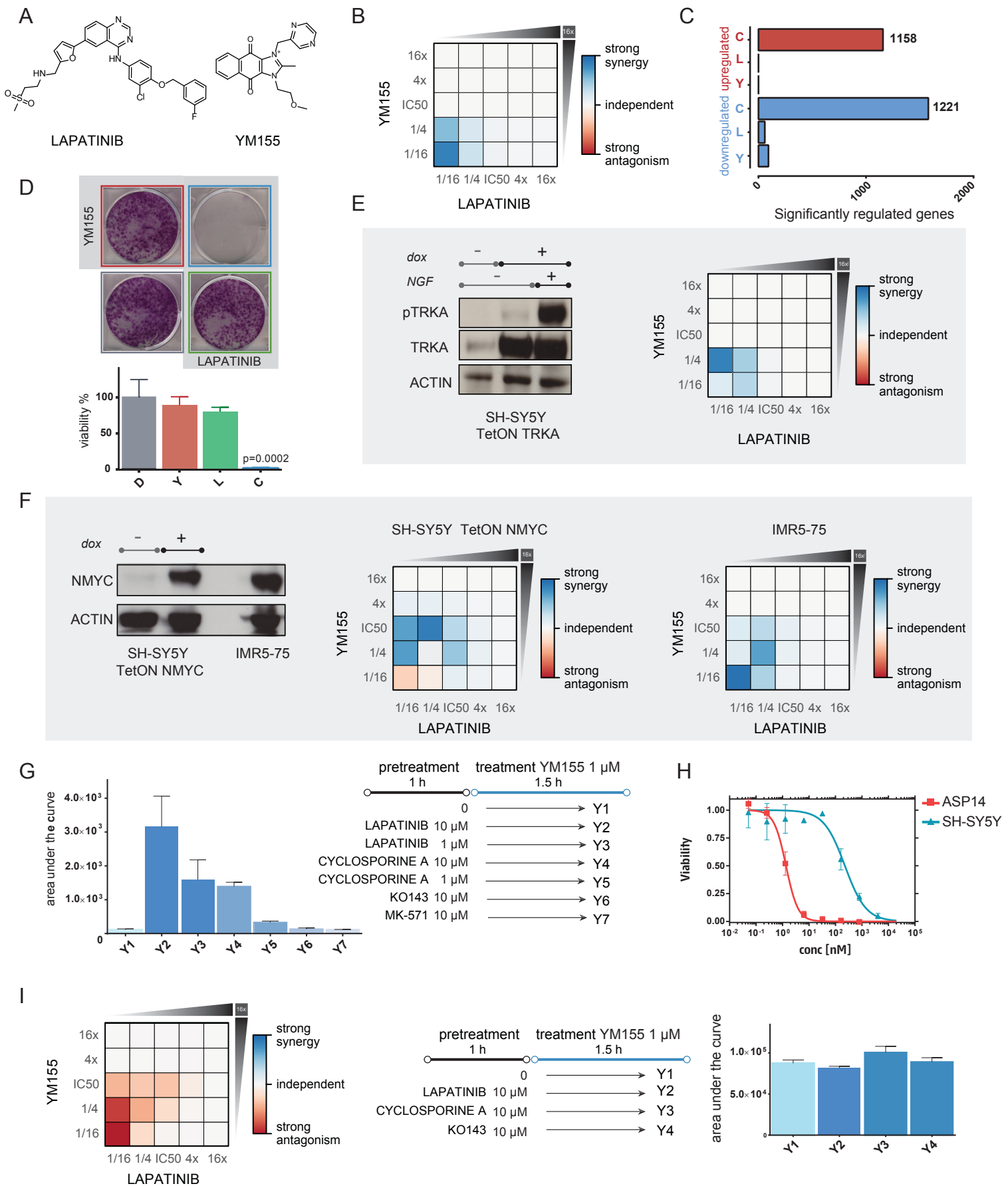


Figure 8. YM155 and lapatinib show high degree of synergy in neuroblastoma regardless of the NMYC and NTRK1 status. (A) chemical structures of YM155 and lapatinib. (B) validation of the synergy by Bliss independence. (C) Bar graphs showing the number of significantly upregulated and downregulated genes in each condition. (D) colony formation assay. (E) and (F) Synergistic effect is preserved in TRKA (E) and NMYC (F) highly expressed state. (G) MRM assay in SH-SY5Y neuroblastoma cell line. Lapatinib inhibits ABCB1 transporter and allows higher intracellular concentration of YM155. (H) Dose response curves of YM155 in ASP14 (red) and SH-SY5Y cell line (blue). (I) Synergy is not preserved in ASP14 Ewing sarcoma cell line, since YM155 levels are not dependent on ABCB1.

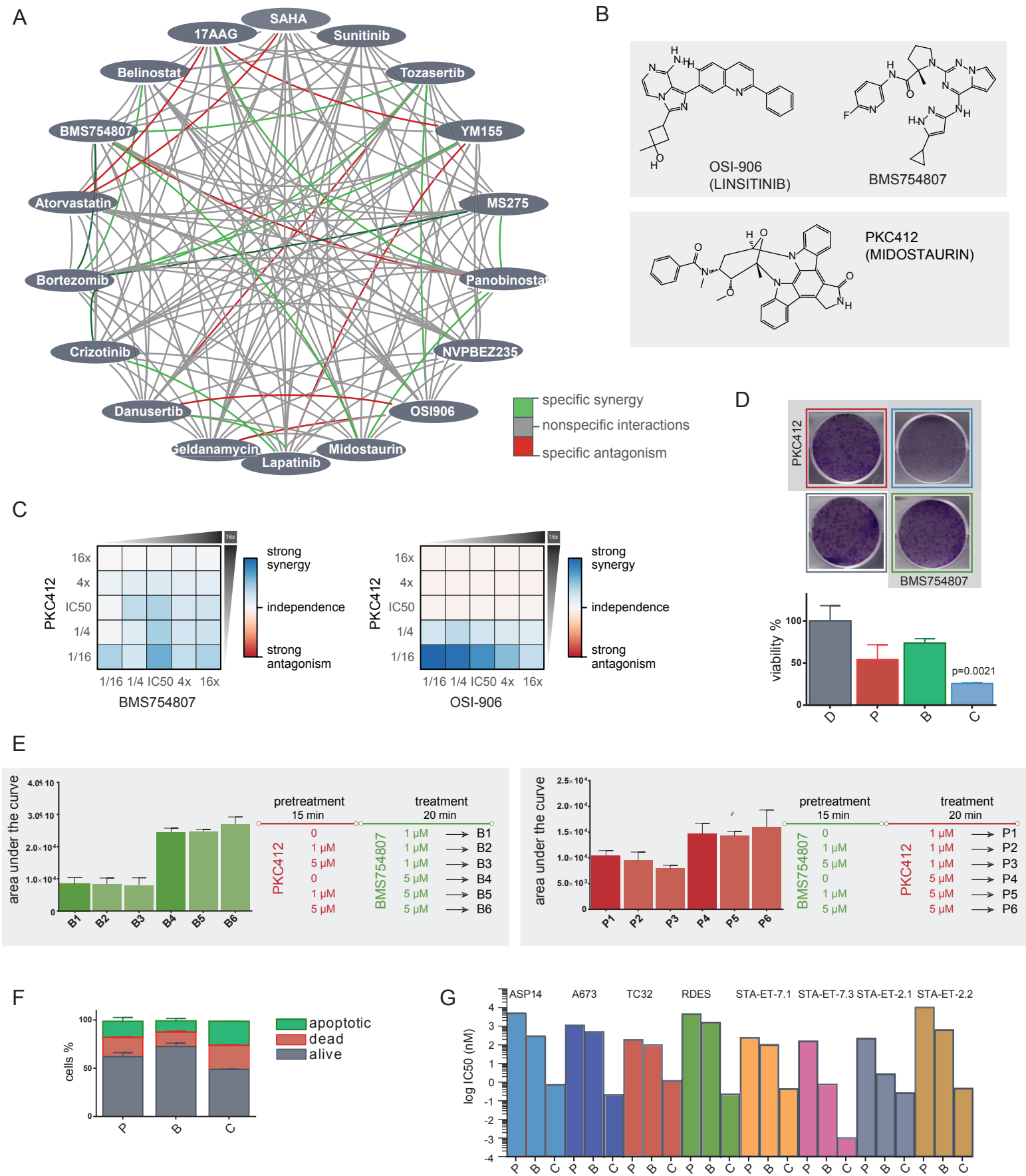


Figure 9. Combinatorial screen reveals Ewing sarcoma specific synergies. (A) Drug-drug interactions specific for ASP14 are shown, specific synergis (green) and specific antagonisms (red). (B) Chemical structures of PKC412 and the two IGF1R inhibitors from the drug panel. (C) Validation of the synergy found in the screen using the Bliss independence model. (D) Colony formation assay. (E) Multiple reaction monitoring assay. (F) Annexin V immunostaining. (G) Comparison of equipotent IC50 concentrations between single drugs and the combination in a panel of Ewing sarcoma cell lines. Analysis done using DDCV version: 4.0 Shiny by RStudio.

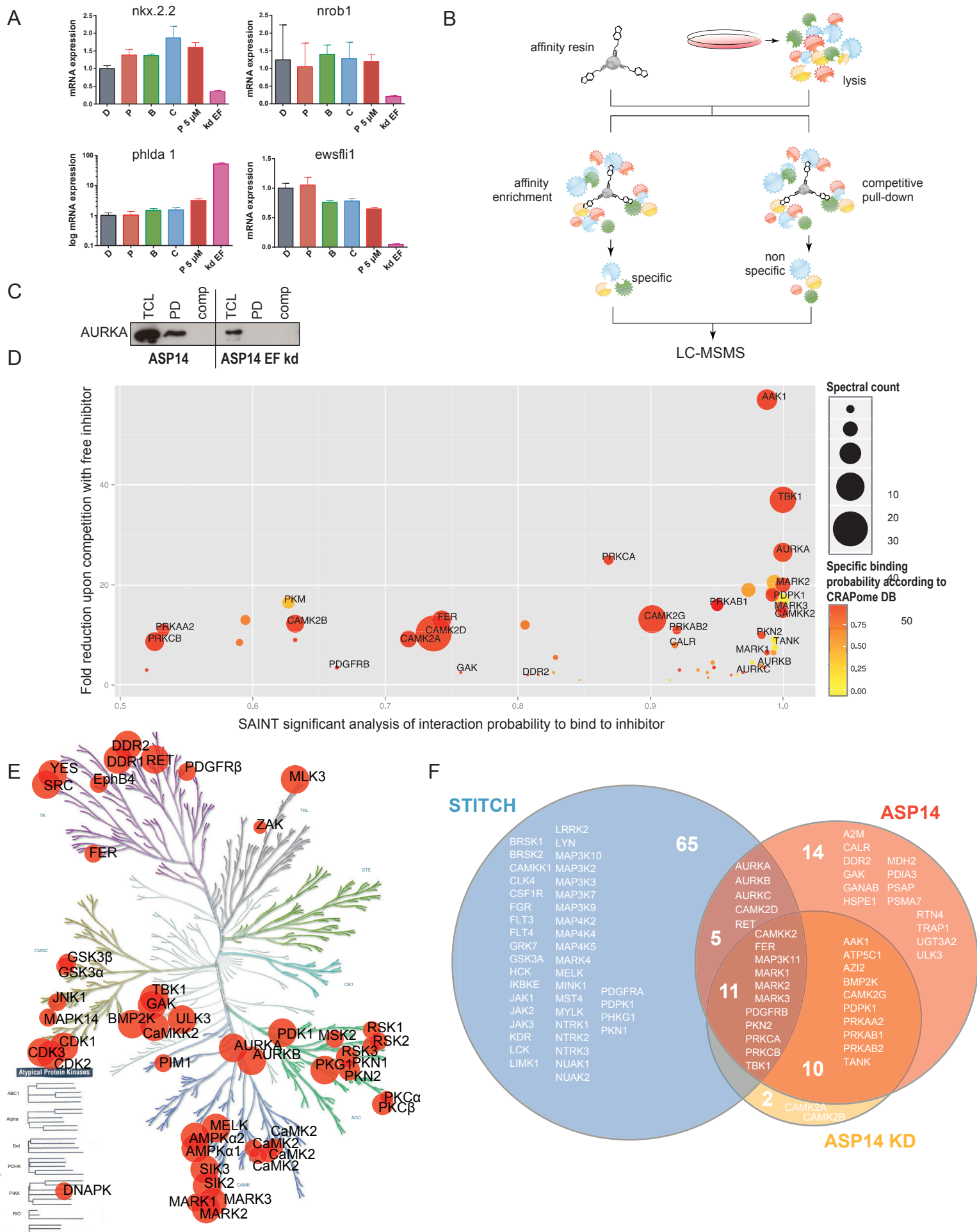
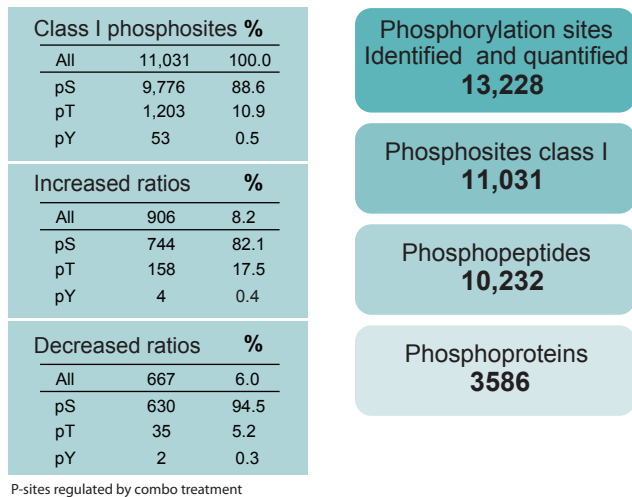
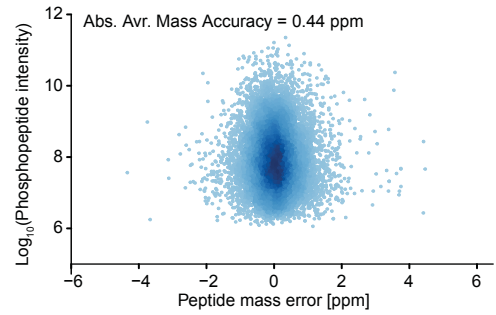


Figure 10. A chemical proteomic approach reveals the EWS-FLI1 determined profile of PKC412. (A) PKC412 does not cause changes on transcriptional level of several EWS-FLI1 target genes. (B) Schematic of the chemical proteomic experiment. (C) Control Western blot for the EWS-FLI1 target gene Aurora kinase A (AURKA). (D) Interactors of PKC412 in ASP14. (E) Distribution of PKC412 targets across the kinome tree. (F) Overlap between PKC412 targets confidently reported in STITCH and interactors found in ASP14 and ASP14 EWS-FLI1 knock-down pull-downs.

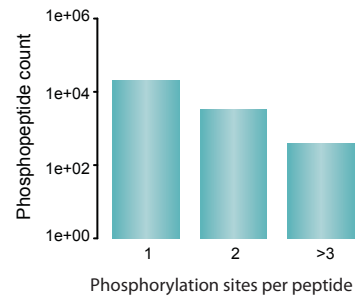
A



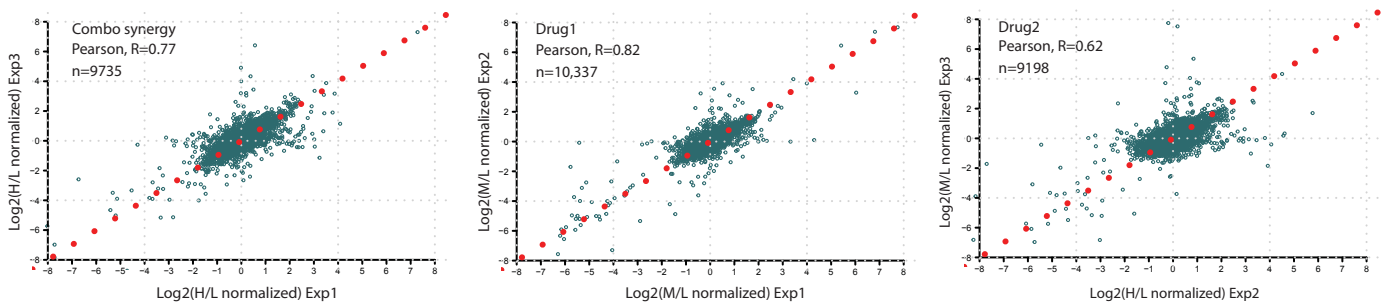
B



C



D



E

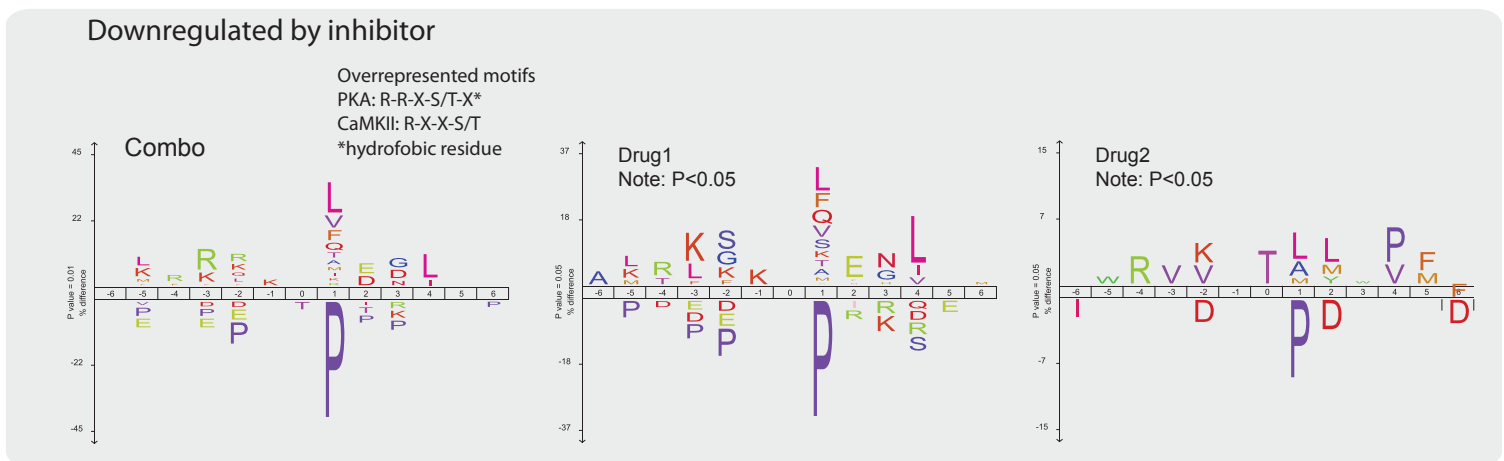


Figure 11. Overview of phosphoproteomic data. (A) Number of identified phosphorylation sites and phosphoproteins, as well as distribution by amino acid from the phosphoproteomic data. (B) Calibrated precursor mass errors measured for all peptides in parts per million (ppm) versus MS signal intensity of the identified phosphopeptides. (C) Distribution of the identified phosphopeptides displaying the number of phosphorylation sites per peptide. (D) Correlation plots of drug effects. (E) Sequence motif analysis (IceLogo). Combo treatment shows overrepresentation for CaMK and PKA motifs for downregulated sites.

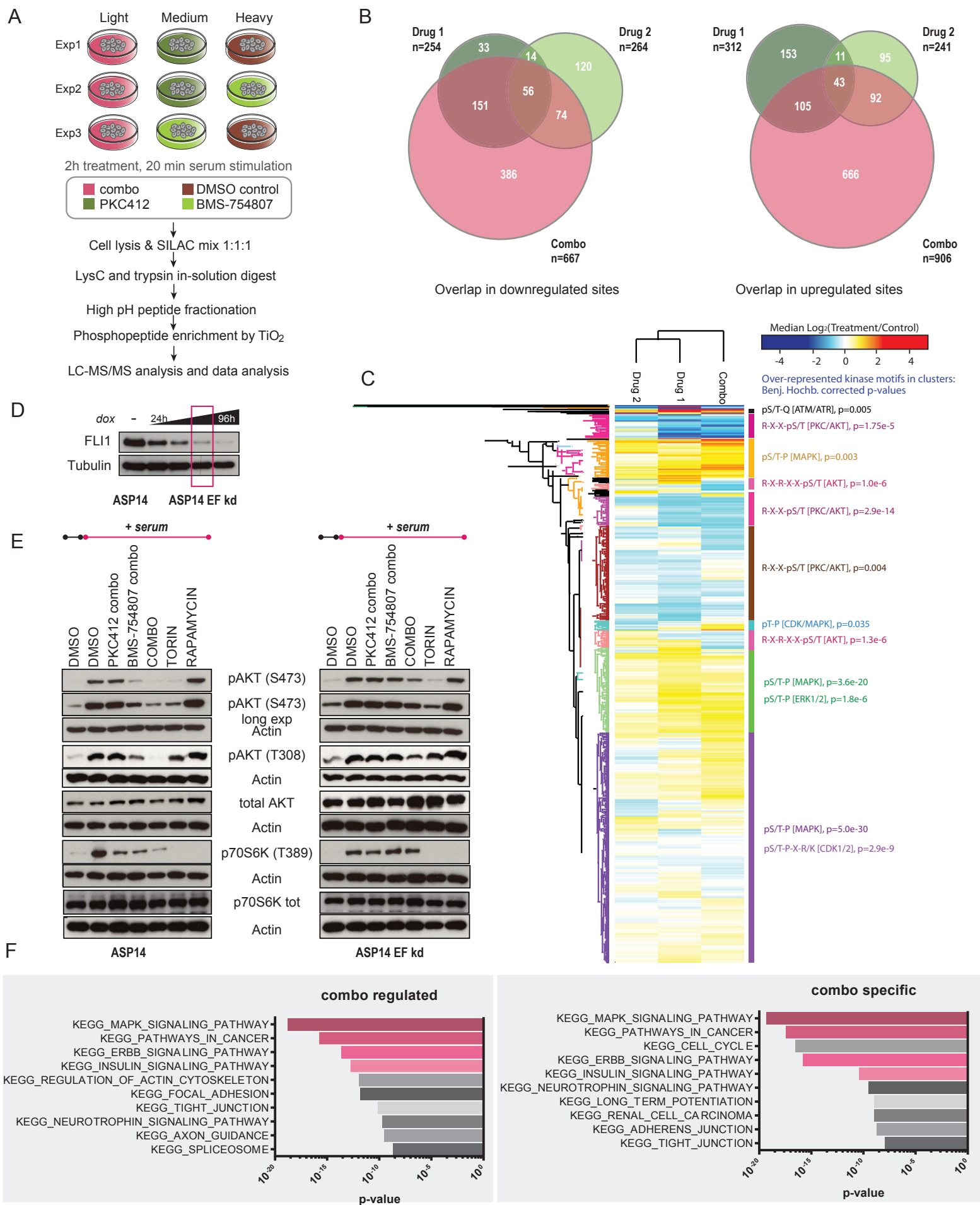


Figure 12. Alteration of phosphorylation events upon combo treatment. (A) schematic of SILAC experiment. (B) Overlap of the phosphorylation sites between single drugs and combinatorial treatment. (C) Cluster-dependent sequence motif analysis of the phosphorylation sites. (D) Temporal resolution of the EWS-FLI1 knockdown. (E) Comparison of downstream signaling events in EWS-FLI1 on and off state upon single drug and combo treatment. (F) KEGG pathway enrichment analysis of combo downregulated sites.

3.4 Manuscript #3: The solute carrier SLC35F2 enables YM155-mediated DNA damage toxicity.

Winter GE, Radic B, Mayor-Ruiz C, Blomen VA, Trefzer C, Kandasamy RK, Huber KV, Gridling M, Chen D, Klampfl T, Kralovics R, Kubicek S, Fernandez-Capetillo O, Brummelkamp TR, Superti-Furga G

Although YM155 was marketed as a survivin suppressor, we did not observe a direct correlation between the efficacy and survivin levels. Moreover, the first clinical trial results were rather disappointing despite a very potent efficacy in preclinical studies. Hence we set out to understand the mechanism of action and to identify genes involved in drug resistance, by the means of a genome-wide insertional mutagenesis approach. We discovered that the primary mode of YM155 induced cytotoxicity is DNA intercalation and that its efficacy is entirely determined by the presence of the influx transporter SLC35F2. This offers the possibility to selectively target tumor cells that highly express this importer, leading to targeted DNA damage induced toxicity.

The solute carrier SLC35F2 enables YM155-mediated DNA damage toxicity

Georg E Winter¹, Branka Radic^{1,4}, Cristina Mayor-Ruiz^{2,4}, Vincent A Blomen³, Claudia Trefzer¹, Richard K Kandasamy¹, Kilian V M Huber¹, Manuela Gridling¹, Doris Chen¹, Thorsten Klampff¹, Robert Kralovics¹, Stefan Kubicek¹, Oscar Fernandez-Capetillo², Thijn R Brummelkamp^{1,3} & Giulio Superti-Furga^{1*}

Genotoxic chemotherapy is the most common cancer treatment strategy. However, its untargeted generic DNA-damaging nature and associated systemic cytotoxicity greatly limit its therapeutic applications. Here, we used a haploid genetic screen in human cells to discover an absolute dependency of the clinically evaluated anticancer compound YM155 on solute carrier family member 35 F2 (SLC35F2), an uncharacterized member of the solute carrier protein family that is highly expressed in a variety of human cancers. YM155 generated DNA damage through intercalation, which was contingent on the expression of SLC35F2 and its drug-importing activity. SLC35F2 expression and YM155 sensitivity correlated across a panel of cancer cell lines, and targeted genome editing verified SLC35F2 as the main determinant of YM155-mediated DNA damage toxicity *in vitro* and *in vivo*. These findings suggest a new route to targeted DNA damage by exploiting tumor and patient-specific import of YM155.

Cancer treatment strategies are facing a transition from the use of broadly cytotoxic substances to the use of custom-designed agents capable of exploiting cancer-specific molecular aberrations. Among others, tumor-selective targeting of otherwise generally toxic agents is a promising approach to reach the goal. Although cell and tissue specificity can be achieved successfully by drug-antibody conjugations, comparable approaches focusing solely on small-molecule compounds are rare^{1–4}. Systematic assessments of transport-cargo relationships in yeast have uncovered a pronounced dependency on active transport mechanisms of most tested small-molecule agents⁵. However, comparable relationships are less well understood in humans, where the general involvement of transporter-mediated mechanisms in drug uptake as opposed to passive diffusion is a matter of active dispute^{6–8}.

YM155 (sepantronium bromide; **Fig. 1a**) is a small-molecule agent with *in vitro* and *in vivo* antitumor activity clinically evaluated for several malignancies, including non-small cell lung cancer, metastatic breast cancer and non-Hodgkin's lymphoma (<http://www.clinicaltrials.gov/>)^{9,10}. The precise mode of action is unknown. Among others, downregulation of the apoptosis inhibitor protein survivin, through binding to the interleukin enhancer-binding factor 3/NF110 transcription factor, has been suggested as a mode of action of YM155 (ref. 11). Despite a remarkable potency in preclinical studies, the first results of clinical trials with YM155 as a single agent proved rather disappointing, possibly reflecting the uncertainty on the molecular nature of the target and the absence of a rationale for patient stratification¹⁰.

With the intention of elucidating the molecular basis of YM155-induced cytotoxicity as well as deciphering potential genetic roadblocks for its clinical efficacy, we devised a genome-wide insertional mutagenesis approach in the near-haploid human cell line KBM7 (ref. 12). This screen allowed assessing gene trap-mediated loss-of-function mutations that would rescue cells from YM155-induced cytotoxicity. We identified a single genomic locus, encoding an

uncharacterized member of the 35F family of solute carrier proteins (SLC35F2), as capable of conferring drug resistance upon retroviral disruption. In the ensuing study, we confirmed transport of YM155 by SLC35F2 and showed that its expression levels across a wide panel of tumor-derived cells are the major determinant of sensitivity to the drug *in vitro* and *in vivo*. The complete dependence on intracellular availability was explained through the elucidation of the primary mode of action of YM155 as a general DNA intercalating and damaging agent. The results led to the concept of targeted induction of DNA damage for the treatment of cancer based on the expression levels of a single solute carrier gene.

RESULTS

Haploid genetics reveals dependency of YM155 on SLC35F2

We mutagenized 1×10^8 near-haploid KBM7 cells with a retroviral gene trap vector that inserts randomly into the genome. Insertions occur genomewide, preferentially at actively transcribed genes; disrupt the genomic locus; and can result in truncation of the expressed protein product via a strong splice acceptor site^{12,13}. Subsequently, the complex mutagenized cell population was selected in the presence of 100 nM YM155, which resulted in the clonal outgrowth of resistant colonies. To identify mutations in genes causally linked to drug resistance, genomic DNA was isolated from the entire KBM7 gene-trapped (KBM7^{GT}) pool and sequenced using an inverse PCR-based protocol described previously¹³. We found enrichment for retroviral insertions in only one gene coding for SLC35F2 with 122 independent insertion events mapping to that single locus (**Fig. 1b,c** and **Supplementary Results, Supplementary Table 1**). In comparison to a large data set of gene trap insertions of a non-selected KBM7 pool, this enrichment was highly significant ($P = 7.58 \times 10^{-299}$)¹². Notably, there was no other locus in the genome that showed statistically significant enrichment for retroviral insertions, suggesting that SLC35F2 is, at the given drug concentrations, the dominant genetic determinant of drug sensitivity.

¹CeMM Research Center for Molecular Medicine of the Austrian Academy of Sciences, Vienna, Austria. ²Genomic Instability Group, Spanish National Cancer Research Centre (CNIO), Madrid, Spain. ³Division of Biochemistry, The Netherlands Cancer Institute, Amsterdam, the Netherlands. ⁴These authors contributed equally to this work. *e-mail: gusuperti@cemm.oeaw.ac.at

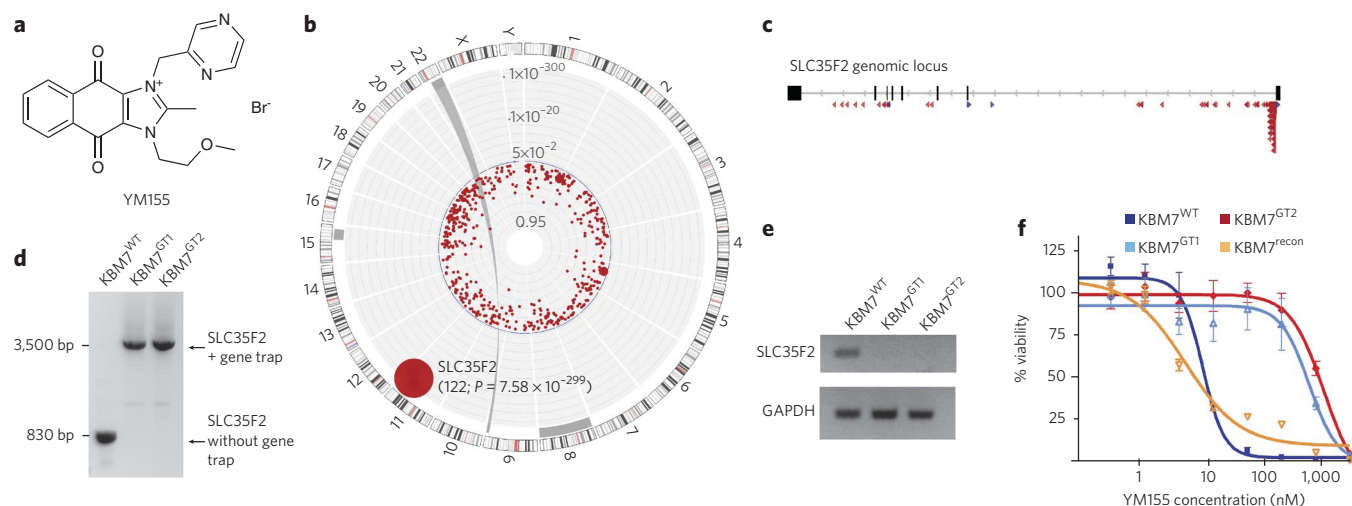


Figure 1 | Mutagenesis of the SLC35F2 locus confers resistance to YM155. (a) The chemical structure of YM155. (b) Circos Plot depiction of sequencing results. Every gene that has been mapped with at least one insertion is depicted as a circle, the localization of which is based on its chromosomal position. The size of a circle correlates with the number of insertions that were mapped for that respective gene. P values decrease from inside to outside and are depicted as $\log_{10}(-\log_{10})$ values. (c) All of the mapped insertions in SLC35F2. Red triangles mark insertions that are in sense orientation compared to SLC35F2, and blue triangles mark antisense orientations. (d) SLC35F2 locus disruption PCR of KBM7^{WT}, KBM7^{GT1} and KBM7^{GT2}. Bp, base pairs. (e) SLC35F2 and GAPDH mRNA levels in KBM7^{WT}, KBM7^{GT1} and KBM7^{GT2}. Data in **d** and **e** are representative of three independent experiments. For uncropped gel images of **d** and **e**, see **Supplementary Figure 11**. (f) Cellular viability of KBM7^{WT}, KBM7^{GT1}, KBM7^{GT2} and KBM7^{recon} after 72-h treatment with various concentrations of YM155. Results represent the mean \pm s.d. of triplicate experiments.

To validate the drug-gene interaction between YM155 and SLC35F2, two independent cell clones carrying gene-trap insertions in SLC35F2 were subcloned (further referred to as KBM7^{GT1} and KBM7^{GT2}). Successful disruption of the underlying genomic locus was shown via a nested PCR strategy (**Fig. 1d** and **Supplementary Fig. 11**). Transcript levels of SLC35F2 were below the limit of detection for both KBM7^{GT1} and KBM7^{GT2} compared to KBM7^{WT} cells (**Fig. 1e** and **Supplementary Fig. 11**). Thus, the retroviral gene-trap approach generated two isogenic loss-of-function alleles for SLC35F2. This allowed for testing the influence of SLC35F2 gene deletion on YM155 efficacy in a dose-dependent manner. After 3 d of drug incubation, we observed a more than 100-fold shift in the half-maximal effector concentration (EC_{50}) of YM155 in the clones deficient of SLC35F2 as compared to wild-type cells. This shift was not observed when using nilotinib, a structurally unrelated control drug that exploits oncogene addiction by targeting the BCR-ABL oncogenic fusion kinase expressed in KBM7 cells (**Fig. 1f** and **Supplementary Fig. 1a**). To prove that the loss of SLC35F2 is causal for the observed resistance to YM155 treatment, we reintroduced C-terminally Flag-tagged SLC35F2 cDNA for stable expression in the KBM7^{GT1} clone (**Supplementary Figs. 1b,c** and **11**). The reconstituted clone (KBM7^{recon}) displayed a strong shift back toward higher sensitivity to YM155, whereas sensitivity to nilotinib remained unaltered (**Fig. 1f** and **Supplementary Fig. 1a**).

YM155 induces DNA damage in cells expressing SLC35F2

Next, we assayed dependence on SLC35F2 in the cellular response to YM155 treatment. We used an RNA sequencing strategy to compare the transcriptional profile of KBM7^{WT} with that of KBM7^{GT1} cells upon 6-h treatment with 1 μ M YM155 (**Supplementary Fig. 2a**). KBM7^{WT} cells showed a clear transcriptional response (431 upregulated and 404 downregulated transcripts; **Supplementary Table 2**) that was almost entirely absent in KBM7^{GT1} cells, the gene-trapped isogenic counterpart (**Fig. 2a,b**). Monitoring the transcriptomic alterations for signatures of chemical or genetic perturbations as well as canonical pathways in a comprehensive gene set compendium (MSigDB)¹⁴, we identified DNA damage response as well as induction of apoptosis to be significantly enriched processes

($P < 0.001$; **Supplementary Fig. 2b**). Neither of these gene sets was enriched in KBM7^{GT1} cells deficient of SLC35F2. To validate a putative DNA damage response caused by YM155 treatment, we treated KBM7^{WT}, KBM7^{GT1} and KBM7^{recon} with increasing concentrations of YM155 and assessed canonical DNA damage. We observed a dose-dependent increase in γ H2AX as well as in phosphorylation of the ATM target KAP1 in KBM7^{WT} cells, indicative of the presence of DNA double-strand breaks¹⁵. Consistent with the toxicity data, this response was not observed in KBM7^{GT1} cells. As expected, reconstitution of KBM7^{GT1} with SLC35F2 cDNA fully reestablished the dose-dependent induction of DNA damage by YM155 (**Fig. 2c** and **Supplementary Fig. 11**). To gain insight on the molecular mechanism of YM155-induced DNA damage, we assessed YM155's ability to interfere with topological changes in plasmid DNA caused *in vitro* by topoisomerase treatment¹⁶. In this assay, YM155 behaved similarly to ethidium bromide, interfering with plasmid relaxation and thus locking the plasmid in a supercoiled state and at the same time, in contrast to the control compound camptothecin, not interfering with the action of topoisomerase. Thus, YM155 has characteristics of a bona fide DNA intercalating chemical agent and not a topoisomerase I inhibitor (**Fig. 2d** and **Supplementary Fig. 11**)¹⁶. DNA intercalating agents such as chloroquine have been shown to interfere with DNA replication and to trigger H2AX phosphorylation^{17,18}. Notably, comet assays revealed that YM155 only generated DNA damage in a fraction of the treated cells (**Supplementary Fig. 3a,b**), which prompted us to explore whether this response was also linked to DNA replication. Accordingly, analysis of 5-ethynyl-2'-deoxyuridine (EdU) incorporation rates revealed that YM155 inhibits DNA replication (**Supplementary Fig. 3c**). Moreover, high-throughput microscopy-mediated analyses showed that the cell cycle distribution of γ H2AX is similar to what is observed with DNA replication inhibitors such as aphidicolin, the response being restricted to replicating cells (**Supplementary Fig. 3d**). Altogether, these analyses provide mechanistic evidence for DNA being the primary target of YM155 action, consistent with the gene expression profile, the biochemical markers and the singular outcome of the primary genetic screen. Given that DNA breaks are highly cytotoxic, we tested the ability of YM155 to induce apoptosis

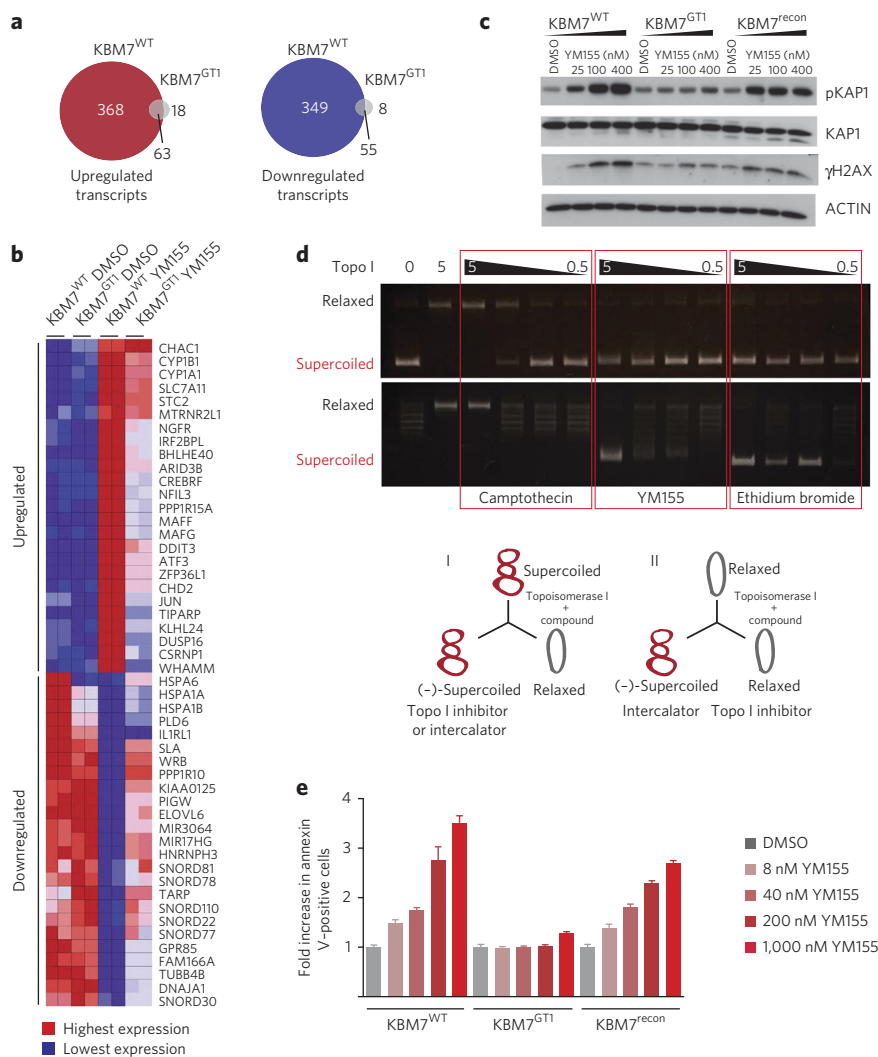


Figure 2 | YM155 induces DNA damage selectively in replicating cells expressing SLC35F2.

(a) Venn diagram depiction quantifying the number of up- and downregulated transcripts after YM155 treatment in KBM7^{WT} and KBM7^{G1T1} cells. (b) Heat map depicting the 25 most up- and downregulated genes after treatment of KBM7^{WT} cells with 1 μ M YM155 for 6 h compared to the respective alterations in KBM7^{G1T1} cells after the same treatment conditions (data are row-normalized). (c) Immunoblot analysis of total KAP1, phospho-KAP1 and γ H2AX compared to actin loading control. KBM7^{WT}, SLC35F2^{G1T1} and SLC35F2^{recon} cells were treated with the indicated concentrations of YM155 for 24 h, and total cell lysates were used for immunoblotting. Data are representative of three independent experiments. (d) DNA intercalation assay. Agarose gel after incubation of relaxed or supercoiled plasmid DNA with different concentrations of topoisomerase I (5 units, 2 units, 1 unit and 0.5 units) in the presence of vehicle control or indicated compounds (camptothecin: 100 μ M; YM155: 100 μ M; ethidium bromide: 10 μ M). (I) and (II) schematically depict the interpretation of the possible results. Data are representative of two independent experiments. For uncropped gel images of **c** and **d**, see **Supplementary Figure 11**. (e) Induction of apoptosis displayed as bar graphs depicting the fold increase in annexin V-positive cells after treatment of KBM7^{WT}, KBM7^{G1T1} and KBM7^{recon} with the indicated concentrations of YM155. Results represent the mean \pm s.d. of triplicate experiments and are normalized to DMSO control values of each cell type.

in the KBM7-based isogenic cell pair monitoring annexin V and propidium iodide staining. The dose-dependent increase of apoptotic cells in KBM7^{WT} was largely absent in KBM7^{G1T1} cells, whereas reintroduction of SLC35F2 reverted the phenotype (**Fig. 2e** and **Supplementary Fig. 4**). In summary, these results indicate that YM155 is dependent on SLC35F2 for its capability to induce DNA damage and to cause apoptotic cell death.

SLC35F2 modulates the cellular uptake of YM155

SLC35F2 is a poorly characterized member of a family of solute carriers that facilitate the transport of nucleotide sugars through biological membranes^{19,20}. As opposed to the majority of SLC35 family members, localized to the Golgi apparatus or the endoplasmic reticulum, SLC35F2 has been reported to localize at the outer cell membrane^{19–21}. In line with this, we assessed whether SLC35F2 facilitates the cellular uptake of YM155 by directly measuring intracellular drug concentration using multiple reaction monitoring (MRM), an MS-based assay. We observed a tenfold decrease in intracellular drug levels in KBM7^{G1T1} cells relative to that in KBM7^{WT} cells. Moreover, we found that in the reconstituted clone, intracellular drug levels were even higher than those in the parental KBM7^{WT} cells, suggesting that SLC35F2 protein levels are proportional to drug uptake (**Fig. 3a**). Indeed, transient overexpression of C-terminal V5-tagged SLC35F2 in HEK293T cells yielded a 15-fold increase in intracellular drug levels compared to empty vector control (**Supplementary Fig. 5**). Hence, the unique reliance of YM155 on the presence or absence of the SLC35F2 gene product may be explained by the role of the protein in determining intracellular YM155 concentrations.

If the levels of SLC35F2 are the main determinant of sensitivity of cells to YM155 action, interference with endogenous expression levels should affect the efficacy of the drug in other cancer cell lines as well. The SW480 colon adenocarcinoma cell line features relatively high SLC35F2 mRNA expression levels²². To validate the importance of SLC35F2 also in this cellular background, we made use of RNA-guided Cas9 nuclease-based genome editing technology (CRISPR)^{23,24}. We derived two independent isogenic clones, SW480^{SLCmut1} and SW480^{SLCmut2}, with frameshift mutations in the SLC35F2 gene (exon 7) resulting from indel mutations (**Supplementary Fig. 6**). These two genomic alterations in SLC35F2 reduced sensitivity of SW480 cells to YM155 more than 100-fold (**Fig. 3b**). This difference in sensitivity was confirmed also in longer-lasting colony formation assays (**Fig. 3c**). To test whether SLC35F2 expression levels not only were required but also could further enhance YM155-induced cytotoxicity, we retrovirally overexpressed C-terminally Flag-tagged SLC35F2 in A549 lung cancer cells that feature average endogenous SLC35F2 mRNA expression levels²². Stable overexpression of SLC35F2 in A549 cells resulted in hypersensitivity to YM155 treatment in short- as well as long-term treatment conditions (**Fig. 3d,e**). Collectively, the data suggested that the importance of SLC35F2 in mediating the efficacy of YM155 extended to cancer cell lines more relevant to the clinical implications of YM155 and that, in general, the expression levels of this uncharacterized transporter may be the major influx-modulating factor.

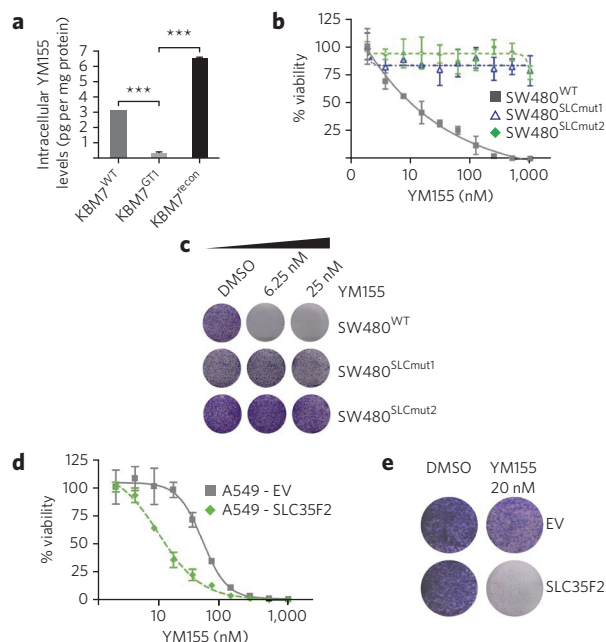


Figure 3 | Validation of the dependency of YM155 on SLC35F2 using genome editing. (a) Intracellular YM155 levels as determined by MRM in KBM7^{WT}, KBM7^{G11} and KBM7^{recon} cells exposed to 2 μ M YM155 for 90 min. Results represent the mean \pm s.d. of triplicate experiments; *** $P < 0.0001$. (b) Cellular viability of SW480^{WT}, SW480^{SLCmut1} and SW480^{SLCmut2} after 72 h treatment with various concentrations of YM155. Results represent the mean \pm s.d. of triplicate experiments. (c) 10-d colony formation assays of SW480^{WT}, SW480^{SLCmut1} and SW480^{SLCmut2} with either vehicle (DMSO) control or the indicated concentrations of YM155. Data are representative of three independent experiments. (d) Cellular viability of A549 (empty vector (EV) control) or A549 cells stably overexpressing C-terminally Flag-tagged SLC35F2 after 72-h treatment with various concentrations of YM155. Results represent the mean \pm s.d. of triplicates. (e) 10-d colony formation assays of A549 (empty vector control) cells or A549 cells stably overexpressing C-terminally Flag-tagged SLC35F2. Data are representative of three independent experiments.

SLC35F2 expression levels predict YM155 efficacy

Given the fact that ectopic expression of SLC35F2 creates a synthetic hypersensitivity to YM155, we charted SLC35F2 expression levels using a patient-data compendium meta-analysis (OncoPrint). We found that SLC35F2 had been reported to be overexpressed in a variety of human malignancies compared to the respective non-tumor tissue (Supplementary Fig. 7). To test whether the efficacy of YM155 could be predicted by SLC35F2 expression levels, we derived EC₅₀ values for YM155 as well as for two structurally different DNA damage-inducing agents (topotecan and idarubicin) from ten-point dose response curves established in 15 cell lines with variable degrees of SLC35F2 expression (Fig. 4a,b and Supplementary Fig. 8)²². By comparing YM155 EC₅₀ values to SLC35F2 expression data, we found a significant ($P = 0.0007$) negative correlation ($R = -0.77$) over the entire cell line panel tested (Fig. 4b). In agreement with our genetically engineered models (KBM7^{GT} and SW480^{SLCmut}), this outlines an enhanced sensitivity to YM155 in cancer cells with endogenously elevated SLC35F2 expression levels. Notably, there was no significant ($P > 0.05$) correlation with either of the other agents tested, illustrating the specificity of the YM155-SLC35F2 relationship (Supplementary Fig. 8). We next calculated the Pearson's correlation values for all of the quantified genes and identified SLC35F2 as one of the most significant ($P = 0.00074$) predictors for YM155 efficacy also on a genome-wide scale (Supplementary Fig. 9 and Supplementary Table 3). Of note, we did not find any significant

($P = 0.496$) correlation between YM155 efficacy and survivin expression levels, suggesting that cell lines with elevated survivin levels are not preferentially killed by YM155. We extended our studies using two members of the cell line panel featuring either high (SW480) or low (HUH7) SLC35F2 expression levels. Also, in colony formation assays and long-term drug treatment, we could confirm the selective toxicity of YM155 for SLC35F2^{high} cells at natural expression level differences (Fig. 4c). To test the hypothesis that the death-inducing mechanism is indeed DNA damage also in cancer cell lines other than KBM7 and mainly depends on intracellular drug concentrations, we monitored DNA damage in SLC35F2^{high} versus SLC35F2^{low} cells. We treated SW480 cells and HUH7 cells with increasing concentrations of YM155 and probed for the canonical double-strand break markers γ H2AX and phospho-KAP1. A pronounced increase of both markers was observable in SW480 cells but not in HUH7 cells, indicating selective DNA damage (Fig. 4d and Supplementary Fig. 11). We measured intracellular drug levels in both cell lines using targeted MS. After treatment with 300 nM or 1 μ M YM155 for 90 min, we observed significantly ($P = 0.001$) higher levels of YM155 in SW480 cells compared to HUH7 cells (Fig. 4e). This confirmed that reduced transporter expression causes lower intracellular YM155 concentrations, hence causing differential induction of DNA damage. However, an additional contribution to the observed differences caused by differential expression of drug efflux pumps should not be excluded. Altogether, this raised the remarkable possibility that, using SLC35F2 levels as discriminating factor, one could predict the efficacy of YM155 also *in vivo*.

SLC35F2 is a major determinant of YM155 efficacy *in vivo*

To test this hypothesis and obtain initial preclinical proof-of-concept for a pharmacological strategy of selective induction of DNA damage, we sought a genetically well-defined experimental setup. We used SW480 cells that were either wild-type for SLC35F2 or had a CRISPR-induced frameshift mutation, as described above, to perform a mouse xenograft experiment and drug treatment (Supplementary Fig. 6). Cells were injected subcutaneously into flanks of SCID mice, and YM155 treatment was initiated after tumors reached a volume of >100 mm³. Although tumors derived from SW480^{WT} cells rapidly receded, there was no marked decrease of tumor growth with the SW480 clone mutant for SLC35F2 (Fig. 4f and Supplementary Fig. 10a). Selective induction of a DNA damage response along with induction of apoptosis was assessed via immunohistochemistry using antibodies for γ H2AX and active caspase 3. In line with the *in vitro* results, we found that YM155 treatment caused a selective induction of DNA damage that was dependent on SLC35F2, as it was not observed in tumors derived from SLC35F2-deficient SW480 cells (Fig. 4g and Supplementary Fig. 10b). Consequently, apoptosis downstream of DNA damage was also only successfully induced in tumors derived from SW480^{WT} cells (Fig. 4h and Supplementary Fig. 10c).

Collectively, these results indicate that YM155 is capable of selectively inducing DNA damage *in vivo* at clinically relevant drug concentrations.

DISCUSSION

Large-scale mutagenesis screens in haploid model organisms such as yeast have provided insights into fundamental biological processes²⁵. Here, we applied global gene disruption in human haploid cells to unravel the cellular consequences of and genetic requirements for exposure to the small-molecule drug YM155. Our data suggest that YM155 confers its cytotoxicity via DNA intercalation, causing a DNA damage response that leads to apoptotic cell death. We did not find evidence for downregulation of survivin on the transcript level, and, over the cell line panel we assayed, survivin levels did not correlate with the efficacy of YM155 to induce cell death. We present evidence for a case where expression levels of only a single,

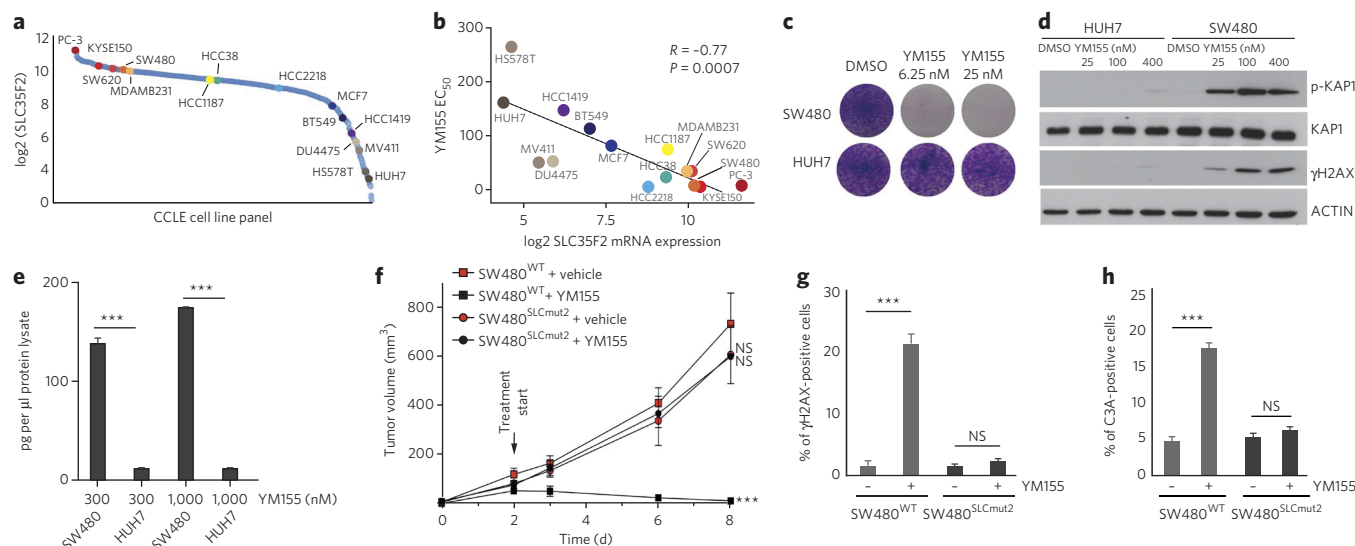


Figure 4 | SLC35F2 is a predictive marker for YM155 efficacy *in vitro* and *in vivo*. (a) SLC35F2 (\log_2) expression values of a large set of cancer cell lines reported elsewhere²². Cell lines with variable degree of SLC35F2 expression used for the correlative study are annotated. (b) EC_{50} values for YM155 were derived for all of the cell lines indicated and are depicted as a function of SLC35F2 expression levels in the respective cell lines. YM155 efficacy was significantly ($P = 0.0007$) negatively correlated with SLC35F2 expression levels ($R = -0.77$). (c) 10-d colony formation assays of SW480 or HUH7 cells treated with either vehicle (DMSO) or the indicated YM155 concentrations. Data are representative of three independent experiments. (d) Immunoblot analysis of phospho-KAP1 (p-KAP1) and γ H2AX compared to total KAP1 and actin loading controls in SW480 and HUH7 cells treated with the indicated concentrations of YM155 for 24 h. Data are representative of three independent experiments. For uncropped gel images, see **Supplementary Figure 11**. (e) Intracellular YM155 levels, as determined by MRM in SW480 and HUH7 cells exposed to 0.3 μ M and 1 μ M YM155 for 90 min. Results represent the mean \pm s.d. of triplicates; *** $P < 0.0001$. (f) Tumor size of SW480^{WT} and SW480^{SLCmut2} xenografts after treatment with YM155 (10 mg per kg body weight per day; $n = 6$). Infusion pumps filled with vehicle or YM155 were implanted on animals when tumors reached 100 mm³ and monitored for growth for 1 week. NS, nonsignificant; *** $P < 0.001$ in f-h. (g) Percentage of γ H2AX-positive cells of SW480^{WT} and SW480^{SLCmut2} xenografts in the absence or presence of YM155 as described in (f). (h) Percentage of C3A-positive cells of SW480^{WT} and SW480^{SLCmut2} xenografts in the absence or presence of YM155 as described in (f). Results represent the mean \pm s.d. of triplicate analysis.

until-now-uncharacterized solute carrier gene can determine the efficacy of a clinically evaluated compound. In this case, the differential activity of members of the ABC family of transporters responsible for drug efflux does not seem to be determinant. Although previous work has established the import of YM155 via OCT1 and OCT2 (SLC22A1 and SLC22A2) as an important pharmacokinetic parameter, we did not observe indication for involvement of these proteins for the uptake of YM155 into the tumor cells assayed^{26,27}. However, the residual activity of YM155 on KBM7^{GT1} and KBM7^{GT2} could result from transport occurring by low levels of SLC22A1 and/or SLC22A2 expression.

Systematic charting of target spectra of an increasing number of solute carriers combined with detailed knowledge on their expression patterns in normal physiologic conditions as well as in pathophysiology should enable better predictions of pharmacokinetic and pharmacodynamic parameters for new small-molecule candidates for clinical assessments. So far, we have not been able to identify the natural substrate of SLC35F2. However, a complete understanding of the endogenous cargo profile of SLC35F2 will be important for understanding the physiological context of differential expression in tissues and tumors.

Collectively, our results indicate that SLC35F2 is an important flux modulator in a way that establishes this carrier as a highly relevant biomarker for further clinical evaluation of YM155. Supported by ectopic overexpression, correlative cell line panel data, genome-engineering loss of function and *in vivo* data, we believe that this unique dependency might expand the therapeutic window for YM155 selectively for patients with elevated intratumoral SLC35F2 expression. Our data clearly establish SLC35F2 expression levels as a mechanism-based biomarker stratification strategy for future clinical evaluations of YM155. We believe that the concluded clinical trials with YM155 would have greatly benefitted from this information

and that the molecular basis for transport across membranes should be part of the knowledge package accompanying drug candidates. Most notably, given the overexpression of SLC35F2 in several malignancies, we propose that this gene-drug interaction might enable a safe and specific targeting strategy of DNA damage to tumor cells with elevated levels of SLC35F2 expression.

Received 4 February 2014; accepted 19 June 2014; published online 27 July 2014

METHODS

Methods and any associated references are available in the [online version of the paper](#).

Accession codes: European Nucleotide Archive: sequence information has been deposited under accession code [PRJEB6449](#). EBI-ArrayExpress: gene expression data have been deposited under accession code [E-MTAB-2627](#).

References

1. Younes, A. *et al.* Brentuximab vedotin (SGN-35) for relapsed CD30-positive lymphomas. *N. Engl. J. Med.* **363**, 1812–1821 (2010).
2. Verma, S. *et al.* Trastuzumab emtansine for HER2-positive advanced breast cancer. *N. Engl. J. Med.* **367**, 1783–1791 (2012).
3. Birsoy, K. *et al.* MCT1-mediated transport of a toxic molecule is an effective strategy for targeting glycolytic tumors. *Nat. Genet.* **45**, 104–108 (2013).
4. Reiling, J.H. *et al.* A haploid genetic screen identifies the major facilitator domain containing 2A (MFSD2A) transporter as a key mediator in the response to tunicamycin. *Proc. Natl. Acad. Sci. USA* **108**, 11756–11765 (2011).
5. Lanthaler, K. *et al.* Genome-wide assessment of the carriers involved in the cellular uptake of drugs: a model system in yeast. *BMC Biol.* **9**, 70 (2011).
6. Dobson, P.D. & Kell, D.B. Carrier-mediated cellular uptake of pharmaceutical drugs: an exception or the rule? *Nat. Rev. Drug Discov.* **7**, 205–220 (2008).

7. Kell, D.B., Dobson, P.D. & Oliver, S.G. Pharmaceutical drug transport: the issues and the implications that it is essentially carrier-mediated only. *Drug Discov. Today* **16**, 704–714 (2011).
8. Giacomini, K.M. *et al.* Membrane transporters in drug development. *Nat. Rev. Drug Discov.* **9**, 215–236 (2010).
9. Tolcher, A.W. *et al.* Phase I and pharmacokinetic study of YM155, a small-molecule inhibitor of survivin. *J. Clin. Oncol.* **26**, 5198–5203 (2008).
10. Giaccone, G. *et al.* Multicenter phase II trial of YM155, a small-molecule suppressor of survivin, in patients with advanced, refractory, non-small-cell lung cancer. *J. Clin. Oncol.* **27**, 4481–4486 (2009).
11. Nakamura, N. *et al.* Interleukin enhancer-binding factor 3/NF110 is a target of YM155, a suppressant of survivin. *Mol. Cell. Proteomics* **11**, M111.013243 (2012).
12. Carette, J.E. *et al.* Haploid genetic screens in human cells identify host factors used by pathogens. *Science* **326**, 1231–1235 (2009).
13. Carette, J.E. *et al.* Global gene disruption in human cells to assign genes to phenotypes by deep sequencing. *Nat. Biotechnol.* **29**, 542–546 (2011).
14. Subramanian, A. *et al.* Gene set enrichment analysis: a knowledge-based approach for interpreting genome-wide expression profiles. *Proc. Natl. Acad. Sci. USA* **102**, 15545–15550 (2005).
15. Glaros, T.G. *et al.* The “survivin suppressants” NSC 80467 and YM155 induce a DNA damage response. *Cancer Chemother. Pharmacol.* **70**, 207–212 (2012).
16. Sappal, D.S. *et al.* Biological characterization of MLN944: a potent DNA binding agent. *Mol. Cancer Ther.* **3**, 47–58 (2004).
17. Cohen, S.N. & Yielding, K.L. Inhibition of DNA and RNA polymerase reactions by chloroquine. *Proc. Natl. Acad. Sci. USA* **54**, 521–527 (1965).
18. Bakkenist, C.J. & Kastan, M.B. DNA damage activates ATM through intermolecular autophosphorylation and dimer dissociation. *Nature* **421**, 499–506 (2003).
19. Ishida, N. & Kawakita, M. Molecular physiology and pathology of the nucleotide sugar transporter family (SLC35). *Pflugers Arch.* **447**, 768–775 (2004).
20. Song, Z. Roles of the nucleotide sugar transporters (SLC35 family) in health and disease. *Mol. Aspects Med.* **34**, 590–600 (2013).
21. Sarangi, A., Bupp, K. & Roth, M.J. Identification of a retroviral receptor used by an envelope protein derived by peptide library screening. *Proc. Natl. Acad. Sci. USA* **104**, 11032–11037 (2007).
22. Barretina, J. *et al.* The Cancer Cell Line Encyclopedia enables predictive modelling of anticancer drug sensitivity. *Nature* **483**, 603–607 (2012).
23. Cong, L. *et al.* Multiplex genome engineering using CRISPR/Cas systems. *Science* **339**, 819–823 (2013).
24. Mali, P. *et al.* RNA-guided human genome engineering via Cas9. *Science* **339**, 823–826 (2013).
25. Hartwell, L.H., Culotti, J., Pringle, J.R. & Reid, B.J. Genetic control of the cell division cycle in yeast. *Science* **183**, 46–51 (1974).
26. Minematsu, T. *et al.* Carrier-mediated uptake of 1-(2-methoxyethyl)-2-methyl-4,9-dioxo-3-(pyrazin-2-ylmethyl)-4,9-dihydro-1H-naphtho[2,3-d]imidazolium bromide (YM155 monobromide), a novel small-molecule survivin suppressant, into human solid tumor and lymphoma cells. *Drug Metab. Dispos.* **37**, 619–628 (2009).
27. Minematsu, T., Iwai, M., Umehara, K., Usui, T. & Kamimura, H. Characterization of human organic cation transporter 1 (OCT1/SLC22A1)- and OCT2 (SLC22A2)-mediated transport of 1-(2-methoxyethyl)-2-methyl-4,9-dioxo-3-(pyrazin-2-ylmethyl)-4,9-dihydro-1H-naphtho[2,3-d]imidazolium bromide (YM155 monobromide), a novel small molecule survivin suppressant. *Drug Metab. Dispos.* **38**, 1–4 (2010).

Acknowledgments

We thank all of the members of the Superti-Furga research laboratory and U. Rix (Moffitt Cancer Center) for skillful advice and discussions. The present work was, in part, financed by the Austrian Academy of Sciences (S.K., R.K.K., G.S.-F., D.C. and T.K.); the Gen-AU initiative of the Austrian Federal Ministry for Science, Research and Economy (G.E.W., PLACEBO); the European Commission (B.R., K.V.M.H. and M.G., grant agreement number 259348, ASSET); the European Research Council (R.K.K., grant agreement number 250179, i-FIVE); and the Swiss National Science Foundation (C.T., Fellowship). T.R.B. is funded by the Cancer Genomics Center (<http://www.cancer-genomics.nl/>) and the Netherlands Organisation for Scientific Research–VIDI grant 91711316. Work in the O.F.-C. laboratory was supported by grants from the Spanish Ministry of Economy and Competitiveness (SAF2011-23753), the Association for International Cancer Research (12-0229), the Howard Hughes Medical Institute and the European Research Council (ERC-617840). C.M.-R. is funded by a PhD fellowship from La Caixa Foundation.

Author contributions

G.E.W. designed and performed experiments, analyzed and interpreted the data, made the figures and wrote the manuscript. B.R. designed and performed experiments, interpreted the data and prepared figures. C.M.-R. performed the mouse xenograft experiments, high-content microscopy and the comet assay. V.A.B. helped perform the haploid genetic screen and conducted statistical analysis. C.T. performed the RNA sequencing experiment and helped to perform MRM measurements. R.K.K. analyzed RNA sequencing data and performed statistical analysis. K.V.M.H. helped to set up MRM measurements and gave experimental advice. M.G. assisted with immunoblot analysis. D.C. created the Circos plot and a graphical display of insertion sites. T.K. operated the next-generation sequencer (Illumina HiSeq 2000) and helped with next-generation sequencing data handling. R.K. gave experimental advice and supervised next-generation sequencing. S.K. gave experimental advice and designed experiments. O.F.-C. designed the mouse xenograft study and analyzed and interpreted data. T.R.B. codesigned the study and gave experimental advice. G.S.-F. codesigned and supervised the study and wrote the manuscript.

Competing financial interests

The authors declare competing financial interests: details accompany the [online version of the paper](#).

Additional information

Supplementary information is available in the [online version of the paper](#). Reprints and permissions information is available online at <http://www.nature.com/reprints/index.html>. Correspondence and requests for materials should be addressed to G.S.-F.

ONLINE METHODS

Cell lines and reagents. A549, HUH7, SW480, SW620, HCC38, HCC1187, HS578T, MDA-MB-231, DU4475, MV4-11, HCC2218, BT-549, MCF-7, HCC1419, PC-3 and HEK 293T cell lines were obtained from the American Type Culture Collection and were cultured in the suggested medium. YM155, idarubicin-HCl, topotecan-HCl and camptothecin were purchased from Selleck Chemicals (Houston, TX, USA), and nilotinib was purchased from LC Laboratories (Woburn, MA, USA). Aphidicolin, neocarzinostatin and ethidium bromide were purchased at Sigma-Aldrich. Antibodies used in these study: anti-Flag (Sigma, F3165, 1:2,000), anti-actin (Cytoskeleton; AAN-01A, 1:5,000), anti-Kap1 (A300-274A, 1:5,000), anti-phospho-Kap1 (A304-146A, 1:1,000; both Bethyl Laboratories) and anti- γ H2AX, (Millipore; 07-627, 1:1,000).

Haploid genetic screen and sequence analysis. Haploid genetic screening was performed as described recently¹³. In brief, virus was produced by transient transfection of the gene-trap plasmid along with packaging plasmids using Lipofectamine 2000 (Invitrogen) in low-passage HEK 293T cells. Virus was concentrated via ultracentrifugation and used to mutagenize 1×10^8 KBM7 cells via spinfection. The mutagenized pool was expanded for another week. Subsequently 1×10^8 gene-trapped cells were selected with 100 nM YM155 in 96-well plates (1×10^5 cells seeded per well). Drug-resistant clones were pooled after 10 d of drug exposure, collected in a T175 flask and expanded to a total cell number of 3×10^7 cells. Genomic DNA was isolated, and retroviral insertion sites were detected via an inverse PCR protocol adapted to next-generation sequencing¹³. The significance of the enrichment of insertions in a given gene was calculated by comparing the number of insertions of the YM155 selected population with an unselected, larger control data set using the one-sided Fisher's exact test. The resulting *P* values were corrected for false discovery rate using the Benjamini and Hochberg method.

Subcloning of SLC35F2 deficient KBM7 mutant cell line. Due to the high mutational burden of SLC35F2 in the YM155 selected pool (approximately 16% of all of the mapped insertions clustered in the SLC35F2 gene), no serial subcloning strategy was required. Instead, KBM7^{GT} cells were seeded at a density of 0.1 cells per well in 384-well plates. Monoclonal colonies were then propagated to 96-well plates, and DNA was isolated when the 96 wells were near confluent. A nested PCR strategy (sequence of primers upon request) was conducted to identify clones harboring a retroviral insertion directly after the first exon of SLC35F2. For final confirmation of gene-trap localization, the identity of the resulting PCR product was confirmed by Sanger sequencing.

Determination of intracellular drug levels via MRM. For YM155, 1×10^6 cells of each assessed genotype (KBM7^{WT}, KBM7^{GT1} and KBM7^{recon}) were treated with 2 μ M YM155 for 2 h at 37 °C. Subsequently, cells have been washed three times with ice-cold PBS and directly lysed in 300 μ l ice-cold methanol. Lysates were then cleared by centrifugation for 20 min at 4 °C at 16,000g, and supernatants were used for subsequent quantifications by MS. MRM settings were automatically generated using the IntelliStart software (Waters), and quantification was conducted on the basis of the intensity of three daughter ions. Quantification in other cell lines has been conducted using the same setup.

RNA sequencing. 5×10^5 cells (KBM7^{WT} and KBM7^{GT1}) were treated for 6 h with 1 μ M YM155 in biological duplicates. RNA was isolated using RNeasy kit (Qiagen), and library preparation was performed with TrueSeq RNA v2 kit (Illumina). Reads were aligned to human reference genome build hg19 using TopHat and Bowtie2 (refs. 28,29). RPKM values were computed using RSeQC package³⁰. Fold changes were calculated using R/DEGseq package applying the MARS (MA-plot-based method with Random Sampling model) method at an FDR \leq 0.001 (refs. 30,31).

Intercalation assay. DNA intercalation assay was performed as described elsewhere¹⁶.

Viability assays. Cellular viability was assayed using the Cell Titer Glo assay (Promega) according to the manufacturer's recommendations. Standard assay setup consists of 72-h drug exposure at various concentrations, with 10,000 cells seeded initially in 96-well plates. EC₅₀ determination and curve fitting was conducted using Prism software (GraphPad Software).

Apoptosis assays. Induction of apoptosis was determined 16 h after drug exposure using the PE Annexin V Apoptosis Detection Kit I (BD Pharmingen) following the manufacturer's recommendations.

CRISPR targeting strategy. CRISPR targeting sites have been extracted from genome browser tracks downloaded at http://www.genome-engineering.org/crispr/?page_id=41 (ref. 23). The following oligos for sense (s) and antisense (as) have been used to generate targeting constructs by cloning into the pX330 backbone as described elsewhere^{31,32}: CACCGAGTGCCACTTCCGTCAACCT (s), AAACAGGTTGACGGAAGTGGCACTC (as). Targeting constructs were transiently transfected with GFPmax vector (Amaya) at a 2:1 ratio. GFP-positive cells of the transfected pools were single-cell-sorted in 96-well plates and grown and expanded monoclonally. For sequence analysis of the targeted locus in SLC35F2 Exon 7, the following primers were used for PCR amplification: forward, 3'-ACATCCACGTGGCAAGCACT-5'; reverse, 3'-GGCCATACCATCGAAGATGA-5'. Eight PCR products each for SW480^{WT}, SW480^{SLCmut1} and SW480^{SLCmut2} were subcloned using the TOPO blunt end cloning kit (Invitrogen) and were sequenced using M13 forward and reverse standard primers.

Xenograft experiments. SW480 cells (2×10^6 cells) were injected into the flanks of 6-week-old *SCID* mice and allowed to reach a tumor volume of $>100 \text{ mm}^3$ (length \times width² \times 0.5). Mice were randomized into groups (*n* = 6) to receive subcutaneous saline control or YM155 (10 mg per kg body weight per day) administered as a 7-d continuous infusion using an implanted osmotic pump (Alzet model 1007D, Durect). YM155 was dissolved and diluted in saline immediately before administration. Statistically significant differences were determined using the Student's *t*-test. *P* < 0.05 was chosen as the threshold for statistical significance. Mice were housed in the pathogen-free animal facility of the Spanish National Cancer Research Centre (CNIO, Madrid) following the animal care standards of the institution. All of the animal protocols were approved by the Instituto de Salud Carlos III committee (Madrid) for animal care and research.

Immunohistochemical studies. Tumor samples were fixed with 4% paraformaldehyde and embedded in paraffin. Subsequently, 5- μ m sections were prepared and stained with either phospho-histone H2AX (Ser139, JBW301, Millipore, 1:1,000) or active caspase-3-specific antibodies (R&D Systems, AF835, 1:1,000).

High-throughput microscopy. High throughput-mediated analysis of the DNA damage response was performed as previously described³³. Briefly, SW480 cells were grown on μ CLEAR bottom 96-well plates (Greiner Bio-One). Treatments were added to the culture medium at the following concentrations: 0.1 μ M YM155, 5 μ M aphidicolin and 50 ng/ml neocarzinostatin. EdU was added to the medium during the last 45 min of incubation with the drug. EdU incorporation into DNA was detected using the Click-iT EdU Alexa Fluor Imaging kit (Invitrogen/Molecular Probes, Eugene, OR). All steps of the Click-iT reaction were performed at room temperature. γ H2AX immunofluorescence was performed using standard procedures. γ H2AX (Upstate Biotechnology, 05-636, 1:1,000) as well as secondary antibody conjugated with Alexa 488 (Molecular Probes, A-11001, 1:250) were used. Images from each well were automatically acquired by an Opera High-Content Screening System (PerkinElmer) at non-saturating conditions with a 20 \times magnification lens. Images were segmented using the DAPI staining to generate masks matching cell nuclei from which the mean signals were calculated. Data were represented with the Prism software (GraphPad Software).

Comet assay. SW480 cells were grown on six-well plates. 100 nM YM155 was added to the culture medium for 3 h. For the irradiation condition, 20 Gy radiation was used. Comet assays were performed with the Comet Assay Kit (Trevigen) following the manufacturer's instructions. Images were acquired with a confocal microscope. Mean tail moments (tail length \times tail DNA %) were automatically scored using the OpenComet analyzing software, and data were represented with the Prism software (GraphPad Software)³⁴.

Statistics. Two-tailed Student's *t*-tests were used for statistical analysis if not stated otherwise in the respective figure legends or Online Methods.

Raw sequencing data. Raw data of the haploid genetic screen is available from the European Nucleotide Archive under the accession number PRJEB6449.

RNA sequencing data is available for EBI-ArrayExpress under the accession number E-MTAB-2627.

28. Trapnell, C., Pachter, L. & Salzberg, S.L. TopHat: discovering splice junctions with RNA-Seq. *Bioinformatics* **25**, 1105–1111 (2009).
29. Langmead, B., Trapnell, C., Pop, M. & Salzberg, S.L. Ultrafast and memory-efficient alignment of short DNA sequences to the human genome. *Genome Biol.* **10**, R25 (2009).
30. Wang, L., Wang, S. & Li, W. RSeQC: quality control of RNA-seq experiments. *Bioinformatics* **28**, 2184–2185 (2012).
31. Wang, L., Feng, Z., Wang, X., Wang, X. & Zhang, X. DEGseq: an R package for identifying differentially expressed genes from RNA-seq data. *Bioinformatics* **26**, 136–138 (2010).
32. Wang, H. *et al.* One-step generation of mice carrying mutations in multiple genes by CRISPR/Cas-mediated genome engineering. *Cell* **153**, 910–918 (2013).
33. Toledo, L.I., Murga, M., Gutierrez-Martinez, P., Soria, R. & Fernandez-Capetillo, O. ATR signaling can drive cells into senescence in the absence of DNA breaks. *Genes Dev.* **22**, 297–302 (2008).
34. Gyori, B.M., Venkatachalam, G., Thiagarajan, P.S., Hsu, D. & Clement, M.V. OpenComet: an automated tool for comet assay image analysis. *Redox Biol.* **2**, 457–465 (2014).

4 General discussion

The current situation in medical care is that for a vast majority of diseases a “proxy” of a patient is being treated: all individuals with the same diagnosis are considered an average patient and receive a very similar therapy. Precision medicine is a medical model that proposes an individualized approach to treating patients. Fortunately, major healthcare representatives and influential political leaders recognized it as a future directive for global healthcare. Due to the current directions in cancer care, precision oncology is set to be the pioneering branch of the whole initiative. Advanced omics technologies and computational techniques will enable better understanding of pathway and network aberrations that will in turn aid selection of drugs and drug combinations that could benefit specific patients (Tsimberidou *et al*, 2014). The aim of precision oncology is thus to provide for highly specific, effective and minimally toxic treatment for each patient. Major hurdles in achieving this are the heterogeneity of tumors, occurrence of resistance to targeted therapies, unexplained mechanisms of action of therapeutics and limited knowledge about combinatorial drug treatment (Collins & Varmus, 2015). Work presented in this thesis is addressing a large portion of these obstacles, from a molecular medicine point of view.

4.1 Occurrence of resistance to targeted therapies

The hype following the appearance of so-called “magic bullet” targeted small molecule was soon blurred by the eventual occurrence of drug resistance that severely interfered with the effectiveness of the therapy. In case of an intrinsic resistance, the major goal is to be able to select the optimal responsive patient group; for acquired resistance, if it is not possible to overcome it with combination therapy or other means, the aim should be to postpone its occurrence. Regardless of the type of resistance, it is an imperative to understand its mechanisms.

Survivin is expressed mostly in cancer cells and usually absent in normal cells; thus the discovery of YM155 (Nakahara *et al*, 2007), a potent anticancer drug that can downregulate survivin, was received with excitement. Although remarkably potent in preclinical studies, the first clinical trials were rather unsuccessful (Giaccone *et al*, 2009), likely reflecting the lack of patient stratification markers and the unknown precise mechanism of action. Therefore, we selected YM155 for investigation, with the aim to decipher the

mechanism of action, determinants of efficacy and the cause of resistance. In order to address this, the near-haploid human KBM7 cell line was mutagenized with a retroviral gene trap virus and subsequent genome-wide insertions resulted in truncation of protein products via a strong splice acceptor site (Carette *et al*, 2009, 2011). A strong selection pressure was applied, using a relatively high concentration of YM155, which led to the outgrowth of resistant colonies. This genome-wide insertional mutagenesis approach allowed us to identify genes involved in drug resistance. Interestingly, only one gene was found with highly significant insertions enrichment – SLC35F2, a poorly annotated member of the solute carrier family of transporters. Expression levels of this transporter are indeed the determining factor of the cellular response to the compound, since SLC35F2 dictates its intracellular concentration, thus allowing the compound to exhibit its effect. Although the natural cargo profile of this transporter is unknown, we could show that it transports YM155 and that high SLC35F2 levels are crucial for the efficacy of the compound *in vitro* as well as *in vivo*. This tight relationship might be explored as a biomarker tool in order to select patients that are likely to respond and thus enlarging the therapeutic index of the compound. Importantly, this influx transporter is highly expressed in a number of cancers, so exploiting the observed interaction might actually lead to a safer use. In contrast to the usual archetype of a transporter in the context of drug resistance, in this case the transporter-compound relationship may actually have beneficial effects. Usually, the overexpression of efflux pumps is a cause of secondary resistance to a compound. Here, case-to-case discrepancies in levels of SLC35F2 support a stratification strategy, on the one hand to divulge resistant patients and on the other the ones most likely to benefit from the effect of the drug.

4.2 Mechanisms of action of therapeutics

Understanding the mechanism of action of drugs is of utmost importance, since it allows their safer and more intelligent use. The majority of drugs are promiscuous, and comprehending their full target profiles (direct, indirect and off-target effects) is not a trivial task, often technically quite challenging. One of the methods to identify small molecule-protein interactions is chemical proteomics – an affinity chromatography based approach coupled to mass spectrometry. Gel-based proteomic workflow, although allowed profiling of a number of clinically relevant small molecules, has shortcomings such as an increased risk of keratin contamination due to multiple sample handling steps, incompatibility with quantitative proteomic methods that utilize post-digestion chemical labeling with isobaric tags and high labor and cost demand. A number of these limitations can be overcome with

the adaptation of a gel-free approach. Despite these advancements, however, few issues remained – we observed a number of cases of impeded cognate target recovery and unsatisfying immunoblot efficiency; thus, it required an optimization. We set to determine whether the elution conditions could critically impact the drug-protein profile by influencing the drug-protein interactions. The aim was to discover a universal method that would improve elution efficiency of a variety of drug targets in both standard drug immobilization protocols and in biotinylated drugs. We found that a double elution with appropriate concentrations of urea and formic acid provides a rapid, mild and efficient elution strategy that resulted in paramount target recovery in both immobilization methods without parallel enrichment of non-specific proteins. Importantly, this effect was not constrained to a particular target type. This generically applicable elution strategy allows for enhanced target profiling of small molecules in a single chemical proteomic experiment.

The chemical proteomic approach was essential in deciphering the target spectrum of crizotinib, a known kinase inhibitor and, as we discovered, a suppressor of human mutT homologue MTH1 (NUDT1) activity, a nucleotide pool sanitizing enzyme. Inhibition of MTH1 induces DNA single-strand breaks, activates DNA repair and suppresses tumor growth. Based on our finding that the phenotypic “RAS inhibitor” SCH51344 directly targets MTH1, we performed an MTH1 inhibitor screen based on thermal shift stability assay. The drug-like features of SCH51344 were limited, so we screened a compound library to find more favorable candidates. The clinically approved kinase inhibitor crizotinib showed high affinity towards MTH1. Curiously, the efficacy of crizotinib blocking MTH1 differed significantly between different batches. Direct-binding assays, long term colony formation assays and *in vitro* K_d measurements led to the conclusion that the cause of this discrepancy is actually the difference between the enantiomers, as crizotinib is a chiral compound. The screening batch seemed to be a racemate, and the effect towards MTH1 was much stronger with the (*S*)-enantiomer than with the clinically used (*R*)-crizotinib. This stereospecificity was undoubtedly confirmed by chemical proteomics. Drug pull-downs with both enantiomers were performed, for which chemical probes of the individual enantiomers were incubated with lysates of RAS-transformed cells. Remarkably, the enantiomers showed completely different target spectra, with (*R*)-crizotinib binding ten times more kinases; among them its cognate targets ALK and MET. (*S*)-crizotinib, on the other hand, did not bind a lot of proteins in general – its most prominent target by far was MTH1. Although (*S*)-crizotinib is a new chemical entity, due to its mirror-like similarity with the clinically approved (*R*)-enantiomer it is an attractive drug candidate. MTH1 levels are increased in RAS-expressing cancers, where the high proliferation rate causes oxidative stress. The role of MTH1 is crucial here, since it can eliminate reactive oxygen species (ROS) induced DNA damage which allows the cancer cell to overcome oncogene induced senescence. In line with that, inhibition of MTH1, as shown

with short interfering RNA, impaired growth of tumor cells. Thus, targeting homeostasis of the cellular nucleotide pool seems a promising option for cancer therapy.

Another approach was applied when we embarked to understand the mechanism of action of YM155. Although marketed as a survivin suppressor, we did not observe a direct correlation between the efficacy of YM155 and survivin levels. A genome-wide insertional mutagenesis approach permitted identification of loss-of-function mutations that would rescue cells from drug-induced toxicity and thus reveal pathways crucial for YM155 activity. We could show that the effect of YM155 is completely dependent on the presence of the influx pump, SLC35F2, which facilitates its transport and is absolutely required for the efficacy of the compound. In order to understand the primary mode of action of YM155, we compared transcriptional profiles of drug responsive (high SLC35F2, KBM7^{WT}) and its isogenic counterpart, a non-responsive cell line (low SLC35F2, KBM7^{GT}) upon YM155 treatment. The most significantly enriched gene sets were the induction of apoptosis and DNA damage response. We observed a dose-dependent increase in DNA double-strand breaks in cells expressing SLC35F2. Moreover, YM155 was coherently exhibiting characteristics of a DNA intercalating agent. When we assayed its ability to interfere with topological forms of plasmid DNA after topoisomerase treatment, it did not behave like a classical topoisomerase I inhibitor but showed similarity to intercalating agents (e.g. ethidium bromide). YM155 inhibited DNA replication and induced apoptotic cell death. Thus, we concluded that DNA intercalation is indeed the primary mode of YM155 induced cytotoxicity and that its efficacy is entirely determined by the presence of SLC35F2. This offers the possibility to selectively target tumor cells that highly express this importer, leading to targeted DNA damage induced toxicity.

Pediatric cancers are different to those occurring in adults. The main characteristic of adult cancers – high mutational burden – is uncommon for childhood tumors, marked by quiet genomes where only a few mutations are found in genes that code for druggable targets, thus making progress in targeted therapy even more difficult. Also, pediatric tumors are very diverse regarding their cells of origin, clinical features and onset time. Mechanism by which a certain chemical entity exhibits its effect is greatly dependent on the availability of its cognate targets and the context of signaling events. Taking all this into consideration, we set out to determine the mode of action of PKC412 (midostaurin) in Ewing sarcoma. Our interest in PKC412 in the Ewing type of tumors spiked when we observed its strong synergistic effect with IGF1R/INSR inhibitors. PKC412 is an orally applicable kinase inhibitor in Phase III development for treating Fms-like tyrosine kinase 3 (FLT3)-mutated acute myeloid leukemia (AML). Interestingly though, FLT3 is not highly expressed in Ewing sarcoma. Moreover, in contrast to our literature-based assumption, we did not observe downregulation of EWS-FLI1 regulated genes on the transcript level upon drug treatment.

To elucidate the target spectrum of PKC412 in Ewing sarcoma, we applied a chemical proteomic approach and tested a chemically derivatized probe compound in two parallel conditions – EWS-FLI1 wild type and EWS-FLI1 knockdown cells. In the absence of its main cognate targets and in a particular signaling context directed by the fusion oncoprotein, PKC412 exhibited its cytotoxic effect primarily by inhibiting a different assortment of proteins. Cytotoxic effects of the compound were predominantly a result of a suppression of prominent signaling routes in Ewing sarcoma, primarily calcium/calmodulin and insulin signaling axes. Compared to its profile in leukemia, the resulting target spectrum of PKC412 was changed and shifted. This should be kept in mind when investigating applications of a drug in a different setting.

4.3 Combinatorial drug treatment

Recently, targeted therapies have shown promise in various cancer types offering an alternative to traditional chemotherapy from the 1950's that is still prevailing. Unfortunately, resistance to targeted agents occurs frequently, caused by various mechanisms that cancer cells adopt when challenged with small molecule drugs. A considerable portion of developing resistance can be successfully addressed with combination treatment, especially in cases where the resistance is a result of either an activation of compensatory pathways or upregulation of efflux transporters that could be blocked by the second drug. We found that FDA approved kinase inhibitor lapatinib strongly synergizes with the DNA damaging compound, YM155, by blocking the ABCB1 pump, whose substrate is YM155. In this way, the intracellular concentration of YM155 was dramatically increased and the effect potentiated and prolonged. Expression levels of ABCB1 are usually high in neuroblastoma tumors, making them intrinsically resistant to YM155. Importantly, the strongest synergistic effect was observed at concentrations much lower than corresponding IC_{50} s; when transformed to plasma concentrations, for both agents they are proved to be well tolerated and easily achieved.

Compensatory pathways can remodel the signaling landscape, thus changing the initial conditions required for the effect of a drug. The effect of the second drug is beneficial if it can act in this alternated environment and/or cause rewiring of deranged signaling networks. The resulting effect of the proper combination would be a synergistic inhibition of crucial signaling routes. Drug-drug interactions are interesting from a mathematical modeling point of view, exclusive of therapeutic potential, since deciphering these correlations in a particular disease context can contribute to knowledge of specific signaling events and

relationships. This is what we aim to achieve in Ewing sarcoma, by charting disease specific drug-drug interactions onto pathways. Mapping these chemical perturbations in a controlled way allow a better understanding of the system as a whole and, additionally, could pave way for in-silico synergy predictions. For this purpose, strong antagonisms are even more interesting than synergies. On the other hand, combinations of drugs producing strong synergistic effect in a range of concentrations achievable in plasma are particularly attractive from a clinical aspect, especially disease specific combinations. Antibody-based and small molecule IGF-1R inhibitors were an exciting new option in precision medicine-based Ewing sarcoma treatment, since this signaling axis was known to be heavily deregulated in this cancer due to a number of related EWS-FLI1 target genes. Yet, it proved to be difficult to identify patients that would benefit from the therapy and even in responsive patients resistance occurred frequently. Combination of PKC412 with two different IGF-1R inhibitors from our screening library was consistently strongly synergistic in a panel of assorted Ewing sarcoma cell lines, while mild antagonism or additivity were observed in parallel screens in neuroblastoma and medulloblastoma. Notably, since we performed a concentration matrix based combinatorial screen, the complete profile of synergy was assessed. Advantageously for a possible therapeutic application, we observed an effect that was spread across a broad range of concentrations of both drugs, arguing for a wide therapeutic window for the synergy. Moreover, for both drugs (PKC412 and BMS-754807) the concentrations with most prominent synergistic effects were below the limit plasma concentrations that are achievable and safe in patients. Thus, the simultaneous use of these two orally applicable agents in therapy would be favorable, also in the context of our short- and long-term experiments due to the observed efficacy of the combination in all Ewing sarcoma cells tested. Although the exact mechanism of the synergistic effect is still unclear, we could show that the combination undoubtedly triggers a different array of responses in cancer cells compared to single drug treatment. For a substantial number of proteins, we observed considerable changes in phosphorylation status upon combinatorial treatment. Furthermore, a significant portion of de-regulated phosphorylated sites was found to be unique for the combo treatment, which strongly argues that the combined effect was more than a simple sum of parts. A very illustrative case of differential phosphorylation was the phosphorylation of p70S6 kinase at T389, a hallmark of the activation of mTOR, that was more inhibited by the combo than either of the drugs alone and – notably – this effect was dependent on the presence of EWS-FLI1 (unlike for the mTOR inhibitor drugs used as a control). Phosphorylation was steadily inhibited by the combination, regardless whether the single drugs or controls were having an effect on their own, which argued for a feedback loop derangements by the simultaneous effect of the two drugs; this could lead to overcoming or postponing the resistance. Our assumption needs a confirmation in clinics, but there is a room for optimism, since both

drugs are safe for use at the required concentrations where they act synergistically in a signaling environment altered by EWS-FLI1.

4.4 Summary and outlook

The advancements in the mass spectrometry based gel-free chemical proteomic approach (reported in the chapter 3.1) already affected our studies, since we applied the newly established method to capture the target profile of PKC412 in the Ewing sarcoma setting. We utilized the new elution strategy and successfully recovered drug interactors; moreover, we managed to capture subtle differences in protein abundances between the EWS-FLI1 on and off state. While achieving this, our approach did not augment the polymer burden (which might mask the target proteins), even though the double elution was applied and therefore we expected more contaminants. Although we already confirmed in the manuscript that the reported enhancement in target recovery was not constrained to a particular branch of the kinome tree or a single drug, solid drug pull-down data that we obtained with PKC412 affirmed that the method allows fast and efficient characterization of small molecule target profiles in a single chemical proteomic experiment. Taking all this into account it seems that this methodology could become a standard elution strategy in the gel-free chemical proteomic approach.

Manuscripts presented in chapters 3.2 and 3.4, both published in 2014, already had an impact on subsequent studies published by our laboratory and others.

The fact that (*S*)-crizotinib is a highly specific MTH1 inhibitor was an excellent starting point for developing a metabolite interaction mapping method, that relies on thermal-stability profiling in combination with mass spectrometry (Huber *et al*, 2015). Indeed, by detecting thermal stabilization of the protein in the intact cells, MTH1 was identified as a top target of the (*S*)-enantiomer of crizotinib. These results encouraged the authors to successfully apply the methodology beyond the identification of established drug-target relationships, but to discover interactors of cellular metabolites. On the other hand, ours and a study of our collaborators (Gad *et al*, 2014) prompted further advancements in understanding the distinct role of MTH1 as the most prominent dNTP pool sensitizing enzyme (Carter *et al*, 2015). MTH1 was shown to be crucial for maintaining KRAS-driven pathways (Patel *et al*, 2015) and required for effective transformation by HRAS (Giribaldi *et al*, 2015). Importantly, the crucial difference in target profiles between the two crizotinib enantiomers was widely recognized in the community.

The absolute dependency of YM155 on an SLC35F2 raised a general interest in investigating SLC-drug interactions. It was acknowledged that this large group of membrane transport proteins was undeservedly understudied. They are involved in fundamental physiological functions, connected with human diseases and are important for drug transport (César-Razquin *et al*, 2015). It was discovered in our laboratory that an SLC protein (SLC38A9) is an important component of the mTOR amino acid sensing machinery (Rebsamen *et al*, 2015) and our group focused further on understanding the roles, functions and specificities of solute carrier membrane transport proteins. We showed that the key to YM155 cytotoxicity are its DNA intercalating properties and the induction of DNA damage pathways that ultimately lead to apoptosis. In this light, it was shown that YM155 caused a DNA damage response that is responsible for its potent effect against leukemia cells (Chang *et al*, 2015). Moreover, the methodology of a haploid genetic resistance screen was useful for succeeding publications by several groups (Tsvetkov *et al*, 2015; Dixon *et al*, 2015).

Phenotypic combinatorial screens in Ewing sarcoma revealed disease specific synergies that offer interesting clinical prospects. Furthermore, chemical perturbations of the system offered an excellent opportunity to better understand signaling pathways involved in creating the specific drug response in Ewing sarcoma through in-depth analysis of specific drug-drug interactions. All combinatorial effects that proved to be specific to Ewing sarcoma cells were mapped out onto the retrieved target space to allow the discovery of specific processes involved in the drug effect. This would enable us to pinpoint signaling circuits that are likely to be crucial for Ewing sarcoma cancer progression. Likewise, we sought to understand the exact mechanism of the synergy between PKC412 and BMS-754807 by means of network modeling. The intersection of target spectra of both drugs with acquired extensive profile of deregulated phosphosites exclusive to the combo treatment would allow us to recognize the response patterns strongly altered by the combination in the EWS-FLI1 modified signaling landscape. We are currently fostering this comprehensive analysis.

We used different approaches to characterize cancer vulnerabilities and profile drugs and drug combinations in order to find alternative regimens. Characteristic traits and particularities of malignant phenotypes that modulate the efficacy of drugs and drug combinations were investigated. We adopted a systems view on complexity of signaling alterations in cancer (global changes caused by EWS-FLI1 oncofusion), but also shed light on the examples of fine-tuning directed by the malignant cells that can prove advantageous (high levels of MTH1 enzyme in cancer, deregulation of drug-transporters). We performed phenotypic screens based on chemical and genetic perturbors, searching for active compounds, investigating drug resistance and exploring drug-drug interactions. In order to decipher the target spectra of drugs and unravel drug synergies, we employed and

optimized diverse approaches. Our studies already contributed to the field, since several publications followed based on our findings.

5 Materials and Methods

5.1 Viability assays

The individual drug effects were determined in proliferation assays using Cell Titer Glo (Promega Inc., Madison WI, USA). Cells were seeded in 96-well plates and treated with drugs the day after. The experiment was done in triplicates. Serial dilutions in a range between 20 μ M and 0.05 μ M were applied for 72 hours. In case of knockdown of EWS/FLI1, the induction with doxycycline was started 24 h prior to drug treatment and the cells were kept in doxycycline until the readout. IC₅₀ values were determined using non-linear regression analysis utilizing the GraphPad Prism software by fitting a dose response curve to the data points.

5.2 Synergy determination

Point-wise synergy screening was performed by deriving drug combination matrices of factorial dilutions of two compounds centered around the IC₅₀ for each drug in a particular cell line. Combinatorial index by Chou-Talalay (Chou & Talalay, 1984) was used to determine synergy based on the Loewe additivity model (Loewe & Muischnek, 1926). In addition to Loewe additivity, the Bliss independence model (Bliss, 1939) was used in validation of synergistic hits. Proliferation rate was determined using Cell Titer Glo (Promega Inc., Madison WI, USA).

5.3 Apoptosis measurements

Induction of apoptosis was measured 24 h after drug exposure. Staining for Annexin V - APC (Firma) and DAPI (Sigma-Aldrich) was done according to the manufacturer's instructions and quantified using a FACS Fortessa (BD) and the Diva software (BD, Version).

1.1 Colony formation assay

1×10^4 cells per well were seeded in six-well plates (in triplicates). After 24 h DMSO (equal to the highest amount of compound dilution, maximum 0.2%) or compounds at combo concentrations were added and cells incubated at 37 °C, 5% CO₂ for 7–10 days. Medium was aspirated, cells were washed with PBS (Gibco), stained with crystal violet solution (0.5% in 6% glutaraldehyde) and left to dry. To quantify the results, ultraviolet absorbance of crystal violet was determined at 570 nm following solubilisation by 70% ethanol.

1.2 Real-time PCR analysis

RNeasy Mini Kit (Qiagen) was used for the isolation of total RNA. Total RNA was quantified using NanoDrop spectrophotometer (Thermo). RevertAid Reverse Transcriptase (Fermentas) was used to generate cDNA from 500 ng of RNA via reverse transcription using oligo(dT) primers. Quantitative real-time PCR was carried out using the SensiMix SYBR kit (Bioline) on a RotorGene RG-600 (Qiagen) PCR machine. Quantification was done with the $2^{-\Delta\Delta C(t)}$ method, where GAPDH expression levels were used for normalization.

1.3 Cell culture

SH-SY5Y cell line and the TRKA-inducible system were kindly provided by Johannes Schulte (University Children's Hospital of Essen, Essen, Germany); NMYC-inducible SH-SY5Y was a gift from Frank Westermann (DKFZ, Heidelberg, Germany); UW228 were a gift from Alexandre Arcaro (University Hospital of Bern, Bern, Switzerland); all Ewing sarcoma cell lines (including the inducible EWS-FLI1 system) were kindly provided by Heinrich Kovar (Children's Cancer Research Institute, Vienna, Austria). A673, ASP14, and UW228 cells were cultured in DMEM (Sigma) media containing 10% fetal bovine serum and 10 U/ml penicillin/streptomycin (Gibco). SH-SY5Y cells were cultured in RPMI 1640 (Sigma) media containing 10% fetal bovine serum and 10 U/ml penicillin/streptomycin (Gibco). TC32, RDES, STA-ET-7.1, STA-ET-7.2, STA-ET-2.1, STA-ET-2.2 were grown on fibronectin (Roche) coated plates, and kept in RPMI 1640 (Sigma) media containing 10% fetal bovine serum and 10 U/ml penicillin/streptomycin (Gibco).

5.7 Cell stimulation and immunoblotting

Cells were cultured in complete medium. The serum starvation was done over night, when indicated. Subsequently, cells were stimulated for 20 minutes with 15% serum media. In case of a knock down of EWS-FLI, cells were treated with doxycyclin (1 mg mL^{-1}) 24 hours before serum stimulation, unless otherwise stated. The following antibodies were used: rabbit anti-actin (AAN01, Cytoskeleton), mouse anti-tubulin (DM1A, Abcam), mouse GAPDH (Santa Cruz, sc-365062), rabbit phospho-Akt (S473) (Cell Signaling, 4060S), rabbit phospho-Akt (Thr308) (Cell Signaling, 2965), rabbit Akt (pan) (11E7) (Cell Signaling, 4685), rabbit phospho-p70 S6 kinase (Thr389) (Cell Signaling, 9234), rabbit p70 S6 kinase α (C-18) (Santa Cruz, sc-230) and rabbit FLI1 (Novus, NB600-537).

5.8 SILAC labeling

ASP14 cells were labeled in SILAC DMEM (PAA Laboratories GmbH) supplemented with 10% dialyzed fetal bovine serum (Sigma), 2 mM L-glutamine (Gibco), penicillin (100 U/ml), and streptomycin (100 mg/ml). One cell population was labeled with natural variants of the amino acids (light label; Lys0, Arg0) (Sigma), the second was labeled with medium variants of amino acids {L-[$^2\text{H}_4$]Lys (+4) and L-[$^{13}\text{C}_6$]Arg (+6)} (Lys4, Arg6), and the third was labeled with heavy variants of the amino acids {L-[$^{13}\text{C}_6,^{15}\text{N}_2$]Lys (+8) and L-[$^{13}\text{C}_6,^{15}\text{N}_4$]Arg (+10)} (Lys8, Arg10). Medium and heavy variants of amino acids were purchased from Cambridge Isotope Laboratories.

6 References

- Alisi A, Cho WC, Locatelli F & Fruci D (2013) Multidrug Resistance and Cancer Stem Cells in Neuroblastoma and Hepatoblastoma. *Int. J. Mol. Sci.* **14**: 24706–24725
- Anderson JL, Denny CT, Tap WD & Federman N (2012) Pediatric sarcomas: translating molecular pathogenesis of disease to novel therapeutic possibilities. *Pediatr Res* **72**: 112–121
- Avnet S, Sciacca L, Salerno M, Gancitano G, Cassarino MF, Longhi A, Zakikhani M, Carboni JM, Gottardis M, Giunti A, Pollak M, Vigneri R & Baldini N (2009) Insulin Receptor Isoform A and Insulin-like Growth Factor II as Additional Treatment Targets in Human Osteosarcoma. *Cancer Res.* **69** : 2443–2452
- Awad O, Yustein JT, Shah P, Gul N, Katuri V, O'Neill A, Kong Y, Brown ML, Toretsky JA & Loeb DM (2010) High ALDH Activity Identifies Chemotherapy-Resistant Ewing's Sarcoma Stem Cells That Retain Sensitivity to EWS-FLI1 Inhibition. *PLoS One* **5**: e13943
- Ban J, Aryee DNT, Fourtouna A, van der Ent W, Kauer M, Niedan S, Machado I, Rodriguez-Galindo C, Tirado OM, Schwentner R, Picci P, Flanagan AM, Berg V, Strauss SJ, Scotlandi K, Lawlor ER, Snaar-Jagalska E, Llombart-Bosch A & Kovar H (2014) Suppression of Deacetylase SIRT1 Mediates Tumor-Suppressive NOTCH Response and Offers a Novel Treatment Option in Metastatic Ewing Sarcoma. *Cancer Res.* **74** : 6578–6588
- Ban J, Bennani-Baiti IM, Kauer M, Schaefer K-L, Poremba C, Jug G, Schwentner R, Smrzka O, Muehlbacher K, Aryee DNT & Kovar H (2008) EWS-FLI1 Suppresses NOTCH-Activated p53 in Ewing's Sarcoma. *Cancer Res.* **68** : 7100–7109
- Barretina J, Caponigro G, Stransky N, Venkatesan K, Margolin AA, Kim S, Wilson CJ, Lehar J, Kryukov G V, Sonkin D, Reddy A, Liu M, Murray L, Berger MF, Monahan JE, Morais P, Meltzer J, Korejwa A, Jane-Valbuena J, Mapa FA, et al (2012) The Cancer Cell Line Encyclopedia enables predictive modelling of anticancer drug sensitivity. *Nature* **483**: 307–603
- Bliss CI (1939) the Toxicity of Poisons Applied Jointly¹. *Ann. Appl. Biol.* **26**: 585–615
- Borgdorff V, Rix U, Winter GE, Gridling M, Muller AC, Breitwieser FP, Wagner C, Colinge J, Bennett KL, Superti-Furga G & Wagner SN (2014) A chemical biology approach

- identifies AMPK as a modulator of melanoma oncogene MITF. *Oncogene* **33**: 2531–2539
- Boro A, Prêtre K, Rechfeld F, Thalhammer V, Oesch S, Wachtel M, Schäfer BW & Niggli FK (2012) Small-molecule screen identifies modulators of EWS/FLI1 target gene expression and cell survival in Ewing's sarcoma. *Int. J. Cancer* **131**: 2153–2164
- Bosse KR & Maris JM (2015) Advances in the translational genomics of neuroblastoma: From improving risk stratification and revealing novel biology to identifying actionable genomic alterations. *Cancer*: n/a–n/a
- Brodeur GM (2003) Neuroblastoma: biological insights into a clinical enigma. *Nat Rev Cancer* **3**: 203–216
- Brodeur GM & Bagatell R (2014) Mechanisms of neuroblastoma regression. *Nat Rev Clin Oncol* **11**: 704–713
- Brodeur GM, Minturn JE, Ho R, Simpson AM, Iyer R, Varela CR, Light JE, Kolla V & Evans AE (2009) Trk Receptor Expression and Inhibition in Neuroblastomas. *Clin. Cancer Res.* **15** : 3244–3250
- Brodeur GM, Seeger RC, Schwab M, Varmus HE & Bishop JM (1984) Amplification of N-myc in untreated human neuroblastomas correlates with advanced disease stage. *Sci.* **224** : 1121–1124
- Brohl AS, Solomon DA, Chang W, Wang J, Song Y, Sindiri S, Patidar R, Hurd L, Chen L, Shern JF, Liao H, Wen X, Gerard J, Kim J-S, Lopez Guerrero JA, Machado I, Wai DH, Picci P, Triche T, Horvai AE, et al (2014) The Genomic Landscape of the Ewing Sarcoma Family of Tumors Reveals Recurrent STAG2 Mutation. *PLoS Genet.* **10**: e1004475
- Burchill SA (2008) Molecular abnormalities in Ewing's sarcoma. *Expert Rev. Anticancer Ther.* **8**: 1675–1687
- Carboni JM, Wittman M, Yang Z, Lee F, Greer A, Hurlburt W, Hillerman S, Cao C, Cantor GH, Dell-John J, Chen C, Discenza L, Menard K, Li A, Trainor G, Vyas D, Kramer R, Attar RM & Gottardis MM (2009) BMS-754807, a small molecule inhibitor of insulin-like growth factor-1R/IR. *Mol. Cancer Ther.* **8** : 3341–3349
- Carette JE, Guimaraes CP, Varadarajan M, Park AS, Wuethrich I, Godarova A, Kotecki M, Cochran BH, Spooner E, Ploegh HL & Brummelkamp TR (2009) Haploid Genetic Screens in Human Cells Identify Host Factors Used by Pathogens. *Sci.* **326** : 1231–1235

- Carette JE, Guimaraes CP, Wuethrich I, Blomen VA, Varadarajan M, Sun C, Bell G, Yuan B, Muellner MK, Nijman SM, Ploegh HL & Brummelkamp TR (2011) Global gene disruption in human cells to assign genes to phenotypes by deep sequencing. *Nat Biotech* **29**: 542–546
- Carter M, Jemth A-S, Hagenkort A, Page BDG, Gustafsson R, Griese JJ, Gad H, Valerie NCK, Desroses M, Bostrom J, Warpman Berglund U, Helleday T & Stenmark P (2015) Crystal structure, biochemical and cellular activities demonstrate separate functions of MTH1 and MTH2. *Nat Commun* **6**:
- César-Razquin A, Snijder B, Frappier-Brinton T, Isserlin R, Gyimesi G, Bai X, Reithmeier RA, Hepworth D, Hediger MA, Edwards AM & Superti-Furga G (2015) A Call for Systematic Research on Solute Carriers. *Cell* **162**: 478–487
- Chang BH, Johnson K, LaTocha D, Rowley JSJ, Bryant J, Burke R, Smith RL, Loriaux M, Müschen M, Mullighan C, Druker BJ & Tyner JW (2015) YM155 potently kills acute lymphoblastic leukemia cells through activation of the DNA damage pathway. *J. Hematol. Oncol.* **8**: 39
- Chen HX & Sharon E (2013) IGF-1R as an anti-cancer target—trials and tribulations. *Chin. J. Cancer* **32**: 242–252
- Chen X, Pappo A & Dyer MA (2015) Pediatric solid tumor genomics and developmental pliancy. *Oncogene* **34**: 5207–5215
- Chen Y, Takita J, Choi YL, Kato M, Ohira M, Sanada M, Wang L, Soda M, Kikuchi A, Igarashi T, Nakagawara A, Hayashi Y, Mano H & Ogawa S (2008) Oncogenic mutations of ALK kinase in neuroblastoma. *Nature* **455**: 971–974
- Chou TC & Talalay P (1984) Quantitative analysis of dose-effect relationships: the combined effects of multiple drugs or enzyme inhibitors. *Adv. Enzyme Regul.* **22**: 27–55
- Cialfi S, McDowell HP, Altavista P, Boldrini R, Bosco S, Clerico A, Jenkner A, Kokai G, Pizer B & Dominici C (2010) ABC drug transporter gene expression in neuroblastoma. *ASCO Meet. Abstr.* **28**: 9524
- Cironi L, Riggi N, Provero P, Wolf N, Suvà M-L, Suvà D, Kindler V & Stamenkovic I (2008) IGF1 Is a Common Target Gene of Ewing's Sarcoma Fusion Proteins in Mesenchymal Progenitor Cells. *PLoS One* **3**: e2634
- Cohn SL, Pearson ADJ, London WB, Monclair T, Ambros PF, Brodeur GM, Faldum A, Hero B, Iehara T, Machin D, Mosseri V, Simon T, Garaventa A, Castel V & Matthay KK (2009) The International Neuroblastoma Risk Group (INRG) Classification System: An

INRG Task Force Report. *J. Clin. Oncol.* **27** : 289–297

- Cole KA & Maris JM (2012) New Strategies in Refractory and Recurrent Neuroblastoma: Translational Opportunities to Impact Patient Outcome. *Clin. Cancer Res.* **18** : 2423–2428
- Collins FS & Varmus H (2015) A New Initiative on Precision Medicine. *N. Engl. J. Med.* **372**: 793–795
- Cong L, Ran FA, Cox D, Lin S, Barretto R, Habib N, Hsu PD, Wu X, Jiang W, Marraffini LA & Zhang F (2013) Multiplex Genome Engineering Using CRISPR/Cas Systems. *Science* **339**: 819–823
- Crompton BD, Stewart C, Taylor-Weiner A, Alexe G, Kurek KC, Calicchio ML, Kiezun A, Carter SL, Shukla SA, Mehta SS, Thorner AR, de Torres C, Lavarino C, Sunol M, McKenna A, Sivachenko A, Cibulskis K, Lawrence MS, Stojanov P, Rosenberg M, et al (2014) The Genomic Landscape of Pediatric Ewing Sarcoma. *Cancer Discov.* **4**: 1326–1341
- Crystal AS, Shaw AT, Sequist L V, Friboulet L, Niederst MJ, Lockerman EL, Frias RL, Gainor JF, Amzallag A, Greninger P, Lee D, Kalsy A, Gomez-Caraballo M, Elamine L, Howe E, Hur W, Lifshits E, Robinson HE, Katayama R, Faber AC, et al (2014) Patient-derived models of acquired resistance can identify effective drug combinations for cancer. *Science* **346**: 1480–6
- Dai C, Tiwari AK, Wu C-P, Su X, Wang S-R, Liu D, Ashby CR, Huang Y, Robey RW, Liang Y, Chen L, Shi C-J, Ambudkar S V, Chen Z-S & Fu L (2008) Lapatinib (Tykerb, GW572016) Reverses Multidrug Resistance in Cancer Cells by Inhibiting the Activity of ATP-Binding Cassette Subfamily B Member 1 and G Member 2. *Cancer Res.* **68** : 7905–7914
- Davies H, Bignell GR, Cox C, Stephens P, Edkins S, Clegg S, Teague J, Woffendin H, Garnett MJ, Bottomley W, Davis N, Dicks E, Ewing R, Floyd Y, Gray K, Hall S, Hawes R, Hughes J, Kosmidou V, Menzies A, et al (2002) Mutations of the BRAF gene in human cancer. *Nature* **417**: 949–954
- Davis MI, Hunt JP, Herrgard S, Ciceri P, Wodicka LM, Pallares G, Hocker M, Treiber DK & Zarrinkar PP (2011) Comprehensive analysis of kinase inhibitor selectivity. *Nat. Biotechnol.* **29**: 1046–1051
- Decock A, Ongenaert M, Vandesompele J & Speleman F (2011) Neuroblastoma epigenetics: From candidate gene approaches to genome-wide screenings. *Epigenetics*

6: 962–970

Delattre O, Zucman J, Plougastel B, Desmaze C, Melot T, Peter M, Kovar H, Joubert I, de Jong P, Rouleau G, Aurias A & Thomas G (1992) Gene fusion with an ETS DNA-binding domain caused by chromosome translocation in human tumours. *Nature* **359**: 162–165

Demetri GD, Chawla SP, Ray-Coquard I, Le Cesne A, Staddon AP, Milhem MM, Penel N, Riedel RF, Bui-Nguyen B, Cranmer LD, Reichardt P, Bompas E, Alcindor T, Rushing D, Song Y, Lee R, Ebbinghaus S, Eid JE, Loewy JW, Haluska FG, et al (2013) Results of an International Randomized Phase III Trial of the Mammalian Target of Rapamycin Inhibitor Ridaforolimus Versus Placebo to Control Metastatic Sarcomas in Patients After Benefit From Prior Chemotherapy. *J. Clin. Oncol.*

Diede SJ (2014) Spontaneous regression of metastatic cancer: learning from neuroblastoma. *Nat Rev Cancer* **14**: 71–72

Dixon SJ, Winter GE, Musavi LS, Lee ED, Snijder B, Rebsamen M, Superti-Furga G & Stockwell BR (2015) Human Haploid Cell Genetics Reveals Roles for Lipid Metabolism Genes in Nonapoptotic Cell Death. *ACS Chem. Biol.* **10**: 1604–1609

Druker BJ, Tamura S, Buchdunger E, Ohno S, Segal GM, Fanning S, Zimmermann J & Lydon NB (1996) Effects of a selective inhibitor of the Ab1 tyrosine kinase on the growth of Bcr-Abl positive cells. *Nat. Med.* **2**: 561–566

Du W & Elemento O (2015) Cancer systems biology: embracing complexity to develop better anticancer therapeutic strategies. *Oncogene* **34**: 3215–3225

Emdal KB, Pedersen A-K, Bekker-Jensen DB, Tsafoou KP, Horn H, Lindner S, Schulte JH, Eggert A, Jensen LJ, Francavilla C & Olsen J V (2015) Temporal proteomics of NGF-TrkA signaling identifies an inhibitory role for the E3 ligase Cbl-b in neuroblastoma cell differentiation. *Sci. Signal.* **8**: ra40–ra40

Fields S & Song O (1989) A novel genetic system to detect protein–protein interactions. *Nature* **340**: 245–246

Fletcher JI, Haber M, Henderson MJ & Norris MD (2010) ABC transporters in cancer: more than just drug efflux pumps. *Nat Rev Cancer* **10**: 147–156

Fouladi M, Stewart CF, Blaney SM, Onar-Thomas A, Schaiquevich P, Packer RJ, Goldman S, Geyer JR, Gajjar A, Kun LE, Boyett JM & Gilbertson RJ (2013) A MOLECULAR BIOLOGY AND PHASE II TRIAL OF LAPATINIB IN CHILDREN WITH REFRACTORY CNS MALIGNANCIES: A PEDIATRIC BRAIN TUMOR CONSORTIUM STUDY. *J.*

Neurooncol. **114**: 173–179

Frei E, Holland JF, Schneidermann MA, Pinkel D, Selkirk G, Freireich EJ, Silver RT, Gold GL & Regelson W (1958) A Comparative Study of Two Regimens of Combination Chemotherapy in Acute Leukemia. *Blood* **13**: 1126–1148

Gad H, Koolmeister T, Jemth A-S, Eshtad S, Jacques SA, Strom CE, Svensson LM, Schultz N, Lundback T, Einarsdottir BO, Saleh A, Gokturk C, Baranczewski P, Svensson R, Berntsson RP-A, Gustafsson R, Stromberg K, Sanjiv K, Jacques-Cordonnier M-C, Desroses M, et al (2014) MTH1 inhibition eradicates cancer by preventing sanitation of the dNTP pool. *Nature* **508**: 215–221

Garofalo C, Manara MC, Nicoletti G, Marino MT, Lollini P-L, Astolfi A, Pandini G, Lopez-Guerrero JA, Schaefer K-L, Belfiore A, Picci P & Scotlandi K (2011) Efficacy of and resistance to anti-IGF-1R therapies in Ewing's sarcoma is dependent on insulin receptor signaling. *Oncogene* **30**: 2730–2740

Gaspar N, Hawkins DS, Dirksen U, Lewis IJ, Ferrari S, Le Deley M-C, Kovar H, Grimer R, Whelan J, Claude L, Delattre O, Paulussen M, Picci P, Sundby Hall K, van den Berg H, Ladenstein R, Michon J, Hjorth L, Judson I, Luksch R, et al (2015) Ewing Sarcoma: Current Management and Future Approaches Through Collaboration. *J. Clin. Oncol.*

Gatta G, Botta L, Rossi S, Aareleid T, Bielska-Lasota M, Clavel J, Dimitrova N, Jakab Z, Kaatsch P, Lacour B, Mallone S, Marcos-Gragera R, Minicozzi P, Sánchez-Pérez M-J, Sant M, Santaquilani M, Stiller C, Tavilla A, Trama A, Visser O, et al (2014) Childhood cancer survival in Europe 1999–2007: results of EURO CARE-5—a population-based study. *Lancet Oncol.* **15**: 35–47

George RE, Sanda T, Hanna M, Frohling S, II WL, Zhang J, Ahn Y, Zhou W, London WB, McGrady P, Xue L, Zozulya S, Gregor VE, Webb TR, Gray NS, Gilliland DG, Diller L, Greulich H, Morris SW, Meyerson M, et al (2008) Activating mutations in ALK provide a therapeutic target in neuroblastoma. *Nature* **455**: 975–978

Giaccone G, Zatloukal P, Roubec J, Floor K, Musil J, Kuta M, van Klaveren RJ, Chaudhary S, Gunther A & Shamsili S (2009) Multicenter Phase II Trial of YM155, a Small-Molecule Suppressor of Survivin, in Patients With Advanced, Refractory, Non-Small-Cell Lung Cancer. *J. Clin. Oncol.* **27** : 4481–4486

Giribaldi MG, Monoz A, Halvorsen K, Patel A & Rai P (2015) MTH1 expression is required for effective transformation by oncogenic HRAS. *Oncotarget; Vol 6, No 13*

Gorlick R, Janeway K, Lessnick S, Randall RL, Marina N & Committee on behalf of the

- COGBT (2013) Children's Oncology Group's 2013 blueprint for research: Bone tumors. *Pediatr. Blood Cancer* **60**: 1009–1015
- Greco WR, Bravo G & Parsons JC (1995) The search for synergy: a critical review from a response surface perspective. *Pharmacol. Rev.* **47** : 331–385
- Greco WR, Faessel H & Levasseur L (1996) The Search for Cytotoxic Synergy Between. *J. Natl. cancer Inst.* **88**: 699–700
- Grohar PJ & Helman LJ (2012) Prospects and challenges for the development of new therapies for Ewing sarcoma. *Pharmacol. Ther.* **137**: 216–224
- Gurney JG, Ross JA, Wall DA, Bleyer WA, Severson RK & Robison LL (1997) Infant Cancer in the U.S.: Histology-Specific Incidence and Trends, 1973 to 1992. *J. Pediatr. Hematol. Oncol.* **19**:
- Hanahan D & Weinberg RA (2011) Review Hallmarks of Cancer : The Next Generation. *Cell* **144**: 646–674
- Hawkins DS (2011) Sarcomas gone bad: What to do about recurrent Ewing sarcoma. *Pediatr. Blood Cancer* **57**: 535–536
- Herrero-Martin D, Fourtouna A, Niedan S, Riedmann LT, Schwentner R & Aryee DNT (2011) Factors Affecting EWS-FLI1 Activity in Ewing's Sarcoma. *Sarcoma* **2011**: 352580
- Holohan C, Van Schaeybroeck S, Longley DB & Johnston PG (2013) Cancer drug resistance: an evolving paradigm. *Nat. Rev. Cancer* **13**: 714–726
- Huang F, Hurlburt W, Greer A, Reeves KA, Hillerman S, Chang H, Fagnoli J, Graf Finckenstein F, Gottardis MM & Carboni JM (2010) Differential Mechanisms of Acquired Resistance to Insulin-like Growth Factor-I Receptor Antibody Therapy or to a Small-Molecule Inhibitor, BMS-754807, in a Human Rhabdomyosarcoma Model. *Cancer Res.*
- Huang M & Weiss WA (2013) Neuroblastoma and MYCN. *Cold Spring Harb. Perspect. Med.* **3** :
- Huber K & Superti-Furga G (2011) After the grape rush: Sirtuins as epigenetic drug targets in neurodegenerative disorders. *Bioorg. Med. Chem.* **19**: 3616–3624
- Huber KVM, Olek KM, Müller AC, Tan CSH, Bennett KL, Colinge J & Superti-Furga G (2015) Proteome-wide drug and metabolite interaction mapping by thermal-stability profiling. *Nat. Methods* **advance on**:
- Iwai M, Minematsu T, Li Q, Iwatsubo T & Usui T (2011) Utility of P-Glycoprotein and Organic

- Cation Transporter 1 Double-Transfected LLC-PK1 Cells for Studying the Interaction of YM155 Monobromide, Novel Small-Molecule Survivin Suppressant, with P-Glycoprotein. *Drug Metab. Dispos.* **39** : 2314–2320
- Janku F (2013) Bringing target-matched PI3King from the bench to the clinic. *Cell Cycle* **12**: 1817–1818
- Janoueix-Lerosey I, Lequin D, Brugieres L, Ribeiro A, de Pontual L, Combaret V, Raynal V, Puisieux A, Schleiermacher G, Pierron G, Valteau-Couanet D, Frebourg T, Michon J, Lyonnet S, Amiel J & Delattre O (2008) Somatic and germline activating mutations of the ALK kinase receptor in neuroblastoma. *Nature* **455**: 967–970
- Jiang Y, Ludwig J & Janku F (2015) Targeted therapies for advanced Ewing sarcoma family of tumors. *Cancer Treat. Rev.* **41**: 391–400
- Junttila MR & de Sauvage FJ (2013) Influence of tumour micro-environment heterogeneity on therapeutic response. *Nature* **501**: 346–54
- Karajannis MA, Legault G, Hagiwara M, Ballas MS, Brown K, Nusbaum AO, Hochman T, Goldberg JD, Koch KM, Golfinos JG, Roland JT & Allen JC (2012) Phase II trial of lapatinib in adult and pediatric patients with neurofibromatosis type 2 and progressive vestibular schwannomas. *Neuro. Oncol.* **14**: 1163–1170
- Kauer M, Ban J, Kofler R, Walker B, Davis S, Meltzer P & Kovar H (2009) A Molecular Function Map of Ewing's Sarcoma. *PLoS One* **4**: e5415
- Kempf-Bielack B, Bielack SS, Jürgens H, Branscheid D, Berdel WE, Exner GU, Göbel U, Helmke K, Jundt G, Kabisch H, Kevric M, Klingebiel T, Kotz R, Maas R, Schwarz R, Semik M, Treuner J, Zoubek A & Winkler K (2005) Osteosarcoma Relapse After Combined Modality Therapy: An Analysis of Unselected Patients in the Cooperative Osteosarcoma Study Group (COSS). *J. Clin. Oncol.* **23** : 559–568
- Kinsey M, Smith R & Lessnick SL (2006) NR0B1 Is Required for the Oncogenic Phenotype Mediated by EWS/FLI in Ewing's Sarcoma. *Mol. Cancer Res.* **4** : 851–859
- Klee CB, Ren H & Wang X (1998) Regulation of the Calmodulin-stimulated Protein Phosphatase, Calcineurin. *J. Biol. Chem.* **273** : 13367–13370
- Kohl NE, Kanda N, Schreck RR, Bruns G, Latt SA, Gilbert F & Alt FW (1983) Transposition and amplification of oncogene-related sequences in human neuroblastomas. *Cell* **35**: 359–367
- Kolch W, Halasz M, Granovskaya M & Kholodenko BN (2015) The dynamic control of signal transduction networks in cancer cells. *Nat. Publ. Gr.* **15**: 515–527

- Konermann S, Brigham MD, Trevino AE, Joung J, Abudayyeh OO, Barcena C, Hsu PD, Habib N, Gootenberg JS, Nishimasu H, Nureki O & Zhang F (2014) Genome-scale transcriptional activation by an engineered CRISPR-Cas9 complex. *Nature* **517**: 583–8
- Kopetz S, Desai J, Chan E, Hecht JR, O'Dwyer PJ, Maru D, Morris V, Janku F, Dasari A, Chung W, Issa J-PJ, Gibbs P, James B, Powis G, Nolop KB, Bhattacharya S & Saltz L (2015) Phase II Pilot Study of Vemurafenib in Patients With Metastatic BRAF-Mutated Colorectal Cancer. *J. Clin. Oncol.*
- Kovar H (2005) Context matters: The hen or egg problem in Ewing's sarcoma. *Semin. Cancer Biol.* **15**: 189–196
- Kreissman SG, Seeger RC, Matthay KK, London WB, Sposto R, Grupp SA, Haas-Kogan DA, LaQuaglia MP, Yu A, Diller L, Buxton A, Park JR, Cohn SL, Maris JM, Reynolds CP & Villablanca JG (2013) Purged versus non-purged peripheral blood stem-cell transplantation for high-risk neuroblastoma (COG A3973): a randomised phase 3 trial. *Lancet Oncol.* **14**: 999–1008
- Kudchadkar R, Ernst S, Chmielowski B, Redman BG, Steinberg J, Keating A, Jie F, Chen C, Gonzalez R & Weber J (2015) A phase 2, multicenter, open-label study of sepantronium bromide (YM155) plus docetaxel in patients with stage III (unresectable) or stage IV melanoma. *Cancer Med.* **4**: 643–650
- Kuhn M, von Mering C, Campillos M, Jensen LJ & Bork P (2008) STITCH: interaction networks of chemicals and proteins. *Nucleic Acids Res.* **36** : D684–D688
- Kurmasheva RT, Dudkin L, Billups C, Debelenko L V, Morton CL & Houghton PJ (2009) The Insulin-like Growth Factor-1 Receptor–Targeting Antibody, CP-751,871, Suppresses Tumor-Derived VEGF and Synergizes with Rapamycin in Models of Childhood Sarcoma. *Cancer Res.* **69** : 7662–7671
- Lamers F, Schild L, Koster J, Versteeg R, Caron HN & Molenaar JJ (2012) Targeted BIRC5 silencing using YM155 causes cell death in neuroblastoma cells with low ABCB1 expression. *Eur. J. Cancer* **48**: 763–771
- Laplanche M & Sabatini DM (2012) mTOR Signaling in Growth Control and Disease. *Cell* **149**: 274–293
- Lawlor ER & Thiele CJ (2012) Epigenetic Changes in Pediatric Solid Tumors: Promising New Targets. *Clin. Cancer Res.* **18** : 2768–2779
- Leavey PJ, Mascarenhas L, Marina N, Chen Z, Krailo M, Miser J, Brown K, Tarbell N, Bernstein ML, Granowetter L, Gebhardt M & Grier HE (2008) Prognostic factors for

- patients with Ewing sarcoma (EWS) at first recurrence following multi-modality therapy: A report from the Children's Oncology Group. *Pediatr. Blood Cancer* **51**: 334–338
- Lee MJ, Ye AS, Gardino AK, Heijink AM, Sorger PK, MacBeath G & Yaffe MB (2012) Sequential Application of Anticancer Drugs Enhances Cell Death by Rewiring Apoptotic Signaling Networks. *Cell* **149**: 780–794
- Lehár J, Krueger AS, Avery W, Heilbut AM, Johansen LM, Price ER, Rickles RJ, Short GF, Staunton JE, Jin X, Lee MS, Zimmermann GR & Borisy A a (2009) Synergistic drug combinations tend to improve therapeutically relevant selectivity. *Nat. Biotechnol.* **27**: 659–666
- Lehár J, Stockwell BR, Giaever G & Nislow C (2008) Combination chemical genetics. *Nat. Chem. Biol.* **4**: 674–81
- Lehár J, Zimmermann GR, Krueger AS, Molnar R a, Ledell JT, Heilbut AM, Short GF, Giusti LC, Nolan GP, Magid O a, Lee MS, Borisy A a, Stockwell BR & Keith CT (2007) Chemical combination effects predict connectivity in biological systems. *Mol. Syst. Biol.* **3**: 80
- Lissat A, Chao MM & Kontny U (2012) Targeted Therapy in Ewing Sarcoma. *ISRN Oncol.* **2012**: 609439
- Loewe S & Muischnek H (1926) Über Kombinationswirkungen. *Naunyn. Schmiedeberg's. Arch. Exp. Pathol. Pharmacol.* **114**: 313–326
- Mali P, Yang L, Esvelt KM, Aach J, Guell M, DiCarlo JE, Norville JE & Church GM (2013) RNA-guided human genome engineering via Cas9. *Science* **339**: 823–6
- Maris JM, Hogarty MD, Bagatell R & Cohn SL (2007) Neuroblastoma. *Lancet* **369**: 2106–2120
- Martini M, Vecchione L, Siena S, Tejpar S & Bardelli A (2011) Targeted therapies: how personal should we go? *Nat. Rev. Clin. Oncol.* **9**: 87–97
- Matthay KK (1998) Stage 4S neuroblastoma: what makes it special? *J. Clin. Oncol.* **16** : 2003–2006
- May WA, Lessnick SL, Braun BS, Klemsz M, Lewis BC, Lunsford LB, Hromas R & Denny CT (1993) The Ewing's sarcoma EWS/FLI-1 fusion gene encodes a more potent transcriptional activator and is a more powerful transforming gene than FLI-1. *Mol. Cell. Biol.* **13** : 7393–7398
- Means AR (2000) Regulatory Cascades Involving Calmodulin-Dependent Protein Kinases.

- Mita MM, Mita AC, Chu QS, Rowinsky EK, Fetterly GJ, Goldston M, Patnaik A, Mathews L, Ricart AD, Mays T, Knowles H, Rivera VM, Kreisberg J, Bedrosian CL & Tolcher AW (2008) Phase I Trial of the Novel Mammalian Target of Rapamycin Inhibitor Deforolimus (AP23573; MK-8669) Administered Intravenously Daily for 5 Days Every 2 Weeks to Patients With Advanced Malignancies. *J. Clin. Oncol.* **26** : 361–367
- Molenaar JJ, Koster J, Zwijnenburg DA, van Sluis P, Valentijn LJ, van der Ploeg I, Hamdi M, van Nes J, Westerman BA, van Arkel J, Ebus ME, Haneveld F, Lakeman A, Schild L, Molenaar P, Stroeken P, van Noesel MM, Ora I, Santo EE, Caron HN, et al (2012) Sequencing of neuroblastoma identifies chromothripsis and defects in neuritogenesis genes. *Nature* **483**: 589–593
- Morrione A, Valentinis B, Xu S, Yumet G, Louvi A, Efstratiadis A & Baserga R (1997) Insulin-like growth factor II stimulates cell proliferation through the insulin receptor. *Proc. Natl. Acad. Sci.* **94** : 3777–3782
- Mosse YP, Laudenslager M, Longo L, Cole KA, Wood A, Attiyeh EF, Laquaglia MJ, Sennett R, Lynch JE, Perri P, Laureys G, Speleman F, Kim C, Hou C, Hakonarson H, Torkamani A, Schork NJ, Brodeur GM, Tonini GP, Rappaport E, et al (2008) Identification of ALK as a major familial neuroblastoma predisposition gene. *Nature* **455**: 930–935
- Naing A, LoRusso P, Fu S, Hong DS, Anderson P, Benjamin RS, Ludwig J, Chen HX, Doyle LA & Kurzrock R (2012) Insulin Growth Factor-Receptor (IGF-1R) Antibody Cixutumumab Combined with the mTOR Inhibitor Temsirolimus in Patients with Refractory Ewing's Sarcoma Family Tumors. *Clin. Cancer Res.* **18** : 2625–2631
- Nakagawara A, Arima-Nakagawara M, Scavarda NJ, Azar CG, Cantor AB & Brodeur GM (1993) Association between High Levels of Expression of the TRK Gene and Favorable Outcome in Human Neuroblastoma. *N. Engl. J. Med.* **328**: 847–854
- Nakahara T, Takeuchi M, Kinoyama I, Minematsu T, Shirasuna K, Matsuhisa A, Kita A, Tominaga F, Yamanaka K, Kudoh M & Sasamata M (2007) YM155, a Novel Small-Molecule Survivin Suppressant, Induces Regression of Established Human Hormone-Refractory Prostate Tumor Xenografts. *Cancer Res.* **67** : 8014–8021
- Nickerson HJ, Matthay KK, Seeger RC, Brodeur GM, Shimada H, Perez C, Atkinson JB, Selch M, Gerbing RB, Stram DO & Lukens J (2000) Favorable Biology and Outcome of Stage IV-S Neuroblastoma With Supportive Care or Minimal Therapy: A Children's Cancer Group Study. *J. Clin. Oncol.* **18** : 477

- Nordling CO (1953) A new theory on cancer-inducing mechanism. *Br. J. Cancer* **7**: 68–72
- Norris MD, Bordow SB, Marshall GM, Haber PS, Cohn SL & Haber M (1996) Expression of the Gene for Multidrug-Resistance–Associated Protein and Outcome in Patients with Neuroblastoma. *N. Engl. J. Med.* **334**: 231–238
- Olsen J V & Mann M (2013) Status of Large-scale Analysis of Post-translational Modifications by Mass Spectrometry. *Mol. Cell. Proteomics* **12** : 3444–3452
- Olsen J V., Blagoev B, Gnäd F, Macek B, Kumar C, Mortensen P & Mann M (2006) Global, In Vivo, and Site-Specific Phosphorylation Dynamics in Signaling Networks. *Cell* **127**: 635–648
- Ong S-E, Blagoev B, Kratchmarova I, Kristensen DB, Steen H, Pandey A & Mann M (2002) Stable Isotope Labeling by Amino Acids in Cell Culture, SILAC, as a Simple and Accurate Approach to Expression Proteomics. *Mol. Cell. Proteomics* **1** : 376–386
- Pappo AS, Anderson JR, Crist WM, Wharam MD, Breitfeld PP, Hawkins D, Raney RB, Womer RB, Parham DM, Qualman SJ & Grier HE (1999) Survival After Relapse in Children and Adolescents With Rhabdomyosarcoma: A Report From the Intergroup Rhabdomyosarcoma Study Group. *J. Clin. Oncol.* **17** : 3487–3493
- Patel A, Burton DGA, Halvorsen K, Balkan W, Reiner T, Perez-Stable C, Cohen A, Munoz A, Giribaldi MG, Singh S, Robbins DJ, Nguyen DM & Rai P (2015) MutT Homolog 1 (MTH1) maintains multiple KRAS-driven pro-malignant pathways. *Oncogene* **34**: 2586–2596
- Peterson TR, Laplante M, Thoreen CC, Sancak Y, Kang SA, Kuehl WM, Gray NS & Sabatini DM (2009) DEPTOR Is an mTOR Inhibitor Frequently Overexpressed in Multiple Myeloma Cells and Required for Their Survival. *Cell* **137**: 873–886
- Pritchard J & Hickman JA (1994) Why does stage 4s neuroblastoma regress spontaneously? *Lancet* **344**: 869–870
- Rebsamen M, Pochini L, Stasyk T, de Araujo MEG, Galluccio M, Kandasamy RK, Snijder B, Fauster A, Rudashevskaya EL, Bruckner M, Scorzoni S, Filipek PA, Huber KVM, Bigenzahn JW, Heinz LX, Kraft C, Bennett KL, Indiveri C, Huber LA & Superti-Furga G (2015) SLC38A9 is a component of the lysosomal amino acid sensing machinery that controls mTORC1. *Nature* **519**: 477–481
- Rezwan M & Auerbach D (2012) Yeast ‘N’-hybrid systems for protein-protein and drug-protein interaction discovery. *Methods* **57**: 423–9
- Riggi N, Knoechel B, Gillespie SM, Rheinbay E, Boulay G, Suvà ML, Rossetti NE, Boonseng

- WE, Oksuz O, Cook EB, Formey A, Patel A, Gymrek M, Thapar V, Deshpande V, Ting DT, Hornicek FJ, Nielsen GP, Stamenkovic I, Aryee MJ, et al (2014) EWS-FLI1 Utilizes Divergent Chromatin Remodeling Mechanisms to Directly Activate or Repress Enhancer Elements in Ewing Sarcoma. *Cancer Cell* **26**: 668–681
- Riggs N & Stamenkovic I (2007) The Biology of Ewing sarcoma. *Cancer Lett.* **254**: 1–10
- Riggs N, Suvà M-L, Suvà D, Cironi L, Provero P, Tercier S, Joseph J-M, Stehle J-C, Baumer K, Kindler V & Stamenkovic I (2008) EWS-FLI-1 Expression Triggers a Ewing's Sarcoma Initiation Program in Primary Human Mesenchymal Stem Cells. *Cancer Res.* **68** : 2176–2185
- Rix U & Superti-furga G (2009) Target profiling of small molecules by chemical proteomics. *Nat. Publ. Gr.* **5**: 616–624
- Roderick HL & Cook SJ (2008) Ca²⁺ signalling checkpoints in cancer: remodelling Ca²⁺ for cancer cell proliferation and survival. *Nat Rev Cancer* **8**: 361–375
- Rodriguez-Mora OG, LaHair MM, McCubrey JA & Franklin RA (2005) Calcium/Calmodulin-Dependent Kinase I and Calcium/Calmodulin-Dependent Kinase Kinase Participate in the Control of Cell Cycle Progression in MCF-7 Human Breast Cancer Cells. *Cancer Res.* **65** : 5408–5416
- Rozengurt E, Soares HP & Sinnett-Smith J (2014) Suppression of feedback loops mediated by PI3K/mTOR induces multiple overactivation of compensatory pathways: an unintended consequence leading to drug resistance. *Mol. Cancer Ther.* **13**: 2477–88
- Sarbassov DD, Guertin DA, Ali SM & Sabatini DM (2005) Phosphorylation and Regulation of Akt/PKB by the Rictor-mTOR Complex. *Sci.* **307** : 1098–1101
- Sausen M, Leary RJ, Jones S, Wu J, Reynolds CP, Liu X, Blackford A, Parmigiani G, Diaz LA, Papadopoulos N, Vogelstein B, Kinzler KW, Velculescu VE & Hogarty MD (2013) Integrated genomic analyses identify ARID1A and ARID1B alterations in the childhood cancer neuroblastoma. *Nat Genet* **45**: 12–17
- Savitski MM, Reinhard FBM, Franken H, Werner T, Savitski MF, Eberhard D, Molina DM, Jafari R, Dovega RB, Klaeger S, Kuster B, Nordlund P, Bantscheff M & Drewes G (2014) Tracking cancer drugs in living cells by thermal profiling of the proteome. *Sci.* **346** :
- Schirle M & Jenkins JL (2015) Identifying compound efficacy targets in phenotypic drug discovery. *Drug Discov. Today*
- Schwab M, Alitalo K, Klempnauer K-H, Varmus HE, Bishop JM, Gilbert F, Brodeur G,

- Goldstein M & Trent J (1983) Amplified DNA with limited homology to myc cellular oncogene is shared by human neuroblastoma cell lines and a neuroblastoma tumour. *Nature* **305**: 245–248
- Schwartz GK, Tap WD, Qin L-X, Livingston MB, Undevia SD, Chmielowski B, Agulnik M, Schuetze SM, Reed DR, Okuno SH, Ludwig JA, Keedy V, Rietschel P, Kraft AS, Adkins D, Van Tine BA, Brockstein B, Yim V, Bitas C, Abdullah A, et al (2015) Cixutumumab and temsirolimus for patients with bone and soft-tissue sarcoma: a multicentre, open-label, phase 2 trial. *Lancet Oncol.* **14**: 371–382
- Scotlandi K, Benini S, Sarti M, Serra M, Lollini P-L, Maurici D, Picci P, Manara MC & Baldini N (1996) Insulin-like Growth Factor I Receptor-mediated Circuit in Ewing's Sarcoma/Peripheral Neuroectodermal Tumor: A Possible Therapeutic Target. *Cancer Res.* **56** : 4570–4574
- Scotlandi K, Manara MC, Nicoletti G, Lollini P-L, Lukas S, Benini S, Croci S, Perdichizzi S, Zambelli D, Serra M, García-Echeverría C, Hofmann F & Picci P (2005) Antitumor Activity of the Insulin-Like Growth Factor-I Receptor Kinase Inhibitor NVP-AEW541 in Musculoskeletal Tumors. *Cancer Res.* **65** : 3868–3876
- Seeger RC, Brodeur GM, Sather H, Dalton A, Siegel SE, Wong KY & Hammond D (1985) Association of Multiple Copies of the N-myc Oncogene with Rapid Progression of Neuroblastomas. *N. Engl. J. Med.* **313**: 1111–1116
- Slamon D, Eiermann W, Robert N, Pienkowski T, Martin M, Press M, Mackey J, Glaspy J, Chan A, Pawlicki M, Pinter T, Valero V, Liu M-C, Sauter G, von Minckwitz G, Visco F, Bee V, Buyse M, Bendahmane B, Tabah-Fisch I, et al (2011) Adjuvant trastuzumab in HER2-positive breast cancer. *N. Engl. J. Med.* **365**: 1273–83
- Slamon DJ, Godolphin W, Jones LA, Holt JA, Wong SG, Keith DE, Levin WJ, Stuart SG, Udove J & Ullrich A (1989) Studies of the HER-2/neu proto-oncogene in human breast and ovarian cancer. *Science* **244**: 707–712
- Smith MA, Altekruse SF, Adamson PC, Reaman GH & Seibel NL (2014) Declining childhood and adolescent cancer mortality. *Cancer* **120**: 2497–2506
- Smith MA, Seibel NL, Altekruse SF, Ries LAG, Melbert DL, O'Leary M, Smith FO & Reaman GH (2010) Outcomes for Children and Adolescents With Cancer: Challenges for the Twenty-First Century. *J. Clin. Oncol.* **28**: 2625–2634
- Smith R, Owen LA, Trem DJ, Wong JS, Whangbo JS, Golub TR & Lessnick SL (2006) Expression profiling of EWS/FLI identifies NKX2.2 as a critical target gene in Ewing's

sarcoma. *Cancer Cell* **9**: 405–416

Subbiah V, Naing A, Brown RE, Chen H, Doyle L, LoRusso P, Benjamin R, Anderson P & Kurzrock R (2011) Targeted Morphoproteomic Profiling of Ewing's Sarcoma Treated with Insulin-Like Growth Factor 1 Receptor (IGF1R) Inhibitors: Response/Resistance Signatures. *PLoS One* **6**: e18424

Surdez D, Benetkiewicz M, Perrin V, Han Z-Y, Pierron G, Ballet S, Lamoureux F, Rédini F, Decouvlaere A-V, Daudigeos-Dubus E, Georger B, de Pinieux G, Delattre O & Tirode F (2012) Targeting the EWSR1-FLI1 Oncogene-Induced Protein Kinase PKC- β Abolishes Ewing Sarcoma Growth. *Cancer Res.* **72** : 4494–4503

Svoboda LK, Harris A, Bailey NJ, Schwentner R, Tomazou E, von Levetzow C, Magnuson B, Ljungman M, Kovar H & Lawlor ER (2014) Overexpression of HOX genes is prevalent in Ewing sarcoma and is associated with altered epigenetic regulation of developmental transcription programs. *Epigenetics* **9**: 1613–1625

Tirado OM, Mateo-Lozano S, Villar J, Dettin LE, Llorca A, Gallego S, Ban J, Kovar H & Notario V (2006) Caveolin-1 (CAV1) Is a Target of EWS/FLI-1 and a Key Determinant of the Oncogenic Phenotype and Tumorigenicity of Ewing's Sarcoma Cells. *Cancer Res.* **66** : 9937–9947

Tirode F, Surdez D, Ma X, Parker M, Le Deley MC, Bahrami A, Zhang Z, Lapouble E, Grossetete-Lalami S, Rusch M, Reynaud S, Rio-Frio T, Hedlund E, Wu G, Chen X, Pierron G, Oberlin O, Zaidi S, Lemmon G, Gupta P, et al (2014) Genomic Landscape of Ewing Sarcoma Defines an Aggressive Subtype with Co-Association of STAG2 and TP53 Mutations. *Cancer Discov.* **4**: 1342–1353

Tomazou EM, Sheffield NC, Schmidl C, Schuster M, Schönegger A, Datlinger P, Kubicek S, Bock C & Kovar H (2015) Epigenome Mapping Reveals Distinct Modes of Gene Regulation and Widespread Enhancer Reprogramming by the Oncogenic Fusion Protein EWS-FLI1. *Cell Rep.* **10**: 1082–1095

Toretzky JA, Kalebic T, Blakesley V, LeRoith D & Helman LJ (1997) The Insulin-like Growth Factor-I Receptor Is Required for EWS/FLI-1 Transformation of Fibroblasts. *J. Biol. Chem.* **272** : 30822–30827

Tsimberidou AM, Eggermont AMM & Schilsky RL (2014) Precision cancer medicine: the future is now, only better. *Am. Soc. Clin. Oncol. Educ. Book* **34**: 61–9

Tsvetkov P, Mendillo ML, Zhao J, Carette JE, Merrill PH, Cikes D, Varadarajan M, van Diemen FR, Penninger JM, Goldberg AL, Brummelkamp TR, Santagata S & Lindquist S

- (2015) Compromising the 19S proteasome complex protects cells from reduced flux through the proteasome. *Elife* **4**: 1–22
- Vogelstein B, Papadopoulos N, Velculescu VE, Zhou S, Diaz LA & Kinzler KW (2013) Cancer Genome Landscapes. *Sci.* **339** : 1546–1558
- Wan PTC, Garnett MJ, Roe SM, Lee S, Niculescu-Duvaz D, Good VM, Project CG, Jones CM, Marshall CJ, Springer CJ, Barford D & Marais R (2004) Mechanism of activation of the RAF-ERK signaling pathway by oncogenic mutations of B-RAF. *Cell* **116**: 855–867
- Wang Y, Zhao R & Zhe H (2015) The emerging role of CaMKII in cancer. *Oncotarget; Vol 6, No 14*
- Werner HMJ, Mills GB & Ram PT (2014) Cancer Systems Biology: a peek into the future of patient care? *Nat. Rev. Clin. Oncol.* **11**: 167–176
- Winter GE, Radic B, Mayor-Ruiz C, Blomen V a, Trefzer C, Kandasamy RK, Huber KVM, Gridling M, Chen D, Klampfl T, Kralovics R, Kubicek S, Fernandez-Capetillo O, Brummelkamp TR & Superti-Furga G (2014) The solute carrier SLC35F2 enables YM155-mediated DNA damage toxicity. *Nat. Chem. Biol.* **10**: 768–773
- Winter GE, Rix U, Lissat A, Stukalov A, Müllner MK, Bennett KL, Colinge J, Nijman SM, Kubicek S, Kovar H, Kontny U & Superti-Furga G (2011) An Integrated Chemical Biology Approach Identifies Specific Vulnerability of Ewing's Sarcoma to Combined Inhibition of Aurora Kinases A and B. *Mol. Cancer Ther.* **10** : 1846–1856
- Yu AL, Gilman AL, Ozkaynak MF, London WB, Kreissman SG, Chen HX, Smith M, Anderson B, Villablanca JG, Matthay KK, Shimada H, Grupp SA, Seeger R, Reynolds CP, Buxton A, Reisfeld RA, Gillies SD, Cohn SL, Maris JM & Sondel PM (2010) Anti-GD2 Antibody with GM-CSF, Interleukin-2, and Isotretinoin for Neuroblastoma. *N. Engl. J. Med.* **363**: 1324–1334
- Yu DMT, Huynh T, Truong AM, Haber M & Norris MD (2015) Chapter Five - ABC Transporters and Neuroblastoma. In *ABC Transporters and Cancer*, Research JDS and TIBT-A in C (ed) pp 139–170. Academic Press
- Yuan K, Chung LWK, Siegal GP & Zayzafoon M (2007) [alpha]-CaMKII controls the growth of human osteosarcoma by regulating cell cycle progression. *Lab Invest* **87**: 938–950
- Zhang H, Pelzer AM, Kiang DT & Yee D (2007) Down-regulation of Type I Insulin-like Growth Factor Receptor Increases Sensitivity of Breast Cancer Cells to Insulin. *Cancer Res.* **67** : 391–397
- Zimmermann GR, Lehár J & Keith CT (2007) Multi-target therapeutics: when the whole is

greater than the sum of the parts. *Drug Discov. Today* **12**: 34–42

7 Abbreviations

| | |
|---------|--|
| ABC | ATP binding cassette |
| ABCB1 | ATP-binding cassette sub-family B member 1 |
| ABL | Abelson murine leukemia viral oncogene homolog 1 |
| AKT | Protein kinase B |
| ALK | Anaplastic lymphoma receptor tyrosine kinase |
| ALL | Acute lymphoblastic leukemia |
| AML | Acute myeloid leukemia |
| ARAF | A-Raf proto-oncogene serine/threonine-protein kinase |
| ARID1A | AT rich interactive domain 1A (SWI-like) |
| ARID1B | AT rich interactive domain 1B (SWI-like) |
| ASM | Aggressive systemic mastocytosis |
| ATM | Ataxia telangiectasia mutated |
| ATP | Adenosine triphosphate |
| ATR | Ataxia telangiectasia and Rad3-related protein |
| ATRX | Alpha thalassemia/mental retardation syndrome x-linked |
| AURKA | Aurora kinase A |
| BCR | Breakpoint cluster region |
| Bcr-Abl | Philadelphia chromosome |
| BRAF | v-raf murine sarcoma viral oncogene homolog B1 |
| CAMK | Calcium/calmodulin-dependent protein kinases |
| CAMK1 | Calcium/calmodulin-dependent protein kinase I |
| CAMK2D | Calcium/calmodulin-dependent protein kinase II delta |

| | |
|--------|---|
| Cas9 | CRISPR associated protein 9 |
| cDNA | Complementary DNA |
| CETSA | Cellular thermal shift assay |
| CI | Combination index |
| CML | Chronic myeloid leukemia |
| CRAF | v-Raf-1 murine leukemia viral oncogene homolog 1 |
| CRISPR | Clustered regularly interspaced short palindromic repeat |
| DAPK2 | Death-associated protein kinase 2 |
| DNA | Desoxyribonucleic acid |
| dNTP | Deoxynucleoside triphosphate |
| E | Glutamic acid (amino acid) |
| EF | EWS-FLI1 |
| EGFR | Endothelial growth factor receptor |
| ERBB2 | Neuro/glioblastoma derived oncogene homolog |
| ERK | Extracellular-signal-regulated kinase |
| ES | Ewing sarcoma |
| ESFT | Ewing sarcoma family of tumors |
| ETS | E26 transformation-specific |
| EWS | Ewing sarcoma breakpoint region 1 |
| FACS | Fluorescence-activated cell sorting |
| FDA | Food and Drug Administration |
| FLI1 | Friend leukemia virus integration 1 |
| FLT3 | Fms-related tyrosine kinase 3 |
| HER2 | v-erb-b2 erythroblastic leukemia viral oncogene homolog 2 |
| HRAS | v-ha-ras harvey rat sarcoma viral oncogene homolog |

| | |
|---------|---|
| IGF-1 | Insulin-like growth factor 1 (somatomedin C) |
| IGF-1R | Insulin-like growth factor 1 receptor |
| InsR | Insulin receptor |
| iTRAQ | Isobaric tags for relative and absolute quantitation |
| KIT | v-kit Hardy-Zuckerman 4 feline sarcoma viral oncogene homolog |
| KRAS | v-ki-ras 2 Kirsten rat sarcoma 2 viral oncogene homolog |
| LC | Liquid chromatography |
| LC-MS | Liquid chromatography mass spectrometry |
| LC-MSMS | Liquid chromatography-tandem mass spectrometry |
| MAPK | Mitogen-activated protein kinases |
| MCL | Mast cell leukemia |
| MDR1 | Multidrug resistance protein 1 |
| MEK | Mitogen-activated protein kinase kinase |
| MET | Hepatocyte growth factor receptor |
| MS | Mass spectrometry |
| MTH1 | 7,8-dihydro-8-oxoguaninetriphosphatase |
| mTOR | Mechanistic target of rapamycin |
| mTORC1 | Mechanistic target of rapamycin complex 1 |
| mTORC2 | Mechanistic target of rapamycin complex 2 |
| MYC | v-myc avian myelocytomatosis viral oncogene homolog |
| NGF | Nerve growth factor |
| NKX.2 | Homeobox protein NK-2 homolog |
| NMYC | v-myc avian myelocytomatosis viral oncogene neuroblastoma derived homolog |

| | |
|--------|---|
| NROB1 | Nuclear receptor subfamily 0, group B, member 1 |
| NSCLC | Non-small-cell-lung cancer |
| NTP | Nucleoside triphosphate |
| NTRK1 | Neurotrophic tyrosine kinase receptor, type 1 |
| NUDT1 | Nudix (nucleoside diphosphate linked moiety X)-type motif 1 |
| OTC | Over the Counter |
| PDGFRB | Platelet-derived growth factor receptor, beta polypeptide |
| PDPK1 | 3-phosphoinositide dependent protein kinase 1 |
| PHLDA1 | Pleckstrin homology-like domain, family A, member 1 |
| PI3K | Phosphatidylinositol-4,5-bisphosphate 3-kinase |
| PKA | cAMP-dependent protein kinase catalytic subunit alpha |
| PKC | Protein kinase C |
| PNET | Peripheral neuroectodermal tumor |
| PRKAA2 | Protein kinase, AMP-activated, alpha 2 catalytic subunit |
| PRKAB1 | Protein kinase, AMP-activated, beta 1 non-catalytic subunit |
| PRKAB2 | Protein kinase, AMP-activated, beta 2 non-catalytic subunit |
| PRKCA | Protein kinase C, alpha |
| PRKCB | Protein kinase C, beta |
| RAF | Family of three serine/threonine-specific protein kinases |
| RAS | Protein superfamily of small GTPases |
| RNAi | RNA-interference |
| S | Serine (amino acid) |
| S6K | Ribosomal protein S6 kinase I |
| SDS | Sodium dodecyl sulfate |

| | |
|----------|---|
| SDS-PAGE | Sodium dodecyl sulfate-polyacrylamide gel electrophoresis |
| SILAC | Stable isotope labeling by amino acids in cell culture |
| SLC | Solute carrier |
| SLC35F2 | Solute carrier family member 35F2 |
| SLC38A9 | Solute carrier family member 38A9 |
| STAG2 | Stromal antigen 2 |
| SV | Structural variation |
| T | Threonine (amino acid) |
| TP53 | Tumor protein P53 |
| TrkA | Tropomyosin receptor kinase A |
| ULK3 | Unc-51 like kinase 3 |
| V | Valine (amino acid) |

Curriculum Vitae

Branka Radić Sarikas

Maiden name: Branka Radić
Citizenship: Serbian
Date of birth: May 5th, 1981
Telephone: +43-680/3208976
E-mail: BRadic@cemm.oeaw.ac.at
branka.radich@gmail.com

Research experience

2010 – present **Predoctoral fellow**

CeMM Research Center for Molecular Medicine of the Austrian Academy of Sciences, Vienna, Austria

under supervision of Prof. Giulio Superti-Furga

Project: Probing network fragilities in embryonal tumors by synergistic drug combinations

2010 **Postgraduate research trainee**

Dept of General Pathology, Second University of Naples, Dipartimento di Biochimica, Biofisica e Patologia Generale, Naples, Italy

under supervision of Prof. Lucia Altucci

Project: Epigenetic modulators in cancer: target genes identification and epigenetic hot spots characterization in AMLs

2009 –2010 **Postgraduate research trainee**

at Dept of Physics, Università degli Studi di Napoli Federico II, Naples, Italy

under supervision of Prof. Raffaele Velotta

Project: Application of visible-UV spectroscopy to molecules of pharmacological interest

Education

Oct 2006 **MPharm**

University of Novi Sad, Faculty of Medicine, Dept of Pharmacy

Diploma thesis: "UV-Visual spectroscopy – the principle and the application in pharmaceutical research"

2008 **State Exam for Pharmacists**

Seminars and Poster Presentations

2015 The second European interdisciplinary Ewing sarcoma research summit, Paris, France

Talk: Phenotypic screens reveal vulnerabilities in Ewing sarcoma.

Meeting report submitted to *Oncotarget*: "Taming the monster through trust, openness and collaboration: The second European interdisciplinary Ewing sarcoma research summit"

2013 Pediatric Cancer Research at the INTERFACE , Vienna, Austria, poster

2013 AACR 104th Annual Meeting, Washington D.C., USA

Poster - Abstract 5038 : Probing network fragilities in neuroblastoma by synergistic drug combinations. *Cancer Research*, Proceedings: AACR 104th Annual Meeting 2013; Apr 6-10, 2013

2012 Days of Molecular Medicine 2012 – The Translational Science Rare Diseases: From Rare to Care, Vienna, Austria, poster

2012 European Chemical Biology Symposium ,Vienna, Austria, poster

2012 8th YSA PhD Symposium , Vienna, Austria

Talk : Probing network fragilities in embryonal tumors by synergistic drug combinations

2011 Methods in Chemical Biology, EMBO Practical Course, Heidelberg, Germany , poster

2011 Molecular mechanisms in signal transduction and cancer, Summer School, Spetses, Greece, poster

Honors and Awards

2013 Awardee of the Second Open Call for Small Scale Collaborative Projects
EpiGeneSys - FP7 European Community-funded Network of Excellence

Project: A novel Boolean model based systems biology approach for prediction of epigenetic drugs synergy

2002-2006 Scholarship for students of excellent scientific achievement by Ministry of Science of Republic of Serbia

Languages

- English (full professional proficiency),
- Italian (professional working proficiency),
- German (elementary proficiency),
- Serbian (native).

Publication List

1. **Branka Radic-Sarikas**, Uwe Rix, Alexey Stukalov, Manuela Gridling, André C. Müller, Jacques Colinge, Giulio Superti-Furga, Keiryn L. Bennett (2015) Enhancing Cognate Target Elution Efficiency in Gel-Free Chemical Proteomics. *EuPA Open Proteom.* **9**: 43-53.
2. Winter GE, **Radic B**, Mayor-Ruiz C, Blomen VA, Trefzer C, Kandasamy RK, Huber KV, Gridling M, Chen D, Klampfl T, Kralovics R, Kubicek S, Fernandez-Capetillo O, Brummelkamp TR, Superti-Furga G (2014) The solute carrier SLC35F2 enables YM155-mediated DNA damage toxicity. *Nat Chem Biol.* **10(9)**: 768-773.
3. Huber KV, Salah E, **Radic B**, Gridling M, Elkins JM, Stukalov A, Jemth AS, Göktürk C, Sanjiv K, Strömberg K, Pham T, Berglund UW, Colinge J, Bennett KL, Loizou JI, Helleday T, Knapp S, Superti-Furga G (2014) Stereospecific targeting of MTH1 by (S)-crizotinib as an anticancer strategy. *Nature.* **508(7495)**: 222-7
4. Franci G, Casalino L, Petraglia F, Miceli M, Menafra R, **Radic B**, Tarallo V, Vitale M, Scarfò M, Pocsfalvi G, Baldi A, Ambrosino C, Zambrano N, Patriarca E, De Falco S, Minchiotti G, Stunnenberg HG, Altucci L (2013) The class I-specific HDAC inhibitor MS-275 modulates the differentiation potential of mouse embryonic stem cells. *Biol Open.* **2(10)**: 1070-1077
5. Tambaro FP, Dell'aversana C, Carafa V, Nebbioso A, **Radic B**, Ferrara F, Altucci L (2010) Histone deacetylase inhibitors: clinical implications for hematological malignancies. *Clin Epigenetics.* **1(1-2)**: 25-44

-